

CHEMICAL WEATHERING AND CONSUMPTION OF ATMOSPHERIC
CO₂ IN VOLCANIC AND ULTRAMAFIC REGIONS IN THE TROPICS

A Dissertation

Presented to the Faculty of the Graduate School

of Cornell University

in Partial Fulfillment of the Requirements for the Degree of

Doctor of Philosophy

by

Herdís Helga Schopka

May 2011

© 2011 Herdís Helga Schopka

CHEMICAL WEATHERING AND CONSUMPTION OF ATMOSPHERIC CO₂ IN
VOLCANIC AND ULTRAMAFIC REGIONS IN THE TROPICS

Herdís Helga Schopka, Ph.D.

Cornell University 2011

Chemical weathering of silicates, in particular mafic rocks, is a major driver of global climate over geological time scales via uptake of atmospheric CO₂, but the magnitude of atmospheric CO₂ consumption by this process is still debated. Chemical weathering of mafic rocks is accompanied by a high consumption of atmospheric CO₂. In spite of mafic watersheds often being small, weathering of mafic rocks is therefore very important for the global carbon cycle. A strong positive correlation between chemical and physical weathering exists, as well as between chemical weathering and temperature. One would therefore expect to find the highest chemical weathering rates and atmospheric CO₂ consumption in tectonically active, hot and humid locations.

I investigate the magnitude of atmospheric CO₂ uptake due to silicate weathering in two different tropical settings, Hawai'i and the Philippines. These two locations have broadly similar climate but vary significantly in their lithology and tectonic style. Rivers and streams were sampled in both locations, as well as hot springs in the Philippines and fresh groundwater in Hawai'i. The water was analyzed for dissolved chemicals and fluxes of atmospheric carbon and other elements from the watersheds were calculated using available hydrological data from the University of Diliman (the Philippines) and the USGS (Hawai'i). In Hawai'i, a runoff kriging model, which was used to calculate discharge in unmonitored watersheds, was created.

The results indicate that atmospheric CO₂-fluxes in the Philippines are among the

highest yet reported from any silicate environment in the world, with an average of $3.58 \pm 0.23 \times 10^6$ mol/km²/yr from volcanic areas. Atmospheric CO₂-fluxes from streams in Hawai'i are close to the global average for basaltic regions. Groundwater discharge is an important part of the hydrological budget in Hawai'i and including chemical fluxes via groundwater increases the total chemical flux from the islands by 30-95%. Importantly, my results imply that groundwater is an important pathway for delivery of dissolved chemicals to the ocean at all stages in the life of a volcanic island.

BIOGRAPHICAL SKETCH

Herdís was born and raised in Reykjavík, Iceland. At an early age she developed an interest in travel and far away places. Her first steps toward nomadism at the tender age of seven took her to Germany, where she studied German in elementary school while her mom studied German at university. After this introduction to life abroad, there was no stopping Herdís. At 17, she went to Bolivia to spend a year learning the ways of the locals as an exchange student and later finished high school at Menntaskólinn í Reykjavík, specializing in ancient languages. The travel bug kept biting and she started traveling around her own fascinating country, first with friends and later with foreign tourists as their guide and cook.

This experience did more than ignite a love of hiking and the great outdoors in Herdís, it also opened her eyes to geology and the fabulous view from the geologist's workplace. All dreams of becoming an anthropologist, astrophysicist or actress were promptly discarded. Instead, she matriculated in the Department of Geology at the University of Iceland, from where she graduated with a B.S. in 2000. While at college studying geology she got an opportunity to study abroad in Svalbard, fell in love with the place and its wild-west atmosphere and spent the next three years there working as a tour guide and expedition leader. From there she headed to Ithaca, NY, to do her graduate work. Of all the things her Ph.D. adviser taught her, the most important one was how to escape the dreary late winters of upstate NY: by doing fieldwork in tropical places such as Hawai'i and the Philippines. She is currently doing a postdoc in Potsdam, Germany and looking forward to more exciting times as a geologist in far away places.

ACKNOWLEDGEMENTS

I am indebted to a large number of people for contributing in many ways, large and small, to this dissertation. I couldn't possibly name them all; for that they are too many. First among equals I want to mention my Ph.D. committee. Lou Derry, Harold van Es, Len Lion and Bryan Isacks have through the years provided me with guidance and support, for which I am very grateful.

Perhaps most importantly, this particular body of work would not have been possible without the professional, cheerful and enthusiastic support of my many field assistants. In Hawai'i these were students and staff of the Cornell Hawai'i Program, as well as Tim Huth, Christopher Hamilton and Shan Mohiuddin. The staff of various municipalities, golf courses and ranches provided access to groundwater wells. In the Philippines my biggest debt is owed to Professor Caloy Arcilla, who single-handedly made my extensive fieldwork there possible by facilitating cooperation with the University of Diliman, Quezon City. The drivers and field assistants - William Tamayo, Gerald Quina, Gerardo Sumat, Cherisse Ferrer, Engielle Mae Paguican, Margaret Grace Honrado and Maria Gracia Collantes – deserve an enormous thank-you for their hard work and enthusiasm. Not least, the large number of locals who in a kind spirit and full of curiosity assisted with sampling and discharge measurements made my stay in the Philippines even more pleasant.

Financial support from the following sources is gratefully acknowledged: NSF (SGER grant # 0738828); BEB small grants in 2006 and 2007, Cornell University Graduate School Research Travel Grant and a semester-long ConocoPhillips Fellowship. The Department of Earth and Atmospheric Sciences at Cornell provided me with TA

funding multiple times.

At Cornell, I enjoyed working with my office mates throughout the years – Chen Chen, Jacob Moore, Adam Goss and Helen Jones. My lab mates in the Derry lab – Meghan Herz, Julie Pett-Ridge, Chris Garvin, Steve Romaniello, Gregg McElwee, Kyle Trostle and Caitlyn Cox - were fun to work with and taught me the tricks of the geochemist's trade. Louise P. McGarry, Brian Ruskin, Stephanie Devlin and many other Snee students have been and still are wonderful friends. Best thanks to them for being there and helping me stay sane and happy through this all.

I was lucky to make great friends outside of Snee Hall, most notably in the Cornell Outing Club. Leslie, Simeon, Ari, Rima, Kata, Jason, Rayko, Caroline, Kara (and many more who I am forgetting), thanks for all the fun and your friendship through the years! My wonderful friend Hrönn Brynjarsdóttir is a gem and so are my fabulous friends *in absentia*, Kristín Vilhjálmisdóttir and Sif Traustadóttir back home in Reykjavík. Shan Mohiuddin and his family are great friends. All these people were always there for me, providing me with company, good cheer and any kind of support I could ask for. Takk!

Last, I want to thank my family back home in Iceland for their unconditional love and support. No matter what crazy thing I have decided to do in my life, I could always count on them to cheerfully support me and do whatever they could to help. I am lucky to have such wonderful people in my life.

TABLE OF CONTENTS

Biographical Sketch.....	iii
Acknowledgments	iv
Table of Contents	vi
List of Figures	x
List of Tables	xii
CHAPTER 1: INTRODUCTION, PREVIOUS WORK AND MAIN RESULTS.....	1
1.1. INTRODUCTION.....	1
1.2. BACKGROUND AND PREVIOUS WORK.....	3
1.2.1. The long-term carbon cycle.....	3
1.2.2. Chemistry of silicate weathering.....	7
1.2.3. Silicate weathering rates – the metrics.....	8
1.2.4. Processes controlling chemical weathering.....	9
1.3. METHODOLOGY.....	14
1.3.1. Chemical analysis and flux calculations.....	14
1.3.2. Study sites.....	15
1.3.2.1. <i>The Philippines</i>	16
1.3.2.2. <i>Hawai'i</i>	17
1.4. RESULTS AND DISCUSSION.....	18
1.5. CONCLUSIONS.....	20
References.....	21
CHAPTER 2: CHEMICAL WEATHERING, RIVER GEOCHEMISTRY AND ATMOSPHERIC CARBON FLUXES FROM VOLCANIC AND ULTRAMAFIC REGIONS ON LUZON ISLAND, THE PHILIPPINES.....	26
Abstract.....	26
2.1. INTRODUCTION.....	27
2.2. GEOLOGY AND CLIMATE.....	31
2.2.1. Zambales and Angat ophiolites	34
2.2.2. Luzon Volcanic Arc	37
2.2.3. Southern Sierra Madre	38
2.2.4. Bicol Volcanic Arc.....	39
2.2.5. Climate	40
2.3. METHODS.....	40
2.3.1. Fieldwork.....	40
2.3.2. Laboratory analyses.....	41
2.3.3. Hydrology	56
2.3.4. Uncertainty propagation in flux calculations.....	58
2.4. RESULTS AND DISCUSSION.....	60
2.4.1. Major elements	60
2.4.2. Sr isotopes	66

2.4.3. Sources of solutes	68
2.4.3.1. <i>Regional trends in sources of solutes – Atmospheric inputs</i>	74
2.4.3.2. <i>Regional trends in sources of solutes – High-temperature weathering</i>	75
2.4.3.3. <i>Regional trends in sources of solutes – Low-temperature weathering</i>	78
2.4.4. Element fluxes	79
2.5. IMPLICATIONS FOR GLOBAL CO ₂ EXPORT.....	85
2.6. CONCLUSIONS.....	89
References	91
CHAPTER 3: WATER BUDGET ANALYSIS FOR THE HAWAIIAN ISLANDS ...	99
Abstract.....	99
3.1. INTRODUCTION.....	100
3.1.1. Motivation.....	100
3.1.2. Study area.....	101
3.1.3. Geology of the Hawaiian Islands.....	104
3.1.4. Climate	106
3.2. METHODS.....	108
3.2.1. Setting up the water budget.....	108
3.2.2. Data sources, data compiling.....	109
3.2.3. Surface runoff and discharge.....	112
3.2.3.1. <i>Uncertainties in discharge modeling</i>	130
3.2.4. Groundwater recharge and SGD.....	131
3.2.4.1. <i>Uncertainties on groundwater recharge estimates</i>	134
3.3. RESULTS.....	135
3.3.1. Discharge and kriging of surface runoff.....	136
3.3.1.1. <i>Big Island of Hawai'i</i>	136
3.3.1.2. <i>Kaua'i</i>	142
3.3.1.3. <i>Unmonitored watersheds</i>	142
3.3.2. Groundwater recharge.....	148
3.3.2.1. <i>Kaua'i</i>	148
3.3.2.2. <i>Maui</i>	155
3.3.2.3. <i>Big Island of Hawai'i</i>	162
3.4. DISCUSSION AND CONCLUSIONS.....	171
References.....	173
CHAPTER 4: SURFACE AND SUBSURFACE CHEMICAL WEATHERING FLUXES FROM THE HAWAIIAN ISLANDS.....	177
Abstract.....	177
4.1. INTRODUCTION.....	178
4.1.1. Motivation and previous studies.....	178
4.1.2. Geology and climate.....	180
4.2. METHODS.....	193

4.2.1. Fieldwork.....	193
4.2.2. Chemistry.....	194
4.2.3. Atmospheric correction.....	205
4.2.3.1. <i>Cyclic salts - method</i>	206
4.2.3.2. <i>Sr-isotopes – method</i>	207
4.2.4. Hydrology.....	208
4.2.5. Geomorphology.....	208
4.3. RESULTS.....	208
4.3.1. Topography and regional division.....	217
4.3.2. Major elements.....	218
4.3.2.1. <i>Surface water</i>	218
4.3.2.2. <i>Groundwater</i>	225
4.3.3. Atmospheric inputs	226
4.3.3.1. <i>Surface water</i>	226
4.3.3.2. <i>Groundwater</i>	232
4.4. DISCUSSION.....	233
4.4.1. Processes controlling chemistry of surface water.....	233
4.4.2. Processes controlling chemistry of groundwater	237
4.4.3. Fluxes, calculation and error propagation.....	238
4.4.4. Fluxes, metrics.....	242
4.4.5. Fluxes, surface water.....	244
4.4.6. Fluxes, groundwater (subsurface).....	253
4.4.7. Magnitude of surface and subsurface fluxes.....	254
4.4.8. Groundwater and geomorphology.....	260
4.4.9. Surface water and geomorphology.....	268
4.5. CONCLUSIONS.....	272
References.....	274

CHAPTER 5: CRITICAL ASSESSMENT OF METRICS TO QUANTIFY THE IMPACT OF CHEMICAL WEATHERING ON RATES OF ATMOSPHERIC CARBON DRAWDOWN.....	279
Abstract.....	279
5.1. INTRODUCTION.....	280
5.2. BACKGROUND.....	281
5.3. DESCRIPTION OF METHODS TESTED.....	283
5.4. CASE STUDIES.....	290
5.4.1. Philippines - arc volcanics and ophiolites.....	291
5.4.2. Hawai'i and Iceland - OIB and MORB.....	294
5.4.3. New Zealand and Russia - felsic volcanics, greywacke, argillite and other mixed silicic rocks.....	294
5.4.4. The impact of lithology.....	300
5.5. RESULTS AND DISCUSSION.....	303
5.5.1. The $2\times\text{Si}$ -method of Edmond and Huh (1997).....	303
5.5.2. Weathering carbon export flux (WCEF).....	304

5.6. CONCLUSIONS.....	305
References.....	307
APPENDICES	310
Appendix 2.1	311
Table A2.1	314
Table A2.2	315
Table A2.3	316
Table A2.4	320
Table A4.1	325
Table A4.2	328

LIST OF FIGURES

Figure 1.1 Schematic of the long-term carbon cycle.....	4
Figure 2.1 Location map of the Philippines.....	29
Figure 2.2 Sampling locations on Luzon.....	32
Figure 2.3 Geological map of the study areas on Luzon.....	35
Figure 2.4 Major element composition of Philippines stream water	61
Figure 2.5 Mineral saturation of Philippines stream water.....	64
Figure 2.6 Na vs. Cl in Philippines stream water	71
Figure 2.7 Fraction of cation load in stream water derived from high-T weathering. .	76
Figure 2.8 Partitioning of elements derived from weathering in stream water.....	83
Figure 3.1 Map of rainfall on the Hawaiian Islands	102
Figure 3.2 Aquifers on Maui and the Big Island of Hawai'i.....	113
Figure 3.3 Semivariogram for runoff on Kaua'i.....	123
Figure 3.4 Location of data points in Kriging model.....	126
Figure 3.5 Kriged runoff surface for the Big Island of Hawai'i.....	137
Figure 3.6 Kriging-derived discharge vs. measured discharge on Kaua'i and the Big Island of Hawai'i.....	140
Figure 3.7 Kriged runoff surface for Kaua'i.....	143
Figure 3.8 Water budget for Maui.....	156
Figure 3.9 Water budget for the Big Island of Hawai'i.....	164
Figure 4.1 Location map of Hawai'i with atmospheric chemistry sampling sites.....	182
Figure 4.2 Shaded relief map of the Big Island of Hawai'i.....	184
Figure 4.3 Cross-sections of topography of Kohala Volcano, Mauna Kea and Mauna Loa on the Big Island of Hawai'i.....	186
Figure 4.4 Shaded relief map of Kaua'i.....	189
Figure 4.5 Cross-sections of topography of Kaua'i.....	191
Figure 4.6 Map of stream sampling sites on the Big Island of Hawai'i.....	195
Figure 4.7 Map of stream sampling sites on Kaua'i.....	197
Figure 4.8 Ternary diagram of major elements in streams and groundwater.....	220
Figure 4.9 Mineral saturation of streams and groundwater.....	223
Figure 4.10 ANOVA of sources of solutes by regions and sub-regions.....	228
Figure 4.11 Comparison of the Sr isotope and cyclic salts -methods for determining atmospheric contribution to the dissolved load.....	230
Figure 4.12 Results from weighted and un-weighted ANOVA of chemical fluxes. .	248
Figure 4.13 Chemical fluxes from the Big Island of Hawai'i and Kaua'i.....	250
Figure 4.14 Ratios of subsurface to surface chemical fluxes from the Big Island of Hawai'i and Kaua'i.....	256
Figure 4.15 Stream profiles for Waimea Canyon, Waipi'o Valley and the Hamakua- Hilo coastline, with Si-concentrations indicated for sampling sites.....	262
Figure 4.16 Correlation between landscape metrics and chemical fluxes in East	

Kaua'i, Kohala and Hamakua-Hilo.....	269
Figure 5.1 Carbon fluxes from ophiolites and volcanic regions, the Philippines.....	292
Figure 5.2 Carbon fluxes from Iceland and Hawai'i.....	295
Figure 5.3 Carbon fluxes from New Zealand and Russia.....	297
Figure 5.4 (WCEF)/WCSF and (2xSi)/WCSF vs. lithology.....	301

LIST OF TABLES

Table 2.1 Sampling locations on Luzon	42
Table 2.2 Major element chemistry of rivers on Luzon	49
Table 2.3 Sr concentration and isotopes of Luzon river water	55
Table 2.4 Cl-normalized molar ratios for solute partitioning calculations.....	70
Table 2.5 Fluxes of silicate-weathering derived solutes and atmospheric carbon from Luzon.....	81
Table 2.6 Fluxes of silicate-weathering derived solutes and atmospheric carbon from rivers globally.....	86
Table 3.1 Data sources used in this study.....	111
Table 3.2 Streams with more than 5 years of published discharge data from the USGS	117
Table 3.3 Parameters of runoff kriging models	129
Table 3.4 Arithmetic average of BF/DR on the Big Island of Hawai'i and Kaua'i.....	133
Table 3.5 Results from aggregated USGS water budgets for the Hawaiian Islands. .	136
Table 3.6 Kriging-derived discharge for unmonitored streams.....	146
Table 3.7 Water budget analysis for all aquifers on Maui.....	149
Table 3.8 Water budget analysis for all aquifers on the Big Island of Hawai'i.....	151
Table 4.1a Stream sampling locations on the Big Island of Hawai'i and on Kaua'i...199	
Table 4.1b Locations of groundwater wells used in this study.....	204
Table 4.2 Cl-normalized ratios of atmospheric deposition in Hawai'i.....	207
Table 4.3a Major element chemistry of rivers the Big Island of Hawai'i and on Kaua'i .	209
Table 4.3b Major element chemistry of groundwater in Hawai'i.....	216
Table 4.4 X/Cl-values for representative rocks in Hawai'i.....	226
Table 4.5a Total surface chemical fluxes from the Big Island of Hawai'i and Kaua'i.....	239
Table 4.5b Area-normalized surface chemical fluxes the Big Island of Hawai'i and Kaua'i.....	240
Table 4.5c Subsurface chemical fluxes from Hawai'i.....	241
Table 4.6 Ratio of subsurface to surface chemical fluxes across the Big Island of Hawai'i and Kaua'i.....	258
Table 5.1 Stoichiometry of congruent dissolution of olivine and pyroxene minerals.....	285
Table 5.2 Stoichiometry of incongruent dissolution of feldspar, amphibole and mica minerals.....	286

CHAPTER 1

INTRODUCTION, PREVIOUS WORK AND MAIN RESULTS

1.1. INTRODUCTION

Uptake of atmospheric inorganic carbon via the chemical weathering of silicate rocks is, along with burial of organic carbon, the main sink of atmospheric CO₂ over geological time. Considerable debate still surrounds the magnitude of this carbon flux from land to the oceans, as well as the mechanisms controlling these fluxes. In this dissertation, I calculate the magnitude of chemical weathering and associated fluxes of dissolved inorganic carbon (DIC) from two tropical, volcanic regions, namely the Hawaiian Islands and the Philippines. Using data from published scientific literature, I compare the result of my work to chemical flux data from other regions spanning a wide range in lithology, climate and relief, and speculate briefly on what processes or characteristics are responsible for the observed variability in chemical weathering fluxes. I also compare different methods that have been developed through the years to quantify chemical weathering, critically assessing the utility of each and making recommendations as to which should be employed by the geochemical community in its quest to understand the impact of chemical weathering of silicates on global paleotemperature and climate.

This dissertation is divided into 5 chapters, including this chapter. Chapters 2 through 5 are written as journal papers and either have been or will be submitted for

publication in peer-reviewed journals. In this introductory chapter, the chapters will be synthesized and the overarching findings of the dissertation explained.

Chapter 2, entitled "Chemical weathering, river geochemistry and atmospheric carbon fluxes from volcanic and ultramafic regions on Luzon Island, the Philippines", details the investigation of riverine chemistry and the associated chemical fluxes from volcanic and ultramafic regions on Luzon Island, the largest of the Philippine Islands. This chapter was published in *Geochimica et Cosmochimica Acta* (Schopka et al., 2011). Chapter 4 ("Surface and subsurface chemical weathering fluxes from the Hawaiian Islands") details a similar study in Hawai'i, although the scope of the Hawai'i study is larger than the one employed in the Philippines, including fluxes of chemicals dissolved in groundwater as well as in surface water. In order to adequately constrain the magnitude of water discharge on land and via groundwater on Hawai'i I conducted a separate hydrological study, described in Chapter 3 ("Water budget analysis for the Hawaiian Islands"). Finally, in Chapter 5, named "Critical assessment of metrics to quantify the impact of chemical weathering on rates of atmospheric carbon drawdown", I compare the three most common methods for calculating the flux of weathering-derived DIC.

The data produced during my work on this dissertation is presented either in the main body of the text or in appendices.

Spelling of Hawaiian place names follows the one employed in the *Atlas of Hawai'i* (Juvik and Juvik, 1998). In Hawaiian, the archipelago, the state and the island of Hawai'i are spelled the same, Hawai'i. To avoid confusion, I will use the term

“Hawai’i” when referring to the entire archipelago and “the Big Island of Hawai’i”, or simply “the Big Island”, when we discuss the island of Hawai’i.

1.2. BACKGROUND AND PREVIOUS WORK

1.2.1. The long-term carbon cycle

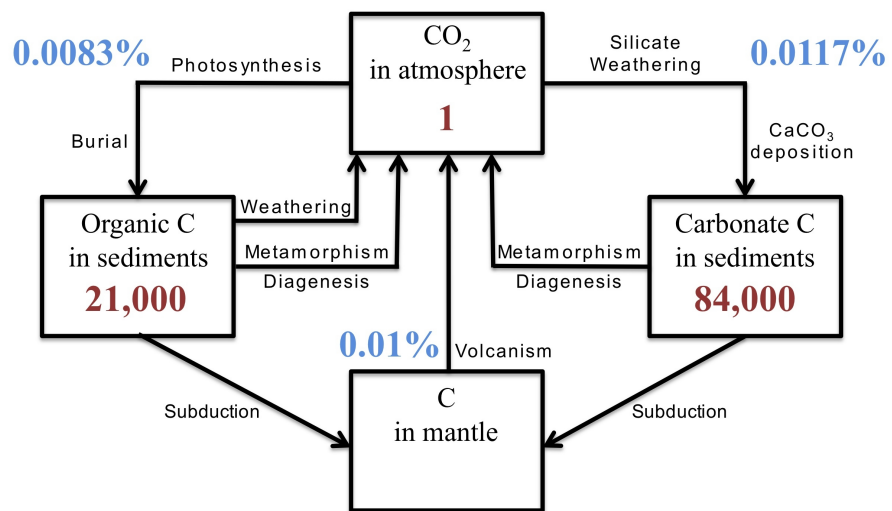
The global carbon cycle is often conceptualized as consisting of two distinct components: the short-term and the long-term cycles. The two terms refer to the rates of transfer between the five main reservoirs of carbon on Earth, namely the oceans, atmosphere, biosphere, soils and rocks (Berner, 2003). The short-term cycle is active in the surface reservoirs only (oceans, atmosphere, biosphere and soils), where organic and inorganic carbon is transferred between reservoirs at rates ranging from seconds to decades and millennia. Conversely, the long-term cycle connects the surface reservoirs to the rocks in the Earth's crust and mantle. Rates of material transfer between the surface and interior are much slower, on the order of hundreds of thousands or millions of years. In the widest sense, this dissertation investigates controls on the long-term transfer of carbon from the atmosphere into carbonate sedimentary rocks.

The time an average carbon atom spends in a reservoir (residence time, τ) is calculated by dividing the reservoir size by the transfer rate:

$$\tau = V/q \tag{1.1}$$

where V is the size (mass, volume) of the reservoir and q is the transfer rate or flux of material into or out of the reservoir. The long-term carbon cycle is shown schematically in Figure 1.1. The reservoir sizes and rates of transfer have been

Figure 1.1. Schematic of the long-term carbon cycle. Main reservoirs and pathways of exchange are shown. The sizes of reservoirs (red) have been normalized to the current inventory of CO₂ in the atmosphere. Rates of exchange (blue) have also been normalized to the current inventory of CO₂ in the atmosphere and are expressed as percentages. Rates and reservoir sizes were adapted from (Berner, 2004), image modified from Figure 1 in (Berner, 2003).



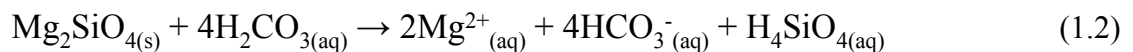
normalized to the current amount of C in the atmosphere, using data on reservoir sizes and fluxes from (Berner, 2004). Sedimentary rocks contain $\sim 100,000$ times more carbon than the atmosphere. On average, photosynthesis and exchange with the ocean turn over all carbon in the atmosphere every five years or so, so the average carbon atom has a residence time, with respect to the Earth's surface carbon reservoirs, of 5 years in the atmosphere (Schlesinger, 1997). The biosphere contains $\sim 0.8 \times$ the amount of carbon in the atmosphere (Berner, 2004) and the average residence time of carbon in the atmosphere with respect to the terrestrial biosphere is therefore approximately 12.5 years. This contrasts with the average residence time of carbon in organic sedimentary rocks: with respect to the uptake of atmospheric CO_2 by burial of organic C, τ is on the order of ~ 250 million years (Myr). Age-area relationships of the global sediment record yield a residence time of sediments of $\sim 100\text{-}300$ Myr (Wold and Hay, 1990; Wilkinson et al., 2009) and carbon isotope modeling yields a similar residence time for sedimentary organic carbon (Derry and France-Lanord, 1996).

The slow rates of transfer between the surface and rock reservoirs of carbon mean that a disruption in the rate will take a comparatively long time to impact the size of the affected reservoirs. Given their enormous size, the sedimentary reservoirs of carbon would need a long-term perturbation of rates of formation or destruction for their size to shift considerably; the magnitude of the perturbation is less significant than its duration. A small shift in the size of these reservoirs is enough, however, to cause an enormous change in the size of the small surficial carbon reservoirs. Thus, the interaction of the sedimentary and surficial carbon reservoirs is the most important determinant of the size of the atmospheric carbon pool over geological time scales,

even if photosynthesis and decomposition of young organic matter constitute the biggest fluxes of carbon out of the atmosphere and into it again.

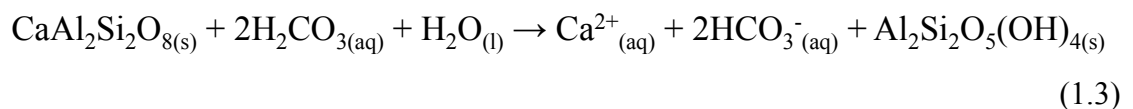
1.2.2. Chemistry of silicate weathering

Weathering of silicate rocks impacts the carbon cycle by neutralizing carbonic acid (H_2CO_3) that forms when CO_2 in the atmosphere dissolves in rainwater. As an example, let us look at the congruent dissolution of Mg-olivine, forsterite:



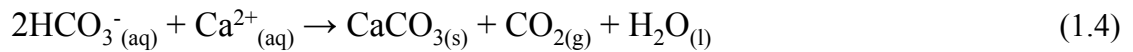
Here, the dissolution of a mole of olivine neutralizes four moles of atmospheric carbon, which is fixed in the water as bicarbonate, HCO_3^- . In addition, two moles of magnesium and one mole of silicic acid are released into solution. No solid products, such as clays, form during this reaction.

Feldspar weathers incongruently to form solutes and clays (kaolinite in this example):



One mole of Ca-feldspar mineral dissolution neutralizes two moles of atmospheric carbon upon dissolution. The ratio of silica to carbon (Si:C) in equation (1.2) is 0.25 and 1 in equation (1.3). The ratio of silica to divalent cations (Si:[divalent cation]) in the products of the reactions is 0.5 in equation (1.2) and 2 in equation (1.3), reflecting the different crystal structure and stoichiometry of the minerals in question. These ratios and their implications for the impact of weathering of different lithologies on the global carbon cycle are discussed further in Chapter 5.

The interplay between silicate weathering and the global carbon cycle is not complete until the alkaline earth metals released by silicate weathering have formed carbonates in the ocean:



Of particular importance here is the observation that to form one mole of carbonate, two moles of bicarbonate are needed. One mole of carbon goes into the carbonate mineral but the other one is degassed to the atmosphere. The implications of this will be discussed in Chapter 5.

1.2.3. Silicate weathering rates – the metrics

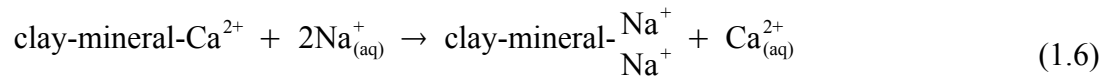
The motivation for this study is curiosity about the impact of silicate weathering on long-term changes in atmospheric CO₂ levels. The metrics used to measure this impact in the literature are varied and Chapter 5 of the dissertation is dedicated to a critical assessment of the utility of each. At this point, it is useful to define two metrics for the purposes of quantifying CO₂ fluxes from the atmosphere via silicate weathering.

The most commonly used metric for assessing the impact of silicate weathering on climate is the so-called carbon "consumption". This is simply the flux of inorganic carbon:

$$\Phi\text{CO}_2 = [\text{HCO}_3^-] \times Q \quad (1.5)$$

where Q refers to the flux of water from a given watershed or region. In Chapter 5, I propose the term **weathering carbon export flux (WCEF, ΦCO_2)** for this metric.

Another metric, introduced by France-Lanord and Derry (1997), accounts for the fact that for every mole of Ca or Mg sequestered in carbonate sediments, one mole of carbon is degassed back to the atmosphere (see equation 1.4). Furthermore, Na and K can become useful agents of carbon sequestration as they exchange for Ca in ion exchange reactions in estuaries and marine sediments (see e.g. Sayles and Mangelsdorf, 1977):



This metric therefore measures the amount of carbon that is likely to be sequestered permanently in sediments:

$$\Delta\text{CO}_2 = \Delta\text{Mg} + \Delta\text{Ca} + 0.15 \times \Delta\text{Na} + 0.1 \times \Delta\text{K} \quad (1.7)$$

where Δ refers to the flux of a given element, in molar units, from a watershed or region. In Chapter 5, I propose the term **weathering carbon sequestration flux (WCSEF, ΔCO_2)** for this metric.

1.2.4. Processes controlling chemical weathering

Many variables impact the rates of chemical weathering, such as climate (temperature, precipitation), vegetation, tectonics (i.e., rate of physical weathering) and lithology. Which of these variables exerts the greatest control over chemical weathering rates is a topic of considerable debate.

One school of thought holds that climate, mainly temperature, is the main driver of chemical weathering rates. The chemical reactions of weathering (e.g. equations 1.1 through 1.3) are temperature-sensitive, as has been verified in multiple studies, both in

the lab (Wollast, 1967; Lagache, 1976; Gislason and Eugster, 1987) and in the field (e.g. White and Blum, 1995; Dessert et al., 2003; Oliva et al., 2003). Studies have also found a correlation between runoff and chemical weathering (e.g. Oliva et al., 2003; Hren et al., 2007). Walker et al. (1981) postulated a feedback mechanism where temperature, largely set by the CO₂-content of the atmosphere, controls chemical weathering rates, partly aided by increased runoff (the saturation pressure of water in the atmosphere increases with increasing temperature, resulting in increased runoff). When temperatures are high, chemical weathering proceeds rapidly and draws CO₂ out of the atmosphere faster than it can be replenished by volcanic degassing and metamorphic decarbonation. Consequently the climate cools, leading to slower rates of chemical weathering. During periods of slow chemical weathering, CO₂ builds up in the atmosphere and eventually weathering rates increase again. This feedback mechanism has been embraced by other workers, such as Berner et al. (1983) and Berner (1992; 1994) and contested by others, e.g. Huh (2003). Importantly, (Walker et al., 1981; Berner et al., 1983; Berner, 1992; 1994) all specify that they are focusing on weathering of Ca- and Mg-silicates.

The idea that tectonics is the main driver of chemical weathering was proposed by Raymo et al. (1988), who proposed that "increasing rates of uplift and erosion in the Himalayas, Andes and Tibetan Plateau have contributed to a significant increase in the global rate of chemical weathering since the late Miocene." (p. 649). This theory was further expounded upon in an influential paper (Raymo and Ruddiman, 1992) where a sharp rise in the global ocean Sr-isotope signal was connected to the uplift of the Himalayan mountains that started around 40 Myr ago. They argued that the increased physical weathering accompanying the uplift led to increased chemical weathering

that again consumed CO₂ from the atmosphere and cooled the climate. Later work revealed that carbon sequestration by chemical weathering in the Himalaya during the Neogene (23-2.7 Myr ago) was only near the world average and not nearly high enough to explain cooler climate (France-Lanord and Derry, 1997).

Although over twenty years have passed since the debate of tectonic or climate control over chemical weathering started, no consensus has yet been reached. Some evidence suggests that both processes are important:

- Without physical erosion the weathering system runs out of fresh material to weather and chemical weathering rates are very low, even in hot and humid locations such as the Amazon and Sri Lanka (Stallard and Edmond, 1983; von Blanckenburg, 2004). This kind of system is often referred to as a transport-limited system (Stallard and Edmond, 1983).
- At very rapid rates of physical erosion, chemical weathering becomes limited by the amount of time that material spends in the weathering zone, regardless of the climate in the basin. This is often referred to as a weathering-limited system (Stallard and Edmond, 1983).
- At multiple combinations of physical erosion rates and climate, chemical weathering rates will depend on lithology (Bluth and Kump, 1994), material age (Gislason et al., 1996), vegetation (Moulton and Berner, 1998) and uplift rates (Riebe et al., 2004).
- Sediment may be eroded from a high-altitude basin with high physical erosion rates and low chemical weathering rates, transported into floodplains far

downstream and undergo extensive chemical weathering there (France-Lanord and Derry, 1997; West et al., 2002). In such cases, chemical weathering rates are largely decoupled from the physical erosion rates and climate in the original basin.

- Dessert et al. (2003) convincingly demonstrated the temperature dependence of chemical weathering rates of basalts worldwide. Their study did not include information on physical weathering rates. They concluded that basalts weather faster than all other silicate lithologies.
- Chemical weathering rates at Earth's surface may be low, even in rapidly dissolving lithologies in a warm and humid climate, if fluid residence time is short enough (Maher, 2010; Chapter 4 of this dissertation).

Numerical modeling of the interplay of chemical weathering, climate and physical weathering suggests that all these factors are indeed important. In their (2005) paper, West et al. compiled data from numerous studies of chemical weathering and physical erosion rates and "show that silicate weathering rates are not governed by any single parameter but require consideration in multiple dimensions" (p. 211). Chemical weathering rates were found to be a function of the square root of physical erosion rates. The square root dependence is purely an empirical relationship and has no obvious physical meaning. To a first approximation, chemical weathering rates are entirely dependent on physical erosion rates at low physical erosion rates, but become dependent on temperature (kinetics) and runoff at higher erosion rates.

Gabet (2007) modeled chemical weathering rates in a rapidly eroding landscape dominated by landslides that expose bedrock. He found a similar dependence of

chemical weathering rates on physical erosion as did West et al. (2005), although the relationship broke down at very high erosion rates. At very high erosion rates, the erosion regime in Gabet's (2007) model is dominated by very large landslides whose recurrence interval is too long for renewal of mineral surfaces to keep up with chemical weathering, which subsequently slows down.

A review of chemical weathering studies in large rivers (Gaillardet et al., 1999) showed that relative rates of chemical weathering (chemical weathering rates normalized to the chemical weathering rate in a reference river) in 60 large rivers correlate well with runoff and relative physical erosion rates (defined in an analogous manner). The temperature dependence of relative chemical weathering rates is clear but not very strong. Basin relief shows no correlation with chemical weathering rates at all. These results show that both climate and tectonics are an important control on chemical weathering rates of silicates, both at the continental scale (Gaillardet et al., 1999) and on intermediate- to small-catchment scale (West et al., 2005). It should be noted, however, that all the studies mentioned in this paragraph were done in continental settings where the bedrock is composed of various lithologies other than basalts. Their results may therefore not be directly transferable to weathering of basaltic terranes.

One important issue that is largely ignored in the literature, especially in physical erosion studies, is the fact that only Ca- and Mg-silicates supply the cations necessary to sequester carbon in the ocean. Na and K do contribute to carbon sequestration but they are an order of magnitude less efficient than the alkaline earth metals at doing so (France-Lanord and Derry, 1997). If the aim of the numerous studies investigating the connection between chemical weathering rates and physical erosion rates of silicates is

to find out if physical erosion rates control global climate through sequestration of carbon, they should focus on the physical erosion rates of Ca- and Mg-rich rocks, rather than the wide range of lithologies that have been studied so far. High physical erosion rates are admittedly very important for burial of organic carbon which can also have large implications for global climate. It is, however, a different process from chemical weathering of silicates.

1.3. METHODOLOGY

1.3.1. Chemical analysis and flux calculations

In order to calculate chemical weathering fluxes from watersheds, we need to know both the chemical composition and discharge of water in a given watershed. By multiplying the average annual concentration of a given element X with the discharge of water from a watershed, the flux of that element from the watershed can be established:

$$F_t = [X] \times Q \quad (1.8)$$

where $X = \{Na^+, K^+, Ca^{2+}, Mg^{2+}, Cl^-, SO_4^{2-}, HCO_3^-, Sr^{2+}\}$ and Q = average annual discharge.

Chemical analyses are generally straight-forward and the methodology is well established. A detailed description of the chemical analytical methods used in this work is presented in Chapter 2, section 3.2. On the other hand, water fluxes are poorly constrained in a large part of the regions I worked in. Because of this, the largest single source of uncertainty in my results comes from the hydrological budget. My

treatment of the hydrology of the Philippines is described in Chapter 2, section 2.3.3, and the hydrology of Hawai'i is described in Chapter 3.

Equation 1.4 gives the total weathering flux from a region or watershed. This information is of limited use because different regions/watersheds are of different sizes - it does not make sense to compare total weathering fluxes from a small creek to those from a large river. To compare watersheds/regions, we need to normalize fluxes to area:

$$F_a = F_t/A \quad (1.9)$$

The term "area" is defined, for the purposes of this dissertation, as the area of a map-view rendition of the watershed. No attempt is made to calculate the "actual" area of the watersheds by taking into account the increased surface area on slopes compared to the area of a projection onto a flat surface. Any such correction would depend on the quality (resolution, accuracy) of the digital terrain data available. This use of the term "area" is in accord with how it is traditionally employed in similar studies.

1.3.2. Study sites

I was interested in investigating the rates of chemical weathering of volcanic and ultramafic rocks in tectonically active regions in the tropics. As explained above, these are the locations where one would expect to find the highest chemical weathering fluxes in the world, due to the combination of high physical erosion rates, high temperature, wet climate and easily dissolved rock type. Hawai'i and the Philippines were chosen as the study sites.

Hawai'i is a particularly well-developed example of hotspot volcanism and the Philippines are a classic example of an island arc shaped by subduction zone volcanism. In terms of rock types, both regions are similar, although the variability in rock composition in the Philippines is considerably greater than in Hawai'i.

Geothermal near-surface occurrences are common on and around volcanoes in the Philippines. Climate is similar in the two regions, but the Philippines are in general warmer and wetter than Hawai'i and regional differences in climate are nowhere near as pronounced in the Philippines as in Hawai'i. Tectonic activity in the Philippines is arguably greater than in Hawai'i, due to the presence of various megathrusts and other features related to the four subduction zones that dip under the archipelago.

1.3.2.1. The Philippines

High-standing oceanic islands (HSIs) in the East Indies, i.e. the main Indonesian islands and Papua New Guinea, were shown to have extremely rapid rates of physical erosion (Milliman and Syvitski, 1992). The Philippines are also HSIs and rates of physical erosion in the Philippines are therefore expected to be very high. Chemical weathering is strongly dependent on mechanical erosion (Gaillardet et al., 1999). This, coupled with the finding that mafic (basalt) rocks weather faster than other silicate rocks (Dessert et al., 2003), suggests that chemical weathering in volcanic and ultramafic regions in the Philippines is very rapid. This leads to the research hypothesis of Chapter 2:

In the Philippines, there should be very high rates of chemical weathering and atmospheric CO₂ consumption.

The hypothesis was tested using water chemistry of almost 100 streams on Luzon Island. The water chemistry and results of flux calculations for the Philippines are described in detail in Chapter 2.

1.3.2.2. Hawai'i

Hawai'i does not have the extremely high physical erosion rates associated with HSI in the equatorial western Pacific. Hawai'i is quite tectonically active. A large number of small and relatively shallow earthquakes occur every year (see USGS earthquake map for Hawai'i, <http://earthquake.usgs.gov/earthquakes/states/hawaii/seismicity.php>), while large earthquakes are less common (e.g. Ando, 1979; Wyss, 1986). This does not translate into uniformly high physical erosion rates on land. Much of mass wasting in Hawai'i occurs as submarine flank collapses (Moore, 1987; Moore et al., 1989). The material transported in submarine flank collapses is only subject to chemical weathering at the Earth's surface prior to the collapse and does not contribute to chemical weathering fluxes from land post-collapse. The material may continue to weather in the ocean (e.g. Révillon et al., 2007; Jones and Gislason, 2008) but that weathering is subject to other controls than silicate weathering on land and is therefore not of immediate interest for this study.

Hawai'i is composed exclusively of mafic rocks, which weather faster than other silicic rock types (Dessert et al., 2003). Indeed, Dessert et al. (2003) remarked on the chemical weathering rates of Hawaiian streams, which seemed anomalously low in comparison with rates on for instance Reunion Island, another hotspot island in the tropics. The anomalously low chemical weathering rates in Hawai'i reported by Dessert et al. (2003) prompted my in-depth study of chemical weathering on the Big

Island of Hawai'i (the youngest island) and on Kaua'i (the oldest island). The RH was formulated around the observations that a) basalt weathers faster than other silicic rocks and b) chemical weathering must be at least locally considerably faster than reported by Dessert et al. (2003), as is evidenced by the presence of well-developed soils on substrate as young as 20 kyr (Vitousek et al., 1997). The research hypothesis for Hawai'i has the same format as the one for the Philippines:

In Hawai'i, there should be high rates of chemical weathering and atmospheric CO₂ consumption.

This hypothesis was tested in the same manner as in the Philippines - by sampling over 50 streams on the two islands and calculating the chemical weathering rate from each basin. Twelve groundwater wells on the Big Island were sampled for chemical analysis. Chemical data from five USGS groundwater wells, available at the USGS online data repository, were used. These included one well on Kaua'i and two wells each on Maui and O'ahu.

1.4. RESULTS AND DISCUSSION

Results from the Philippines show that fluxes of silicate weathering-derived bicarbonate (WCEF) from volcanic regions in Luzon are some of the highest reported worldwide. Sequestration of atmospheric CO₂ by silicate weathering (WCSF) in Luzon is also on the far upper end of values reported so far. Ophiolites contribute a significant amount of Ca- and Mg-alkalinity to the oceans, equaling the highest fluxes found in volcanic terranes.

The results from Hawai'i indicate that when only surface weathering fluxes are considered, the observations of Dessert et al. (2003) are largely valid and that chemical weathering rates in Hawai'i are anomalously low given the rock type and climate. If the flux of chemical weathering products in groundwater, which is largely discharged directly into the ocean (Chapter 4, this dissertation), is included, the chemical fluxes increase dramatically. This suggests that weathering by groundwater is an integral part of the oceanic hotspot island's weathering mechanism.

On the Big Island of Hawai'i, groundwater chemical fluxes are indeed 10-18 times higher than surface chemical weathering fluxes. This ratio diminishes to around 0.5 on Kaua'i, the oldest island. This demonstrates that groundwater is a very important component of the weathering system from the very birth of a volcano until island collapse and subsidence. Ignoring the solute flux via groundwater is therefore bound to give a thoroughly skewed image of chemical weathering fluxes from Hawai'i and, by extension, other oceanic islands.

The details of my study of Hawai'i are described in Chapter 3 (hydrology) and Chapter 4 (chemical weathering). In short, the results confirm the research hypothesis that Hawai'i has high rates of atmospheric CO₂ consumption but with a caveat: the surface chemical weathering rates are not quite as high as expected based on lithology, and the addition of groundwater solute fluxes to the overall solute flux budget is very important.

1.5. CONCLUSIONS

Work by (Marty and Tolstikhin, 1998; Taran, 2009) and many others suggests that island arcs are an important source of CO₂ to the atmosphere. This carbon comes from metamorphic decarbonation and volcanic degassing. My work in the Philippines, and a limited number of other studies (Dessert et al., 2003; 2009; Rad et al., 2006; 2007; Goldsmith et al., 2010), suggests that not only are arcs an important source of CO₂ to the atmosphere but also act as an important sink for atmospheric CO₂. At our present level of understanding, it is not clear if these two processes are in balance or not. Currently, a large fraction of island arcs on Earth is in the tropics, where large runoff and high temperatures contribute to very high chemical weathering rates. It is still largely unknown how arcs in higher latitudes (Kuril Islands, Aleutian Islands) behave (Dessert et al., 2009).

References

- Ando M. (1979) Hawaii earthquake of November 29, 1975: Low dip angle faulting due to forceful injection of magma. *Journal of Geophysical Research* **84** (B13), 7616-7626.
- Berner R.A. (1992) Weathering, plants, and the long-term carbon cycle. *Geochimica et Cosmochimica Acta* **56**, 3225-3231.
- Berner R.A. (1994) GEOCARB II: A revised model of atmospheric CO₂ over Phanerozoic time. *American Journal of Science* **294**, 56-91.
- Berner R.A. (2003) The long-term carbon cycle, fossil fuels and atmospheric composition. *Nature* **426**, 323-326.
- Berner R.A. (2004) *The Phanerozoic Carbon Cycle*. 1st ed. Oxford University Press.
- Berner R.A., Lasaga A.C. and Garrels R.M. (1983) The carbonate-silicate geochemical cycle and its effect on atmospheric carbon dioxide over the past 100 million years. *Am J Sci* **283**, 641-683.
- Bluth G.J.S. and Kump L.R. (1994) Lithologic and climatologic controls of river chemistry. *Geochimica et Cosmochimica Acta* **58**, 2341-2359.
- Derry L.A. and France-Lanord C. (1996) Neogene Growth of the Sedimentary Organic Carbon Reservoir. *Paleoceanography* **11**, 267-275.
- Dessert C., Dupre B., Gaillardet J., Francois L.M. and Allegre C.J. (2003) Basalt weathering laws and the impact of basalt weathering on the global carbon cycle. *Chemical Geology* **202**, 257-273.
- Dessert C., Gaillardet J., Dupre B., Schott J. and Pokrovsky O.S. (2009) Fluxes of high- versus low-temperature water-rock interactions in aerial volcanic areas: Example from the Kamchatka Peninsula, Russia. *Geochimica et Cosmochimica Acta* **73**, 148-169.

- France-Lanord, C. and Derry L.A. (1997) Organic carbon burial forcing of the carbon cycle from Himalayan erosion. *Nature* **390**, 65-67.
- Gabet E.J. (2007) A theoretical model coupling chemical weathering and physical erosion in landslide-dominated landscapes. *Earth and Planetary Science Letters* **264**, 259-265.
- Gaillardet J., Dupre B., Louvat P. and Allegre, C.J. (1999) Global silicate weathering and CO₂ consumption rates deduced from the chemistry of large rivers. *Chemical Geology* **159**, 3-30.
- Gislason S.R. and Eugster H.P. (1987) Meteoric Water-Basalt Interactions .1. A Laboratory Study. *Geochimica et Cosmochimica Acta* **51**, 2827-2840.
- Gislason S.R., Arnorsson S. and Armannsson H. (1996) Chemical weathering of basalt in Southwest Iceland; effects of runoff, age of rocks and vegetative/glacial cover. *American Journal of Science* **296**, 837-907.
- Goldsmith S.T., Carey A.E., Johnson B.M., Welch S.A., Lyons W.B., McDowell W.H. and Pigott J.S. (2010) Stream geochemistry, chemical weathering and CO₂ consumption potential of andesitic terrains, Dominica, Lesser Antilles. *Geochimica et Cosmochimica Acta* **74**, 85-103.
- Hren M.T., Chamberlain C.P., Hilley G.E., Blisniuk P.M. and Bookhagen B. (2007) Major ion chemistry of the Yarlung Tsangpo-Brahmaputra river: Chemical weathering, erosion, and CO₂ consumption in the southern Tibetan plateau and eastern syntaxis of the Himalaya. *Geochimica et Cosmochimica Acta* **71**, 2907-2935.
- Huh Y. (2003) Chemical weathering and climate — a global experiment: A review. *Geosciences Journal* **7**, 277-288.
- Jones M.T. and Gislason S.R. (2008) Rapid releases of metal salts and nutrients following the deposition of volcanic ash into aqueous environments. *Geochimica et Cosmochimica Acta* **72**, 3661-3680.

- Juvik, S.P. and Juvik, J.O. (1998) *Atlas of Hawaii*. 3rd ed. Honolulu, University of Hawai'i Press.
- Lagache M. (1976) New data on the kinetics of the dissolution of alkali feldspars at 200°C in CO₂ charged water. *Geochimica et Cosmochimica Acta* **40**, 157-161.
- Maher K. (2010) The dependence of chemical weathering rates on fluid residence time. *Earth and Planetary Science Letters* **294**, 101-110.
- Marty B. and Tolstikhin I.N. (1998) CO₂ fluxes from mid-ocean ridges, arcs and plumes. *Chemical Geology* **145**, 233-248.
- Milliman J.D. and Syvitski J.P.M. (1992) Geomorphic/tectonic control of sediment discharge to the ocean; the importance of small mountainous rivers. *Journal of Geology* **100**, 525-544.
- Moore J.G. (1987) Subsidence of the Hawaiian Ridge. In: *Volcanism in Hawaii*. USGS Professional Paper. Washington, DC, USGS, 85-100.
- Moore J.G., Clague D.A., Holcomb R.T., Lipman P.W., Normark W.R. and Torresan M.E. (1989) Prodigious Submarine Landslides on the Hawaiian Ridge. *Journal of Geophysical Research* **94** (B12), 17,465-17,484.
- Moulton K.L. and Berner R.A. (1998) Quantification of the effect of plants on weathering: Studies in Iceland. *Geology* **26**, 895 -898.
- Oliva P., Viers J. and Dupre B. (2003) Chemical weathering in granitic environments. *Chemical Geology* **202**, 225-256.
- Rad S., Louvat P., Gaillardet J. and Allegre C.J. (2006) Time scale of erosion in volcanic islands: relationship with chemical and physical erosion. In: *Eos Trans. AGU*.
- Rad S.D., Allegre C.J. and Louvat P. (2007) Hidden erosion on volcanic islands. *Earth and Planetary Science Letters* **262**, 109-124.

- Raymo M.E., Ruddiman W.F. and Froelich P.N. (1988) Influence of late Cenozoic mountain building on ocean geochemical cycles. *Geology* **16**, 649 -653.
- Raymo M.E. and Ruddiman W.F. (1992) Tectonic Forcing of Late Cenozoic Climate. *Nature* **359**, 117-122.
- Réveillon S., Teagle D.A.H., Boulvais P., Shafer J. and Neal C.R. (2007) Geochemical fluxes related to alteration of a subaerially exposed seamount: Nintoku seamount, ODP Leg 197, Site 1205. *Geochemistry Geophysics Geosystems* **8**, 26p.
- Riebe C.S., Kirchner J.W. and Finkel R.C. (2004) Erosional and climatic effects on long-term chemical weathering rates in granitic landscapes spanning diverse climate regimes. *Earth and Planetary Science Letters* **224**, 547-562.
- Sayles F.L. and Mangelsdorf Jr. P.C. (1977) The equilibration of clay minerals with sea water: exchange reactions. *Geochimica et Cosmochimica Acta* **41**, 951-960.
- Schlesinger W. (1997) *Biogeochemistry: An Analysis of Global Change, 2nd edition*. San Diego, Calif., Academic Press.
- Schopka H.H., Derry, L.A. and Arcilla C.A. (2011) Chemical weathering, river geochemistry and atmospheric carbon fluxes from volcanic and ultramafic regions on Luzon Island, the Philippines. *Geochimica et Cosmochimica Acta*, **75**, 978-1002.
- Stallard R.F. and Edmond J.M. (1983) Geochemistry of the Amazon .2. The Influence of Geology and Weathering Environment on the Dissolved-Load. *Journal of Geophysical Research-Oceans and Atmospheres* **88**, 9671-9688.
- Taran Y.A. (2009) Geochemistry of volcanic and hydrothermal fluids and volatile budget of the Kamchatka-Kuril subduction zone. *Geochimica et Cosmochimica Acta* **73**, 1067-1094.

- Vitousek P.M., Chadwick O.A., Crews T.E., Fownes J.H., Hendricks D.M. and Herbert D. (1997) Soil and ecosystem development across the Hawaiian Islands. *GSA Today* **7**, 1-10.
- von Blanckenburg F. (2004) Cosmogenic nuclide evidence for low weathering and denudation in the wet, tropical highlands of Sri Lanka. *Journal of Geophysical Research* **109** (F3).
- Walker J.C.G., Hays P.B. and Kasting J.F. (1981) A negative feedback mechanism for the long-term stabilization of Earth's surface temperature. *Journal of Geophysical Research* **86** (C10), 9776–9782.
- West A.J., Bickle M.J., Collins R. and Brasington J. (2002) Small-catchment perspective on Himalayan weathering fluxes. *Geology* **30**, 355-358.
- West A.J., Galy A. and Bickle, M. (2005) Tectonic and climatic controls on silicate weathering. *Earth and Planetary Science Letters* **235**, 211-228.
- White A.F. and Blum A.E. (1995) Effects of climate on chemical weathering in watersheds. *Geochimica et Cosmochimica Acta* **59**, 1729-1747.
- Wilkinson B.H., McElroy B.J., Kesler S.E., Peters S.E. and Rothman E.D. (2009) Global geologic maps are tectonic speedometers—Rates of rock cycling from area-age frequencies. *Geological Society of America Bulletin* **121**, 760 -779.
- Wold C.N. and Hay W.W. (1990) Estimating ancient sediment fluxes. *Am J Sci* **290**, 1069-1089.
- Wollast R. (1967) Kinetics of the alteration of K-feldspar in buffered solutions at low temperatures. *Geochimica et Cosmochimica Acta* **31**, 635-648.
- Wyss M. (1986) Seismic quiescence precursor to the 1983 Koaiki (MS = 6.6), Hawaii, earthquake. *Bulletin of the Seismological Society of America* **76**, 785-800.

CHAPTER 2

CHEMICAL WEATHERING, RIVER GEOCHEMISTRY AND ATMOSPHERIC CARBON FLUXES FROM VOLCANIC AND ULTRAMAFIC REGIONS ON LUZON ISLAND, THE PHILIPPINES¹

Abstract

We investigated the rates of chemical weathering of volcanic and ophiolitic rocks on Luzon Island, the Philippines. Luzon has a tropical climate and is volcanically and tectonically very active, all factors that should enhance chemical weathering. Seventy-five rivers and streams (10 draining ophiolites, 65 draining volcanic bedrock) and two volcanic hot springs were sampled and analyzed for major elements, alkalinity and ⁸⁷Sr/⁸⁶Sr. Cationic fluxes from the volcanic basins are dominated by Ca²⁺ and Mg²⁺ and dissolved silica concentrations are high (500 – 1900 μM). Silica concentrations in streams draining ophiolites are lower (400 – 900 μM), and the cationic charge is mostly Mg²⁺. The areally weighted average CO₂ export flux from our study area is $3.89 \pm 0.21 \times 10^6$ mol/km²/yr, or $5.99 \pm 0.64 \times 10^6$ mol/km²/yr from ophiolites and $3.58 \pm 0.23 \times 10^6$ mol/km²/yr from volcanic areas (uncertainty given as ± 1 standard error, s.e.). This is ~6-10 times higher than the current best estimate of areally averaged global CO₂ export by basalt chemical weathering and ~2-3 times higher than the current best estimate of CO₂ export by basalt chemical weathering in the tropics.

¹ This chapter has been published in *Geochimica et Cosmochimica Acta*: Schopka, H.H., Derry, L. and Arcilla, C. Chemical weathering, river geochemistry and atmospheric carbon fluxes from volcanic and ultramafic regions on Luzon Island, the Philippines. *Geochimica et Cosmochimica Acta* **75**, 978–1002.

Extrapolating our findings to all tropical arcs, we estimate that around one tenth of all atmospheric carbon exported via silicate weathering to the oceans annually is processed in these environments, which amount to ~1% of the global exorheic drainage area. Chemical weathering of volcanic terranes in the tropics appears to make a disproportionately large impact on the long-term carbon cycle.

2.1. INTRODUCTION

Weathering of Ca- and Mg-rich silicate rocks and burial of organic carbon are the two main mechanisms responsible for the removal of CO₂ from the atmosphere over geological timescales. These processes are counteracted by volcanic degassing of CO₂, oxidation of organic matter and decarbonation of carbonate rocks during metamorphism. Chemical weathering of silicate minerals is mediated by carbonic acid formed as atmospheric CO₂ dissolves in water (or, equivalently, by organic acids derived from soil organic matter). An example is the incongruent dissolution of anorthite, Ca-feldspar:



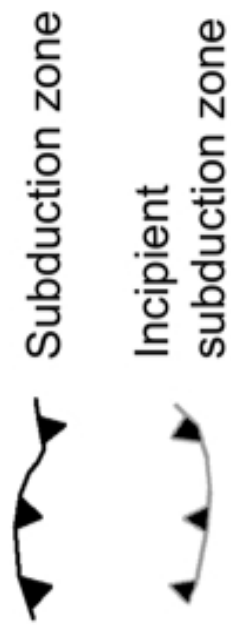
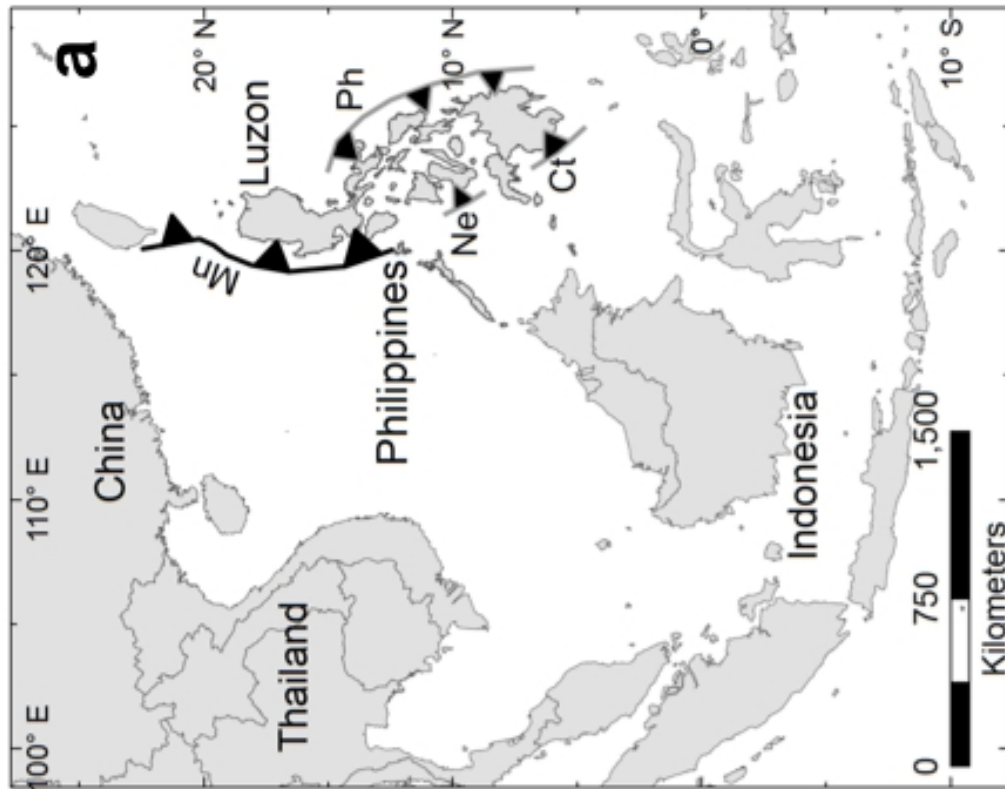
The products of the reaction are a clay mineral (kaolinite in this example), dissolved cations and bicarbonate. The bicarbonate and cations formed in the above reaction are transported to the oceans where they may precipitate as carbonates. The net result of the weathering process is the removal of carbon dioxide from the ocean-atmosphere system. The mechanisms that control weathering fluxes on large scales remain incompletely understood. Temperature, rainfall, lithology, basin relief, and erosion rate

are among the variables that have been investigated in an effort to identify the key control mechanisms on global weathering fluxes.

Meybeck (1987) showed that basalt weathers at faster rates than other silicate rocks, such as granitoids and metamorphics. Several studies have confirmed that elevated rates of atmospheric carbon consumption accompany fast weathering rates in basaltic and andesitic regions (Gislason et al., 1996; Louvat and Allegre, 1997; Dessert et al., 2003, Das et al., 2005). Gaillardet et al. (1999), in their study of the CO₂ consumption by rock weathering in the largest river basins in the world, report a correlation between rates of physical and chemical erosion. Milliman and Syvitski (1992) showed that sediment fluxes from high-standing oceanic islands (HSIs) are of the same order of magnitude as sediment fluxes from all the large rivers of the world combined, and went on to demonstrate that the HSI of the East Indies alone (comprising ~2% of global land area) contribute 20-25% of the global sediment export from land to sea (Milliman et al., 1999). These regions have abundant ultramafic to intermediate volcanic rocks, are tectonically active, experience warm and wet climate, and high erosion rates. All of these factors should act to enhance chemical weathering. Work by Lyons et al. (2005) confirmed the high chemical erosion rates associated with rapid physical erosion rates in sedimentary rocks on New Zealand and Goldsmith et al. (2008) reported very high chemical erosion rates in areas of intermediate volcanism in New Zealand. Rad et al. (2006) and Goldsmith et al. (2010) found comparably high chemical weathering rates in watersheds with intermediate lithology on various islands in the Lesser Antilles. We therefore hypothesize that chemical weathering rates, and the associated CO₂ consumption rates, in the volcanic island arcs in tropical regions of Oceania and Central America should be high.

Figure 2.1. The Philippines, adjacent land masses and locations referred to in the text.

a) Location of the Philippines in SE Asia. Subduction zones around the Philippines are modified from Schellart and Rawlinson (2010); Mn: Manila, Ne: Negros, Ct: Cotabato and Ph: Philippine Trenches. The dark box denotes the region shown in b). b), Names of regions used in text.



The Philippines (Figures 2.1a, 2.1b) is an ideal place to investigate the rates of consumption of atmospheric CO₂ by weathering processes in a volcanic arc in a young, tectonically active tropical setting. Oceanic crust is subducted under the archipelago in four different subduction zones (Schellart and Rawlinson, 2010) and earthquakes and volcanic eruptions are consequently very common. Located at between 5 and 20°N, the over 1000 islands that comprise the archipelago lie within the tropical cyclone track in the western Pacific and have an area of just under 300,000 km². The climate is hot and humid. We focused our field work on the largest island, Luzon. Since our intent was to investigate controls on chemical weathering rates of mafic and ultramafic rocks we avoided watersheds known to contain significant amounts of carbonate rocks, while including watersheds that cover the entire range of mafic and intermediate lithologies and climate found on Luzon. Several of the watersheds studied are influenced by hydrothermal activity related to volcanism; the weathering component derived from the hydrothermal activity is referred to as high-temperature, or “high-T”, weathering (Evans et al., 2001) in the following text, as opposed to low-temperature, or “low-T”, weathering proceeding at ambient temperatures.

2.2. GEOLOGY AND CLIMATE

Most of the streams and rivers studied drain the major currently active volcanic regions on Luzon; the Bataan Volcanic Arc, the Macolod Corridor and the Bicol Volcanic Arc (Figures 2.1b, 2.2 and 2.3). We also sampled streams draining older volcanic rocks in the Southern Sierra Madre and on the Bicol Peninsula, as well as streams draining ultramafic rocks (ophiolites) in Zambales and Rizal Provinces. The geology of each region is described in the following, geological maps are shown in

Figure 2.2. Sampling locations on Luzon. Thin grey lines are contour lines with 400 m interval; bold grey lines represent main rivers and streams. a) Sampling locations in the Zambales ophiolite, around Pinatubo and on the Bataan Peninsula. b) Sampling locations in Taal, the Macolod Corridor, around Laguna de Bay and in the southern Sierra Madre mountains. c) Sampling locations in the provinces of Camarines Norte and Camarines Sur. d) Sampling locations in Bicol and Sorsogon provinces.

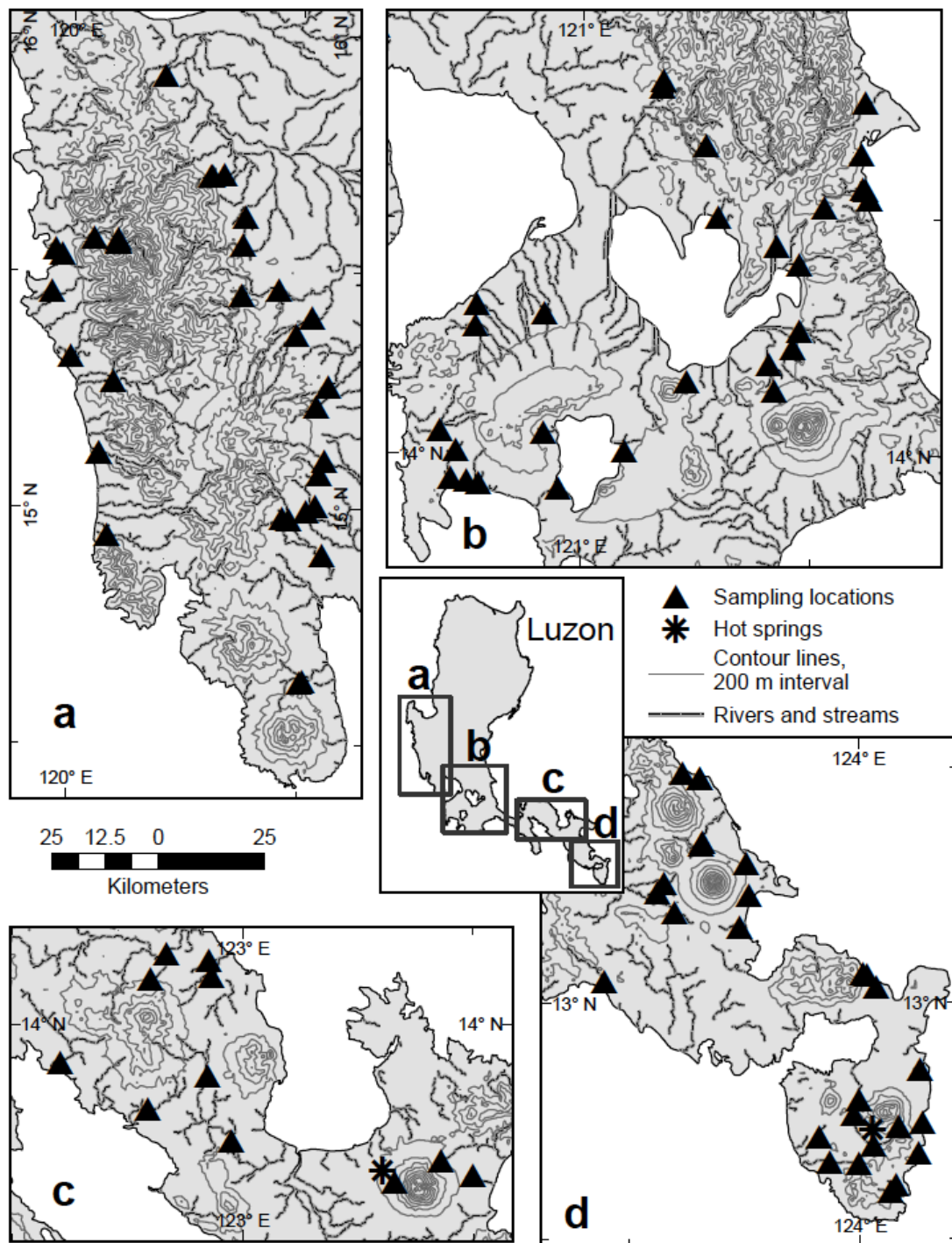


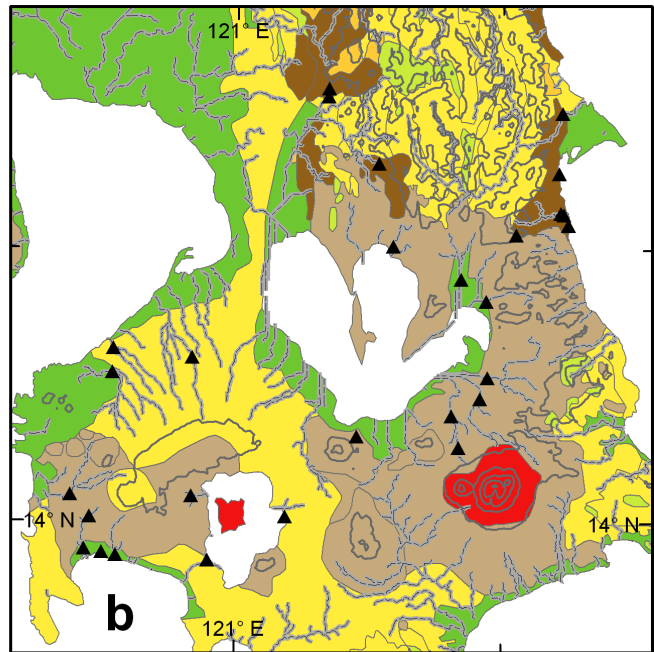
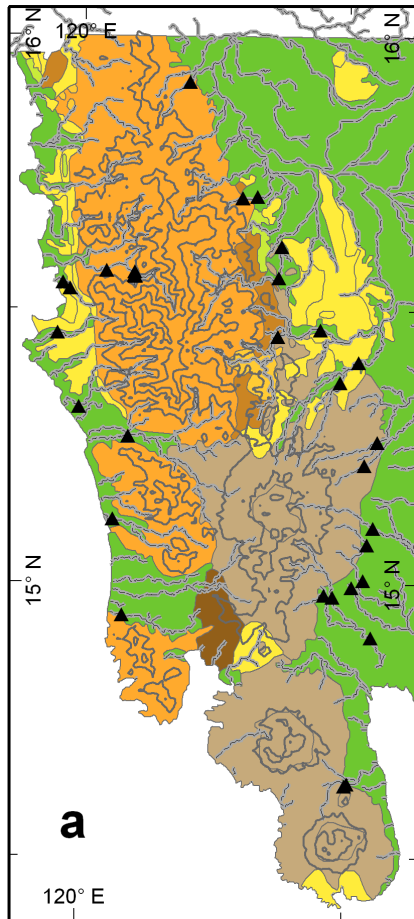
Figure 2.3, and sources are listed where they are discussed. The major element chemistry and Sr-isotope composition of representative volcanic rocks from the study area, collected from published sources, are listed in Table A2.1 and Table A2.2, respectively.

2.2.1. Zambales and Angat ophiolites

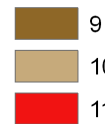
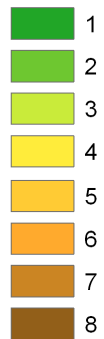
The Zambales Ophiolite (Figures 2.2a and 2.3a) is a supra-subduction-zone ophiolite (Hawkins and Evans, 1983; Evans et al., 1991; Yumul et al., 2000) NW of Manila. It comprises extensive outcrops of peridotite, dunite and gabbro, as well as diabase dike complexes. The rocks of the Zambales ophiolite are altered into various alteration assemblages, from greenschist to amphibolites (Evans et al., 1991). Evans et al. (1991) also noted that the average $^{87}\text{Sr}/^{86}\text{Sr}$ value of whole rock samples from the Zambales ophiolite (0.70451 ± 0.00084 (2σ)) are higher than expected for oceanic crust and attribute this to pervasive alteration by seawater.

The Angat Ophiolite (Figures 2.2b and 2.3b) is located NE of Manila. It is an incomplete and structurally dissected ophiolite comprised of gabbros, diabase sheeted dikes, tonalites and pillow basalts (Arcilla et al., 1989). No ultramafic rocks are exposed. All the rocks have undergone alteration up to greenschist facies and the primary minerals, especially olivine, have been largely replaced by alteration products such as chlorite and amphibole. Encarnación et al. (1993) report zircon U-Pb ages of 45-48 Ma for both the Zambales and Angat ophiolites. There are no $^{87}\text{Sr}/^{86}\text{Sr}$ data available for the Angat ophiolite but based on the similar age and degree of alteration of the Angat and Zambales ophiolites, we infer that they have similar $^{87}\text{Sr}/^{86}\text{Sr}$ values.

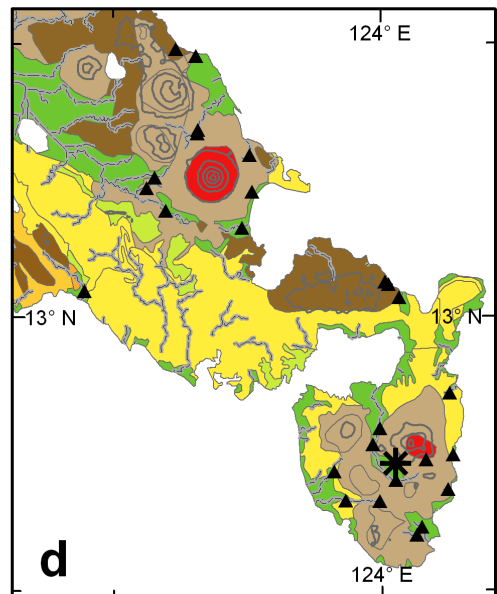
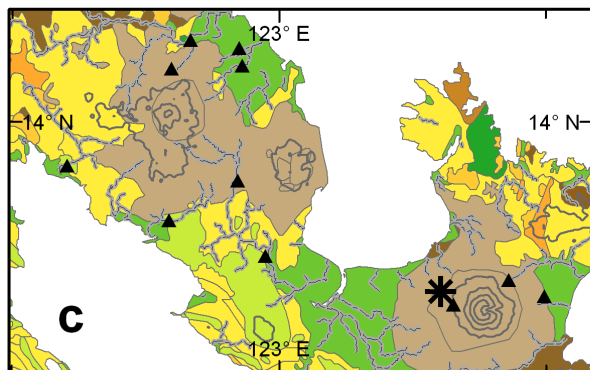
Figure 2.3. Geological map of the study areas. The division into parts a-d is the same as in Fig. 2. Legend: 1=Unknown lithology, 2=Alluvium, Recent; 3=Limestone; 4=Sedimentary and metamorphic rocks, undifferentiated; 5=Intrusive rocks, undifferentiated; 6=Ultramafic rocks; 7=Volcanics, undifferentiated; 8=Volcanics, Cretaceous-Eocene; 9=Volcanics, Miocene-Pliocene; 10=Volcanics, Pliocene-Holocene; 11=Volcanics, active. a) Geology of the Zambales ophiolite and the NW section of the LVA. b) Geology of the Macolod Corridor (SE section of the LVA and adjacent volcanoes) and the southern Sierra Madre mountains. c) Geology of Camarines Norte and Camarines Sur provinces, in the NW section of the BVA. d) Geology of Bicol and Sorsogon provinces in the SE section of the BVA. Modified from the Geological Map of the Philippines published by the Bureau of Mines (Anonymous, 1963).



Geology legend



- ▲ Sampling locations
- * Hot springs
- Contour lines, 400 m interval
- Rivers and streams



2.2.2. Luzon Volcanic Arc

Subduction of the South China Sea plate along the Manila Trench has caused volcanism along the Luzon Arc since the Miocene. This subduction zone is about 1200 km long and stretches from Taiwan through Northern and Central Luzon down to Mindoro (Defant et al., 1989). It comprises six distinct segments, namely Mindoro, Macolod Corridor, Bataan, Northern Luzon, Babuyan and Taiwan. This study included the Bataan (Figures 2.2a-b, 2.3a-b) and the Macolod Corridor (Figures 2.2b, 2.3b) segment of the Luzon Arc. The Bataan segment is an N-S trending arcuate zone that follows the western coast of Luzon from the Gulf of Lingayen south to Central Luzon. This segment gives way to the Macolod Corridor in the immediate vicinity of Lake Taal, where the volcanic trend changes to NE-SW.

Both the Bataan segment and the Macolod Corridor produce high to medium-K calc-alkaline rocks. The Bataan segment consists of two sub-parallel lines of volcanoes. The arc front volcanoes (AFV) are located closer to the shore and thus closer to the trench. Activity in the AFV has been dated at 7-0.2 Myr although volcanism continues there to the present day, most notably at Pinatubo (Pallister et al., 1992) and at Taal Volcano. Four volcanoes comprise the back arc volcanoes, formed between 1.7 to 0.1 Myr (Defant et al., 1989).

The Macolod Corridor is a 40-km wide zone of intense volcanism, comprising two calderas, several stratovolcanoes and hundreds of monogenetic volcanic edifices such as maars and scoria cones. It is interpreted as a pull-apart zone between the Manila Trench and the Philippine Fault, crossing Luzon in a NE-SW direction, perpendicular to the trend of both the remaining segments of the Luzon Volcanic Arc (LVA) and the

Bicol Volcanic Arc (Section 2.4) (Förster et al., 1990). Volcanic activity in the Macolod Corridor has migrated from the NE to the SW through time. Explosive activity commenced in the northern part ~2 Myr ago and lasted to 1.36 Myr ago, when the volcanic front started to move to the southwest. Quiescent, monogenetic volcanism dominated until ~0.5 Ma, when the volcanic front had moved to the southwestern part of the area. At that point, explosive eruptions returned and continue to the present day (Ku et al., 2009).

2.2.3. Southern Sierra Madre

The basement of the Southern Sierra Madre mountain range (Figures 2.2b, 2.3b) consists of volcanic, plutonic and sedimentary rocks, much of them metamorphosed. The sequence is believed to be a volcanic arc/back arc basin pair dating back to late Mesozoic to early Tertiary times. The basement rocks are covered with sedimentary sequences deposited in a marine shelf environment from the late Oligocene to Quaternary times, and more recent terrigenous sediments. This marine sedimentary sequence comprises extensive limestones, tuffaceous and other volcanoclastic sediments, shale, sandstone and conglomerate. Nonmarine volcanoclastic sediments make their first appearance in the Early Pleistocene and are composed mainly of tuffs and welded volcanic breccias (Bachman et al., 1983). No chemistry data or Sr isotope values are available for the rocks in this region, as far as the authors are aware. In the following discussion, streams in the Southern Sierra Madre region are grouped with streams in the LVA.

2.2.4. Bicol Volcanic Arc

The Bicol Peninsula (Figures 2.2c-d, 2.3c-d) is the southernmost extension of Luzon. About a dozen volcanic centers are found on the peninsula. Three are currently active (Mayon, Bulusan and Iriga) and three more are considered potentially active (Labo, Isarog and Malinao) (<http://www.phivolcs.dost.gov.ph/>). Streams draining all of these volcanoes, except for Iriga, were sampled. The peninsula has a basement of ultramafic and metamorphic rocks that are capped with limestone, deep marine sediments and volcanic rocks. Young carbonates and alluvium mantle the low-lying regions of the peninsula (Andal, 2002).

Current volcanism in the Bicol Volcanic Arc (BVA) is related to the subduction of the Philippine Sea Plate along the Philippine Trench under the Philippine Archipelago. The volcanic rocks on the Bicol Peninsula span the range from basalts through basaltic andesites and andesites to dacites and rhyolites. They all belong to the calc-alkaline series, except for Mt. Mayon which is unique among Bicol volcanoes in that it erupts two magma series, arc tholeiite and calc-alkaline (Andal et al., 2005 and references therein). The current subduction regime started 7 Ma ago. Volcanic rocks formed in the current subduction regime show a younging-southward trend that implies that subduction propagated towards the south (Ozawa et al., 2004). Currently, the youngest volcanic rocks in Bicol are found on and around Mt. Mayon and Mt. Bulusan, both of which have been very active in recent decades. The oldest volcanic rocks that have been identified in Bicol to date are 43 Ma and are not considered to have formed as a result of subduction along the Philippine Trench (Ozawa et al., 2004).

2.2.5. Climate

Temperatures vary very little throughout the area studied. The average annual temperature as measured at 15 weather stations distributed throughout the study area is 27.3 ± 0.8 (2σ) °C. The warmest months are April through June (27-30°C) and the coolest months are December and January (24-27°C). Variations in precipitation are considerable across the study region. The western part of the study area (from Zambales east to Taal) shows a strong seasonality in rainfall, with nearly 80% of annual rain falling from June to September and the remainder of the year being quite dry. In Quezon and on the Bicol peninsula, around 45% of the annual rainfall occurs from October through December and the remaining 55% of annual rainfall is fairly evenly distributed through the remainder of the year. The average total annual precipitation is significantly ($p = 0.03$) higher in the eastern part of the study area than in the west, or 3344 ± 1020 ($\pm 2\sigma$) mm/yr vs. 2446 ± 1704 mm/yr. Both temperature and precipitation data were extracted from the NOAA GHCN-Monthly V2 dataset, accessed at http://bonnet19.cs.qc.edu:7778/pls/rschdata/rd_start.main in February 2009.

2.3. METHODS

2.3.1. Fieldwork

We conducted stream sampling in January and February of 2007 and 2008. This corresponds with the dry period in W-Luzon and the end of the wet period in the Bicol Peninsula. Discharge data was collected in the field at the time of sampling using an FP111 Global Water flow probe. A cross-section was measured across the stream and discharge measured at regular intervals along the transect. At water depths of <20 cm,

the flow meter was moved slowly up and down through the water column for approximately one minute to get an averaged flow rate. Where the water was deeper than ~20 cm, discharge was measured at discreet intervals up the water column at each station, and the results averaged. Long-term discharge data for some of the streams was obtained from the Department of Hydraulics at the University of the Philippines, Diliman (see Chapter 2.3.3).

During sampling, pH and temperature of the water was measured *in situ* using a Beckman-Coulter portable pH/T meter. Samples were collected from a fast-flowing section of the stream into plastic syringes that were rinsed 3-4 times in the stream water prior to sample collection. The samples were hand filtered through 0.2 μm nitrate-cellulose filters into acid-washed LDPE bottles. Usually we collected 2 bottles of 125 mL each, with little to no airspace. The samples were kept in cold, dark conditions until arrival at Cornell University. Upon arrival there, one of the bottles for each sample was acidified with ultrapure HNO_3 to a pH of ~2 and all the samples were kept refrigerated.

In total, 105 samples were collected from 75 river basins and 2 hot springs. Table 2.1 shows the names and locations of the streams studied. Several rivers were sampled twice. The hot spring data were used to estimate hydrothermal inputs to streams. Four river samples are excluded from analysis. These samples show significant seawater contamination ($\text{TDS} > 1000 \text{ mg/L}$) and are labeled such in Table 2.1 and Table 2.2.

2.3.2. Laboratory analyses

For all samples collected in 2007, major cations (Na^+ , K^+ , Ca^{2+} and Mg^{2+}) were analyzed at Cornell University on a Dionex ICS-2000. Cations (Na^+ , K^+ , Ca^{2+} , Mg^{2+}

Table 2.1. Sampling locations in Luzon, 2007 and 2008

Table 2.1.

Location name	Type	Region	Sample ID	Longitude	Latitude	m a.s.l.	Basin elevation, maximum (m a.s.l.)	Basin average elevation, (m a.s.l.)	Basin relief (m)	Area (km ²)	Average annual discharge, 10 ⁶ m ³ /yr
RIVERS											
Angat Ophiolite, region ZA²											
Hanginan River	Main	ZA ²	PH-07-01	121.173	14.779	80	643	309	564	10	25
Lacotan River	Main	ZA	PH-07-02	121.174	14.794	142	773	394	644	7	19
Zambales Ophiolite, region ZA²											
Alasa River	Main	ZA	PH-08-04	119.955	15.456	14	2034	537	2026	80	203
Bancal River	Main	ZA	PH-08-03*	119.999	15.310	6	1786	631	1782	134	86
Bulsa River, us	Tributary	ZA	PH-08-62	120.450	15.465	90	1613	464	1529	295	749
Bulsa River, ds	Main	ZA	PH-07-34	120.370	15.452	123	1613	530	1493	442	1122
Mababo River	Tributary	ZA	PH-07-39, PH-07-40	120.300	15.704	136	1559	798	1428	27	68
Cabarabuan River	Main	ZA	PH-07-36	120.329	15.708	72	1559	663	1503	38	97
Camiling River, us	Tributary	ZA	PH-07-35	120.370	15.559	91	1764	773	1677	256	650
Camiling River, ds	Main	ZA	PH-08-61	120.375	15.616	45	1764	677	1724	298	757
Dumloc River	Main	ZA	PH-07-37	120.199	15.916	23	781	332	758	38	97
Lawis River, ds ¹	Tributary	ZA	PH-08-05	120.100	15.560	167	2009	1033	1847	115	292
Lawis Tributary I	Tributary	ZA	PH-08-06	120.100	15.562	157	1759	875	1600	21	53
Lawis River, ds ¹	Main	ZA	PH-07-04, PH-07-33	120.099	15.569	165	2009	999	1861	138	350
Lawis Tributary II	Main	ZA	PH-08-07	120.045	15.571	100	1149	650	1049	8	21
Masinloc River	Main	ZA	PH-07-05, PH-08-08*	119.977	15.538	14	1301	461	1288	40	101
Bicol Volcanic Arc, region Bicol											
Bulawan River	Main	Bicol	PH-07-16	123.755	13.296	95	2382	621	2289	17	36
Dobgon River	Main	Bicol	PH-08-40	123.578	13.256	87	2445	495	2358	38	80

Table 2.1. (continued)

Location name	Type	Region	Sample ID	Longitude	Latitude	m a.s.l.	Basin elevation, maximum (m a.s.l.)	Basin average elevation, (m a.s.l.)	Basin relief (m)	Area (km ²)	Average annual discharge, 10 ⁶ m ³ /yr
Guinobatan River	Main	Bicol	PH-08-38	123.599	13.195	73	2379	261	2307	65	137
Joroel River	Main	Bicol	PH-08-44	123.618	13.491	20	989	402	971	10	21
Kinastillohan River	Main	Bicol	PH-07-24	123.658	13.336	103	1242	445	1153	4	9
Naga River	Main	Bicol	PH-08-42	123.656	13.478	2	139	46	132	14	30
Naga River Tributary	Main	Bicol	PH-08-43	123.656	13.478	2	1398	492	1387	8	17
Paulog River	Main	Bicol	PH-08-21	123.563	13.237	67	1271	220	1210	29	61
Pio Duran River	Main	Bicol	PH-08-39	123.446	13.048	14	504	174	495	66	138
Quinale River	Main	Bicol	PH-08-41	123.659	13.342	64	1920	426	1860	86	180
Santo Domingo River	Main	Bicol	PH-07-19	123.760	13.229	58	2414	672	2361	8	17
Yawa River	Main	Bicol	PH-07-15	123.741	13.163	12	2406	269	2397	57	119
Bicol Volcanic Arc, region Camarines											
Daet River	Main	Camarines	PH-08-47	122.932	14.103	14	1490	302	1481	69	146
Inarihan River	Main	Camarines	PH-07-11	123.327	13.666	399	874	574	489	1.4	3
Kilbay River	Main	Camarines	PH-08-19*	122.603	13.920	6	968	168	964	331	326
Matogdon Tributary	Tributary	Camarines	PH-07-26	122.799	14.098	168	324	222	165	2	4
Matogdon River	Main	Camarines	PH-08-49	122.835	14.150	14	1329	306	1319	28	58
Pinaglabanan River	Main	Camarines	PH-08-45	123.430	13.710	166	1916	639	1750	12	26
Ragay River	Main	Camarines	PH-08-20	122.794	13.820	11	975	204	971	120	252
Rangas River	Main	Camarines	PH-07-13	123.497	13.681	69	1983	808	1919	18	38
San Vicente River	Main	Camarines	PH-08-48	122.926	14.135	10	19	13	11	1.3	3
Pulantuna River	Tributary	Camarines	PH-08-46	122.923	13.893	62	1495	306	1446	189	398
Sipocot River	Main	Camarines	PH-07-25	122.975	13.755	16	1495	199	1486	487	1025
Bicol Volcanic Arc, region Sorsogon											
Bacolod River	Main	Sorsogon	PH-08-23	123.997	12.796	25	1500	379	1483	10	22
Bacon River	Main	Sorsogon	PH-08-37	124.034	13.035	15	1030	373	1017	12	25
Bangon River	Main	Sorsogon	PH-08-30	124.075	12.615	9	624	150	619	24	50

Table 2.1. (continued)

Location name	Type	Region	Sample ID	Longitude	Latitude	m a.s.l.	Basin elevation, maximum (m a.s.l.)	Basin average elevation, (m a.s.l.)	Basin relief (m)	Area (km ²)	Average annual discharge, 10 ⁶ m ³ /yr
Barcelona River	Main	Sorsogon	PH-08-34	124.128	12.861	16	1176	148	1169	27	56
Karangan Stream	Tributary	Sorsogon	PH-07-23	124.083	12.738	282	630	423	352	1.1	2
Cadacan River, us	Tributary	Sorsogon	PH-08-27	124.027	12.701	41	1520	346	1488	34	71
Cadacan River, ds	Main	Sorsogon	PH-07-20	123.984	12.767	58	1520	212	1503	125	263
Pawa River	Main	Sorsogon	PH-08-29	124.066	12.601	14	581	187	575	26	55
San Bartolome River	Main	Sorsogon	PH-08-32	124.124	12.684	7	599	222	597	17	36
San Francisco River	Main	Sorsogon	PH-08-24	123.912	12.718	31	791	160	769	23	49
San Juan Stream	Main	Sorsogon	PH-08-35	124.014	13.059	39	908	323	875	5	10
San Juan II Stream	Main	Sorsogon	PH-08-36	124.008	13.064	91	363	235	288	0.8	2
Solinao River	Tributary	Sorsogon	PH-08-28	123.997	12.662	35	413	165	378	17	37
San Ramon (Magsaysay River)	Main	Sorsogon	PH-08-25	123.933	12.664	21	413	127	401	53	111
Unnamed waterfall	Main	Sorsogon	PH-08-33	124.134	12.748	12	109	70	97	0.2	0
Luzon Volcanic Arc, region BLM³											
Balanac River	Main	BLM	PH-08-55	121.460	14.227	12	2158	451	2147	160	337
Buso-Buso River	Main	BLM	PH-08-50	121.268	14.657	211	940	404	738	18	39
Catmon River	Tributary	BLM ³	PH-07-08	120.504	14.631	45	1038	316	1004	18	39
Diwa River	Main	BLM	PH-07-09	120.508	14.635	29	1403	379	1375	94	198
Pagsanjan River	Main	BLM	PH-07-32	121.473	14.266	35	533	325	522	207	437
Pangil River	Main	BLM	PH-08-54	121.471	14.405	9	529	348	520	53	111
San Antonio River	Main	BLM	PH-08-52	121.423	14.445	8	405	102	398	13	27
Santa Cruz River, us	Tributary	BLM	PH-07-31	121.419	14.138	196	2139	816	1953	22	47
Santa Cruz River, ds	Main	BLM	PH-08-56	121.406	14.196	46	2139	460	2095	107	226
Tanay River	Main	BLM	PH-08-51	121.296	14.505	14	648	309	637	44	92
Luzon Volcanic Arc, region Pinatubo⁴											
Bamban River	Main	Pinatubo	PH-08-65	120.560	15.261	89	1084	345	1000	88	186

Table 2.1. (continued)

Location name	Type	Region	Sample ID	Longitude	Latitude	m a.s.l.	Basin elevation, maximum (m a.s.l.)	Basin elevation, average (m a.s.l.)	Basin relief (m)	Area (km ²)	Average annual discharge, 10 ⁶ m ³ /yr
Bucao River	Main	Pinatubo	PH-07-06, PH-08-02	120.088	15.279	33	1668	419	1640	557	1173
Gumain River, us	Tributary	Pinatubo	PH-08-71	120.478	14.977	38	n.a.	n.a.	n.a.	127	268
Caulaman River	Tributary	Pinatubo	PH-08-72	120.461	14.981	42	957	320	923	49	103
Gumain River, ds	Main	Pinatubo	PH-08-74	120.569	14.917	7	1568	357	1561	255	536
Maloma River	Main	Pinatubo ⁴	PH-07-03, PH-08-01	120.062	15.117	8	1020	275	1013	153	322
Bangot River	Tributary	Pinatubo	PH-08-64	120.488	15.369	103	1464	337	1364	96	203
O'Donnell River	Main	Pinatubo	PH-08-63	120.523	15.406	87	1464	354	1381	279	587
Pasig River	Main	Pinatubo	PH-08-67	120.553	15.103	112	1457	649	1348	56	118
Porac River us	Tributary	Pinatubo	PH-08-68	120.542	15.073	75	1117	361	1046	42	89
Porac River ds	Main	Pinatubo	PH-08-73	120.535	15.008	35	1117	274	1090	120	252
Sacobia River	Main	Pinatubo	PH-08-66	120.536	15.218	147	972	396	830	33	70
Santol River	Main	Pinatubo	PH-08-70	120.513	14.994	34	214	72	184	18	39
Tabang River	Main	Pinatubo	PH-07-07	120.081	14.942	15	999	140	992	167	425
Luzon Volcanic Arc, region Quezon											
Agus River	Main	Quezon	PH-07-44, PH-08-58	121.608	14.750	47	1510	501	1501	931	1961
Balabag River	Main	Quezon	PH-07-43, PH-08-60	121.625	14.545	25	411	231	403	3	7
Kiloloram River	Main	Quezon	PH-08-57	121.607	14.640	7	295	133	291	0.5	1
Llabak River	Main	Quezon	PH-07-41	121.526	14.527	331	686	481	356	6	13
Tignoan River	Main	Quezon	PH-07-42, PH-08-59	121.610	14.567	35	1030	361	1013	87	184
Luzon Volcanic Arc, region Taal											
Obispo Stream	Tributary	Taal	PH-08-13	120.728	14.010	56	723	206	668	19	40

Table 2.1. (continued)

Location name	Type	Region	Sample ID	Longitude	Latitude	m a.s.l.	Basin elevation, maximum (m a.s.l.)	Basin average elevation, (m a.s.l.)	Basin relief (m)	Area (km ²)	Average annual discharge, 10 ⁶ m ³ /yr
Balayan River	Main	Taal	PH-08-14	120.718	13.950	14	723	126	713	82	173
Dacanlao River	Main	Taal	PH-08-17	120.778	13.939	15	766	283	755	56	118
Langgangan River	Main	Taal	PH-08-15	120.751	13.944	16	47	29	31	0.5	1
Laurel River	Main	Taal	PH-07-29	120.919	14.048	26	638	313	619	32	67
Mabacao River	Main	Taal	PH-08-11	120.770	14.273	32	665	299	643	244	514
Mangapol River	Main	Taal	PH-08-09	120.920	14.301	116	671	379	563	39	82
Naic River	Main	Taal	PH-08-10	120.771	14.317	16	664	218	651	77	162
Palico River	Main	Taal	PH-08-12	120.693	14.049	23	713	238	692	161	338
Palsara River	Main	Taal	PH-07-30	121.096	14.011	11	379	280	352	15	31
Pansipit River	Main	Taal	PH-08-18*	120.950	13.931	8	936	126	936	624	1314
Pele River	Main	Taal	PH-07-28	121.228	14.157	134	1074	516	950	2	4
HOT SPRINGS - Bicol Volcanic Arc											
Inarihan hot spring		Camarines	PH-07-12	123.321	13.671	331					
San Benon hot spring		Sorsogon	PH-07-22	124.026	12.731	53					

1: ds = downstream, us = upstream

2: ZA = Zambales and Angat

3: BLM = Bataan, Laguna and Macolod

4: Pinatubo = comprises both streams draining exclusively Pinatubo and streams draining both Pinatubo and the adjacent Zambales ophiolite

*: Sample not included in flux analysis due to possible seawater contamination

and Sr^{2+}) in samples collected in 2008, and Sr^{2+} in samples from 2007, were analyzed using a Jobin Yvon Ultima ICP-AES at Boston University. Precision in cation analyses was generally better than 6%. Anions in all samples were measured at Cornell University on a Dionex ICS-2000 ion chromatograph with a precision better than 5%. Alkalinity was measured by Gran titration, with a precision better than 2%. Dissolved Si was measured at Cornell University using the molybdate blue method (Mortlock and Froelich, 1989) with a precision better than 2%. Sr isotope values were measured using a VG 54 multicollector thermal ionization mass spectrometer (TIMS) at Cornell University with an average error of 0.01%. Repeat measurements of the NBS987 standard give $^{87}\text{Sr}/^{86}\text{Sr}$ of 0.71025 ± 0.00001 . Repeat analyses of the M178 standard from the USGS indicate that the accuracy of our methods is better than 6% for anions, 5% for cations (9% for Na) and 3% for Si. Major element data are presented in Table 2.2 and Sr isotope data in Table 2.3.

In nine out of every ten samples collected in 2007 the normalized inorganic charge balance or NICB $((\text{TZ}^+ - \text{TZ}^-)/(\text{TZ}^+) * 100)$ ranges between -10% and 10%. In samples collected in 2008, NICB is lower than -20% in 16% of cases and -20% - -10% in 41% of cases. It is not clear what causes the large NICB in the 2008 sample batch; 1) both the elemental analysis and alkalinity titrations were repeated in an effort to identify sources of error, 2) the samples from 2008 are from either from the same streams as the 2007 samples or from streams that are very similar to the 2007 streams in terms of watershed characteristics, and 3) the samples from the two different field campaigns received the same post-collection treatment. Our best guess is that this discrepancy is linked to the different instruments used to analyze cations, i.e. that the ICP-OES systematically yields low values relative to the ion chromatograph. Systematic differences between calculated and titrated alkalinity in river waters have also been

Table 2.2. Major element chemistry of Luzon rivers, 2007 and 2008

Table 2.2.

sample ID	Date	Q at		T	pH	F	Cl	SO ₄	NO ₃	µmol/L				µeq/L				TDS ²
		sampling	m ³ /sec							Na	K	Ca	Si	Alk	Alk type ¹	ppm		
																	°C	
PH-07-01	1/11/07	0.3	29.0	8.23	4	201	98	n.d.	478	3	559	769	724	2610	a	275		
PH-07-02	1/11/07	0.3	26.1	7.71	2	31	64	n.d.	284	3	610	702	802	2724	a	271		
PH-07-03	1/12/07	0.9	30.4	8.13	4	61	111	n.d.	330	45	963	321	912	2574	a	270		
PH-07-04	1/13/07	4.6	23.2	8.31	n.d. ⁵	30	23	3	62	2	769	94	434	1523	a	146		
PH-07-05	1/13/07	0.7	29.9	7.65	n.d.	39	44	2	114	6	999	277	614	2542	b	236		
PH-07-06	1/13/07	2.5	29.0	8.34	11	337	2196	n.d.	1499	104	1043	1861	928	2544	a	573		
PH-07-07	1/14/07	2.2	25.8	8.06	5	211	895	n.d.	693	98	684	666	1220	1389	a	315		
PH-07-08	1/14/07	0.8	27.4	7.36	3	77	32	n.d.	306	37	229	336	951	1275	a	168		
PH-07-09	1/14/07	1.5	27.2	7.47	3	123	90	9	437	58	222	377	989	1334	a	187		
PH-07-11	1/17/07	1.3	22.1	7.58	2	66	14	n.d.	263	64	47	154	1027	629	a	120		
PH-07-12 ³	1/17/07		36.8	6.13	13	756	4761	n.d.	5400	395	4129	3566	2215	10755	a	1657		
PH-07-13	1/17/07	0.8	30.5	5.14	8	115	2025	7	375	57	235	1592	919	13	a	336		
PH-07-15	1/18/07	2.8	30.3	7.80	13	521	1355	30	1609	156	1275	924	1055	2795	a	496		
PH-07-16	1/18/07	2.8	26.4	7.91	12	109	75	n.d.	424	84	152	324	1118	1191	a	181		
PH-07-19	1/18/07	0.8	25.7	7.62	13	112	88	11	557	98	216	392	1202	1521	a	216		
PH-07-20	1/19/07	40.4	27.9	7.04	8	527	624	18	1041	123	751	795	1340	2403	a	386		
PH-07-22 ³	1/19/07		43.4	6.46	18	2238	3260	23	4669	266	3610	2305	2203	7792	a	1300		
PH-07-23	1/19/07	1.4	23.2	7.51	23	141	124	2	313	49	98	282	997	705	a	143		
PH-07-24	1/20/07	0.7	28.1	7.92	9	102	43	18	403	98	140	311	991	1177	a	170		
PH-07-25	1/20/07	56.0	27.9	7.48	3	146	34	n.d.	291	30	176	374	468	1196	a	137		
PH-07-26	1/21/07	0.1	24.6	6.87	n.d.	106	22	4	265	40	77	127	717	557	a	98		
PH-07-28	1/30/07	0.0	22.2	7.95	9	147	147	19	343	82	153	252	1192	849	a	169		
PH-07-29	1/30/07	0.5	27.1	8.12	27	166	241	82	999	242	521	794	1545	3035	a	390		
PH-07-30	1/30/07	0.1	26.1	8.15	17	172	197	136	1637	376	737	1348	1257	5477	a	568		
PH-07-31	1/31/07	2.6	23.1	7.60	9	85	41	99	344	103	192	241	1154	1025	a	172		
PH-07-32	1/31/07	2.1	22.9	7.40	5	115	27	3	294	47	153	298	626	1043	a	133		

Table 2.2. (continued)

sample ID	Date	Q at sampling m ³ /sec	T °C	pH	F	Cl	SO ₄	NO ₃	Na	K	Mg	Ca	Si	Alk		TDS ² ppm
														Alk µeq/L	Alk type ¹	
PH-07-33	1/29/07		23.2	8.69	n.d.	39	31	4	55	2	833	63	390	1665	a	154
PH-07-34	2/1/07	2.5	27.5	8.60	3	41	118	n.d.	358	10	612	500	632	2340	a	237
PH-07-35	2/2/07	1.2	23.0	8.20	n.d.	33	51	n.d.	213	5	842	460	603	2669	a	249
PH-07-36	2/2/07	0.2	24.6	8.30	4	40	57	n.d.	203	7	792	546	552	2737	a	253
PH-07-37	2/2/07	0.1	29.9	7.80	n.d.	50	73	10	294	5	1000	698	885	3445	a	332
PH-07-39	3/5/07			8.40	n.d.	29	43	2	206	4	837	589	605	2887	a	267
PH-07-40	3/5/07			8.56	n.d.	23	43	n.d.	191	3	842	581	614	2906	a	267
PH-07-41	3/11/07	0.8	24.0	7.50	n.d.	108	16	9	215	23	106	150	495	572	a	85
PH-07-42	3/11/07	3.3	27.0	8.20	n.d.	133	34	2	320	10	264	469	655	1576	a	177
PH-07-43	3/11/07	0.4	26.0	7.90	3	148	50	2	355	19	180	508	691	1489	a	176
PH-07-44	3/11/07	0.8	28.0	7.40	2	129	28	2	252	7	165	327	488	1021	a	122
PH-08-01	1/24/08	1.5	35.6	8.07	n.d.	67	154	0	264	53	871	345	908	2395	a	261
PH-08-02	1/24/08		31.0	8.18	12	577	2966	0	2235	145	1075	2033	1006	2515	a	685
PH-08-03 ⁴	1/24/08		30.6	7.87	11	136752	7126	n.d.	98199	3276	14062	2457	555	-16717	b	7390
PH-08-04	1/24/08		28.7	7.68	n.d.	2318	158	5	911	36	804	222	465	355	b	198
PH-08-05	1/25/08	3.7	23.3	8.10	0	36	28	3	61	0	708	100	415	1612	a	150
PH-08-06	1/25/08	0.4	23.6	8.13	n.d.	41	33	2	51	0	850	44	421	1790	a	163
PH-08-07	1/25/08	0.1	24.9	8.03	0	38	32	n.d.	55	0	1291	53	729	2814	a	255
PH-08-08 ⁴	1/25/08		32.1	7.76	4	20185	1092	n.d.	13874	482	2885	648	625	-982	b	1234
PH-08-09	1/26/08	0.7	25.3	7.97	13	701	264	210	1267	190	454	671	1672	2209	b	375
PH-08-10	1/26/08		26.8	7.96	15	330	152	189	1236	281	551	770	1324	3338	a	408
PH-08-11	1/26/08	2.5	26.1	7.98	13	149	113	81	703	159	401	639	1597	2733	a	343
PH-08-12	1/26/08		27.5	7.79	14	156	140	54	678	153	406	690	1577	2779	a	347
PH-08-13	1/26/08	0.3	28.5	6.77	17	154	202	245	632	178	426	641	1906	2371	a	358
PH-08-14	1/26/08		30.1	6.75	17	212	228	n.d.	805	232	511	823	1818	3267	a	411
PH-08-15	1/27/08	0.0	26.1	7.00	25	265	493	354	989	264	643	1067	1646	3325	a	473

Table 2.2. (continued)

sample ID	Date	Q at sampling m ³ /sec	T °C	pH	F	Cl	SO ₄	NO ₃	Na	K	Mg	Ca	Si	Alk		
														Alk	Alk	TDS ²
														µmol/L	µeq/L	ppm
PH-08-17	1/27/08	0.3	26.9	7.13	20	280	227	137	929	209	562	812	1727	3124	a	411
PH-08-18 ⁴	1/27/08		27.1	8.33	30	11122	1089	n.d.	9989	850	1370	1044	34	2300	b	982
PH-08-19 ⁴	1/30/08		28.9	7.44	n.d.	26234	1449	n.d.	19104	787	2932	709	549	850	a	1727
PH-08-20	1/30/08		29.0	7.47	4	190	37	0	318	56	172	406	913	1401	a	181
PH-08-21	1/31/08	0.4	29.3	7.45	18	222	238	45	629	127	343	498	1315	1676	b	263
PH-08-23	1/31/08	0.4	26.1	6.59	5	321	278	0	592	84	340	627	1559	1949	a	301
PH-08-24	1/31/08	0.7	29.3	6.77	4	187	53	0	354	77	169	236	1434	939	b	180
PH-08-25	1/31/08	1.2	28.6	6.46	3	182	112	n.d.	407	71	162	247	1272	885	b	174
PH-08-27	2/1/08		25.9	7.25	8	499	494	7	609	98	539	558	1299	1398	b	282
PH-08-28	2/1/08	0.5	25.9	7.02	n.d.	142	64	0	359	50	134	195	1015	856	a	146
PH-08-29	2/1/08	0.9	26.0	6.56	4	234	211	0	300	40	138	200	731	357	b	114
PH-08-30	2/1/08		26.0	6.56	n.d.	1207	79	n.d.	941	58	245	206	803	535	b	169
PH-08-32	2/1/08		25.8	7.60	n.d.	173	25	n.d.	292	38	168	252	902	941	b	143
PH-08-33	2/1/08	0.0	24.3	7.16	17	183	85	12	282	52	64	178	923	432	b	115
PH-08-34	2/1/08	3.2	26.3	7.85	n.d.	148	47	n.d.	319	64	146	189	1231	810	b	154
PH-08-35	2/2/08	0.2	25.7	7.96	n.d.	144	35	0	307	41	130	307	1184	1002	b	165
PH-08-36	2/2/08	0.2	24.9	8.11	n.d.	137	26	0	281	39	108	282	1161	908	b	154
PH-08-37	2/2/08	0.4	28.0	7.67	n.d.	184	78	n.d.	344	49	233	423	1003	1365	b	190
PH-08-38	2/2/08		29.7	7.75	17	365	369	48	665	105	586	1156	1174	3461	a	414
PH-08-39	2/2/08	0.8	29.3	8.15	n.d.	140	238	0	432	31	1155	1235	667	4717	a	444
PH-08-40	2/3/08	1.3	24.8	8.12	13	117	58	0	363	84	193	306	1250	1191	b	186
PH-08-41	2/3/08	12.4	24.8	8.06	n.d.	92	47	8	273	65	157	251	1162	959	b	159
PH-08-42	2/3/08	3.3	27.4	7.23	n.d.	199	162	6	282	64	128	221	921	513	b	131
PH-08-43	2/3/08	0.6	27.7	7.40	5	211	346	0	280	56	122	288	800	245	b	127
PH-08-44	2/3/08	2.4	26.3	8.11	n.d.	100	76	2	197	44	117	197	789	612	b	113
PH-08-45	2/3/08	2.2	26.0	6.85	n.d.	193	759	n.d.	452	62	216	363	1074	123	a	189

Table 2.2. (continued)

sample ID	Date	Q at sampling m ³ /sec	T °C	pH	F	Cl	SO ₄	NO ₃	Alk						TDS ² ppm		
									Na	K	Mg	Ca	Si	Alk		Alk	Alk
									µmol/L							µeq/L	
PH-08-46	2/4/08	1.4	25.7	7.52	n.d.	136	25	n.d.	176	28	93	117	466	438	b	74	
PH-08-47	2/4/08	8.9	26.2	7.64	n.d.	130	26	n.d.	202	37	100	153	728	559	b	100	
PH-08-48	2/4/08		28.0	7.05	n.d.	187	23	9	257	54	96	179	826	619	b	114	
PH-08-49	2/4/08		27.9	7.53	n.d.	128	38	n.d.	259	47	123	199	894	835	a	132	
PH-08-50	2/7/08	0.2	23.9	8.33	7	61	141	n.d.	451	10	436	763	811	2508	b	270	
PH-08-51	2/7/08	0.2	27.1	8.12	6	83	105	27	229	40	271	1552	515	3954	a	363	
PH-08-52	2/7/08	0.8	27.1	7.45	7	307	76	78	471	52	305	469	803	1528	b	204	
PH-08-54	2/7/08	0.9	25.7	8.09	3	128	25	n.d.	252	60	167	213	788	981	a	135	
PH-08-55	2/7/08	8.1	26.4	8.60	5	302	42	24	344	87	293	258	1085	1106	b	178	
PH-08-56	2/7/08		26.3	8.23	9	373	64	75	434	108	389	331	1320	1379	b	225	
PH-08-57	2/8/08	1.2	23.6	7.86	n.d.	141	35	0	243	9	241	431	722	1385	b	165	
PH-08-58	2/8/08		24.0	7.72	3	92	56	0	203	11	197	657	533	1716	b	182	
PH-08-59	2/8/08	5.7	24.2	8.22	3	131	39	0	233	9	259	442	765	1430	b	171	
PH-08-60	2/8/08	0.3	24.0	8.32	3	267	56	0	270	16	179	480	819	1220	b	169	
PH-08-61	2/9/08	2.2	27.7	8.61	3	91	81	0	222	7	933	488	612	3009	a	279	
PH-08-62	2/9/08	3.6	29.7	8.40	12	71	128	27	308	13	696	486	712	2594	a	262	
PH-08-63	2/9/08	1.7	30.7	8.17	14	4926	3286	6	1720	181	884	2549	1097	2073	b	854	
PH-08-64	2/9/08	0.4	28.2	8.18	n.d.	117	526	0	581	95	431	845	1129	2047	b	309	
PH-08-65	2/9/08	0.9	28.8	7.96	n.d.	756	798	n.d.	1115	99	538	1233	1339	2837	a	450	
PH-08-66	2/10/08	0.3	28.0	8.24	21	766	4712	n.d.	2447	235	848	3621	1369	1830	a	906	
PH-08-67	2/10/08	0.5	29.3	7.99	15	1832	4486	0	3249	291	1107	3220	1237	1691	a	916	
PH-08-68	2/10/08	1.1	29.6	7.95	n.d.	775	2820	71	1675	203	990	1927	1481	1398	a	625	
PH-08-70	2/10/08	0.0	33.7	7.41	n.d.	244	336	113	666	167	295	481	1297	1349	b	257	
PH-08-71	2/10/08	2.0	29.0	8.29	n.d.	1321	612	0	1389	94	440	894	876	2005	a	363	
PH-08-72	2/10/08	0.2	30.0	7.63	n.d.	66	143	n.d.	414	77	265	455	1158	1574	b	219	
PH-08-73	2/10/08	1.9	31.2	7.47	n.d.	579	1963	35	1304	192	765	1495	1437	1810	a	524	

Table 2.2. (continued)

sample ID	Date	Q at sampling	T	pH	F	Cl	SO ₄	NO ₃	Na	K	Mg	Ca	Si	Alk		
														Alk type ¹	TDS ²	
														μeq/L	ppm	
PH-08-74	2/10/08	0.3	29.6	8.22	n.d.	1239	1109	n.d.	1556	146	719	1507	913	3027	a	510
MI78	n.a.	n.a.	n.a.	-	14	1768	1938	27	36	6	19	51	242	5463	b	603

1: a = determined by Gran titration, b = determined by charge balance

2: TDS = Na + K + Ca + Mg + F + Cl + SO₄ + Br + NO₃ + PO₄ + HCO₃ + SiO₂

3: Hot spring

4: Sample not included in flux analysis due to possible seawater contamination

5: n.d. = not detected

Table 2.3. Sr concentration and isotopes of Luzon rivers, 2007 and 2008

Sample ID	Sr	$^{87}\text{Sr}/^{86}\text{Sr}$	$\pm (2\sigma)$
	nmol/L		
PH-07-01	438	0.70441	0.00012
PH-07-02	436	0.70335	0.00008
PH-07-03	808	0.70469	0.00010
PH-07-05	911	0.70802	0.00008
PH-07-06	3760	0.70421	0.00012
PH-07-07	2093	0.70438	0.00010
PH-07-08	892	0.70446	0.00008
PH-07-09	1278	0.70449	0.00010
PH-07-12 ¹	6760	0.70364	0.00008
PH-07-13	4053	0.70359	0.00007
PH-07-15	2742	0.70394	0.00007
PH-07-16	1221	0.70379	0.00007
PH-07-19	1337	0.70380	0.00007
PH-07-20	2031	0.70402	0.00008
PH-07-22 ¹	3895	0.70396	0.00007
PH-07-25	1953	0.70639	0.00010
PH-07-26	927	0.70384	0.00008
PH-07-28	872	0.70432	0.00007
PH-07-29	914	0.70394	0.00008
PH-07-30	1452	0.70382	0.00007
PH-07-31	1186	0.70465	0.00007
PH-07-32	1058	0.70479	0.00008
PH-07-33	137	0.70383	0.00012
PH-07-34	600	0.70433	0.00008
PH-07-35	423	0.70394	0.00008
PH-07-36	467	0.70381	0.00012
PH-07-37	469	0.70433	0.00008
PH-07-39	464	0.70383	0.00012
PH-07-40	462	0.70377	0.00012

Table 2.3. (continued)

Sample ID	Sr	$^{87}\text{Sr}/^{86}\text{Sr}$	$\pm (2\sigma)$
	nmol/L		
PH-07-41	691	0.70430	0.00008
PH-07-42	637	0.70438	0.00007
PH-07-43	552	0.70480	0.00008
PH-07-44	350	0.70418	0.00007
PH-08-01	747	0.70451	0.00010
PH-08-03 ²	19732	0.70904	0.00010
PH-08-06	61	0.70488	0.00012
PH-08-07	72	0.70527	0.00012
PH-08-08 ²	3586	0.70890	0.00015
PH-08-09	1162	0.70491	0.00007
PH-08-10	1706	0.70494	0.00007
PH-08-11	1192	0.70467	0.00038
PH-08-12	1319	0.70512	0.00015
PH-08-13	1019	0.70520	0.00007
PH-08-15	1413	0.70485	0.00007
PH-08-17	1135	0.70504	0.00007
PH-08-18 ²	1614	0.70552	0.00022
PH-08-21	1504	0.70382	0.00010
PH-08-23	1459	0.70399	0.00009
PH-08-24	947	0.70414	0.00015
PH-08-27	1482	0.70412	0.00008
PH-08-28	903	0.70439	0.00010
PH-08-30	1157	0.70481	0.00008
PH-08-41	1112	0.70380	0.00008
PH-08-45	1383	0.70359	0.00013
PH-08-54	836	0.70435	0.00007
PH-08-58	769	0.70593	0.00008
PH-08-68	5782	0.70421	0.00008
M178	389	-	-

1: Hot spring

2: Possible seawater contamination

reported by Wolff-Boenisch et al. (2009). For the majority of our samples we used the Gran alkalinity values in flux calculations (see Table 2.2). In samples from 2008 where $\text{NICB} < -10\%$ (i.e., in samples where satisfactory charge balance was not achieved using the Gran alkalinity for HCO_3^-) we used the calculated alkalinity for HCO_3^- instead. The sole exception was sample PH-08-63 where the calculated alkalinity was negative.

2.3.3. Hydrology

Calculations of chemical fluxes are strongly dependent on hydrological data such as river discharge. Historical and/or recent discharge data are available for a number of rivers in the regions under study here ($n = 55$, see below). Nevertheless, no discharge data are available for most of the rivers that we sampled ($n = 54$, or 72% of the streams sampled). A common strategy to estimate river discharge in studies comparable to ours, where the focus is on chemistry rather than on hydrology and where hydrology data is sparse, is to use the average reported runoff (discharge normalized to watershed area) for a region to calculate discharge of individual streams. We sought to improve predicted runoff by using spatial statistics on simple landscape metrics. We used a 90-m resolution digital elevation model (DEM) obtained from CGIAR-CSI (<http://srtm.csi.cgiar.org/>) to define watersheds for the streams and rivers studied and to calculate their area. This dataset is based on the finished-grade 3 arc-second NASA SRTM data. SRTM data suffer from data voids, especially over water bodies and in mountainous areas, and the CGIAR-CSI dataset has been processed to fill those data voids using auxiliary data (Reuter et al., 2007). The CGIAR DEM was processed in ArcGIS 9.3 and ArcINFO (ESRI, 2009). Sinks in the DEM were identified and filled with ArcGIS Spatial Analyst functions. Watersheds

were created for all rivers and streams sampled, as well as for all rivers for which historical runoff data is available.

The runoff data used was collected by the National Water Resources Council (NWRC) of the Philippines and made accessible to us by Professor Glenn Tabios at the Department of Hydraulics at the University of the Philippines, Diliman. The NRWC divides the Philippines into 10 water resources regions (WR); the ones we worked in are WR 3 (Central Luzon), WR 4 (Southern Tagalog) and WR 5 (Bicol). We used two data sets, one from 1944-1970 and another from 1982-2000 (only a few streams were monitored for the entire period). The average duration of data collection for the streams we used was 10 years for streams draining ophiolites and 12 years for streams draining volcanic areas, with minimum of 6 and 2 years and maximum of 14 and 24 years, respectively. The data do not contain any estimates of uncertainty for individual discharge measurements. Most of the rivers and streams have approximately normally distributed yearly discharge, allowing us to use arithmetic average and standard deviation to assess uncertainty in the dataset.

Simple *t*-tests, performed using the JMP 8.0 software package (SAS, 2009), reveal no significant differences between average runoff by geographic region or lithology. The variation in runoff (coefficient of variation (CV , %) = standard deviation/mean \times 100%) in ophiolitic regions is significantly less ($CV = 25\%$), than in volcanic regions ($CV = 47\%$). We cannot tell if the difference in CV between lithologies is caused by variations in data availability and duration of records or if it is caused by variability in climate in the different regions. The spatial distribution of the mean runoff was investigated using ArcGIS 9.3 software (ESRI, 2009). No spatial trends in average runoff were detected, rendering spatial interpolation methods such as Kriging or

nearest neighbor interpolation inappropriate for predicting runoff in unmonitored basins.

Multiple linear regression was performed on the calculated average runoff for each basin using JMP 8.0. The predictors we used were landscape metrics that are readily available for each basin, namely the average, minimum, maximum and standard deviation of each of the following; elevation, slope and aspect. Individually, any of these variables have very little predictive potential for mean runoff ($r^2 = 0 - 0.4$). Multiple linear regression models of average runoff yielded better r^2 for several combinations of independent variables (r^2 of modeled vs. observed runoff > 0.98), but cross-correlation between variables and unrealistic model parameters indicate that the good fit is artificial. In short, the results of statistical treatment of the runoff data indicate that none of the potential predictor variables we tested have any real predictive potential.

We therefore use the regionally averaged observed runoff to calculate discharge in unmonitored watersheds. We distinguish between watersheds in ophiolitic and volcanic regions, using the average runoff (2539 mm/yr and 2106 mm/yr, respectively) for unmonitored streams. Several of the streams we studied drain a mix of ophiolitic and volcanic bedrock. For these streams, we use the statistics for rivers draining volcanic regions.

2.3.4 Uncertainty propagation in flux calculations

Uncertainty in chemical analyses, watershed area and stream discharge were propagated through flux calculations according to the methods presented in Bevington and Robinson (2002).

Chemical fluxes of a given element, X , from a watershed, i , are calculated as the concentration of that element, $[X]$, multiplied by the discharge, Q , through the watershed, Q_i : $[X] \times Q_i$. Q_i is the product of runoff through the watershed and the area of the watershed, A_i . Uncertainties in the area of watersheds are taken from Oksanen and Sarjakoski (2005). Their study utilized DEMs with a cell size of 10m, and we apply their results unchanged to the 90m-resolution DEM used in our study. According to Oksanen and Sarjakoski (2005), CV is 24% in watersheds smaller than 2 km², 16% in watersheds between 2 and 22 km² and less than 3% in watersheds larger than 22 km².

The CV for total (t) chemical fluxes (F) in a single watershed i , (Ft,i), is calculated as:

$$CV_{Ft,i} = \sqrt{CV_{[X]}^2 + CV_{Q_i}^2} \quad (2.2)$$

In the case of area-normalized (a) fluxes (F) through a single watershed i , (Fa,i), the equation becomes:

$$CV_{Fa,i} = \sqrt{CV_{Ft,i}^2 + CV_{A_i}^2} \quad (2.3)$$

Watersheds are aggregated into regions. The CV for the total chemical fluxes from a region j , (Ft,j), is calculated as:

$$CV_{Ft,j} = \sqrt{\frac{\sum_{n=1}^i [CV_{Ft,i}^2 \times Q_i]}{\sum_{n=1}^i Q_i}} \quad (2.4)$$

In the case of area-normalized fluxes from a region j , (Fa,j), the equation becomes:

$$CV_{Fa,j} = \sqrt{\frac{\sum_{n=1}^i [CV_{Fa,i}^2 \times A_i]}{\sum_{n=1}^i A_i}} \quad (2.5)$$

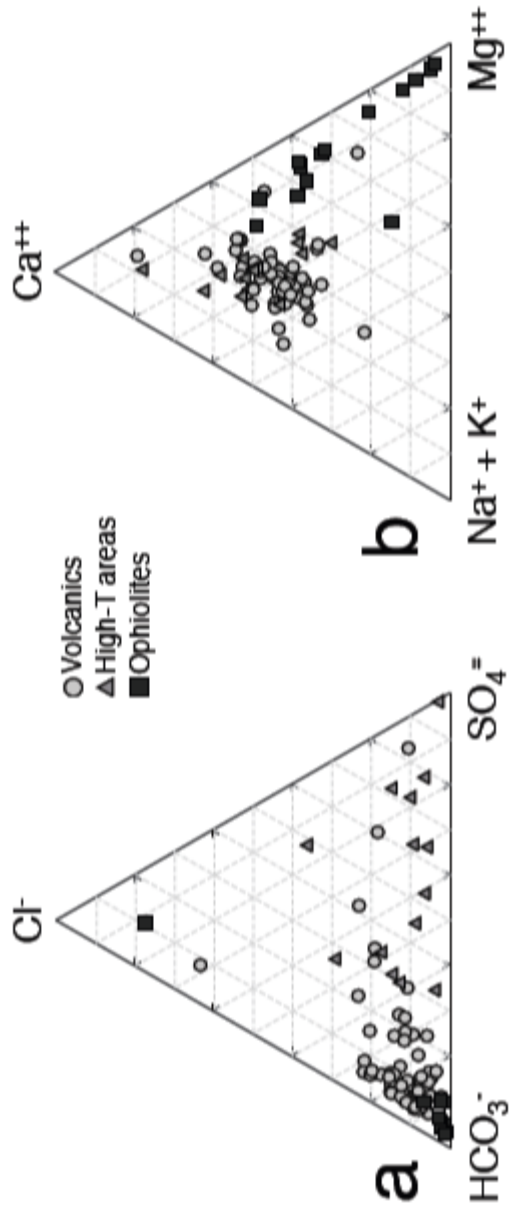
2.4. RESULTS AND DISCUSSION

2.4.1. Major elements

In Table 2.2, chemical analyses of samples from 2007 and early 2008 are listed. We divide the rivers studied into two very broad classes, ophiolites and volcanic regions. Within each class the major element chemistry of the streams (Na^+ , K^+ , Ca^{2+} , Mg^{2+} , Cl^- , SO_4^{2-} and HCO_3^-) is broadly similar, but there are pronounced differences between the two classes. Rivers draining ophiolites have significantly (at 95% significance level) higher pH values and a smaller range in pH than volcanic rivers (average pH of 8.2 and 7.6, respectively). The higher pH in ophiolite waters may be caused by low-temperature serpentinization (Neal and Shand, 2002). The large range in the pH of volcanic rivers is a result of some, but not all, of those rivers receiving addition of magmatic gases and acids.

Bicarbonate is the dominant anion in most of the rivers sampled (Figure 2.4). Cl^- contributes the major negative charge to only two rivers, Salaza River in Zambales (PH-08-04) and Bangon River in Sorsogon (PH-08-30). Neither of the two rivers shows other obvious signs of seawater input (such as high $^{87}\text{Sr}/^{86}\text{Sr}$). Sulfate is a major contributor to the negative charge in rivers draining Mount Pinatubo and in a few rivers draining volcanic craters on the Bicol Peninsula.

Figure 2.4. Ternary diagrams of the major anion and cation composition of the rivers studied. The diagrams show the river water composition in terms of charge equivalents and are not corrected for atmospheric or hydrothermal inputs. Bicarbonate is the dominant anion in systems other than those with active volcanic activity. Ophiolite streams are, as expected, Mg-rich.

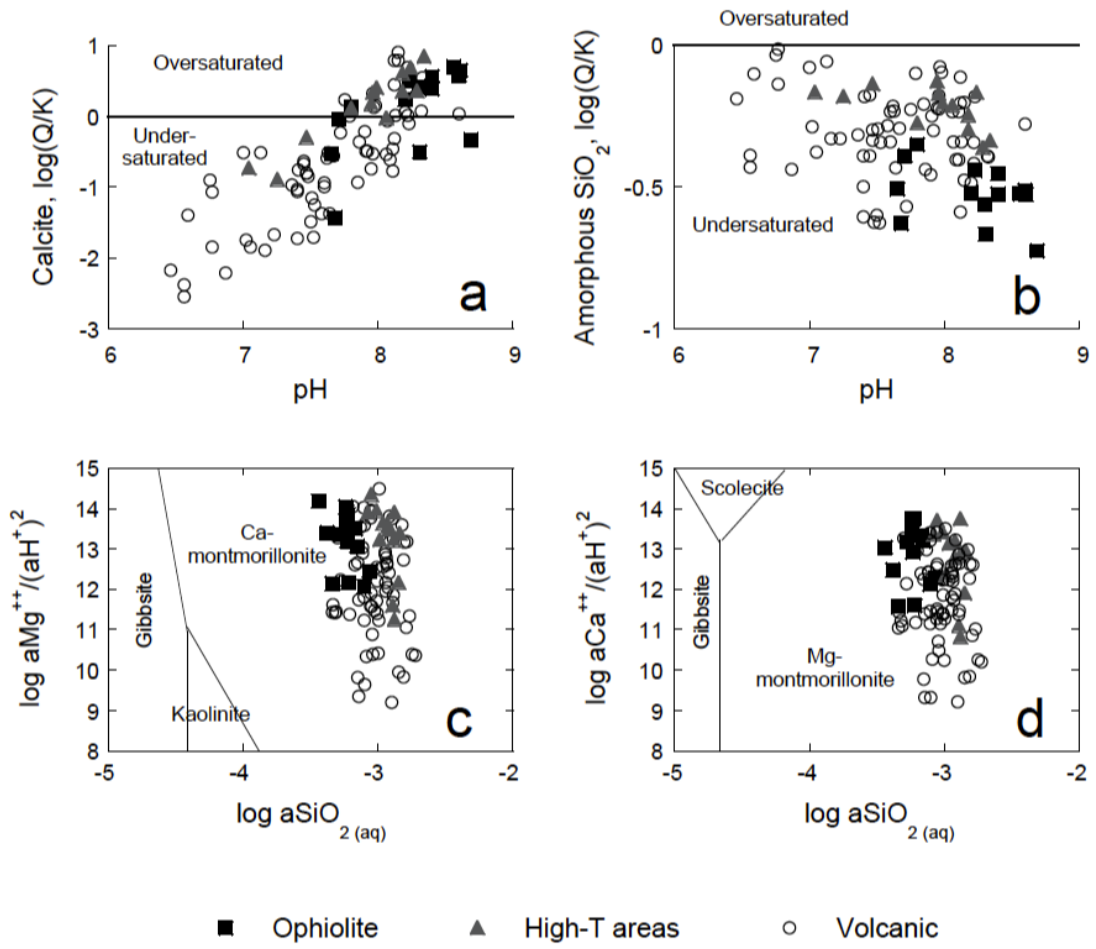


Mg^{2+} is a major contributor to the positive charge in ophiolitic rivers, especially in the Zambales ophiolite, and most of these rivers contain insignificant amounts of Na^+ and K^+ . The cation component of volcanic rivers has roughly subequal contributions from the major components; in most cases $Ca^{2+} > Mg^{2+} > (Na^+ + K^+)$. No systematic difference in either anion or cation composition exists between rivers draining the BVA versus the LVA, indicating similar weathering conditions and processes in these two regions.

We calculated the saturation state of the waters studied with respect to primary and secondary minerals using Geochemist's Workbench 7.0 (Bethke, 2007). Calcite saturation is prevalent in waters at $pH > 8$, regardless of whether the lithology is volcanic or ophiolitic (Figure 2.5a). In general, rivers draining ultramafic rocks have higher pH and are more likely to be supersaturated with calcite. Rivers draining the BVA are usually undersaturated with calcite, even at pH over 8, while rivers draining the LVA are more likely to be saturated with calcite. The streams we studied generally have high concentrations of dissolved Si: 412-885 μM in ophiolites, 466-1906 μM in volcanics. These values are similar to or higher than those reported from basaltic islands: 270-1250 μM in Sao Miguel rivers (Louvat and Allegre, 1998), 420-2700 μM in Iceland rivers (Gislason et al., 1996) and 280-570 μM in Reunion rivers (Louvat and Allegre, 1997). Many of our samples are close to opal saturation (Figure 2.5b) but we have not attempted to determine the influence of plant uptake on silica fluxes (Derry et al., 2005).

Total dissolved solids (TDS) in streams in Luzon (150-332 mg/L and 82-916 mg/L in ophiolite and volcanic streams, respectively) are high compared to world rivers (50 mg/L in the Amazon) (Meybeck and Ragu, 1995) and similar to or higher than TDS

Figure 2.5. Mineral saturation diagrams for the rivers under study. Calculated using Geochemist's Workbench 7 at T=25°C. Saturation index as a function of pH for a) calcite and b) amorphous silica. Stability diagrams for c) Mg and d) Ca indicate that the river water is in the stability field of secondary smectite minerals.



observed in other volcanic regions mentioned above. Luzon streams tend to have high cation concentrations compared to other volcanic provinces such as the Stikine terrane (Gaillardet et al., 2003), the Azores (Louvat and Allegre, 1998), New Zealand (Goldsmith et al., 2008) and Iceland (Gislason et al., 1996). This is especially true for Mg^{2+} and Ca^{2+} , even when excluding ophiolite streams. The high cation concentrations coupled with the high Si concentration put the water into the stability fields of smectites (Figure 2.5c and 2.5d); smectites are the most common clay mineral in river sediments on Luzon (smectites on average comprise 86% of clay abundances, Liu et al. (2009)). These observations are consistent with expectations of fast weathering of ultramafic to intermediate compositions with fine-grained to glassy textures, in a volcanically and tectonically active area with a warm and humid climate.

2.4.2. Sr isotopes

Measured Sr concentrations in the rivers and streams sampled here are 61-911 nmol/L for ophiolites and 426-9884 nmol/L for volcanics. The highest values are generally found in the Pinatubo area and are likely caused by high-temperature weathering (hydrothermal) activity, low flow at time of sampling or a combination of those two factors. The only other study to report dissolved river data from the Philippines, as far as the authors are aware, is that of Goldstein and Jacobsen (1987) where values of 102-172 ppb Sr (1164-1963 nmol/L) were reported for four rivers draining central and northern Luzon. The $^{87}Sr/^{86}Sr$ values for dissolved riverine Sr reported by Goldstein and Jacobsen (1987) are somewhat higher than those reported here, ranging from 0.70452-0.70628. None of those four rivers drains exclusively volcanic lithologies and the presence of Sr derived from sedimentary sources likely explains the higher values.

The Sr isotope signature of river water reflects the relative contribution of atmospheric inputs and chemical weathering of the various lithologies that make up the watershed to the solute load. We consider three end members; rainwater, limestones and igneous rocks. We take the value of Sr in precipitation to be that of modern seawater, 0.7092. Marine limestones in the Philippines are mostly Miocene and younger and we adopt an average value of 0.7088 for limestone in this work (McArthur et al., 2001). The Sr isotope signature of volcanic rocks in the study area is given in Table A2.2. For regions without published $^{87}\text{Sr}/^{86}\text{Sr}$ data we use the overall mean of the data from volcanic regions, $^{87}\text{Sr}/^{86}\text{Sr} = 0.70400 \pm 0.00066$ (Knittel-Weber and Knittel, 1990; Castillo and Newhall, 2004; McDermott et al., 2005; DuFrane et al., 2006). We measured Sr isotopes on 53 of the water samples presented here. A large majority of these samples (45 of 53 samples, or 85%) has $^{87}\text{Sr}/^{86}\text{Sr}$ ranging between 0.7036-0.7050, showing little evidence of dissolution of marine carbonate or any large contribution of rainwater.

Eight samples, or 15% of measured samples, have $^{87}\text{Sr}/^{86}\text{Sr}$ higher than 0.7050. These samples were assumed to reflect a mix of Sr from igneous rocks and limestone (where geological map revealed presence of marine carbonate within the basin) or igneous rocks and rain (where, according to geological maps, no marine carbonate is present in the basin). We used a simple two-component mixing model to partition the Sr in those high- $^{87}\text{Sr}/^{86}\text{Sr}$ samples into relative proportions derived from igneous rock and limestone/rain:

$$f_i = \frac{R_{spl} - R_a}{R_i - R_a} \times 100 \quad (2.6)$$

where “*f*” refers to fractional contribution, “*R*” refers to $^{87}\text{Sr}/^{86}\text{Sr}$ and the subscripts “*i*” and “*spl*” refer to igneous rock and sample, respectively. The subscript “*a*” refers to limestone or rain, as the case may be.

Of the watersheds we studied ($n = 75$), available geological maps indicate that only three basins have appreciable amounts of marine carbonates. Sr-isotope analyses were made on all of those rivers; the Masinloc River on the west coast of the Zambales ophiolite, the Sipocot River which drains Mt. Labo and the surrounding lowlands in the provinces of Camarines Norte and Sur, and the Agus River in the Southern Sierra Madre Mountains. The contribution of weathering of limestone to the dissolved Sr load of these rivers is 82, 52 and 25%, respectively. Of the remaining 72 watersheds, only 4 have significantly elevated $^{87}\text{Sr}/^{86}\text{Sr}$. Three of those drain Taal Volcano in Batangas Province, (Palico, Obispo and Dacanlao streams). Geological maps do not show any carbonate outcrops in these watersheds but the Sr isotope data and the spatial arrangement of the affected watersheds, which all lie adjacent to each other, indicate the likely presence of a subsurface body of carbonate rocks. The proportion of limestone-derived Sr in those streams ranges from 11-15%. The fourth stream is an ephemeral tributary of the Lawis River in the Zambales Ophiolite, which has about 16% rain-derived Sr.

2.4.3. Sources of solutes

In volcanic areas, stream chemistry is influenced not only by low-temperature (low-T) weathering and atmospheric deposition but also by geothermal processes, which we refer to as high-temperature (high-T) weathering. During high-T weathering, strong acids (HCl , H_2SO_4 , HNO_3) of volcanic origin replace carbonic acid as chemical

weathering agents. Since no neutralization of atmospheric-derived carbonic acid accompanies these reactions, they do not directly consume atmospheric carbon. The mass-balance equation for a conservative element X is:

$$[X]_{tot,i} = [X]_{rain,i} + [X]_{high-T,i} + [X]_{low-T,i} \quad (2.7)$$

where $X = \{Na^+, K^+, Ca^{2+}, Mg^{2+}, SO_4^{2-}\}$, the subscript “ i ” refers to each individual stream, “ tot ” refers to the total concentration of X , and “ $rain$ ” refers to solutes derived from atmospheric inputs.

We calculate the contributions from atmospheric and geothermal inputs from end member models and assume that low-T weathering makes up the rest. To correct for the atmospheric deposition of the major elements, we use sea salt X/Cl ratios, listed in Table 2.4, and $[Cl]_{rain,i}$ for all streams, such that:

$$[X]_{rain,i} = \left(\frac{X}{Cl}\right)_{sea\ salt} \times [Cl]_{rain,i} \quad (2.8a)$$

Combined high- and low-temperature weathering products are referred to as X^* :

$$[X]^* = [X]_{tot,i} - [X]_{rain,i} \quad (2.8b)$$

A significant contribution of Na^+ from weathering is evident in a plot of Na^+ vs. Cl^- , showing $(Na^+/Cl^-)_{stream} > (Na^+/Cl^-)_{seawater}$ (Figure 2.6). We assume that the maximum plausible Cl^- concentration in volcanic streams unaffected by hydrothermal activity is 200 μM . If $[Cl^-]_{tot,i} < 200 \mu M$, all Cl^- is assumed to come from atmospheric deposition. The value of $[Cl^-]_{rain} = 200 \mu M$ derives from the assumption that rainfall in the region

Table 2.4. Cl-normalized molar ratios used in solute partitioning calculations

	SO ₄ /Cl	Na/Cl	Ca/Cl	K/Cl	Mg/Cl	HCO ₃ /Cl
Rainfall ¹	0.052	0.858	0.019	0.019	0.098	0.000
Hydrothermal fluids ²	1.065	0.636	0.535	0.181	0.326	1.122

1: Sea salt ratios from Schlesinger (1997)

2: Average of published data (see text for references) and samples PH-07-12 and PH-07-22

has an average chloride concentration of 100 μM (Eklund et al., 1997; Waterloo et al., 1997; Fujita et al., 2000; Kyoung Lee et al., 2000) and the evapotranspiration factor is around 2. Inputs from Cl⁻ bearing minerals such as amphiboles are believed to be minor and in any case are not well constrained by our data. All Cl⁻ in streams draining ultramafic areas is attributed to atmospheric input since no hydrothermal activity is reported in these areas. Next, we correct for hydrothermal (high-T) contribution to streams draining volcanic regions. We adopt the method used by Dessert et al. (2009) to calculate the contribution of high-temperature weathering to the dissolved load:

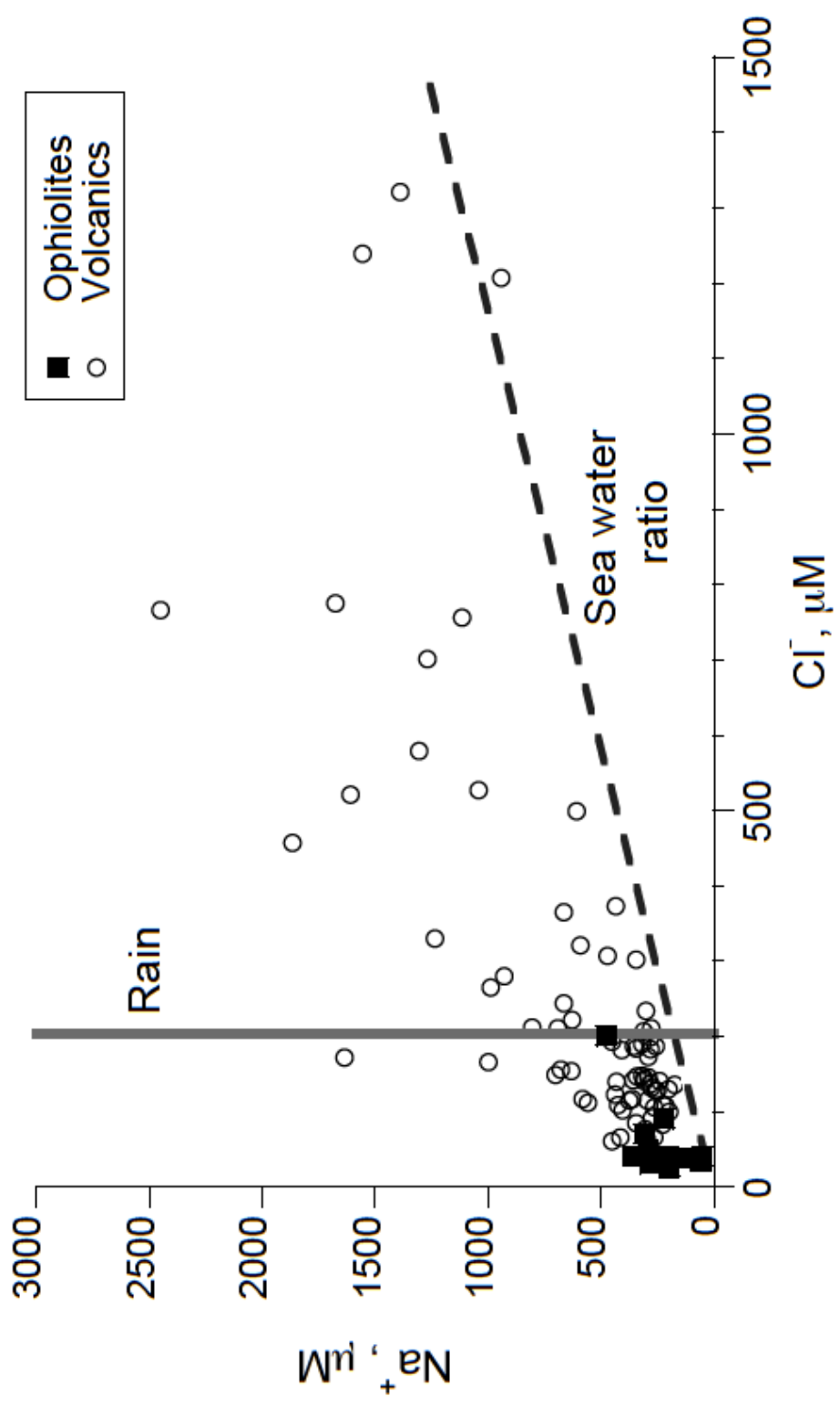
$$[Cl]_{high-T,i} = [Cl]_{tot,i} - [Cl]_{rain,i} \quad (2.9a)$$

and

$$[X]_{high-T,i} = \left(\frac{X}{Cl}\right)_{hot\ springs} \times [Cl]_{high-T,i} \quad (2.9b)$$

The only exception from this order of corrections is HCO₃⁻. First we correct for hydrothermal input using the HCO₃/Cl ratio of hydrothermal waters and then we attribute the remaining HCO₃⁻ to atmospheric origin. For the hot spring end member X/Cl we use the average of our own data from hot springs sampled on Mt. Isarog and

Figure 2.6. Significant enrichment of Na^+ in river water from what would be expected if all Na^+ originated in rainfall with Na/Cl of 0.86. The excess Na^+ is derived from weathering. The estimate of $200 \mu\text{M Cl}^-$ in rain is derived from regional average rainfall values ($100 \mu\text{M}$) and an evapotranspiration factor of 2.



Mt. Bulusan and published data from three Philippine hydrothermal areas; Pinatubo (Stimac et al., 2004), Taal (Delmelle et al., 1998) and Manito-Bacon (Baltasar, 1980), see Table 2.4. Model runs where we used the regional average of $(X/Cl)_{\text{hot springs}}$ did not yield significantly different results than using the average of all available data. Given that result and the fact that the range in composition of hydrothermal fluids is quite large, we prefer to use all the data available to us to constrain the end-member ratios for the hot springs.

We carried out a sensitivity analysis to investigate the impact of the varying the end member assumptions on the solute source allocations (Appendix 1), investigating 27 different scenarios. The sensitivity analysis was carried out independently of the flux calculations and their associated uncertainties (see Chapter 2.3.4), and deals with the possible variability in the fractional contribution of the three sources (rain, hydrothermal end member, low-temperature weathering end member) to the total chemical flux.

In volcanic areas, variability in the composition of rainfall causes variability in the fraction of solutes derived from rainfall of 11% (Mg^{2+}) to 67% (Ca^{2+}). The observed variability in the composition of hydrothermal fluids leads to variability in the fraction of solutes derived from these fluids of 16% (the alkali metals) to 22% (Mg^{2+}). These values may seem high, but it should be kept in mind that both rainfall and high-T weathering are relatively small components of the overall solute flux. A confirmation of this effect is evident in the modeled variability in the fraction of solutes from low-T weathering; it is small, ranging from 2.4% (the alkaline earths) to 9.6% (K^+). In ophiolite regions the variability in source allocation is much smaller; it is always less than 1% in the case of precipitation and in the case of low-T weathering solutions, it

ranges from >1% (the alkaline earths) to 35% (K^+). We therefore conclude that our estimates of absolute solute fluxes from the three different sources are relatively insensitive to the exact ratios used in solute partitioning calculations.

The Philippines is a densely populated country (89 million) with nearly 300 inhabitants/km². Agriculture is a major land use in the Philippines, covering some 32% of the islands (<http://countrystat.bas.gov.ph>). Significant soil erosion and modification of the natural ecosystem by humans has occurred in the Philippines over the 20th century (see e.g. Kastner 2009). Furthermore, many of the streams sampled run through urban areas where untreated wastewater is channeled directly into streams and lakes (Dyer et al., 2003). These conditions can influence the dissolved load chemistry of streams, although their impact on silicate weathering budgets is less clear. Unfortunately, we are not aware of any studies that can be used to quantify the impact of human land use in the Philippines on weathering chemistry. For the present, we simply note that land use is an additional source of uncertainty in our weathering flux calculations but one that is not currently constrained.

2.4.3.1. Regional trends in sources of solutes – Atmospheric inputs

No spatial trends were observed in the exports of rain-derived solutes. In terms of species concentrations in individual samples, Cl^- from rainfall ranges from nearly 0% in the Pinatubo region (O'Donnell River) to 100% in the majority of volcanic streams and ophiolite streams. The regional average $\%Na_{rain}$ ranges from 13% (Pinatubo) to 46% (Quezon) and the average $\%K_{rain}$ is 2%-6% in volcanic areas and ~27% in the ophiolites and in Quezon. Rain-derived Ca^{2+} never exceeds 2% of the total Ca^{2+} concentration in any region studied and the $\%Mg_{rain}$ is only slightly higher than

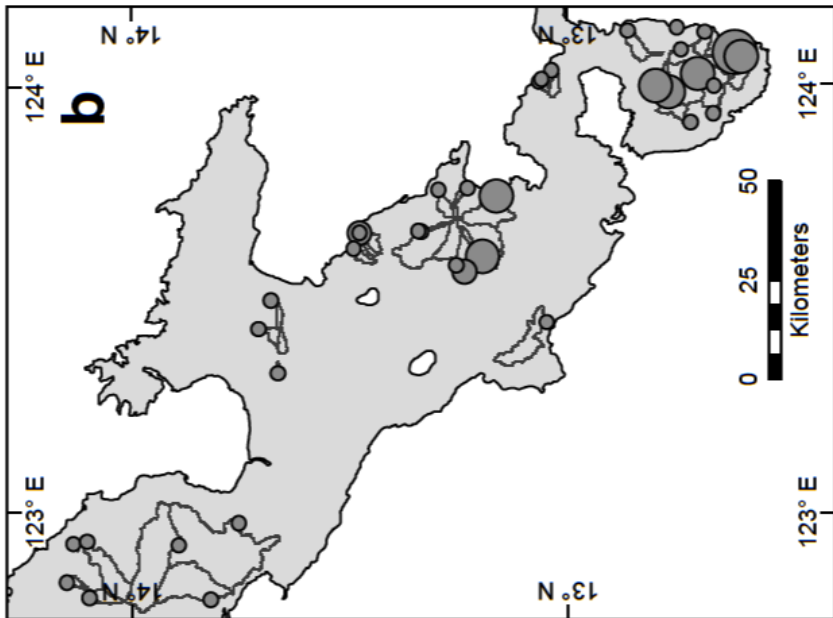
$\%Ca_{\text{rain}}$ in most regions. Uncertainties in estimates of atmospheric inputs are therefore very small for Ca and Mg and do not contribute greatly to the overall uncertainty in the weathering fluxes.

2.4.3.2. Regional trends in sources of solutes – High-temperature weathering

We assessed the validity of the method of Dessert et al. (2009) by plotting the cation load derived from high-temperature processes as a percentage of the total cation load due to silicate weathering on a map of Luzon (Figure 2.7). As described above, this method relies on Cl^- as indicator element for hydrothermal activity and this may limit its usefulness in hydrothermal systems dominated by other acids than HCl. Overall, the method yields plausible results although it fails to replicate large observed inputs of hydrothermal fluids into Rangas River on the Bicol Peninsula, which drains the crater of Isarog volcano. This system appears to be dominated by sulfuric acid, judging by the large proportion of sulfate in the water and strong smell of sulfur at the river.

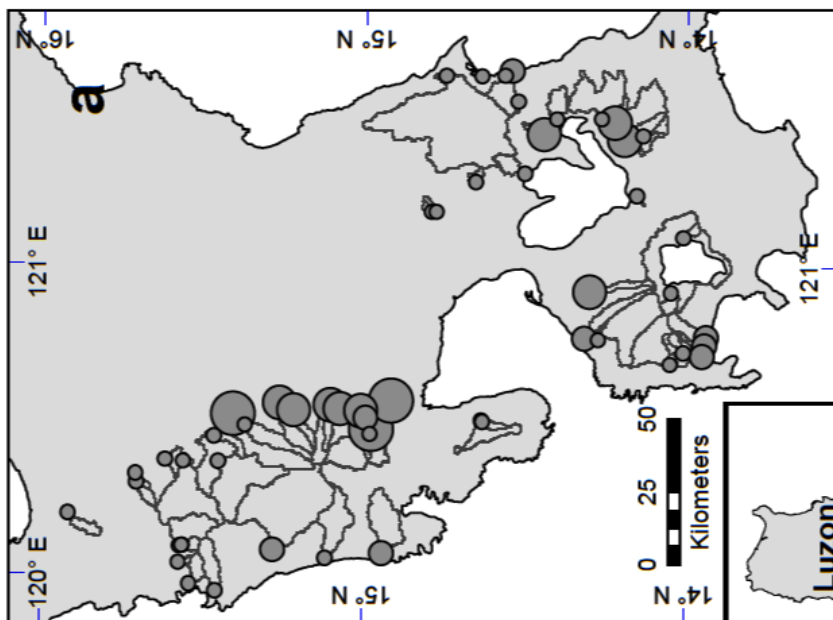
The highest percentages of hydrothermal inputs cluster around major volcanoes (Pinatubo, Mayon, Bulusan), just as expected from field observations and published data. The exception is rivers on the flanks of Taal Volcano, where the Dessert method predicts only small amounts of high-temperature inputs, contrary to what might be expected from the presence of a very active hydrothermal system inside the Taal caldera (Delmelle et al., 1998). Most of the streams sampled on Taal drain the outside flanks of the caldera and we infer that the impact of the hydrothermal system extends only to a small extent to the outer flanks of the caldera. Hydrothermal inputs into the

Figure 2.7. Percent of total cation load derived from high-temperature weathering, calculated using Cl as indicator for high-T weathering (Dessert et al., 2009). The method correctly identifies numerous streams draining active volcanoes as heavily impacted by high-T weathering activity but fails to identify one stream that is heavily impacted by inputs of magmatic sulfuric acid.

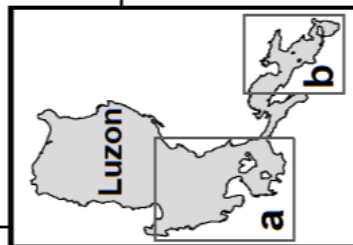


**Cations from high-T weathering,
% of total cation load**

- 0%
- 0% - 10%
- 10% - 50%
- 50% - 100%



□ Watersheds studied



streams SE of Laguna de Bay most likely come from the numerous maars that dot the landscape in that area.

Hydrothermal activity supplies on average approximately 10% of the dissolved cation load in the volcanic rivers we studied. The range is very large; most streams are not affected by hydrothermal activity while others get most of their solutes from hydrothermal activity.

2.4.3.3. Regional trends in sources of solutes – Low-temperature weathering

Area-normalized exports of cations produced by low-temperature weathering are largest in the Pinatubo area ($5.44 \pm 0.81 \times 10^6$ mol/km²/yr) but smallest in the Camarines region ($1.26 \pm 0.22 \times 10^6$ mol/km²/yr). Most valleys draining the Pinatubo complex are still filled with voluminous lahar deposits from the cataclysmic 1991 eruption (Montgomery et al., 1999) and the large surface area of these deposits no doubt contributes to the high weathering fluxes in the region. It is also quite possible that our method underestimates inputs of hydrothermal inputs somewhat and that the solute load is differently distributed between low- and high-temperature sources. The relatively small low-temperature cation exports from the Camarines region may be biased by the relatively high discharge, and thus low solute concentrations, of rivers when sampling took place.

If calcium and magnesium are investigated separately, area-normalized low-temperature fluxes from Pinatubo and Camarines are still the largest and smallest, respectively. The Zambales and Angat ophiolites have the second largest fluxes of Ca and Mg, consistent with their ultramafic lithology.

Area-normalized exports of Si from the Bicol Peninsula show a weak but highly significant ($r^2 = 0.27$, $p_{\text{slope}} < 0.001$) correlation with age of the substrate, increasing from a regional average of $1.27 \pm 0.21 \times 10^6$ mol/km²/yr in Camarines, the oldest part of the currently active BVA, through $2.23 \pm 0.31 \times 10^6$ mol/km²/yr in Bicol to a regional average of $2.54 \pm 0.35 \times 10^6$ mol/km²/yr in Sorsogon, the youngest part of the Bicol Peninsula. Two factors may contribute to this trend. The basins developed on younger substrates have more hydrothermal input, while weathering of the older substrates may have partially depleted Si as soils evolve, resulting in lower modern Si fluxes.

2.4.4. Element fluxes

A full understanding of the controls on weathering fluxes in tectonically or volcanically active regions includes disentangling the signatures of high- and low-temperature inputs (Evans et al., 2004; Dessert et al., 2009). We argue that the once in the ocean, base cations derived from high-T weathering (i.e., released by the action of strong acids such as HCl and H₂SO₄) of silicate rocks have the same potential to form sedimentary carbonates and sequester carbon as solutes from low-temperature weathering, even if no carbon was consumed and exported during the release of these cations (for carbon to be consumed during weathering of silicate rocks, the acid dissolving the rocks must be carbonic acid). This is because in the ocean, where solutes from a large number of weathering systems come together, these high-T cations can form carbonates with bicarbonate derived from silicate weathering of alkali metals in other weathering systems. In particular, sulfate reduction generates alkalinity that can then be removed by reaction with cations that were originally dissolved by sulfuric acid. Consequently, high-T weathering of silicate rocks has

similar implications for the long term carbon cycle as silicate low-T weathering. In the following discussion, we therefore treat high- and low-temperature weathering products as a single category, solutes derived from silicate weathering (X^*).

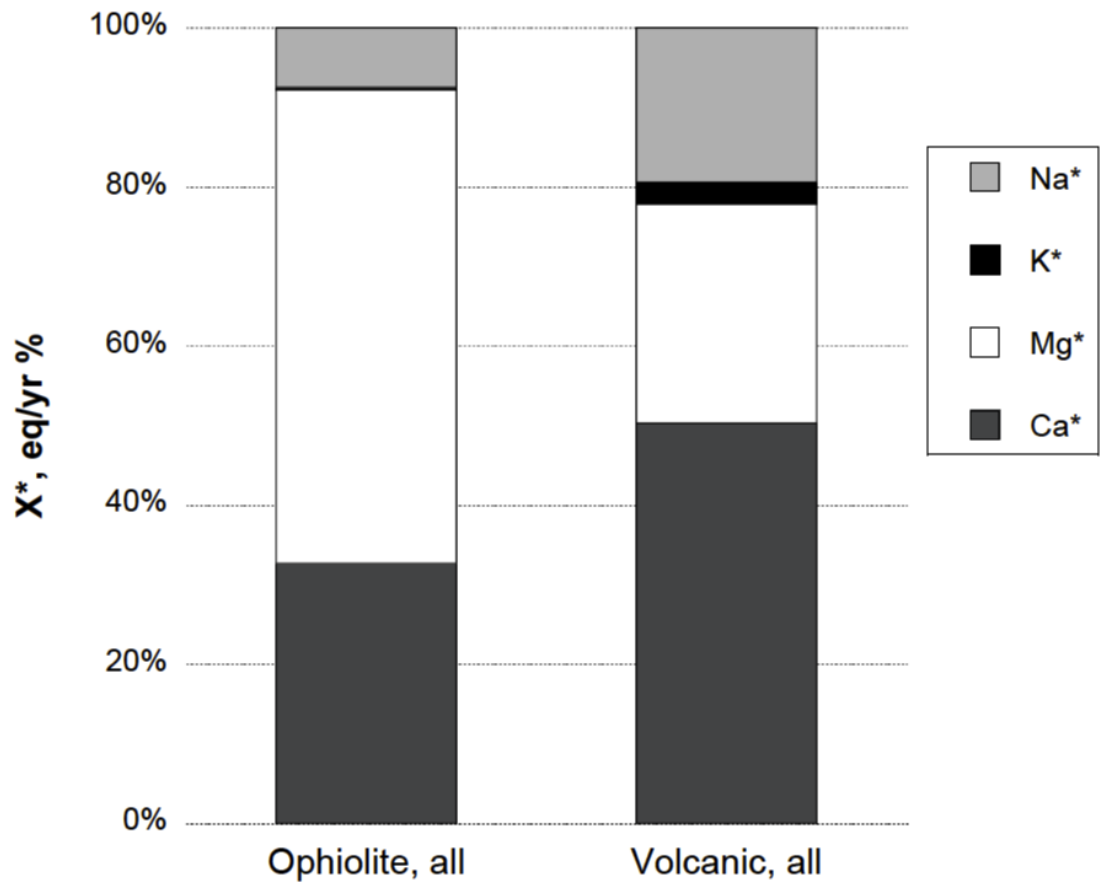
The area-normalized fluxes of major elements from the Philippine watersheds studied are among the highest recorded anywhere in the world (see Tables 2.5, A2.3 and A2.4). Export of cations derived from silicate weathering is 35-241 t/km²/yr in volcanic areas and 54-147 t/km²/yr in ophiolitic regions. Silicate weathering rates (cation weathering rate plus silica, calculated as SiO₂) are 108-380 t/km²/yr in volcanic and 119-283 t/km²/yr in ophiolitic regions, respectively. This compares to silicate weathering rates of 0.8 (Ob) to 72 t/km²/yr (Irrawaddy) in some of the world's largest rivers (Gaillardet et al., 1999) and of 15-310 t/km²/yr in volcanic regions of New Zealand (Goldsmith et al., 2008).

The volume-weighted average composition of waters draining ophiolitic and volcanic areas is shown in Figure 2.8. The data has been corrected for precipitation inputs and limestone dissolution where necessary. Ophiolitic rivers are very Mg-rich compared to volcanic rivers (~60% vs. ~30% on equivalent basis, respectively) and the combined Mg and Ca contribution to the solute load in these rivers is over 95%. This explains the very high alkalinity of rivers draining ultramafic rocks. Ca and Mg are also the most important components of volcanic rivers, accounting for a little less than 80% of the cationic charge. Area-normalized fluxes of dissolved Ca and Mg from ultramafic areas ($2.95 \pm 0.25 \times 10^6$ mol/km²/yr) are on the high end of the range observed in volcanic regions ($0.76-4.86 \times 10^6$ mol/km²/yr), mainly due to the large contribution of Mg to the dissolved load. Dissolved Si flux in ophiolite rivers ($1.55 \pm 0.13 \times 10^6$

Table 2.5. (continued)

-
- 1: Silicate cation weathering rate = $\text{Na}^* + \text{K}^* + \text{Ca}^* + \text{Mg}^*$
 - 2: Silicate weathering rate = Silicate cation weathering rate + SiO_2
 - 3: Total bicarbonate flux, also called "carbon consumption" in published studies
 - 4: See France-Lanord and Derry (1997), p. 66.
 - 5: ZA = Zambales and Angat ophiolites
 - 6: BLM = Bataan, Laguna and Macolod
 - 7: Pinatubo = comprises both streams draining exclusively Pinatubo and streams draining both Pinatubo and the adjacent Zambales ophiolite

Figure 2.8. Partitioning of elements (by charge) derived from weathering in rivers draining ophiolites and volcanic regions on Luzon. The dominance of Ca and Mg in both classes of rivers is apparent. Mg is the dominant cation in ophiolitic rivers and Ca in volcanic rivers. K is almost completely absent in the solute load of ophiolitic rivers, reflecting its scarcity in ultramafic rocks (and possible uptake by vegetation).



mol/km²/yr) is on the low end of the range for volcanic rivers ($1.35\text{-}3.29 \times 10^6$ mol/km²/yr).

The weathering carbon export flux (i.e. alkalinity flux derived from silicate alteration) from the Philippines is $3.89 \pm 0.21 \times 10^6$ mol/km²/yr weighted over both volcanic and ophiolitic regions. In volcanic regions, the export flux is $3.58 \pm 0.23 \times 10^6$ mol/km²/yr, and in ophiolitic regions it is $5.99 \pm 0.64 \times 10^6$ mol/km²/yr. These values are on the high end of atmospheric carbon export fluxes reported globally (Table 2.6).

Importantly, these values are significantly higher than the global average values for export fluxes in tropical arcs, reported in Dessert et al. (2003) as 1.6×10^6 mol/km²/yr. If our values are typical for fluxes from tropical volcanic arcs, it would appear that current estimates of the magnitude of weathering carbon fluxes from mafic and intermediate lithologies in tropical arc terranes are too low.

2.5. IMPLICATIONS FOR GLOBAL CO₂ EXPORT

In order to extrapolate our findings to other volcanic arcs in the tropics, we express the total export fluxes from the LVA and BVA as a function of arc length. We then assess the total length of volcanic arcs in the tropics (within 20 degrees of the Equator) and calculate the total fluxes expected from these arcs, assuming the fluxes we calculate for Luzon are representative of all tropical arcs. The length of arc studied in this paper is around 530 km. The segment of the LVA studied here is approximately 250 km long and the segment of the BVA studied is approximately 280 km long. We use values from von Huene and Scholl (1991) for length of arcs in the tropics. We adjusted the values given by von Huene and Scholl (1991) if a substantial part of an arc lies outside of the tropics, such as the Tonga and Mariana trenches. We also modified the lengths

Table 2.6. Carbon export fluxes, silicate cation weathering fluxes and silicate chemical weathering fluxes in different regions of the world.

River Name	Country / Region	Lithology	Area km ²	Runoff mm/yr	Silicate weathering		Silicate cation		Silicate chemical	
					carbon export flux ¹ 10 ⁶ mol/km ² /yr	Silicate weathering flux ¹ t/km ² /yr	carbon export flux ² 10 ⁶ mol/km ² /yr	Silicate weathering flux ² t/km ² /yr	carbon export flux ³ t/km ² /yr	weathering rate ³ t/km ² /yr
Columbia Plateau	USA	Basalt		1,053	0.37	7.7		24		a
Deccan Traps	India	Basalt		463	1.26	25		37		a
Hawaii	USA	Basalt		1,612	0.66	12		34		a
Java	Indonesia	Basalt		4,052	6.41	152		342		a
Massif Central	France	Basalt		406	0.30	5.6		13		a
Mt. Cameroon	Cameroon	Basalt		2,120	3.44					a
Parana Traps	Brazil	Basalt		1,020	0.82	21		60		a
La Reunion	La Reunion	Basalt		2,433	2.26	48		106		a
Sao Miguel	Azores	Basalt		734	0.56	13		35		a
Iceland	Iceland	Basalt		2,432	1.11	21		58		b
Siberian Traps	Central S	Basalt	700,000		0.1-0.3	5.7-6.1				h
Baltic Shield	NW Russia	Basalt		300-700		2.3		3.6		i
Irrawady	Myanmar	Mixed	410,000	1,185	2.03	42		72		e
Brahmaputra	S Asia	Mixed	580,000	879	0.15	2.6		10		e
Ganges	S Asia	Mixed	1,050,000	470	0.45	7.9		14		e
Orinoco	S America	Mixed	1,100,000	1,032	0.07	2.3		10		e
Nelson	Canada	Mixed	1,132,000	79	0.04	0.8		1.2		e
Mississippi	USA	Mixed	2,980,000	195	0.07	1.7		3.8		e
Ob	Siberia	Mixed	2,990,000	135	0.02	0.3		0.8		e
Congo-Zaire	W Africa	Mixed	3,698,000	324	0.05	0.8		4.2		e
Amazon	S America	Mixed	6,112,000	1,078	0.05	2.2		13		e
Haut Glacier d'Arolla	Switzerland	Mixed	12	2,009	0.002	13		18		g
Zambales/Angat	Philippines	Ultramafic	1,813	2,539	6.07	100		192		f
Waitara	New Zealand	Volcanic	705		0.852*			113		c
Manganui, ds	New Zealand	Volcanic	200		2.39*			240		c

Table 2.6. (continued)

River Name	Country / Region	Lithology	Area km ²	Runoff mm/yr	Silicate weathering		Silicate cation		Silicate
					carbon export flux ¹ 10 ⁶ mol/km ² /yr	weathering flux ² t/km ² /yr	weathering flux ² t/km ² /yr	weathering rate ³ t/km ² /yr	chemical weathering rate ³ t/km ² /yr
Kamchatka River, outlet	Russia	Volcanic	45,600	520	0.46 [#]	8.03 [#]	20.55 [#]		d
Volcanic, all	Philippines	Volcanic	6,236	2,106	3.58	116	225		f

Sources: a - Dessert et al., 2003; b - Gislason et al., 1996; c - Goldsmith et al., 2008; d - Dessert et al., 2009; e - Gaillardet et al., 1999; f - this study; g - Sharp et al., 1995; h - Pokrovsky et al., 2005; i - Zakharova et al., 2005

1: Total bicarbonate flux, also called "carbon consumption" in published studies

2: Silicate cation weathering flux = Na* + K* + Ca* + Mg*

3: Silicate chemical weathering rate = Na* + K* + Ca* + Mg* + SiO₂

*: Carbon export flux calculated as twice the silica flux, as proposed by Edmond and Huh (1997).

#: These values refer to low-temperature weathering only

reported for the trenches surrounding the Philippine archipelago and for the Andaman-Sunda-Java trenches, since we were unable to verify the lengths given by von Huene and Scholl (1991). According to these calculations, volcanic arcs in the tropics stretch for 16,600 km.

The total weathering carbon export flux from the studied watersheds is 28×10^9 mol/yr, or 54×10^6 mol/km of arc length. Extrapolating this to the 16,600 km of volcanic arcs in the tropics, the total weathering carbon export flux from these systems is on the order of 0.9×10^{12} mol/yr. These calculations are subject to considerable uncertainty (e.g. uncertainty in the exact length of arcs in the tropics, inclusion of non-volcanic regions and/or exclusion of volcanoes, variable width/length ratios of arcs) and should be regarded as order of magnitude calculations only.

The weathering carbon export fluxes presented above represent about 10% of the global export of carbon by silicate weathering (Gaillardet et al., 1999). Because the composition of the cation flux is heavily weighted toward Ca + Mg, the long term sequestration potential of this flux is even greater than 10% of the global total (France-Lanord and Derry, 1997), although at present it is difficult to scale this with precision. As defined here the tropical volcanic arcs correspond to ~1% of the exorheic drainage area worldwide (Syvitski et al., 2005). Put another way, a fraction, perhaps as much as 15-20%, of all atmospheric carbon ultimately sequestered by silicate weathering may be processed through an area corresponding to ~1% of Earth's surface.

2.6. CONCLUSIONS

We initiated this study to test the hypothesis that chemical erosion rates in tectonically active, tropical volcanic arc terrains are very high. The data support this hypothesis; the silicate-weathering derived bicarbonate and cation fluxes and associated potential sequestration of atmospheric CO₂ are among the highest yet reported from any environment in the world. We found the highest area-normalized cation weathering fluxes in streams draining the lahar-dominated flanks of Mt. Pinatubo, and the lowest area-normalized cation weathering fluxes in Quezon, where volcanism ceased during the Pleistocene, and in Camarines. It is worth noting that even if these regions have the lowest weathering rates in this study, they still have some of the highest reported weathering rates in the world. Weathering rates in ultramafic rocks on Luzon are comparable to rates measured for low-temperature weathering rates in volcanic rocks, although the chemical composition differs.

We estimate that hydrothermal activity supplies around 10% of the dissolved cation load to streams on Luzon. This activity is restricted to areas surrounding known active volcanic centers. The estimate of the magnitude of hydrothermal contribution is subject to uncertainty, mainly because of the uncertainties in the composition of the hydrothermal end-member fluids, but because the total hydrothermal contribution is ca. 10% the uncertainties do not have a large impact on the overall flux estimate.

Extrapolating our findings to the entire length of volcanic arcs in the tropics yields a total weathering carbon export flux from tropical arcs of 0.9×10^{12} mol/yr. These values agree broadly with the values for global silicate weathering carbon export fluxes estimated by Gaillardet et al. (1999) and Dessert et al. (2003). Furthermore, we

estimate that volcanic arcs in the tropics, while areally small, process around 10% of all atmospheric carbon exported by silicate weathering worldwide. Chemical weathering of volcanic arcs in the tropics thus has a markedly disproportionate impact on the long-term carbon cycle, an impact that exceeds by an order of magnitude the expected impact based on areal extent alone.

References

- Andal E.S. (2002) Geological and geochemical characterization of the Plio-Pleistocene to recent volcanic rocks of the southeastern Luzon Volcanic Arc Chain: Implications to arc evolution. M.Sc. thesis, University of the Philippines.
- Andal E.S., Yumul G.P., Listanco E.L., Tamayo R.A., Dimalanta C.B. and Ishii T. (2005) Characterization of the Pleistocene Volcanic Chain of the Bicol Arc, Philippines: Implications for Geohazard Assessment. *Terr. Atmos. Ocean. Sci.* **16**, 865-883.
- Anonymous (1963) Geological Map of the Philippines. Department of Agriculture and Natural Resources Bureau of Mines, Manila.
- Arcilla C.A., Ruelo H.B. and Umbal J. (1989) The Angat ophiolite, Luzon, Philippines: lithology, structure, and problems in age interpretation. *Tectonophysics* **168**, 127-135.
- Bachman S.B., Lewis S.D. and Schweller W.J. (1983) Evolution of a forearc basin, Luzon Central Valley, Philippines. *AAPG Bull.* **67**, 1143-1162.
- Baltasar A.J. (1980) Interpretations of the water and gas chemistry from three geothermal areas in the Philippines - Manito in Albay, Biliran Island and Tongonan in Leyte. Orkustofnun: United Nations University.
- Bethke C. (2007) The Geochemist's Workbench. Hydrogeology Program, University of Illinois.
- Bevington, P.R. and Robinson, D.K. (2002) Data Reduction and Error Analysis for the Physical Sciences, 3rd ed. McGraw-Hill, New York
- Castillo P.R. and Newhall C.G. (2004) Geochemical Constraints on Possible Subduction Components in Lavas of Mayon and Taal Volcanoes, Southern Luzon, Philippines. *J. Petrol.* **45**, 1089-1108.

- Das A., Krishnaswami S., Sarin M.M., and Pande K. (2005) Chemical weathering in the Krishna Basin and Western Ghats of the Deccan Traps, India: Rates of basalt weathering and their controls. *Geochim. Cosmochim. Acta* **69**, 2067–2084.
- Defant M.J., Jacques D., Maury R.C., De Boer D. and Joron J. (1989) Geochemistry and tectonic setting of the Luzon arc, Philippines. *Geol. Soc. Am. Bull.* **101**, 663-672.
- Delmelle P., Kusakabe M., Bernard A., Fischer T., de Brouwer S. and del Mundo E. (1998) Geochemical and isotopic evidence for seawater contamination of the hydrothermal system of Taal Volcano, Luzon, the Philippines. *B. Volcanol.* **59**, 562-576.
- Derry L.A., Kurtz A.C., Ziegler K. and Chadwick O.A. (2005) Biological control of terrestrial silica cycling and export fluxes to watersheds. *Nature* **433**, 728-731.
- Dessert C., Dupre B., Gaillardet J., Francois L.M. and Allegre C.J. (2003) Basalt weathering laws and the impact of basalt weathering on the global carbon cycle. *Chem. Geol.* **202**, 257-273.
- Dessert C., Gaillardet J., Dupre B., Schott J. and Pokrovsky O.S. (2009) Fluxes of high- versus low-temperature water-rock interactions in aerial volcanic areas: Example from the Kamchatka Peninsula, Russia. *Geochim. Cosmochim. Acta* **73**, 148-169.
- DuFrane S.A., Asmerom Y., Mukasa S.B., Morris J.D. and Dreyer B.M. (2006) Subduction and melting processes inferred from U-Series, Sr-Nd-Pb isotope, and trace element data, Bicol and Bataan arcs, Philippines. *Geochim. Cosmochim. Acta* **70**, 3401-3420.
- Dyer S. D., Peng C., McAvoy D.C., Fendinger N.J., Masscheleyn P., Castillo L.V. and Lim J.M.U. (2003) The influence of untreated wastewater to aquatic communities in the Balatuin River, The Philippines. *Chemosphere* **52**, 43-53.
- Edmond J.M. and Huh Y. (1997) Chemical Weathering Yields from Basement and

Orogenic Terrains in Hot and Cold Climates. In: Tectonic uplift and climate change. New York, Plenum Press, pp.330-351.

Eklund T.J., McDowell W.H. and Pringle C.M. (1997) Seasonal variation of tropical precipitation chemistry: La Selva, Costa Rica. *Atmos. Environ.* **31**, 3903-3910.

Encarnación J.P., Mukasa S.B. and Obille Jr E.C. (1993) Zircon U-Pb Geochronology of the Zambales and Angat Ophiolites, Luzon, Philippines: Evidence for an Eocene Arc-Back Arc Pair. *J. Geophys. Res.* **98(B11)**, 19,991-20,004.

ESRI (2009) ArcGIS – The Complete Geographic Information System [online]. Redlands: ESRI. Available from <http://www.esri.com/software/arcgis/index.html> (accessed April 2, 2010).

Evans C.A., Casteneda G. and Franco H. (1991) Geochemical Complexities Preserved in the Volcanic Rocks of the Zambales Ophiolite, Philippines. *J. Geophys. Res.* **96(B10)**, 16251-16262.

Evans, M. J, Derry L. A., Anderson S. P. and France-Lanord C. (2001) Hydrothermal source of radiogenic Sr to Himalayan rivers. *Geology* **29**, 803-806.

Evans M.J., Derry L.A. and France-Lanord C. (2004) Geothermal fluxes of alkalinity in the Narayani river system of central Nepal. *Geochem. Geophys. Geosy.* **5**, Q08011.

Förster H., Oles D., Knittel U., Defant M.J. and Torres R.C. (1990). The Macolod Corridor: A rift crossing the Philippine island arc. *Tectonophysics* **183**, 265-271.

France-Lanord C., and Derry L.A. (1997) Organic carbon burial forcing of the carbon cycle from Himalayan erosion. *Nature* **390**, 65-67.

Fujita S., Takahashi A., Weng J., Huang L., Kim H., Li C., T.C. Huang F. and Jeng F. (2000) Precipitation chemistry in East Asia. *Atmos. Environ.* **34**, 525-537.

Gaillardet J., Dupre B., Louvat P. and Allegre C.J. (1999) Global silicate weathering and CO₂ consumption rates deduced from the chemistry of large rivers. *Chem.*

Geol. **159**, 3-30.

- Gaillardet J., Millot R. and Dupré B. (2003) Chemical denudation rates of the western Canadian orogenic belt: the Stikine terrane. *Chem. Geol.* **201**, 257-279.
- Gislason S.R., Arnorsson S. and Armannsson H. (1996) Chemical weathering of basalt in Southwest Iceland; effects of runoff, age of rocks and vegetative/glacial cover. *Am. J. Sci.* **296**, 837-907.
- Goldsmith S.T., Carey A.E., Lyons W.B. and Hicks D.M. (2008) Geochemical fluxes and weathering of volcanic terrains on high standing islands: Taranaki and Manawatu-Wanganui regions of New Zealand. *Geochim. Cosmochim. Acta* **72**, 2248-2267.
- Goldsmith S.T., Carey A.E., Johnson B.M., Welch S.A., Lyons W.B., McDowell W.H. and Pigott J.S. (2010) Stream geochemistry, chemical weathering and CO₂ consumption potential of andesitic terrains, Dominica, Lesser Antilles. *Geochim. Cosmochim. Acta* **74**, 85-103.
- Goldstein S.J. and Jacobsen S.B. (1987) The Nd and Sr Isotopic Systematics of River-Water Dissolved Material - Implications for the Sources of Nd and Sr in Seawater. *Chem. Geol.* **66**, 245-272.
- Hawkins J. and Evans C. (1983) Geology of the Zambales Range, Luzon, Philippine Islands: ophiolite derived from an island arc-back-arc pair. In *The Tectonics and Geologic Evolution of Southeast Asian Seas and Islands, Part 2, AGU Geophys. Mono.* **27** (ed. D.E. Hayes). pp 124-138.
- Kastner, T. (2009) Trajectories in human domination of ecosystems: Human appropriation of net primary production in the Philippines during the 20th century. *Ecol. Econ.* **69**, 260-269.
- Knittel-Weber C. and Knittel U. (1990) Petrology and genesis of the volcanic rocks on the eastern flank of Mount Malinao, Bicol arc (southern Luzon, Philippines). *J. Southe. Asian. Earth* **4**, 267-280.

- Ku Y., Chen C., Song S., Iizuka Y. and Shen J.J. (2009) A 2 Ma record of explosive volcanism in southwestern Luzon: Implications for the timing of subducted slab steepening. *Geochem. Geophys. Geosy.* **10**, Q06017.
- Kyoung Lee B., Hee Hong S., and Soo Lee D. (2000) Chemical composition of precipitation and wet deposition of major ions on the Korean peninsula. *Atmos. Environ.* **34**, 563-575.
- Liu Z., Zhao Y., Colin C., Siringan F.P. and Wu Q. (2009) Chemical weathering in Luzon, Philippines from clay mineralogy and major-element geochemistry of river sediments. *Appl. Geochem.* **24**, 2195-2205.
- Louvat P. and Allegre C.J. (1997) Present denudation rates on the island of Reunion determined by river geochemistry: Basalt weathering and mass budget between chemical and mechanical erosions. *Geochim. Cosmochim. Acta* **61**, 3645-3669.
- Louvat P. and Allegre C.J. (1998) Riverine erosion rates on Sao Miguel volcanic island, Azores archipelago. *Chem. Geol.* **148**, 177-200.
- Lyons W.B., Carey A.E., Hicks D.M. and Nezat C.A. (2005) Chemical weathering in high-sediment-yielding watersheds, New Zealand. *J. Geophys. Res.* **110**, F01008.
- McArthur J., Howarth R.J. and Bailey T.R. (2001) Strontium Isotope Stratigraphy: LOWESS Version 3: Best Fit to the Marine Sr-Isotope Curve for 0-509 Ma and Accompanying Look-up Table for Deriving Numerical Age. *J. Geol.* **109**, 155-170.
- McDermott F., Delfin Jr. F., Defant M., Turner S. and Maury R. (2005) The petrogenesis of volcanics from Mt. Bulusan and Mt. Mayon in the Bicol arc, the Philippines. *Contrib. Mineral. Petr.* **150**, 652-670.
- Meybeck M. (1987) Global chemical weathering of surficial rocks estimated from river dissolved loads. *Am. J. Sci.* **287**, 401-428.

- Meybeck M. and Ragu A. (1995) GEMS/Water Contribution to the Global Register of River Inputs (GLORI), Provisional Final Report. Geneva: UNEP/WHO/UNESCO.
- Milliman J.D. and Syvitski J.P.M. (1992) Geomorphic/tectonic control of sediment discharge to the ocean; the importance of small mountainous rivers. *J. Geol.* **100**, 525-544.
- Milliman J.D., Farnsworth K.L. and Albertin C.S. (1999) Flux and fate of fluvial sediments leaving large islands in the East Indies. *J. Sea Res.* **41**, 97-107.
- Montgomery D.R., Panfil M.S. and Hayes S.K. (1999) Channel-bed mobility response to extreme sediment loading at Mount Pinatubo. *Geology* **27**, 271-274.
- Mortlock R. and Froelich P. (1989) A simple method for the rapid determination of biogenic opal in pelagic marine sediments. *Deep-sea Res.* **36**, 1415-1426.
- Neal C. and Shand P. (2002) Spring and surface water quality of the Cyprus ophiolites. *Hydrol. Earth Syst. Sci.* **6**, 797-817.
- Oksanen, J. and Sarjakoski, T. (2005) Error propagation analysis of DEM-based drainage basin delineation. *Int. J. Remote Sens.* **26**, 3085-3102.
- Ozawa A., Tagami T., Listanco E.L., Arpa C.B. and Sudo M. (2004) Initiation and propagation of subduction along the Philippine Trench: evidence from the temporal and spatial distribution of volcanoes. *J. Asian Earth Sci.* **23**, 105-111.
- Pallister J.S., Hoblitt R.P. and Reyes A.G. (1992) A Basalt Trigger for the 1991 Eruptions of Pinatubo Volcano? *Nature* **356**, 426-428.
- Pokrovsky O. S, Schott J., Kudryavtzev D. I. and Dupre B. (2005) Basalt weathering in Central Siberia under permafrost conditions. *Geochim. Cosmochim. Acta* **69**, 5659-5680.
- Rad S., Louvat P., Gorge C., Gaillardet J. and Allegre C.J. (2006) River dissolved and solid loads in the Lesser Antilles: New insight into basalt weathering processes. *J. Geochem. Explor.* **88**, 308-312.

- Reuter H.I., Nelson A. and Jarvis A. (2007) An evaluation of void-filling interpolation methods for SRTM - data. *Int. J. Geogr. Inf. Sci.* **21**, 983-1008.
- SAS (2009) JMP, Version 8.0. SAS Institute, Inc., Cary, North Carolina, USA.
- Schellart W. and Rawlinson N. (2010) Convergent plate margin dynamics: New perspectives from structural geology, geophysics and geodynamic modelling. *Tectonophysics* **483**, 4-19.
- Schlesinger W. (1997) Biogeochemistry: An Analysis of Global Change, 2nd edition. San Diego, Calif., Academic Press.
- Sharp M., Tranter M., Brown G.H. and Skidmore M. (1995) Rates of chemical denudation and CO₂ drawdown in a glacier-covered alpine catchment. *Geology* **23**, 61-64.
- Stimac J.A., Goff F., Counce D., Larocque A.C.L., Hilton D.R. and Morgenstern U. (2004) The crater lake and hydrothermal system of Mount Pinatubo, Philippines: evolution in the decade after eruption. *B. Volcanol.* **66**, 149-167.
- Syvitski J.P.M., Vorosmarty C.J., Kettner A.J. and Green P. (2005) Impact of Humans on the Flux of Terrestrial Sediment to the Global Coastal Ocean. *Science* **308**, 376-380.
- von Huene R. and Scholl D.W. (1991) Observations at Convergent Margins Concerning Sediment Subduction, Subduction Erosion, and the Growth of Continental-Crust. *Rev. Geophys.* **29**, 279-316.
- Waterloo M.J., Schelleken J., Bruijnzeel L.A., Vugts H.F., Assenberg P.N. and Rawaqa T.T. (1997) Chemistry of Bulk Precipitation in Southwestern Viti Levu, Fiji. *J. Trop. Ecol.* **13**, 427-447.
- Wolff-Boenisch D., Gabet E.J., Burbank D.W., Langner H. and Putkonen J. (2009) Spatial variations in chemical weathering and CO₂ consumption in Nepalese High Himalayan catchments during the monsoon season. *Geochim. Cosmochim. Acta* **73**, 3148-3170.

Yumul G.P., Dimalanta C.B. and Jumawan F.T. (2000) Geology of the southern Zambales Ophiolite Complex, Luzon, Philippines. *Isl. Arc* **9**, 542-555.

Zakharova E.A., Pokrovsky O. S., Dupre B. and Zaslavskaya M.B. (2005) Chemical weathering of silicate rocks in Aldan Shield and Baikal Uplift: insights from long-term seasonal measurements of solute fluxes in rivers. *Chem. Geol.* **214**, 223-248.

CHAPTER 3

WATER BUDGET ANALYSIS FOR THE HAWAIIAN ISLANDS

Abstract

Hydrological fluxes in Hawai'i are poorly constrained, especially with respect to submarine groundwater discharge. This is a severe disadvantage for studies of fluxes of dissolved chemicals from the islands. In this chapter, I present an analysis of the hydrology of the Hawaiian Islands, in particular for the Big Island of Hawai'i and Kaua'i, performed using data from the USGS. A kriging model is used to derive surface runoff for the Big Island of Hawai'i and for Kaua'i. Submarine groundwater discharge is adopted from the results of USGS water balance reports for individual islands. On Kaua'i, it is necessary to adjust the USGS submarine groundwater discharge estimate for the base flow component of runoff. This is accomplished by calculating the total surface runoff on Kaua'i from the runoff kriging model, and subtracting baseflow from the total runoff using data from the USGS.

On the Big Island, the youngest island in the Hawaiian archipelago, submarine groundwater discharge greatly exceeds surface runoff. In the youngest parts of the island, nearly no surface runoff is observed. As the bedrock gets progressively older, the importance of surface runoff increases. On the Big Island of Hawai'i (the youngest island) the ratio of surface runoff to submarine groundwater discharge is 0.27, whereas on Kaua'i (the oldest island), this same ratio is 1.77. Landscape and climate also play a

role in the partition of water fluxes between submarine discharge and surface runoff. These results show that submarine groundwater discharge is a key component of the hydrological cycle throughout the life cycle of a hot spot volcano. This implies that current estimates of chemical fluxes from volcanic islands, where only surface waters are investigated, may be too low.

3.1. INTRODUCTION

The hydrological balance of volcanic oceanic islands is often under-constrained and major fluxes are poorly known. Poorly quantified hydrological processes such as evapotranspiration and submarine groundwater discharge, as well as a large number of small and mostly unmonitored streams, are the leading sources of this uncertainty. A knowledge of hydrological fluxes is a major requisite for constraining fluxes of chemical weathering products from oceanic islands and is therefore of significance to geochemists.

3.1.1. Motivation

This study of the water balance of the Hawaiian Islands has been undertaken as a necessary sub-task in a larger project that aims to quantify the fluxes of dissolved products of chemical weathering from the Hawaiian Islands via surface runoff and submarine groundwater discharge.

A large number of streams were sampled for chemical analyses on Kaua'i and the Big Island. Many of these streams have no discharge records, either historical or current. Since the chemistry of the streams is quite variable from place to place it is important

to have good estimates of discharge for individual streams in order to weight the chemical fluxes properly.

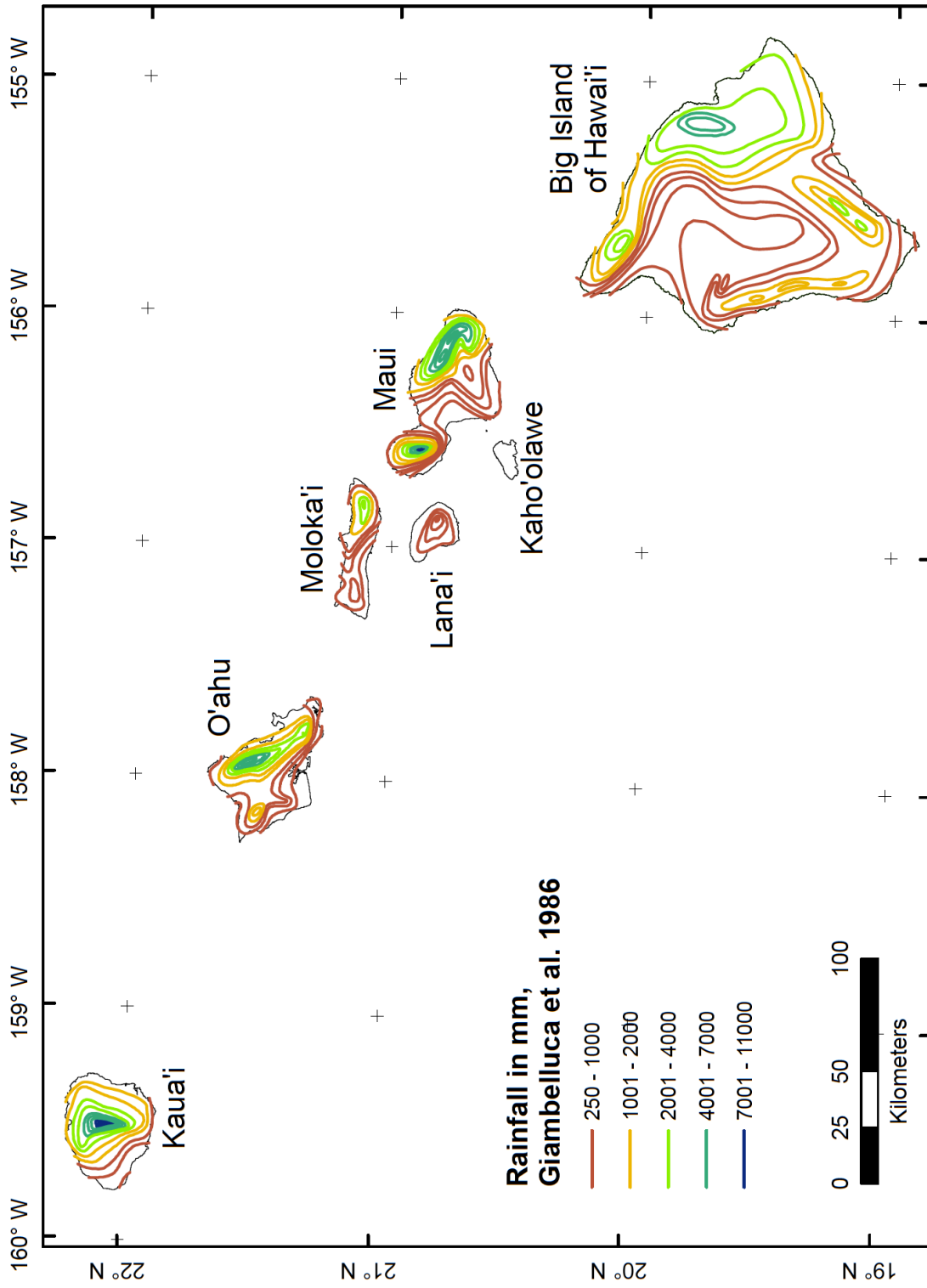
We also sampled several groundwater wells on the Big Island. The variability in groundwater chemistry is much smaller than in stream chemistry so we do not need to account for fluxes through each individual well, or even aquifer, in the same way as we need to do with streams. An assessment of the fluxes of groundwater is, however, needed in order to quantify the fluxes of solutes via groundwater discharge.

The two main data products desired from this study are 1) total runoff values for the Big Island and Kaua'i, converted into discharge in unmonitored watersheds, and 2) values for the submarine groundwater discharge from all the Hawaiian Islands, especially Kaua'i and the Big Island.

3.1.2. Study area

The 600 km long, NW-SE trending Hawaiian Archipelago consists of five main islands (Big Island of Hawai'i, Maui, Moloka'i, O'ahu and Kaua'i) and several smaller ones, of which Lana'i, Kaho'olawe and Niihau are the most important ones (Figure 3.1). The Hawaiian Islands are located at the northern edge of the tropics, between 19°N and 22°N, in the middle of the Pacific Ocean. The islands comprise the youngest volcanoes in the 6000 km long Hawaiian-Emperor Volcanic Chain that was formed by the interaction of the Hawaiian mantle plume with the Pacific Plate. Volcanism over the plume head produced volcanic islands on the overlying Pacific Plate. As the Pacific Plate drifted steadily to the NW relative to the mantle plume, the volcanoes were transported away from the plume and the zone of active volcanism. In this manner, a chain of islands, successively younger towards the SE, was formed.

Figure 3.1. A map of the Hawaiian Islands, showing the average yearly amount of rainfall (Giambelluca et al., 1986) on the major islands. This study focuses on Kaua'i and the Big Island.



3.1.3. Geology of the Hawaiian Islands

The Hawaiian volcanoes go through a well-documented succession of eruptive stages (Peterson and Moore, 1987). At the birth of a volcano alkaline magma predominates, replaced by tholeiites that prevail during the submarine and subaerial shield building stage. During the shield building stage over 95% of the volume of the edifice is emplaced. Thin and volumetrically insignificant alkaline lava caps are erupted in the waning phase of shield building. After a period of erosion and volcanic quiescence, many of the Hawaiian volcanoes have a post-erosional phase with formation of alkaline cinder cones. The oldest subaerial island in Hawai'i is Kaua'i, where the oldest shield-building rocks have been dated at 5.1 Myr old (McDougall, 1979). The islands decrease in age towards the SE. Representative ages of shield building rocks are ~ 3-2.5 Myr on O'ahu, ~ 1.5 Myr on Moloka'i and around 1 Myr on Maui (McDougall, 1964). On the Big Island, rock ages range from 0.45 Myr on Kohala Peninsula (McDougall and Swanson, 1972) to zero for the lavas from the current eruptive episode of Kilauea. At the site of the submarine volcano Lo'ihi, a new island will most likely form in the future.

Up to 90% of the volume of Hawaii's volcanoes may be hidden from view under sea level (Schmincke, 2004). The Big Island of Hawai'i is, in terms of volume and absolute height, the largest mountain on Earth. It reaches from the sea floor more than 5000 m to sea level, and additional 4000 m to the peak of its two massive volcanoes, Mauna Kea and Mauna Loa. The total elevation is higher than that of the Himalayas. The Hawaiian volcanoes cause isostatic subsidence of the underlying Pacific Plate, forming a canoe-shaped trough around the islands called the Hawaiian Deep (Moore, 1987). The isostatic compensation is complete within a million years or so (Moore,

1987) and thermal contraction of the underlying plate becomes the dominant cause of subsidence of the volcanic edifice (Watts, 1978). Some 200 km east of the Big Island, a flexural bulge of several hundred meters (Watts and ten Brink, 1989) causes temporary uplift as the volcanoes ride over it (Grigg and Jones, 1997).

As volcanic activity wanes and ceases, the islands lose mass by river erosion and submarine landslides. Eventually, the combined efforts of thermal subsidence and erosion reduce the islands to below sea level. The resulting seamounts are transported on the Pacific Plate to the Kurile-Kamchatka Trench, where the seamount chain is eventually subducted under the Kamchatka Peninsula.

The mantle plume produces mainly tholeiite, a volcanic rock of mafic composition. Tholeiite magma can solidify as either paho'eho'e or a'a lava. Paho'eho'e flows are generally much less viscous than a'a lavas and can flow quite far from the vent in lava tubes. Paho'eho'e lava fields are composed of thin (1-10m), interfingering tongues of lava that stack up to form thick lava piles. Paho'eho'e lavas are often very rich in vesicles formed by exsolved magmatic gases. The surface of a'a lava flows is rugged and blocky, in stark contrast to the smooth surface characteristic of paho'eho'e lavas. During emplacement, blocks of cinder and rubble from the surface of the advancing a'a flow fall down the front and are overridden by the lava flow itself. This results in lavas that have highly porous basal and surface breccias and a very dense, impermeable core. Paho'eho'e and a'a and lavas are chemically identical. The former may turn into the latter (but not vice versa) during emplacement as viscosity increases due to cooling and crystallization.

Most Hawaiian extrusive volcanic rocks have very high porosity and permeability. Hydraulic conductivity ranges from 150 - 10,000 m/d (all hydraulic conductivity values from Oki et al., 1999 and references therein) in unweathered basalt but is reduced to between 0.02 - 85 m/d in weathered basalts. Pyroclastic flows have intermediate hydraulic conductivity of 0.3 - 150 m/d. Dikes have very low hydraulic conductivity (10^{-6} - 10^{-3} m/d) and act as important aquitards in Hawai'i. For comparison, hydraulic conductivity in granite is on the order of 10^{-8} - 10^{-6} m/day, rising to 10^{-4} - 10^{-2} m/day in sandstone (Bear, 1988). Because of the different hydrologic properties of the various rock morphologies, ground water aquifers in Hawai'i are either basal (fresh ground water sitting on top of sea water), dike-confined or perched on weathered soil horizons or pyroclastic flows.

To sum up, the bedrock on Hawai'i is extremely porous and has generally very high permeability. On the youngest volcanoes of the Big Island, Kilauea and Mauna Loa, there are no permanent streams and only very few ephemeral ones, because all precipitation that does not evaporate goes straight to ground water recharge. As landscapes age and lavas weather, soils form and infiltration into the groundwater system is reduced. Consequently, stream flow starts to cut into the lava pile and valleys form. Surface runoff from the landscape becomes more persistent in terms of temporal occurrence, although it remains highly variable in magnitude.

3.1.4. Climate

River runoff, or river discharge normalized by watershed area, is highly variable in Hawai'i. Both the hydrological properties of the rocks and the patterns and magnitude of rainfall are important in shaping the hydrology of the regions under study here. The magnitude of rainfall in Hawai'i is fairly well known and has been monitored since the

1840's by various entities, such as plantation owners and private citizens, the National Weather Service and the USGS (Giambelluca et al., 1986). Currently, there are over 100 rain gages operating in the state (see http://www.prh.noaa.gov/hnl/hydro/daily_archive/HRS_archive.php). Figure 3.1 shows a map of the rainfall distribution in Hawai'i (Giambelluca et al., 1986). This rainfall data compilation is the most widely used one for water budget calculations in the state.

The following discussion of climate in Hawai'i is based largely on the rainfall distribution map of Figure 3.1 and on Juvik and Juvik (1998). Trade winds from the northeast prevail throughout most of the year. These moisture-laden winds rise when they encounter the steep topography of the islands, causing the pronounced orographic rainfall maxima in the eastern parts of all the islands. A temperature inversion, where warm, descending air overlies cooler, ascending air, traps surface air masses below elevations of between 1500 and 3000 m. The upper slopes of the high mountains of Hawai'i, Mauna Loa and Mauna Kea on the Big Island and Mt. Haleakala on Maui, receive very little moisture because of this temperature inversion and contribute negligibly to both ground water recharge and surface runoff. The most extreme orographic rain falls on Kaua'i, where extremely steep topography leads up to Mt. Wai'ale'ale (1569 m a.s.l.). Annual rainfall at the weather station at the summit of Mt. Wai'ale'ale has reached over 11000 mm/yr, making it one of the wettest places on Earth.

A secondary rainfall maximum is observed in the Waianae Mountains in western O'ahu, caused by further orographic rising of the trade winds blowing over the island. The air masses have at that point lost much of their moisture content so the second rainfall maximum is much smaller than the first one. In the Kona and Ka'u regions of

the Big Island secondary rainfall maxima are also observed. These regions are largely sheltered from the persistent trade winds by the massive volcanoes Mauna Loa and Mauna Kea. Temperature differences between land and sea can therefore build up over the day. During the afternoon, the heated air over land rises and the cooler air over the ocean rushes in and cools convectively as it rises over land, precipitating the moisture it held.

The intense orographic rainfall on the windward side of the islands leaves little moisture in the air and a rain shadow exists on the leeward side of the islands. This effect is very pronounced on the NW side of the Big Island where rainfall drops below 250 mm/yr, often regarded as the threshold for desert conditions. The spatially uneven distribution of rainfall is one of the main reasons for the spectacular diversity of ecosystems and environmental conditions observed in Hawai'i.

Hawaiians recognize two seasons - winter and summer. Winters are cool, breezy and wet and generally last from October through April. Summer lasts from May through September. The climate is equitable with low day-to-day and month-to-month variability. In Honolulu, the range of annual maximum and minimum temperature is 21.2 - 29.3°C, with a mean of 25.3°C. Temperatures are significantly cooler at altitude.

3.2. METHODS

3.2.1. Setting up the water budget

A common conceptualization of water budgets has the following components: Rainfall (P), direct runoff (DR), actual evapotranspiration (AE), groundwater recharge (G) and change in soil moisture storage (Δ SS) (Thornthwaite, 1948; Thornthwaite and Mather,

1955). In Hawai'i, the water budget is most often balanced on the groundwater recharge so that the mass balance equation takes the form of (see for instance Shade, 1995a):

$$G = P - DR - AE - \Delta SS \quad (3.1a)$$

The residual from the mass balance equation will contain all the errors associated with the input parameters and therefore it is important to use as input those parameters that have the least error associated with them. This formulation is generally the most convenient one because groundwater recharge is the hardest component of the water budget to calculate directly. Much of the groundwater recharge in Hawai'i discharges directly into the ocean (often referred to as submarine groundwater discharge, or SGD) and although many attempts (Knee et al., 2005; Street et al., 2008; Peterson et al., 2009) have been made to quantify that discharge directly, none have been successful at the scale needed for this study (all the Hawaiian Islands). The calculation of actual evapotranspiration is also problematic, especially over large, non-homogeneous areas. Pan evaporation is fairly well constrained in Hawai'i and although the conversion of pan evaporation rates into rates of AE is not straightforward, it is nonetheless a considerably more developed science than the direct modeling, or direct measuring, of groundwater recharge.

An important component of all the studies used here is the separation of stream flow into base flow and direct runoff. Base flow refers to rain water that initially drains into the groundwater system, be it shallow or deep, and later enters streams when the stream bed intersects the groundwater table. Direct runoff is rainwater that does not infiltrate deep into the subsurface but instead drains directly into the stream either

from direct overland flow or through soil. In this dissertation, the term "direct runoff" is used in this sense, whereas the terms "total runoff" and "surface runoff" are used interchangeably for the sum of direct runoff and base flow (i.e., total discharge), normalized over the watershed area.

Changes in soil moisture storage are important for modeling the water balance on short timescales, i.e. days or weeks. We assume that on average, it equals zero on an annual timescale and omit it from our calculations, reducing equation 3.1a to

$$G = P - DR - AE \quad (3.1b)$$

3.2.2. Data sources, data compiling

We made use of published data to perform this study and no new hydrological data were produced in the field. Some of the data we used unchanged from the source, while other data were processed to better meet the needs of our study of chemical fluxes. A complete list of all data sources and how they were used is presented in Table 3.1. In summary, the water budget studies were used to derive values for groundwater recharge and discharge data from the USGS were used to model total runoff on Kaua'i and the Big Island to produce discharge values for unmonitored watersheds.

The following is a short description of the methodology employed in the water budget studies. The reports for Kaua'i and Moloka'i treat each island as a single aquifer system, the other three islands are divided up into several discrete aquifers. All the listed studies take the approach to water budgeting described in equation 3.1a above. Discharge data from the USGS are used to estimate base flow and direct runoff using

various hydrograph separation procedures. Actual evapotranspiration is estimated on a daily, weekly or monthly timescale by combining the potential evapotranspiration data of Ekern and Chang (1985) with a soil water storage budget that propagates soil moisture excess and deficit through time. Groundwater recharge is found by balance in most of the studies, except for in the study of Shade (1997) of the water budget of Moloka'i, where a slightly more complex procedure is used that involves averaging of two models. In the first model, soil water excess is allocated to groundwater recharge, and in the second model, it is allocated to actual evapotranspiration. Results from the two models are averaged to yield the final water budget for Moloka'i.

Table 3.1. Overview of the data sources used in this study.

Island	Data source	Authors	Used for
All	USGS Water Data for the Nation, Historical Surface Water Data	USGS, 2010	R*
All (Hawai'i)	Water Resources Protection Plan, Volumes I and II	State of Hawaii, 1990	G*
Kaua'i	Water Budget for the Island of Kauai, Hawaii	Shade, 1995a	G
O'ahu	Water Budget and the Effects of Land-Use Changes on Ground-Water Recharge, Oahu, Hawaii	Shade and Nichols, 1996	G, R
Moloka'i	Water Budget for the Island of Molokai, Hawaii	Shade, 1997	G, R
Maui	Water Budget of East Maui, Hawaii	Shade, 1999	G, R
Maui	Effects of Agricultural Land-Use Changes and Rainfall on Ground-Water Recharge in Central and West Maui, Hawaii, 1926-2004	Engott and Vana, 2007	G
Hawai'i	Water Budget for the Kohala Area, Island of Hawai'i	Shade, 1995b	G
Hawai'i	Ground Water in Kilauea Volcano and Adjacent Areas of Mauna Loa Volcano, Island of Hawai'i	Takasaki, 1993	G, R
Hawai'i	Water Resources of the South Kona/Ka'u Master Plan Area	Waimea Water Services, Inc., 2004	G, R

* G = ground water recharge, R = surface runoff

Separate USGS water budgets for E and W Maui were combined into a comprehensive water budget for Maui (Figure 3.2a). Many reports describe and calculate the water budget for various regions of the Big Island but no island-wide synthesis was found. Four water budget studies were used to compile a comprehensive water budget for the Big Island (Figure 3.2b). The smaller islands of Lana'i, Kaho'olawe and Ni'ihau were omitted from this study.

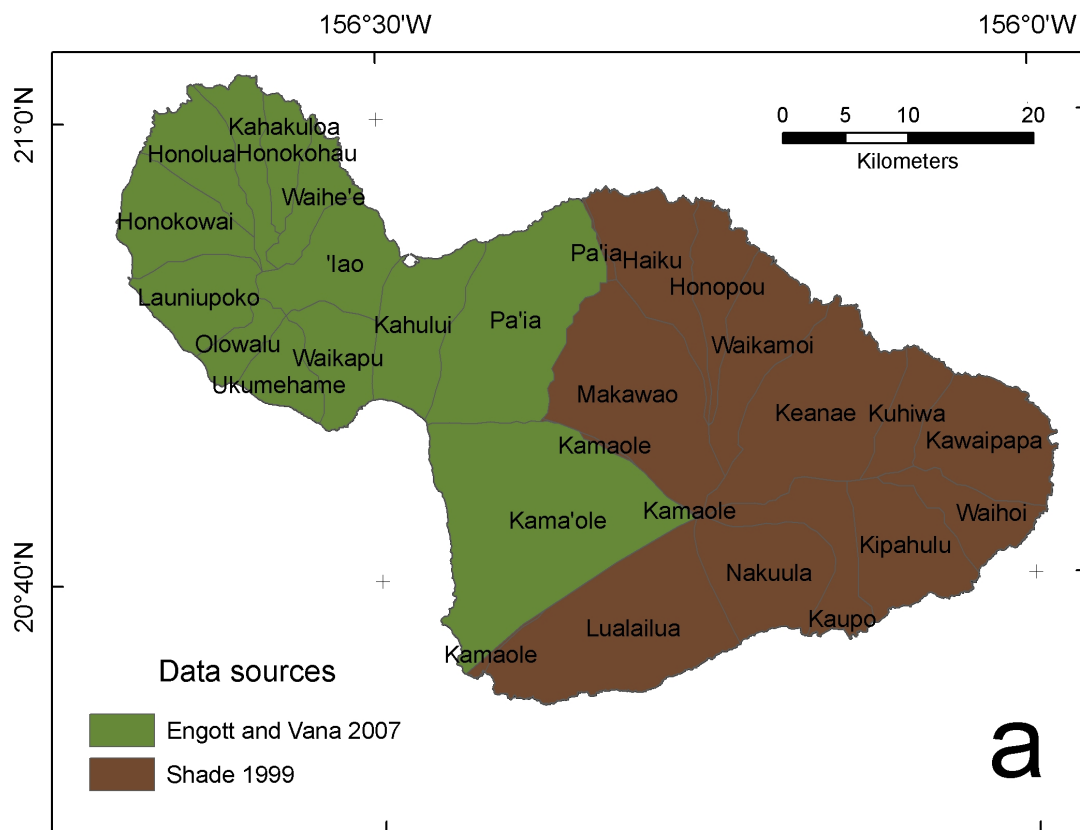
The regions of study in the two water reports on Maui overlap in the central portion of the island. We digitized aquifer maps from both of these studies and merged them so that the more recent dataset was retained in areas of overlap. Water budget data for the Big Island were treated in the same way; data from more recent reports superseded data from older reports wherever they overlapped.

The reports we use always give water fluxes in units of volume. We normalized the fluxes to aquifer area to facilitate the comparison of fluxes between aquifers and between different methods of estimating fluxes.

3.2.3. Surface runoff and discharge

In addition to the water budget studies of the USGS, we used published data for stream discharge from the USGS to estimate total runoff for individual unmonitored streams on Kaua'i and the Big Island. Long-term discharge data are available from the USGS for a large number of streams in Hawai'i. The largest concentration of monitored catchments is on Kaua'i and on O'ahu (30 and 45 streams with more than 5 years of discharge data, respectively (see Table 3.2).

Figure 3.2. Maps showing the aquifers of Maui and the Big Island and what data source was used for each aquifer in the comprehensive water budgets presented in this chapter. a) Maui b) Big Island.



All available discharge measurements for all watersheds on the Big Island and on Kaua'i were compiled and the average discharge was computed. We included data from all streams that had been monitored for 5 years or more, regardless of when the monitoring took place. The average was calculated on an $n \times 12$ month basis, $n \geq 2$. This yielded time series spanning, for instance, August 1912 to August 1914, June 1915 to June 1918 and finally July 1919 to July 2007 (USGS station nr. 16068000, East Branch of the North Fork of Wailua River, near Lihue, Kaua'i, HI). No stream was included that has a total of less than 5 years of discharge data. Discharge in these basins is very variable from year to year and using less than 5 years worth of data for inferring the long-term discharge carries the risk of either significantly over- or underestimating the long-term annual discharge. We excluded discharge data from the W and S parts of the Big Island. These regions have nearly no surface runoff and the little surface runoff that does occur only happens in flash floods and for a few days after very heavy rains, in very few and rather small basins. Discharge in the few gauged streams in these regions is therefore not likely to be representative for discharge from these regions as a whole.

Once the discharge data had been compiled, the discharge was divided by the area of the drainage basin (extracted from the USGS database and/or computed from a watershed shapefile in ArcGIS) to arrive at the average total runoff, in mm/yr, for each basin. The total runoff was plotted in ArcMap and the Geostatistical Analyst extension used to derive parameters for a kriging model, which predicts modeled values (here, total runoff) in places where no measurements exist.

Discharge and total runoff are related, but not identical, quantities. Discharge is the total volume of water that is transported through a watershed past a gauging point.

Table 3.2. List of streams with more than 5 years of published discharge data from the
USGS

Table 3.2

USGS Site name	USGS Site Number	Area km ²	Kriging model inputs		Kriging model outputs		Period of record used
			Mean annual Q	CV, annual Q	Mean annual Q	Q	
			10 ⁶ m ³ /yr	%	10 ⁶ m ³ /yr	10 ⁶ m ³ /yr	
Big Island							
Wailuku River at Piihonua	16704000	386	243	40	n.a.	01/71-01/01	
Wailuku River at Hilo	16713000	638	449	46	n.a.	3/77-3/79, 6/80-6/87, 10/88-10/95	
Honolii Stream near Papaikou	16717000	31.90	115	33	85	01/71-01/01	
Alia Stream near Hilo	16717600	1.61	11	15	5	5/62-5/72	
Pohakupuka Stream near Papaaloa	16717800	5.66	24	34	24	5/62-5/79	
Manowaiopae Stream near Laupahoehoe	16717820	4.23	7	46	9	9/65-9/71	
Kawainui Stream near Kamuela	16720000	3.99	14	27	17	01/71-01/01	
Kawaiiki Stream near Kamuela	16720300	1.24	3	36	7	01/71-01/99	
Alakahi Stream near Kamuela	16725000	2.17	7	31	5	01/71-01/01	
Wailoa Stream near Waipio	16732200	37.50	67	13	96	3/64-3/69	
Waiilikahi Stream near Waimanu	16737000	1.97	9	23	10	4/39-4/59	
Kaimu Stream near Waimanu	16738000	2.33	8	52	6	4/39-4/47, 7/50-7/52	
Punalulu Stream near Waimanu	16739000	1.71	6	38	3	4/39-4/52	
Waiaalala Stream near Waimanu	16740000	0.31	1	50	3	4/39-4/52	
Paopao Stream near Waimanu	16741000	0.83	3	31	3	3/39-3/52	
E. Br. Honokane Nui Stream near Nuilii	16747500	12.90	24	10	37	6/63-6/69	
Kohakohau Stream near Kamuela	16756000	6.06	8	48	16	4/56-4/66	
Keanuiomano Stream near Kamuela	16756500	2.87	9	28	3	11/63-10/72	
Waikoloa Str at Marine Dam near Kamuela	16758000	3.06	9	33	10	01/71-01/01	
Hauani Gulch near Kamuela	16759000	1.22	2	47	2	01/71-01/01	

Table 3.2 (continued)

USGS Site name	USGS Site Number	Area km ²	Kriging model inputs		Kriging model outputs		Period of record used
			Mean annual Q	CV, annual Q	Mean annual Q	Mean annual Q	
			10 ⁶ m ³ /yr	%	10 ⁶ m ³ /yr	10 ⁶ m ³ /yr	
Kaua'i							
Kawai'oi Stream near Waimea	16010000	10.2	30	28	29	07/19-07/09	
Waimea River at alt. 840 ft near Waimea	16016000	51.8	47	31	79	6/25-6/48, 3/51-3/68	
Waialae Stream at alt 3,820 ft near Waimea	16019000	4.64	18	30	17	02/20-02/32, 07/52-07/09	
Waimea River below Kekaha Ditch intake near Waimea	16028000	114	68	63	189	05/25-05/47, 2/48-02/55	
Waimea River near Waimea	16031000	150	110	51	203	08/10-08/17, 12/43-12/63, 10/65-	
Koula River at Koula near Eleele	16047000	32.6	79	26	8	09/10-09/16, 7/37-7/39	
Huleia Stream near Lihue	16055000	45.6	33	38	45	01/13-01/16, 03/67-03/70	
South Fork of Wailua River near Lihue	16060000	58.0	106	43	129	01/12-01/18, 06/19-06/20, 05/21-	
North Fork of Wailua River at alt 650 ft near Lihue	16063000	13.7	65	32	54	07/15-07/18, 07/19-07/85	
East Branch of North Fork of Wailua River near Lihue	16068000	16.2	43	25	46	08/12-08/14, 06/15-06/18, 07/19-07/07	
North Fork Wailua River near Kapaa	16071000	46.4	98	39	130	01/71-01/01	
Left Branch Opaekaa Stream near Kapaa	16071500	1.68	2	43	5	01/71-01/01	
Kapaa Stream near Kealia	16078000	7.90	30	26	18	4/11-4/14, 4/16-4/20	
Kapaa Stream at Kapahi Ditch intake near Kapaa	16080000	10.0	15	66	23	01/71-10/85	
Halaulani Stream at alt 400 ft near Kilauea	16097500	3.08	10	26	11	01/71-01/01	

Table 3.2 (continued)

USGS Site name	USGS Site Number	Area km ²	Kriging model inputs		Kriging model outputs		Period of record used
			Mean annual Q	CV, annual Q	Mean annual Q	Mean annual Q	
			10 ⁶ m ³ /yr	%	10 ⁶ m ³ /yr	10 ⁶ m ³ /yr	
Anahola Stream near Kealia	16089000	11.1	18	43	23	01/71-01/01	
Pohakuhonu Stream near Kilauea	16097000	4.48	7	31	12	11/57-10/72	
Kalihiwai River near Hanalei	16098000	9.43	44	17	28	4/14-4/15, 7/15-7/23	
Hanalei River at alt 625 ft near Hanalei	16101000	18.6	70	39	83	2/14-1/52, 7/52-8/55	
Hanalei River near Hanalei	16103000	48.4	203	18	216	1/12-1/19, 1/63-1/07	
Waioli Stream near Hanalei	16105000	4.69	28	25	25	7/14-7/18, 7/19-7/32	
Lumahai River near Hanalei	16106000	18.0	104	21	86	7/14-7/17, 7/20-7/33	
Waiiha River near Hanalei	16108000	26.4	122	23	118	01/71-01/01	
Hanakapiai Stream near Hanalei	16115000	7.07	15	25	20	01/32-01/52	
Hanakoa Stream near Hanalei	16116000	1.29	5	30	9	1/1/32-12/31/51	
Kalalau Stream near Hanalei	16117000	4.01	6	24	9	01/32-01/55	

Taking this value and dividing it evenly over the area of the watershed gives the total runoff. Discharge has units of volume/time, whereas runoff has units of length/time. Runoff can be conceptualized as the depth of water that leaves each point in the watershed over a given amount of time, usually a year. Discharge between basins is not comparable unless the basins are of the same size, whereas runoff enables the comparison of water budgets of different basins of widely different sizes. The basin-size-independence of runoff allows us to model it spatially, something we cannot do with discharge. Once the runoff has been modeled, it is possible to convert it back to discharge by multiplying the modeled runoff with the area of the pixels in the model. This is an important point to keep in mind for the following discussion.

Kriging is a geostatistical technique used to interpolate values between measured locations to predict values at unmeasured locations. Originally developed for mining applications, the technique is in widespread use today in environmental sciences and geology, to name a few applications. Kriging "provides a best linear unbiased estimate of an unmeasured value calculated from weighted values measured in a local neighborhood" (Nielsen and Wendroth, 2003, p. 119) and can also provide the user with the magnitude of the error of the interpolated variable. A brief summary of the kriging procedure will be given here; the reader is referred to Chapter 5 in Nielsen and Wendroth (2003) for a more detailed treatment of the subject. The following discussion is largely based on chapters 4 and 5 in Nielsen and Wendroth's book (2003).

The first step to fitting a kriging model is to investigate the spatial auto-correlation in the data. Auto-correlation is similar to the concept of correlation between two different variables, except that in auto-correlation we are interested in the correlation between

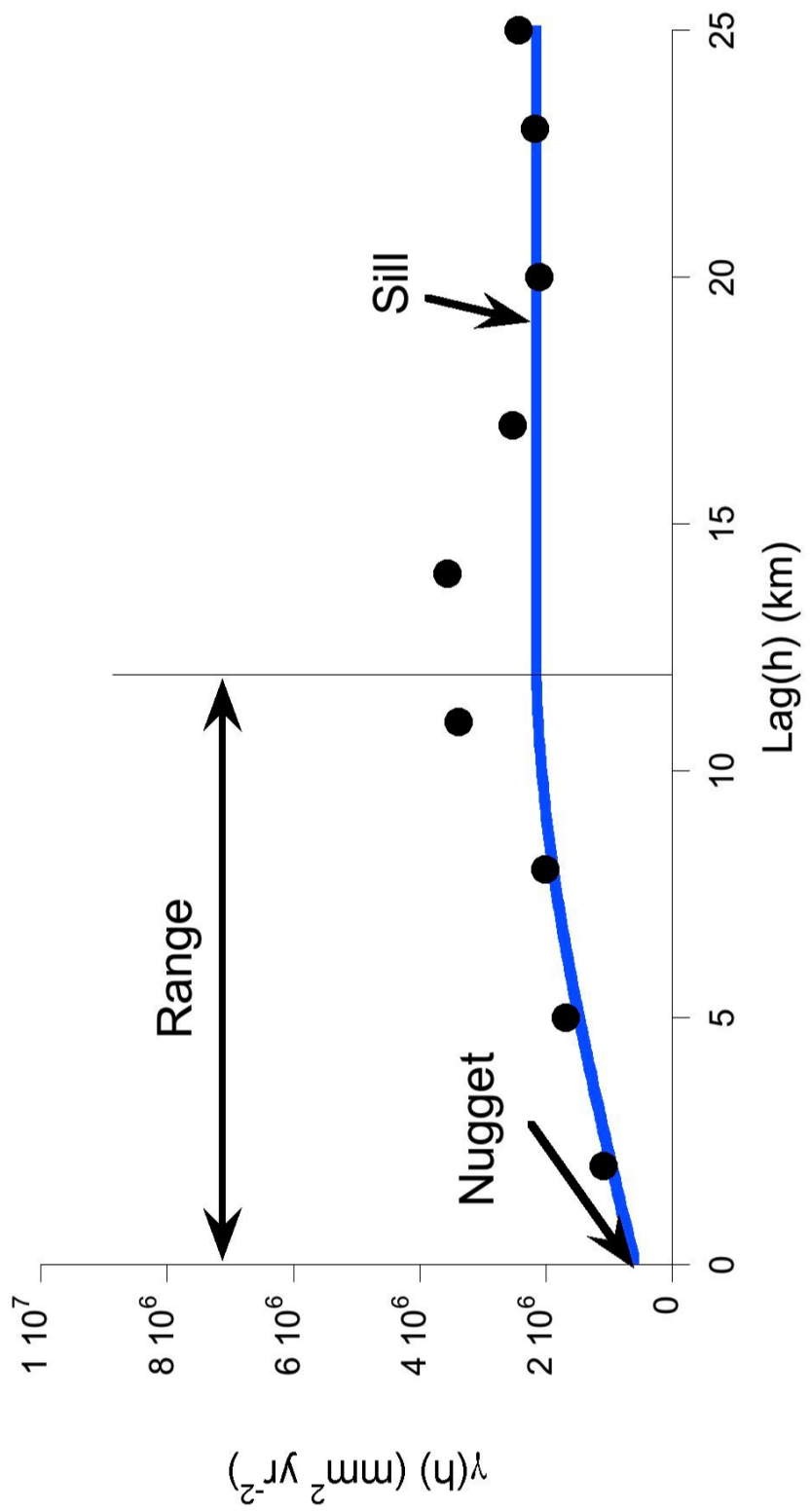
values for the same variable, measured at different locations. As the distance between pairs of locations varies, so the correlation between the variable at the two locations may vary in a systematic manner, in which case the variable is said to be spatially auto-correlated.

A semivariogram for surface runoff in the USGS-monitored watersheds on Kaua'i is shown in Figure 3.3. The variance (γ) is shown on the y-axis as a function of the lag (h), or distance between pairs of observations. In this case, there is considerable scatter in the data but it is obvious that at short distances, surface runoff values are on the average more similar (low values of γ) than dissimilar (large values of γ). The blue line on the semivariogram is a theoretical model for the shape of the variance as a function of the lag distance. We used a spherical model that rises relatively fast up to the maximum variance (termed sill) and then levels off to be invariant as the lag distance increases. The y-intercept is the nugget variance, 582622 mm²/yr² or 763 mm/yr, for the theoretical standard deviation at $h = 0$ km. The distance at which the variance in surface runoff becomes invariant to increased distance is called the range of the semivariogram. In this dataset, the range is at 12.6 km, as is seen by the slope of the spherical semivariogram model leveling off at that distance.

We followed the methodology laid out by Hengl (2006) to select an appropriate grid cell size in our kriging model. We used the equation for inspection density of point data (see Table 1, Hengl, 2006). As a compromise between the coarsest and the finest legible resolution, Hengl recommends using the equation

$$p = 0.0791 \times \sqrt{\frac{A}{N}} \quad (3.2)$$

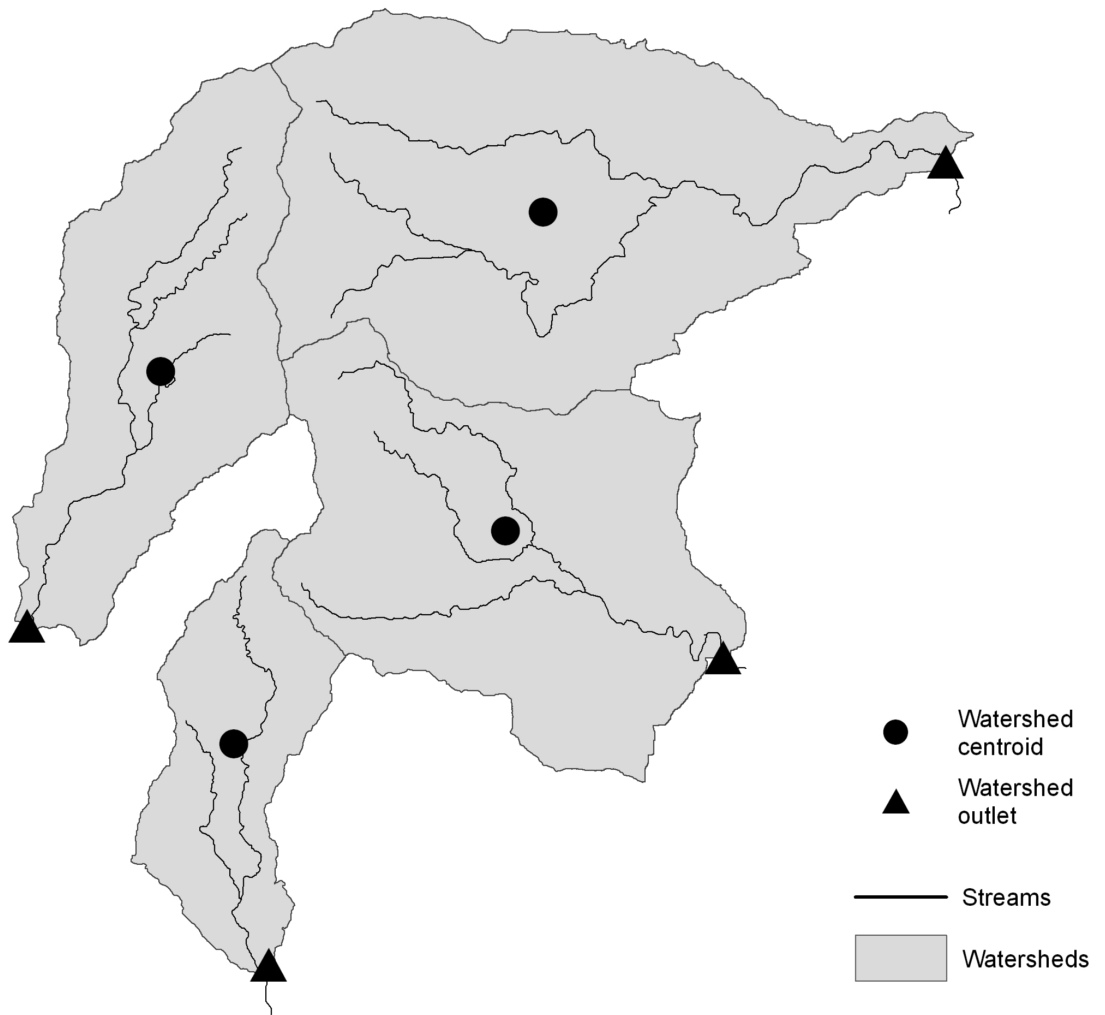
Figure 3.3. Semivariogram for runoff on Kauai.



where A = area and N = number of point observations. On Kaua'i, $A = 1432 \text{ km}^2$ and N = number of streams employed in kriging = 26. On the Big Island, we kriged over an area that is 2277 km^2 , using $N = 20$ streams. The resulting optimal cell sizes are 588 m for Kaua'i and 844 m for the Big Island. We, somewhat conservatively, set the grid cell size in our models for both islands at 890 m, to be consistent across the two islands and to make the total runoff grid cell size compatible with other rasters we used in this study, such as precipitation rasters.

In kriging, each data point is assumed to represent an area around itself. There may be directional trends in the data, where the spatial autocorrelation is larger in a given direction, but every pixel is nonetheless assumed to impact others around it in every direction to at least some extent. This is important in our study because average surface runoff is a value that represents an entire watershed and yet discharge is monitored at one end of a watershed, such that the integrated average surface runoff at a gauging site does not contain any information about surface runoff in the downstream direction. We investigated the effect of locating the data point for surface runoff at both the gauging site at the outlet of the watershed and at the centroid of the watershed as determined by ArcGIS (Figure 3.4). For each island, we constructed two kriging models - one where the data points are located at the gauging site and the other where the data points are located at the centroid of the watershed. The results from the two models were compared to measured discharge for each of the streams monitored by the USGS and used as input for the model. Based upon the correlation with measured discharge, discharge for streams where no measurements exist was calculated using the model that performed better on each island.

Figure 3.4. Runoff modeling for each island was performed twice, once where the runoff data point were located in the center of the watersheds (centroids) and once where the data points were located at the outlet of the watershed (outlets).



On the Big Island, we limited our kriging total runoff model to the Kohala Peninsula, the Hamakua Coast and North Hilo, including the town of Hilo. The surface runoff model does not include all of Wailuku River (the largest river on the Big Island) but long-term discharge measurements do exist for the river and thus modeled surface runoff is not needed. No eligible streams were omitted from the kriging on Kaua'i. The kriging surfaces calculated for Kaua'i and the surface runoff-active parts of the Big Island are best defined in the immediate neighborhood of the input (total runoff) data points and the method does not define a surface beyond the extent of the spatially outermost data points.

On the Big Island, we inserted “dummy” data points, where total runoff = 0 mm/yr (see Chapter 3.3.1.1.), in order to cover a larger area and more of the streams sampled than would have been possible given the number and locations of gauged streams. This approach, to insert 'dummy' or additional data points with a user-defined value into a kriging model, is sometimes applied when data are missing but the value of the missing data can be estimated with a reasonable degree of confidence (see for instance Berman and Turner, 1992; Baddeley and Turner, 2005; Waagepetersen, 2008). In the current case, it is reasonable to assume that there is no surface runoff, beyond occasional flash floods, where the dummy points were inserted. The same is not true for Kaua'i and no attempt was made to extend the kriging surface there beyond the reach of monitored streams. Table 3.3 contains parameters related to the kriging models for the Big Island and Kaua'i.

The total runoff rasters generated in the kriging models were cut to the outlines of the watersheds we needed discharge data for. The resulting watershed rasters were exported as ascii-files and processed in Excel; discharge (total runoff × area) was

computed for each pixel and summed up to give the total discharge (referred to as "kriged discharge") per watershed. To check the quality of our models, we calculated the kriged discharge for all the gauged streams used as inputs into our model and compared the results with the actual measured discharge.

Table 3.3. Parameters related to the kriging models for the Big Island and Kaua'i

	Big Island of Hawai'i	Kaua'i
General model properties		
Type of kriging	Ordinary	Ordinary
Trend order	None	First
Semivariogram properties		
Variogram model type	Spherical	Spherical
Lag size (m)	265.5	2111
# lags	12	12
Nugget (mm ² /yr ²)	0	582622
Sill (mm ² /yr ²)	4108916	1571228
Range (m)	31102	12560
Neighbor search		
Type	Standard	Smooth
Continuous factor	n.a.	0.5
Search radius	Variable	Variable
# neighbors	12	10-30

We did not employ a one-out methodology (model a separate kriging surface for each monitored stream from all the monitored streams except for the one being modeled),

because of time constraints. The fit between observed and modeled discharge that is presented in Chapter 3.3, “Results”, may therefore be somewhat artificially high.

3.2.3.1. *Uncertainties in discharge modeling*

Kriging models do not explicitly account for the actual observed error in the input variables. Instead, the kriging variance is often used as a measure of error in the model. The kriging variance is indeed a measure of the spatial variability of the input variable, but it is not a measure of the reliability of the kriging estimate (Nielsen and Wendroth, 2003) and is therefore not suitable as the single estimate of uncertainty in modeled discharge.

The standard deviation of discharge is known for all the streams used as input into our kriging model. We calculated the coefficient of variation ($CV = \text{standard deviation} / \text{mean}$) of discharge for each stream and kriged the resulting dataset to estimate the error in unmonitored catchments. The kriging model parameters are listed in Table 3.3. We cut the CV -rasters to the outlines of the unmonitored watersheds and exported the resulting watershed rasters to ascii-format. The average total CV for each watershed was calculated according to the following formula:

$$CV_{Q, measured} \% = \sqrt{\frac{\sum_{n=1}^i R_i \times (CV_{i, measured Q})^2}{\sum_{n=1}^i R_i}} \quad (3.3)$$

where $CV = \text{coefficient of variation}$, $\{1,2,3,\dots,n\}$ refers to individual pixels in the watershed rasters and $n = \text{total number of pixels in a given raster}$. R refers to kriged runoff. These calculations were done on a pixel-by-pixel basis.

The kriging variance of runoff was calculated during runoff modeling. The variance rasters were converted to standard deviation rasters before being cut to watersheds. The weighted standard deviation of runoff was then calculated according to equation (3.3), with the obvious modification that the standard deviation replaced CV in the equation. Finally, the weighted standard deviation of runoff for each watershed was divided by the kriged average runoff to get a CV of kriged runoff, $CV_{runoff,kriged}$.

To get a composite CV , $CV_{composite}$, of modeled Q in each watershed, we combined the two CV s:

$$CV_{composite} \% = \sqrt{\frac{(CV_{Q,measured})^2 + (CV_{runoff,kriged})^2}{\sqrt{2}}} \quad (3.4)$$

This value is used in the final error assessment of the modeled discharge from Kaua'i and the Big Island of Hawai'i. It is also compared with both the $CV_{Q,measured}$ and $CV_{runoff,kriged}$ in chapters 3.3., “Results” and 3.4., “Discussion and conclusions”.

3.2.4. Groundwater recharge and SGD

We use the area-normalized groundwater recharge values from the water budget reports in Table 3.1 as-is, with no further processing. It is important to note, though, that the groundwater recharge value given is not necessarily identical to the actual SGD, for reasons discussed below.

Hydrologists split stream discharge into two components - base flow and direct runoff. Base flow is the groundwater component of stream flow and is usually regarded as the discharge in a stream after a prolonged absence of precipitation. Direct runoff is

defined as the amount of precipitation that discharges directly from the surface and shallow subsurface into streams without interacting with the ground water system.

The methodology used in all the reports we cite here counts only direct runoff as "runoff". Base flow, the ground water-fed component of stream flow, is counted as groundwater recharge. Our limited sampling of river water for chemical analyses cannot distinguish between these two components of discharge (the two components are mixed in the stream). We therefore use the total measured discharge of streams to model the total runoff field for our study areas. The total discharge already includes the base flow and we must correct the groundwater recharge estimates presented in the reports cited in order to avoid double-counting the base flow component.

Modifying equation (3.1b), we re-define several variables:

$$G = \text{SGD} + \text{BF} \quad (3.1c)$$

where SGD = submarine groundwater discharge and BF = base flow.

Inserting equation (3.1c) into equation (3.1b), we get

$$\text{SGD} + \text{BF} = P - \text{DR} - \text{AE} \quad (3.1d)$$

We do not know the base flow component, BF, but we do know the direct runoff, DR.

To calculate BF, we define:

$$Q = \text{BF} + \text{DR} \quad (3.1e)$$

The ratio BF/DR is known (see below) and is used to calculate BF. Solving equation (3.1e) for DR and inserting into the ratio BF/DR we get:

$$\frac{BF}{DR} = \frac{BF}{(Q - BF)} \quad (3.1f)$$

which becomes:

$$BF = DR \times \frac{BF}{DR} \quad (3.1g)$$

DR is known and available in the reports we use. We calculated BF/DR for six streams (4 on Kaua'i, 2 on the Big Island) from data given in (Oki, 2004) (Table 3.4). The arithmetic average of BF/DR was computed for each island and used to correct G for BF, to yield SGD, which is the term used to calculate chemical fluxes via groundwater discharge. The sample sizes are very small and the confidence intervals should be interpreted with caution.

Table 3.4. Arithmetic averages of BF/DR on the Big Island and Kaua'i.

	# of streams	BF/DR
Big Island of Hawai'i	2	0.21 ± 0.16
Kaua'i	4	0.89 ± 0.48

An alternative approach to correct the ground water flux is to combine equations 3.1d and 3.1e to get:

$$SGD = P - Q - AE \quad (3.1h)$$

As discussed above, the total discharge (Q) is not known for a large part of the Hawaiian Islands but was modeled on the Big Island and Kaua'i in this study.

3.2.4.1. *Uncertainties on groundwater recharge estimates*

Uncertainty on our groundwater recharge estimates is poorly constrained. None of the reports we used for our study deal with uncertainty explicitly. The USGS water budget for Molokai (Shade, 1997) contains estimates of groundwater recharge calculated using two different water budget methods: the first one allocates excess soil-moisture to groundwater recharge before evapotranspiration and the second method allocates excess soil moisture first to evapotranspiration and second to groundwater recharge. The average recharge value from the two methods is presented as the final value and that is the value we report here. The *CV* of the three different groundwater recharge estimates is 35% and that is the value we assign to the uncertainty on all groundwater recharge estimates in our data compilation.

An error of 35% on groundwater recharge estimates is intermediate between the only two other studies we are aware of where error analysis on Hawaiian water budgets is performed. Oki (2002) performed a revised assessment of the water budget of the Hawi aquifer on Kohala Peninsula (labeled "B" in Shade (1995 b) and this study) and included a rigorous error analysis. His results indicate that groundwater recharge can be estimated with as little as 21% error (i.e., $CV \leq 21\%$). This low error is mainly attributed to using daily water budgeting, which avoids errors associated with averaging processes like evapotranspiration and soil moisture recharge over monthly or yearly intervals. Evapotranspiration and soil moisture recharge are highly variable temporally and respond mainly to rainfall events of typically short duration, on the order of hours to days. The low error reported by Oki (2002) cannot be expected to apply to the studies we used, mainly because all the studies we used in our compilation, except for one (Engott and Vana, 2007), use monthly or yearly water

budgets. We treat the error reported by (Oki, 2002) as a lower limit on the error associated with estimates of groundwater recharge in Hawai'i.

Giambelluca et al. (1996) investigated groundwater recharge uncertainty on land under both pineapple and sugarcane cultivation on O'ahu, using a water balance method that incorporates irrigation. Their results indicate that estimates of groundwater recharge in such settings are subject to *CV*'s of 49-58%. We take this as an upper limit on the error associated with estimates of groundwater recharge in Hawai'i.

3.3. RESULTS

Results from the aggregation of water budget data are presented in Table 3.5. The table lists values for rainfall, direct runoff, actual evapotranspiration and groundwater recharge as totals for each island.

There is a slight imbalance in the budget for the Big Island, caused by rounding. The imbalance is less than 1% and thus well within error. Table 3.5 also lists the ratio of direct runoff to groundwater recharge (R/G) averaged over each island. Kaua'i, the oldest and most weathered island, is the only one where direct runoff exceeds groundwater recharge. Several individual aquifers on Maui and the Big Island also have $R/G > 1$. Direct runoff tends to dominate over groundwater flow in regions where drainage networks are (relatively) well developed, or where precipitation is especially heavy.

Table 3.5. Results from the aggregation of water budget data, total fluxes for each island.

Island	Rain-fall (P)	Run-off (R)	Actual evapotranspiration (AE)	Ground-water recharge (G)	R/G	Area	Residual in water budget	Source
	10 ⁶ m ³ /yr					km ²		
Kaua'i	3761	1600	1260	901	1.77	1432	G	a
Moloka'i	774	125	385	264	0.47	675	Average of AE and G	b
O'ahu	2733	424	1214	1095	0.39	1542	Various	c
Maui	4021	1110	1395	1517	0.73	1888	G	d, e
Big Island of Hawai'i	18087	2045	8343	7729	0.27	10456	Various	f, g, h, i

Sources: a, (Shade, 1995a); b, (Shade, 1997); c, (Shade and Nichols, 1996); d, (Shade, 1999); e, (Engott and Vana, 2007); f, (State of Hawaii, 1990); g, (Takasaki, 1993); h, (Shade, 1995b); i (Waimea Water Services, Inc., 2004).

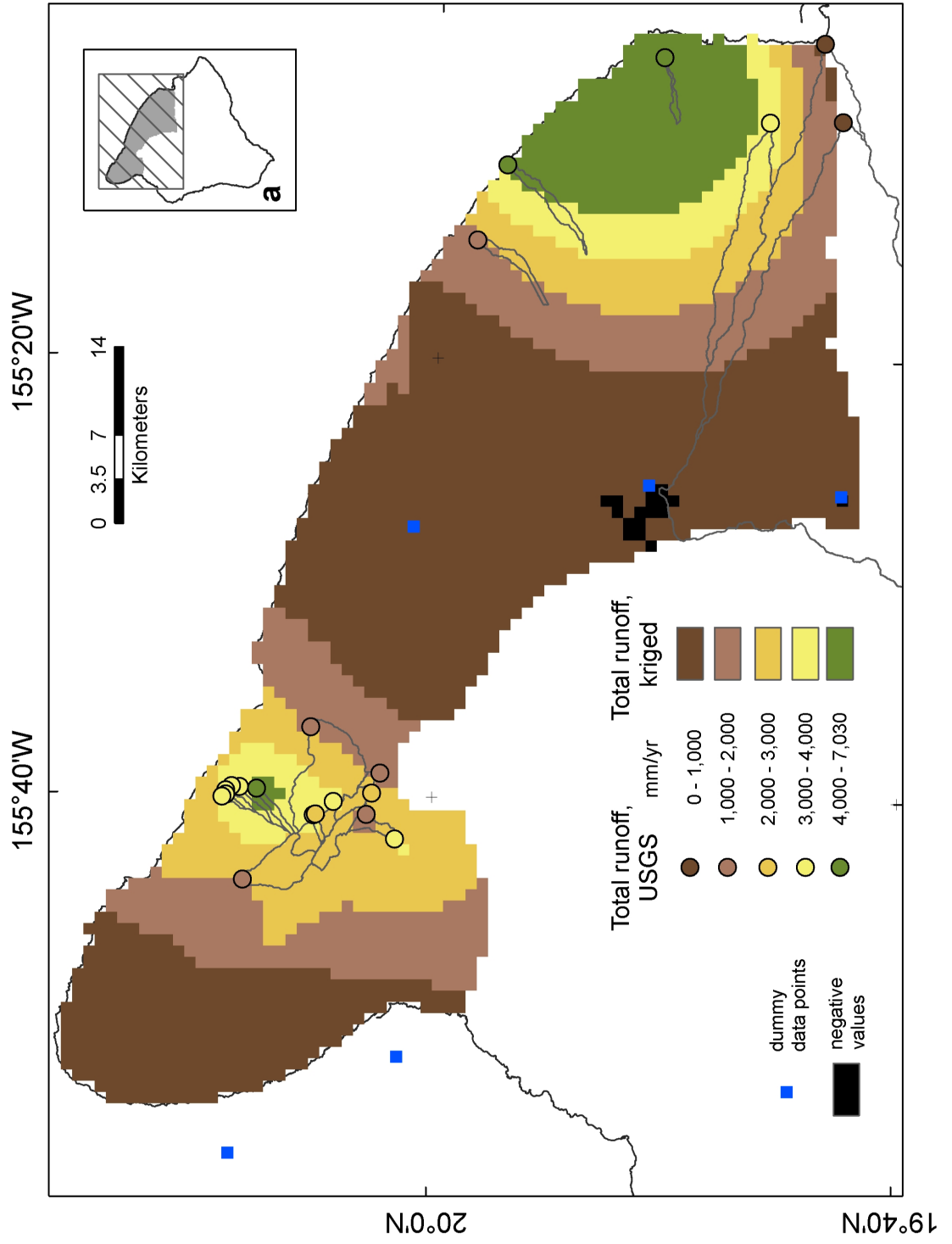
3.3.1. Discharge and kriging of surface runoff

3.3.1.1. Big Island of Hawai'i

On the Big Island, we found that the kriging model that uses data points located at the gauging sites gave better results than the centroid model both in terms of predicting observed surface runoff values at gauge sites ($r^2 = 0.98$) and in terms of predicting actual discharge (Figure 3.5.). This was somewhat unexpected, for reasons outlined in the Methods-section (3.2.3.).

We suspect that this is caused by the unusual hydrology of the Big Island (described above), where large portions of (primarily the far upstream) area that a GIS-model

Figure 3.5. Results from the kriging runoff model for the Big Island described in the text are shown as a raster cut to the extent of the aquifers we classify as runoff-active in Chapter 4. The location and runoff values for selected USGS monitored streams on the Big Island, used as input data for the kriging, are shown as filled circles and dummy data points used to extend the raster reach are shown as filled boxes. The black pixels in the kriged runoff raster have values less than zero.

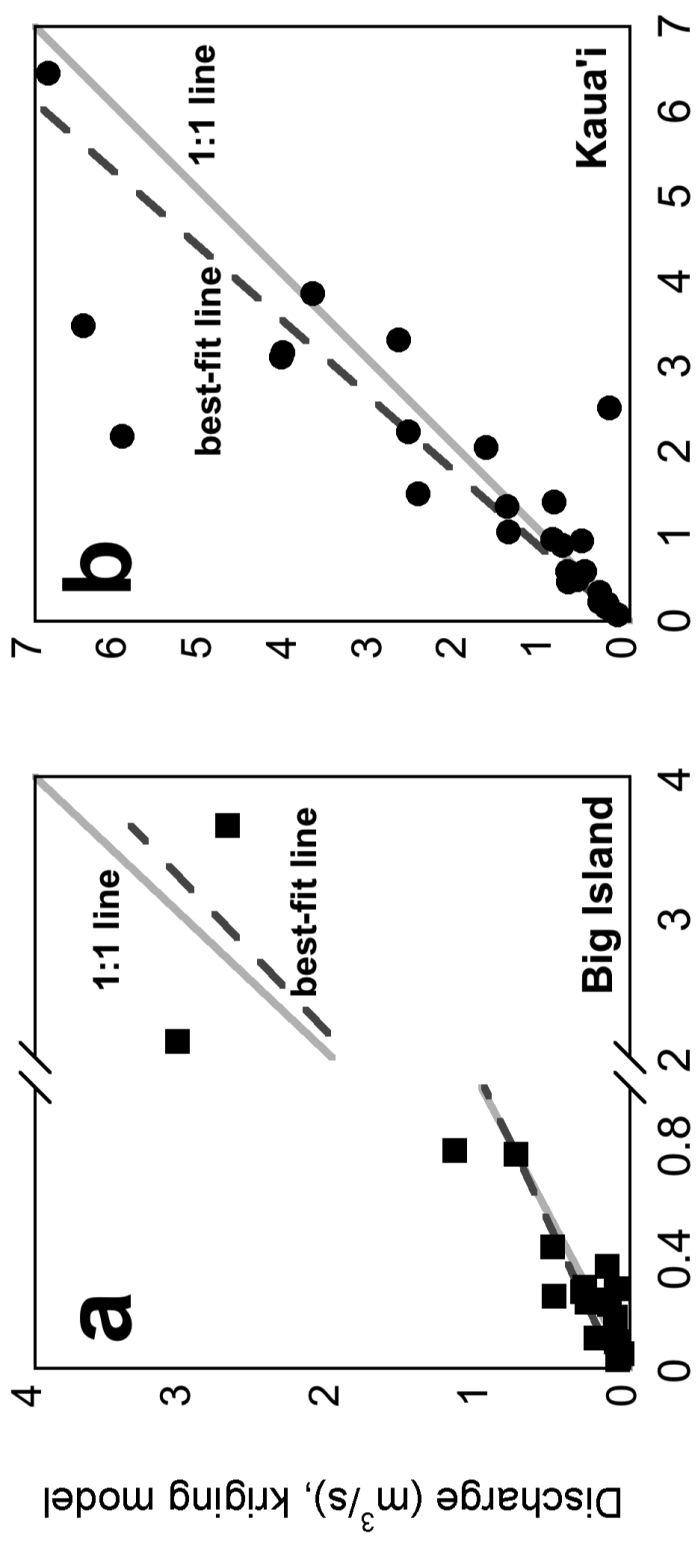


defines as watershed do not in reality contribute to the surface runoff. The lack of contribution may be due to lack of rainfall, for instance due to the temperature inversion, or due to all rainfall (that does not evaporate) being diverted directly to groundwater. These processes would tend to result in a watershed that is most likely smaller than the basin as outlined by GIS (although it is hard to predict how underground routing of groundwater would impact the effective size of the watershed). The streams would also receive most of their rainfall in the lower reaches of the basin.

To the author's best knowledge there is no accepted way to define contributing vs. non-contributing watershed area and no attempt is made to modify watershed shape and/or size to reflect the hydraulic realities on and in the ground. In any case, if the upper reaches of the Big Island watersheds do not contribute significantly to total runoff generation and may in fact be considered to not be a part of the "real" watershed, one would not expect our ability to model total runoff in space to improve by moving the data point, that reflects total runoff, upstream. Indeed, such a move might be expected to negatively impact spatial modeling of runoff.

The discharge computed from the kriged total runoff surfaces was compared to the discharge measured by the USGS for 18 of the streams used as input to our model on the Big Island. Wailuku River and its tributaries were not included in the regression because the kriging surface doesn't extend over their entire watersheds and any discharge estimate would be too low. A least-squares regression yields a best-fit line with slope = 0.90 ± 0.20 ($\alpha = 0.05$) and $r^2 = 0.85$ (Figure 3.6a). The slope is significant with $p < 0.0001$.

Figure 3.6. Kriging-derived discharge values (i.e., total runoff multiplied by area of pixels, see end of Chapter 3.2.3., "Methods - Surface runoff and discharge") for streams monitored by the USGS, plotted as a function of the measured discharge. a) Big Island b) Kaua'i. The regression lines discussed in the text are shown with a dark-grey dashed line. For reference, the 1:1 line is shown in light grey. Note the break in the x-axis in the plot for the Big Island.



3.3.1.2. *Kaua'i*

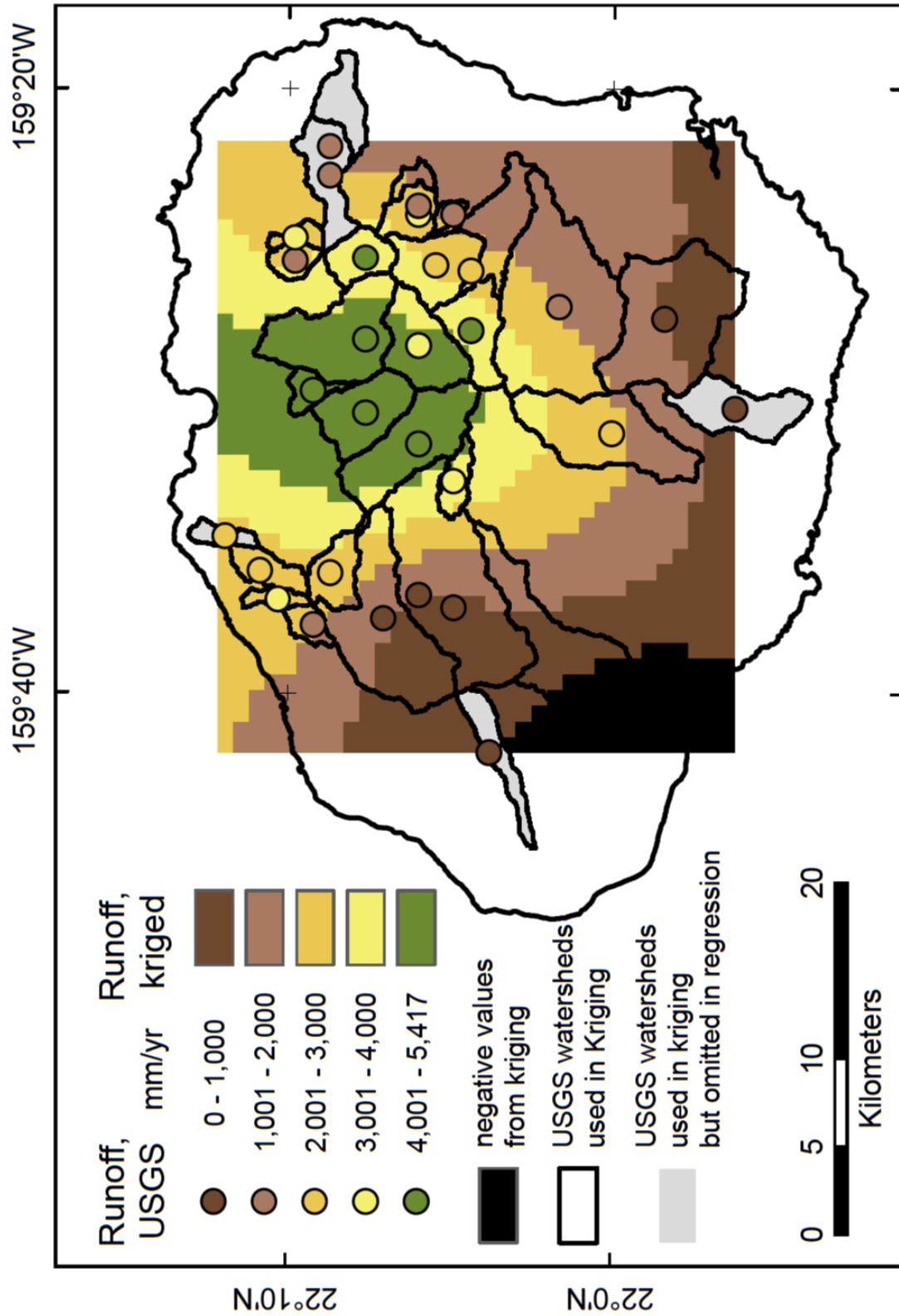
Specifying the surface runoff as a point attribute at the gauge site yielded a model that gave excellent correlation ($r^2 = 0.92$) between modeled and observed discharge values. However, the slope of the regression was 1.8 ($r^2_{slope} = 0.56$) and the model was therefore not adequate for predicting discharge in unmonitored streams.

When total runoff was kriged using the centroid of each respective watershed as the location for the surface runoff points, and using the smoothing interpolation function (Gribov and Krivoruchko, 2004) in the ArcGIS geostatistical analyst kriging module, the results improved significantly (Figure 3.7). Least-squares regression of measured and calculated discharge for the 30 USGS gauging stations on Kaua'i gave $r^2 = 0.74$ and a highly significant ($p < 0.0001$) slope of 1.13 ± 0.31 (Figure 3.6b). On Kaua'i, the entire watershed is active, in the sense that runoff is generated everywhere in the basin. This is in stark contrast to most watersheds on the Big Island, where only the lowermost part of a given basin is expected to receive rainfall that contributes to total runoff. This is the crucial difference between the two islands that explains why the data points for spatial modeling of runoff need to be placed in different parts of the GIS-defined watersheds on the two islands.

3.3.1.3. *Unmonitored watersheds*

We extracted total runoff rasters for individual unmonitored watersheds on Kaua'i and the Big Island in ArcGIS. The total runoff rasters were converted into discharge values in the same manner as the total runoff rasters for the USGS monitored streams. The results for kriged discharge in unmonitored streams are presented in Table 3.6.

Figure 3.7. Results of kriging runoff on Kaua'i using ordinary kriging and a smoothing function in ArcGIS Geostatistical Analyst. The kriging raster prediction surface is compared to the input runoff values.



Individual pixels in the runoff raster generated by kriging are 0.79 km². Several streams sampled in this study are smaller than an individual runoff pixel. We applied a criterion where streams under 1 km² are considered too small to have a runoff raster extracted. Instead, these streams were assigned the runoff value of the pixel that covered the largest part of the watershed, as judged by eye. It should be noted that these small streams account for around 0.2% of the area studied and an even smaller portion of the total discharge. Even with very large error bars, these fluxes will be a trivial component of the overall water budget.

All CV -values calculated for unmonitored streams on Kaua'i and Hawai'i and discussed here are presented in Table 3.6. The uncertainty on the modeled Q on the Big Island (for method, see Section 2.2.3.1.) ranges from 8% to 34% (minimum and maximum values, respectively) when only $CV_{Q,measured}$ is considered. These values increase significantly ($p < 0.001$) when looking only at $CV_{runoff,kriged}$; here uncertainty values (CV) range from 19% to 234%. The very high $CV_{runoff,kriged}$ values occur in two streams on the Kohala Peninsula, outside the range of monitored streams.

Combining the $CV_{Q,measured}$ and $CV_{runoff,kriged}$ yields a range of $CV_{composite}$ from 26% to 196% with a mean value of 56%. Again, the highest values correspond to two streams on Kohala Peninsula. Without these two streams, the average CV would drop by 9%, down to 47%.

On Kaua'i, uncertainty in modeled runoff is significantly larger than on the Big Island of Hawai'i. This applies both to the $CV_{Q,measured}$ and $CV_{runoff,kriged}$. $CV_{Q,measured}$ ranges from 28% to 46% with an arithmetic average of 39%. This is still significantly lower than the average for $CV_{runoff,kriged}$ and $CV_{composite}$, which have a range of 32% to 440%

Table 3.6. Kriged discharge in unmonitored streams.

River name	Area km ²	Runoff, annual mean, kriged		Runoff, standard error, kriged		Q, annual mean 10 ⁶ m ³ /yr	CV _{Q,measured} %	CV _{runoff,kriged} %	CV _{composite} %
		mm/yr	mm/yr	mm/yr	mm/yr				
Big Island									
Makeha Stream ¹	0.066	1826	663	36	0.120	26	37		
Waipi'o Tributary ¹	0.066	2007	803	40	0.132	26	40		
Pu'u O Umi stream ¹	0.150	2535	1041	41	0.379	28	42		
Kahua Ranch stream ¹	0.368	1969	1116	57	0.724	22	51		
Kapehu Rd. Stream	1.98	2615	971	37	5.18	34	42		
Kilohana Gulch	2.30	3128	1175	38	7.20	25	38		
Hapahapai Gulch	3.86	651	1521	234	2.51	8	196		
Honomu Stream	4.16	5801	1114	19	24.1	25	26		
Kawaihae Uka Stream	4.57	2853	1156	41	13.0	26	40		
Waikama Gulch	6.65	1695	1244	73	11.3	20	64		
Hanawi Stream	10.8	5138	1168	23	55.4	27	30		
Laupahoehoe Stream	12.2	1449	1067	74	17.6	33	68		
Walaohia Gulch	12.4	1094	1408	129	13.5	14	109		
Aamakao Gulch	12.5	1535	1369	89	19.2	18	76		
Hi'ilawe Stream	16.2	1661	949	57	26.9	29	54		
Kawainui I Stream	21.9	4953	1184	24	108.7	27	30		
Hakalau Stream	22.4	5236	1364	26	117.2	27	31		
Kapue Stream	24.3	3331	1311	39	81.0	27	40		
Honokane Nui	26.1	2316	888	38	60.5	23	38		
Waikaumalo Stream	35.5	2373	1480	62	84.3	26	57		
Nanue Stream	37.5	1793	1496	83	67.3	26	73		
Kolekole River	53.8	3104	1468	47	167.1	25	45		
Umauma Stream	54.2	2458	1545	63	133.1	25	57		

Table 3.6. (continued)

River name	Area km ²	Runoff, annual mean, standard error, kriged		Runoff, kriged mm/yr	CV _{runoff,kriged} %	Q, annual mean 10 ⁶ m ³ /yr	CV _{Q,measured} %	CV _{composite} %
		mm/yr	mm/yr					
Kaua'i								
Dam Gulch ¹	0.104	417	1273	1273	305	0.043	46	260
Tributary A ¹	0.229	499	1347	1347	270	0.114	45	230
Tributary@Po'o Kaeha	0.452	385	1278	1278	332	0.578	46	282
Tributary @ Mauka Powerhouse	1.011	378	1664	1664	440	0.382	45	372
Wiliwili Gulch	2.655	408	1326	1326	325	1.08	46	276
Koke'e Stream	4.909	1376	1234	1234	90	6.75	39	82
Keahua Stream	9.251	3046	1015	1015	33	28.2	34	40
Waikomo Stream ²	11.5	684	1227	1227	179	1.58	38	154
Nawiliwili Stream ²	11.7	993	1593	1593	160	11.6	40	139
Opaka'a Stream ²	13.3	1687	1232	1232	73	22.4	40	70
Kilauea Stream	23.0	2956	1147	1147	39	68.1	32	42
Anahola Stream ²	23.9	1438	1044	1044	73	34.4	36	68
Hanama'ulu Stream ²	25.6	1348	1516	1516	112	34.5	40	100
Koai'e Stream	29.3	2094	1124	1124	54	61.4	36	54
Kapa'a Stream ²	36.2	1634	1075	1075	66	59.1	38	64
Wainiha Stream ²	58.3	3641	1160	1160	32	212.3	28	36
Makaweli River	68.7	2166	1330	1330	61	148.8	36	60
Hanapepe River	69.2	1575	1283	1283	81	109.0	36	75

1: Watershed too small to extract from kriged runoff raster. Runoff given here is found by manually selecting the runoff pixel that covers the greatest area of the watershed polygon.

2: Watershed extends beyond the kriged runoff surface. Discharge calculated by extending the average runoff over the modeled part of the basin to the entire basin.

and 36% to 372%, respectively. The large range in both CV -metrics on Kaua'i is caused by five small ($< 3 \text{ km}^2$) watersheds in the Waimea Canyon that have $CV_{runoff,kriged}$ of 270% and up. Without these outliers, the arithmetic average $CV_{composite}$ goes down to 76% from 134%.

3.3.2. Groundwater recharge

Compilation and inspection of extant data reveals that groundwater recharge exceeds direct runoff by a factor of 1 to 4, up to a high of 11, in most aquifers on the islands (Table 3.5). The exceptions are Kaua'i, far eastern Maui (see Chapter 3.3.2.2.) and four aquifers on the Big Island. See Table 3.7 for complete water budget analysis for all aquifers on Mau'i and Table 3.8 for complete water budget analysis for all aquifers on the Big Island.

3.3.2.1. Kaua'i

We used the BF/DR method (equation 3.1g), coupled with the BF/DR values given in Table 3.4, to compute base flow for Kaua'i. The BF/DR method yielded base flow larger than the estimates of groundwater recharge of Shade (1995 a) and thus negative SGD. It has been established by other workers (e.g. Knee et al., 2006; 2008) that SGD from Kaua'i is indeed present, although its magnitude is not comparable to river (surface) runoff - Knee et al. (2008) estimate that SGD is equivalent to 10-20% of river discharge in Hanalei Bay on the north coast of Kaua'i. The negative SGD values yielded by the subtraction of base flow from groundwater recharge estimates must be caused by either the groundwater recharge estimates being too low or the BF/DR, as computed from data in Oki (2004) and presented in Table 3.4, being too high. Assuming that the groundwater recharge values are more representative than the

Table 3.7. Complete water budget analysis for all aquifers on Maui.

Aquifer name/code	Area ¹ km ²	10 ⁶ m ³ /yr				mm/yr				Residual in water budget	Source ²	
		Rainfall (P)	Runoff (R)	Actual evapotran- spiration (AE)	Ground water recharge (G)	Rainfall (P)	Runoff (R)	Actual evapotran- spiration (AE)	Ground water recharge (G)			
Haiku	75	225	47	94	84	3001	626	1252	1123	0.56	G	a
Honokohau	36	110	28	35	46	3050	772	988	1290	0.60	G	b
Honokowai	61	99	21	42	37	1619	337	681	601	0.56	G	b
Honolua	46	101	20	47	34	2171	432	1004	734	0.59	G	b
Honopou	42	169	43	47	80	3982	1012	1110	1893	0.53	G	a
'Iao	65	149	44	43	62	2283	669	656	959	0.70	G	b
Kahakuloa	28	66	18	22	26	2359	632	790	937	0.67	G	b
Kahului	71	30	2	19	9	427	26	272	129	0.20	G	b
Kamaole	4	2.9	0.2	2.1	0.6	689	46	492	145	0.32	G	a
Kama'ole	237	142	2	88	52	601	7	372	221	0.03	G	b
Kaupo	55	122	18	54	50	2230	329	988	912	0.36	G	a
Kawaipapa	84	365	129	86	151	4336	1527	1018	1790	0.85	G	a
Keanae	140	676	271	147	260	4847	1943	1051	1863	1.04	G	a
Kipahulu	75	294	82	80	133	3947	1093	1075	1779	0.61	G	a
Kuhiwa	33	223	144	35	43	6726	4345	1044	1295	3.35	G	a
Launiupoko	54	87	15	26	46	1616	281	486	849	0.33	G	b
Luailua	160	170	8	126	36	1062	52	786	224	0.23	G	a
Makawao	148	133	11	98	21	896	75	663	140	0.53	G	a
Nakuula	79	95	4	69	22	1210	53	877	281	0.19	G	a
Olowalu	21	36	6	8	23	1739	262	376	1099	0.24	G	b
Pa'ia	2	1.4	0.1	1.0	0.3	703	27	495	153	0.18	G	a

Table 3.7. (continued)

Aquifer name/code	Area ¹ km ²	10 ⁶ m ³ /yr				mm/yr				Residual in water budget	Source ²	
		Rainfall (P)	Runoff (R)	Actual evapotranspiration (AE)	Ground water recharge (G)	Rainfall (P)	Runoff (R)	Actual evapotranspiration (AE)	Ground water recharge (G)			
Pa'ia	154	96	1	68	27	623	8	441	174	0.05	G	b
Ukumehame	31	31	3	9	19	1000	102	282	616	0.16	G	b
Waie'e	32	87	22	23	41	2688	687	719	1282	0.54	G	b
Waihoi	41	158	51	40	66	3812	1237	970	1605	0.77	G	a
Waikamoi	68	308	115	69	126	4506	1677	1010	1839	0.91	G	a
Waikapu	45	45	7	17	21	997	155	382	460	0.34	G	b

1: The area given in this table is in some cases smaller than the area given in the respective reports. This is because the process of merging aquifers from the different reports diminished the size of some aquifers considerably.

2: a = Shade 1999, b = Engott and Vana 2007

Table 3.8. Complete water budget analysis for all aquifers on the Big Island

Table 3.8.

Aquifer name/code	Area ¹ km ²	Actual Ground			Actual Ground			R/G	Residual in water budget	Source ²		
		Rainfall (P)	Runoff (R)	evapotran- spiration (AE)	Rainfall (P)	Runoff (R)	evapotran- spiration (AE)					
		10 ⁶ m ³ /yr			mm/yr							
2	74	109	0	51	58	1483	0	695	789	0	(G+AE)/2	a
3	111	80	0	53	28	721	0	472	248	0	(G+AE)/2	a
4	28	24	0	15	8	852	0	551	301	0	(G+AE)/2	a
5	158	116	0	69	47	733	0	436	297	0	(G+AE)/2	a
6	47	71	0	36	35	1495	0	762	733	0	(G+AE)/2	a
7	10	10	0	7	3	935	0	668	267	0	(G+AE)/2	a
8	122	129	0	69	59	1055	0	567	488	0	(G+AE)/2	a
9	37	35	0	21	14	930	0	558	372	0	(G+AE)/2	a
10	106	134	0	84	50	1263	0	795	469	0	(G+AE)/2	a
11	81	106	0	50	58	1310	0	613	715	0	(G+AE)/2	a
12	31	43	0	21	22	1382	0	669	713	0	(G+AE)/2	a
13	25	36	0	17	19	1411	0	651	760	0	(G+AE)/2	a
14	75	105	0	64	41	1402	0	848	553	0	(G+AE)/2	a
15	77	77	0	47	29	1001	0	608	375	0	(G+AE)/2	a
16	1	2	0	1	1	1620	0	850	1012	0	(G+AE)/2	a
17	66	123	0	87	35	1852	0	1311	520	0	(G+AE)/2	a
18	24	41	0	29	11	1746	0	1222	466	0	(G+AE)/2	a
19	119	165	0	94	71	1386	0	792	594	0	(G+AE)/2	a
20	218	202	0	118	84	926	0	539	387	0	(G+AE)/2	a
21	53	58	0	35	24	1099	0	654	445	0	(G+AE)/2	a
22	66	58	0	44	14	884	0	673	210	0	(G+AE)/2	a
23	30	19	0	17	1	637	0	546	46	0	(G+AE)/2	a
A [#]	156	552	183	147	224	3543	1172	941	1438	0.81	G	b

Table 3.8. (continued)

Aquifer name/code	Area ¹ km ²	Actual Ground				Actual Ground				Residual in water budget	Source ²	
		Rainfall Runoff		evapotran- spiration		Rainfall Runoff		evapotran- spiration				
		(P)	(R)	(AE)	(G)	(P)	(R)	(AE)	(G)			
		10 ⁶ m ³ /yr										
		mm/yr										
B [#]	101	252	32	137	83	2484	314	1351	819	0.38	G	b
C [#]	427	261	55	173	33	612	129	405	78	1.67	G	b
Mauna Loa												
Slope NY	917	2813	0	912	1901	3067	0	994	2073	0	G	c
Northeast												
Rift	590	1387	0	488	899	2352	0	828	1524	0	G	c
Mauna Loa												
Slope S	829	1142	0	796	346	1378	0	961	417	0	G	c
Kaioiki Fault												
System	106	128	0	109	19	1207	0	1025	183	0	G	c
Southwest												
Rift	125	150	0	128	22	1196	0	1020	177	0	G	c
Kilauea Slope												
NE	544	1901	0	698	1203	3495	0	1284	2212	0	G	c
East Rift	253	579	0	261	318	2287	0	1032	1255	0	G	c
Kilauea Slope												
S	386	562	0	368	194	1456	0	954	501	0	G	c
Mahukona	8	5	0	4	1	635	25	432	178	0.14	G	d
Waimanu [#]	22	80	33	22	25	3658	1524	1016	1118	1.36	G	d
Honokaa [#]	275	399	21	280	119	1448	76	1016	432	0.18	G	d
Waimea	742	339	19	245	75	457	25	330	102	0.25	G	d
Anaehoomalū	687	402	17	297	87	584	25	432	127	0.20	G	d
Kiholo	393	250	10	180	60	635	25	457	152	0.17	G	d
Keauhou	414	473	11	347	116	1143	25	838	279	0.09	G	d

Table 3.8. (continued)

Aquifer name/code	Area ¹ km ²	Actual 10 ⁶ m ³ /yr			Actual mm/yr			R/G	Residual in water budget	Source ²		
		Rainfall (P)	Runoff (R)	Actual evapotran- spiration (AE)	Ground water recharge (G)	Rainfall (P)	Runoff (R)				Actual evapotran- spiration (AE)	Ground water recharge (G)
Kealakekua	448	376	11	273	91	838	25	610	203	0.13	G	d
Naalehu	134	204	14	136	54	1524	102	1016	406	0.25	G	d
Hilo [#]	13	43	3	13	28	3404	203	1016	2184	0.09	G	d
Hakalau [#]	441	1603	673	448	482	3632	1524	1016	1092	1.40	G	d
Onomea [#]	456	1818	915	463	452	3988	2007	1016	991	2.03	G	d
Paauilo [#]	385	626	49	392	186	1626	127	1016	483	0.26	G	d

1: The area given in this table is in some cases smaller than the area given in the respective reports. This is because the process of merging aquifers from the different reports diminished the size of some aquifers considerably.

#: Aquifers classified as runoff-active in Chapter 3.

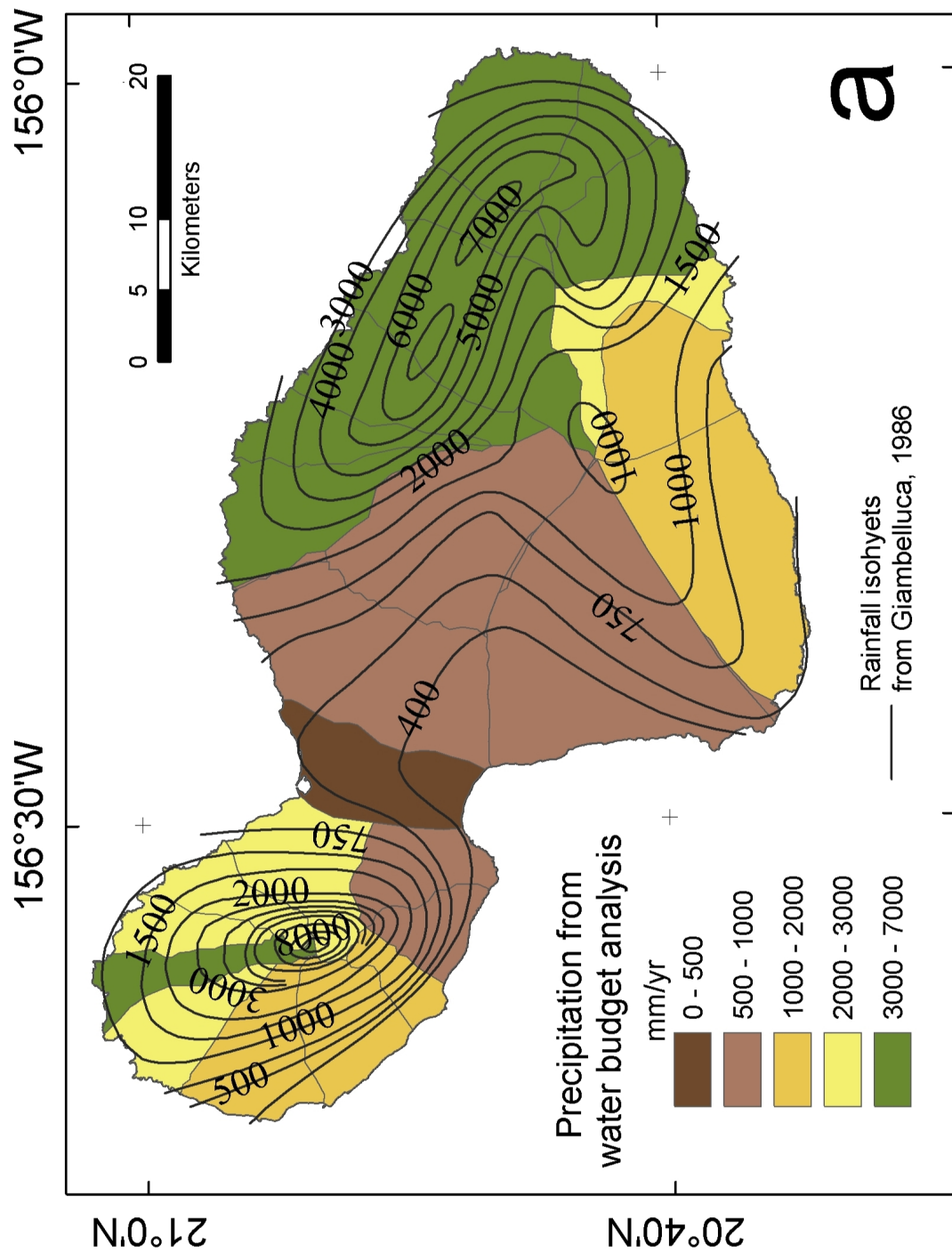
2: a = WWW 2004, b = Shade 1995b, c = Takasaki 1993, d = State of Hawaii 1990

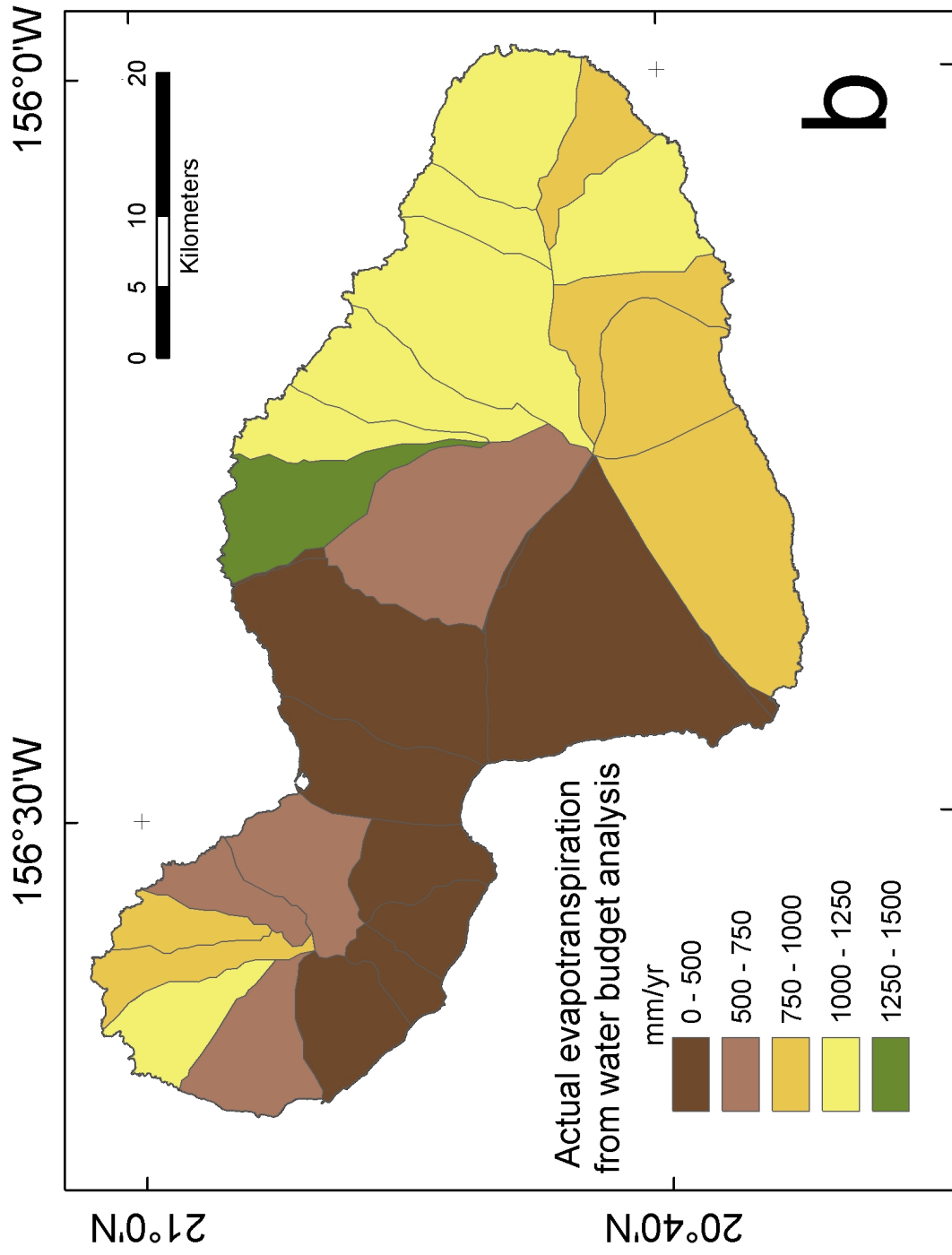
BF/DR values, we used the kriged total discharge (Q) for Kaua'i to constrain SGD (equation 3.1h). As explained above and shown in Figure 3.7, the kriged total runoff surface does not cover all of Kaua'i and the island-wide discharge calculated using the total runoff raster must therefore be regarded as the minimum discharge. Using USGS values for P and AE and the kriging results for Q, we compute SGD on the order of $390 \times 10^6 \text{ m}^3/\text{yr}$, or just under half of the USGS computed groundwater recharge. This value for SGD on Kaua'i is a maximum value, since the kriging surface used to compute total discharge does not cover the entire island.

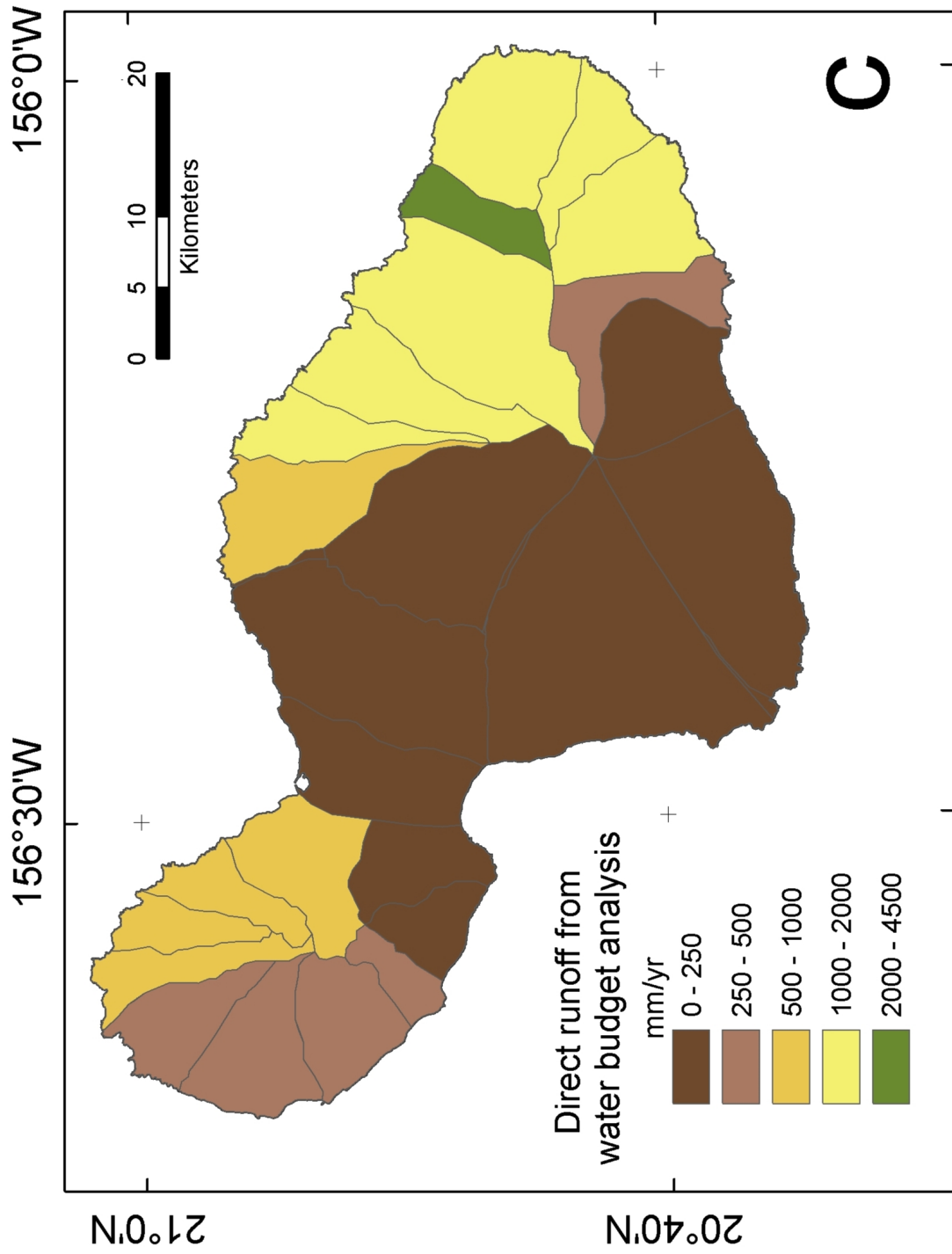
3.3.2.2. *Maui*

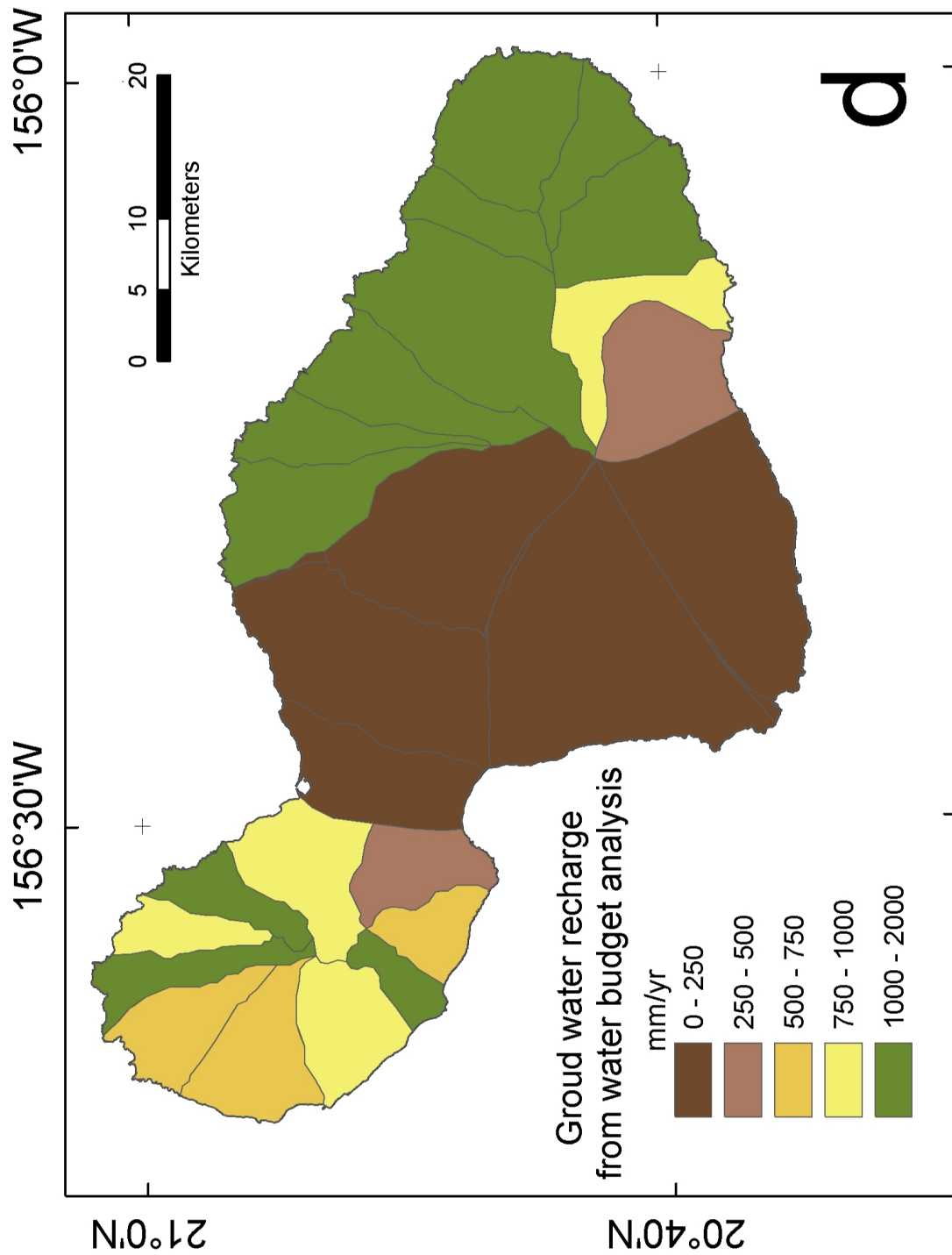
The two reports (Figure 3.2a) used to create the maps shown below (Figure 3.8a - e) give very similar results for both groundwater recharge and rainfall in the region of Central Maui, where the two studies overlap geographically. The eastern slopes of Mt. Haleakala receive by far the largest amount of rainfall on the island (Figure 3.8a) but the western slope of the volcano and the Central Maui Isthmus, in the rain shadow of Mt. Haleakala, receive significantly less rainfall. Actual evapotranspiration (Figure 3.8b) and direct runoff (Figure 3.8c) follow similar patterns, although the magnitudes differ. Groundwater recharge on Maui is also highest on the eastern slopes of Mt. Haleakala (Figure 3.8d). Groundwater recharge exceeds direct runoff in all aquifers, except for in Keanae and Kuhiwa (Figure 3.8e), which lie in the zone of greatest rainfall (Figure 3.8a).

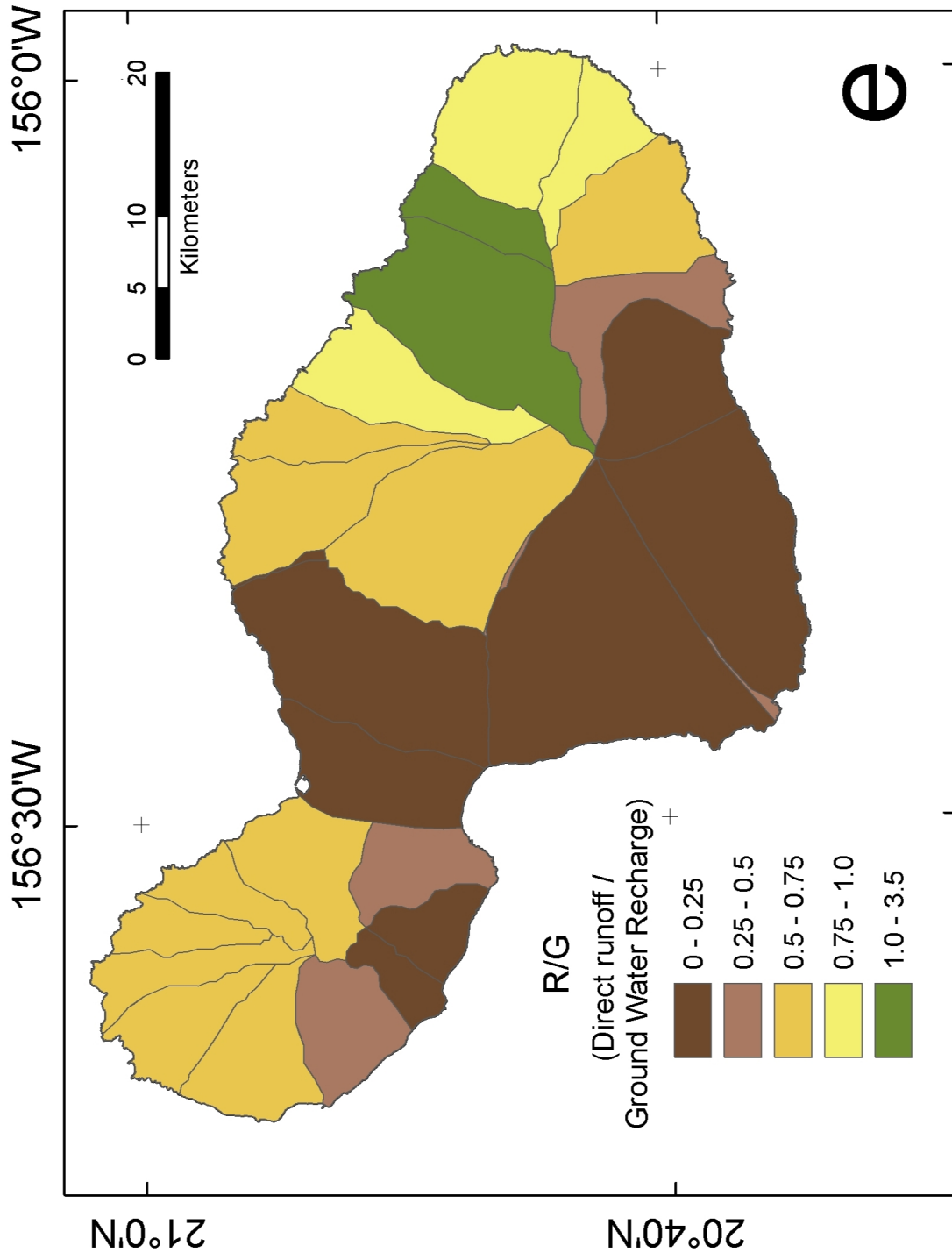
Figure 3.8. Maps of water budget analysis for all aquifers on Mau'i. a) Precipitation from water budget analysis, b) Actual evapotranspiration from water budget analysis, c) Total runoff from water budget analysis, d) Ground water recharge from water budget analysis, e) Total runoff versus ground water recharge (R/G).











3.3.2.3. *Big Island of Hawai'i*

We used the BF/DR method to correct groundwater recharge values on the Big Island for the base flow component of discharge, although it is hard to constrain its effectiveness with only two data points. The method predicts base flow of around 6% of total ground water recharge. This value is well within uncertainty for the water budget and the correction has been ignored.

The results of combining the four reports cited in Table 3.1 are shown in the maps of Figure 3.9. Precipitation in each aquifer is shown in Figure 3.9a and compared with the precipitation map of Giambelluca et al. (1986) (also shown in Figure 3.1), which was used to calculate precipitation in all the studies except for the South Kona/Ka'u study (Waimea Water Services, Inc., 2004). As is to be expected, the composite precipitation from the water budget studies and the precipitation map of Giambelluca et al. (1986) correlate very well. Figure 3.9b shows the composite of actual evapotranspiration from water budget studies, with locations of stream and groundwater samples from our 2005, 2006 and 2008 sampling campaigns indicated as well. Interestingly, AE south of Hilo (in NE Rift-aquifer and, especially, in the NE Slope of Mauna Loa-aquifer) is relatively low given the large volume of rainfall in the area. This can probably be explained by the extremely porous nature of the rocks on Mauna Loa. Furthermore, although rainfall on the Kohala Peninsula is considerably larger in aquifer A than in aquifer B, AE is considerably lower in aquifer A. AE is obviously not limited by moisture ability in aquifer A. More likely, persistent cloud cover limits AE. Figure 3.9c compares the water budget-derived AE with pan evaporation data from Ekern and Chang (1985) and calculated AE from Nullet et al. (1995). Ekern and Chang in their (1985) report collect pan evaporation data from a

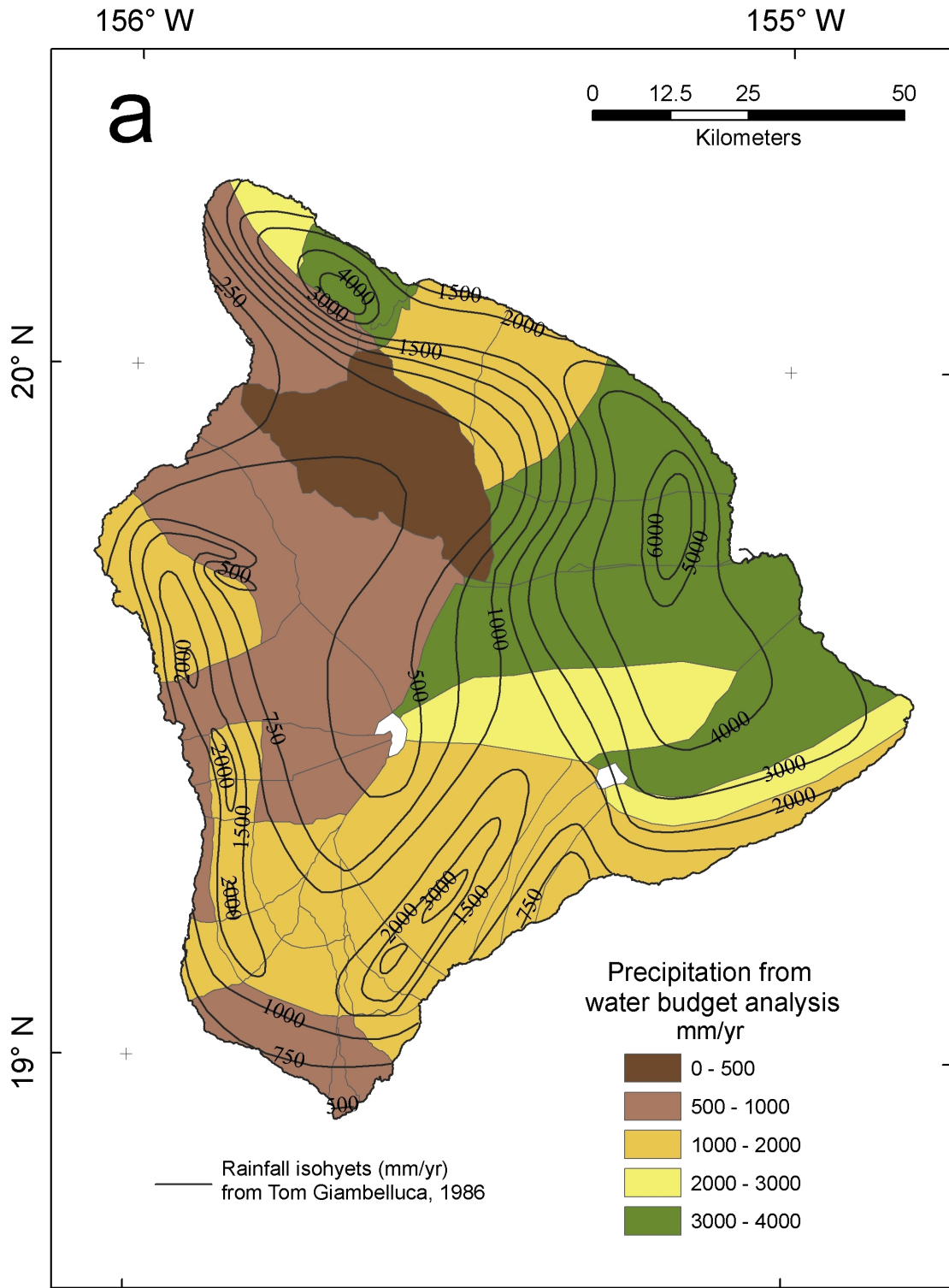
number of different sources on the Big Island, mostly from plantations. The pan ET values measure rates of water evaporation from pans that are kept continuously full of water, so moisture is never a limiting factor. This severely limits the usefulness of the method to estimate AE under natural conditions, where moisture deficit (pan ET > AE) may prevail during certain times of year or even year round. The dataset of Ekern and Chang (1985) is widely used in the reports we cite here as a basis for calculating AE. For details on how that is done, the reader is referred to the individual reports.

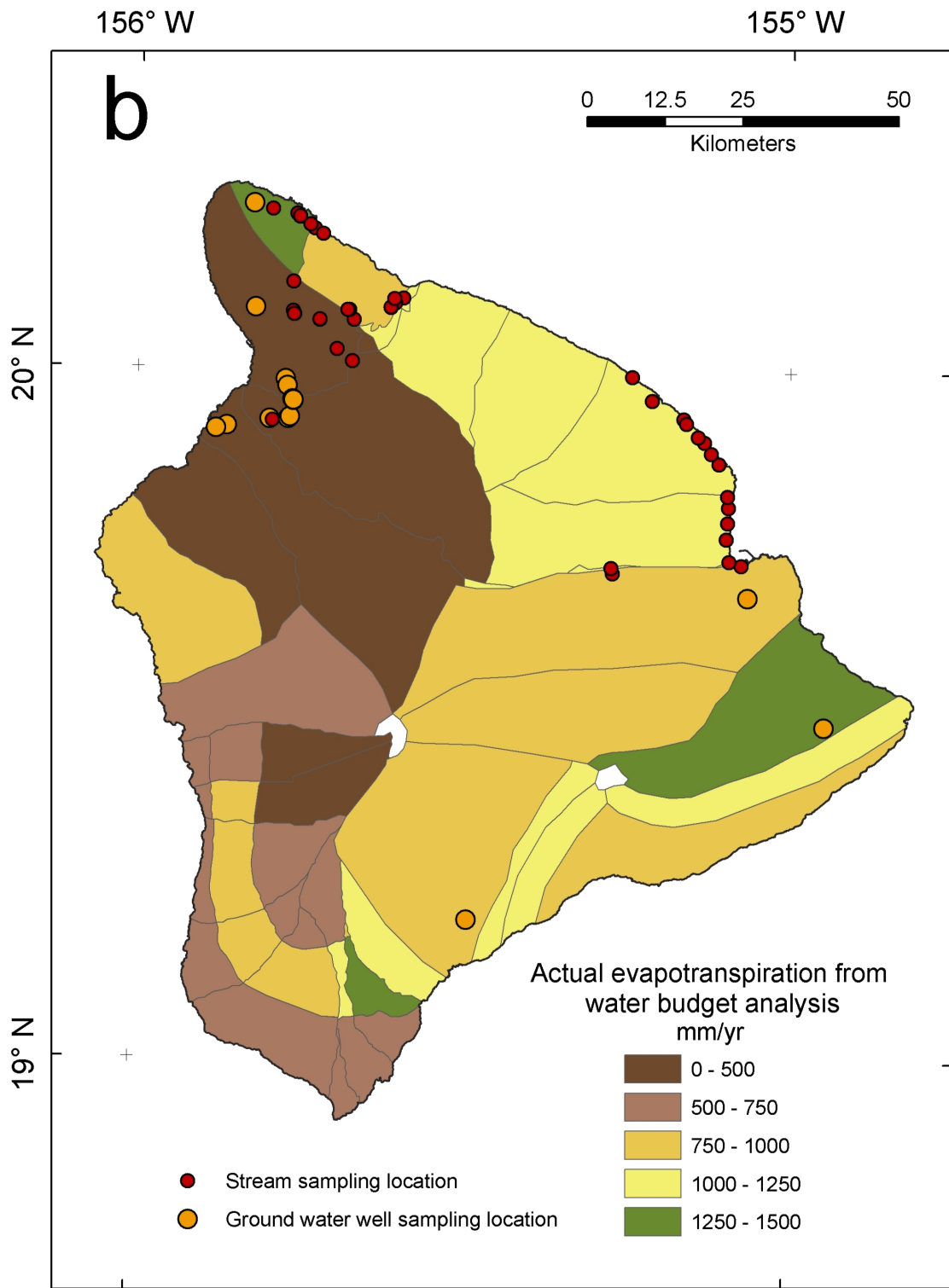
Direct runoff as compiled from water budget data is shown in Figure 3.9d. Note that the values presented here are not directly comparable to the map of total kriged runoff in Figure 3.5 and instead are expected to be consistently lower than the total runoff of Figure 3.5.

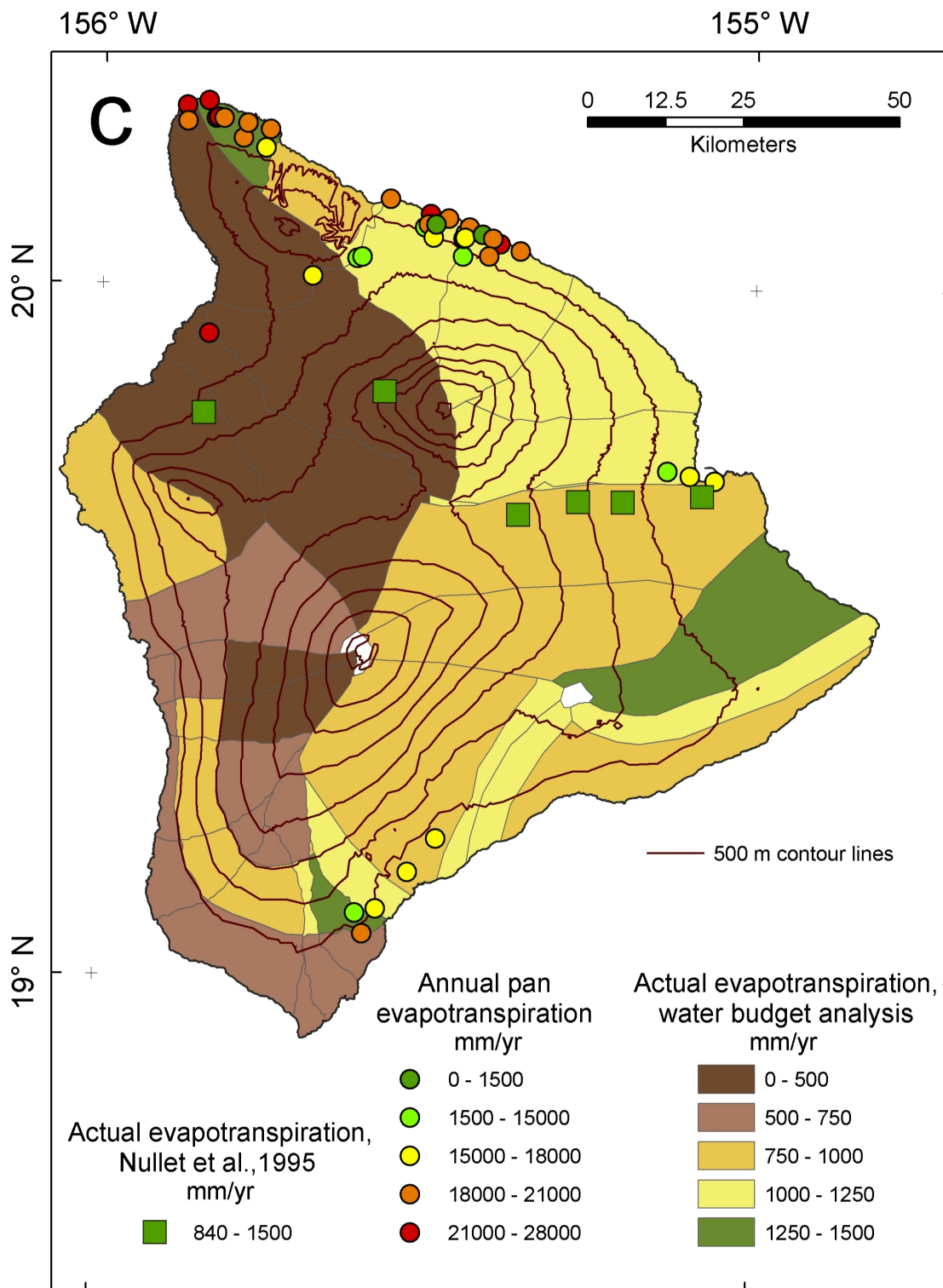
Groundwater recharge from the water budget compilation is shown in Figure 3.9e. By far the largest amounts of groundwater recharge occurs on the east slope of Mauna Loa and Mauna Kea and on the eastern Kohala Peninsula. A second recharge maximum is located in South Kona, near the southern tip of the island. This maximum is coincident with the rainfall maximum observed in that region. Finally, very little groundwater recharge occurs in the North Kona region on the west coast.

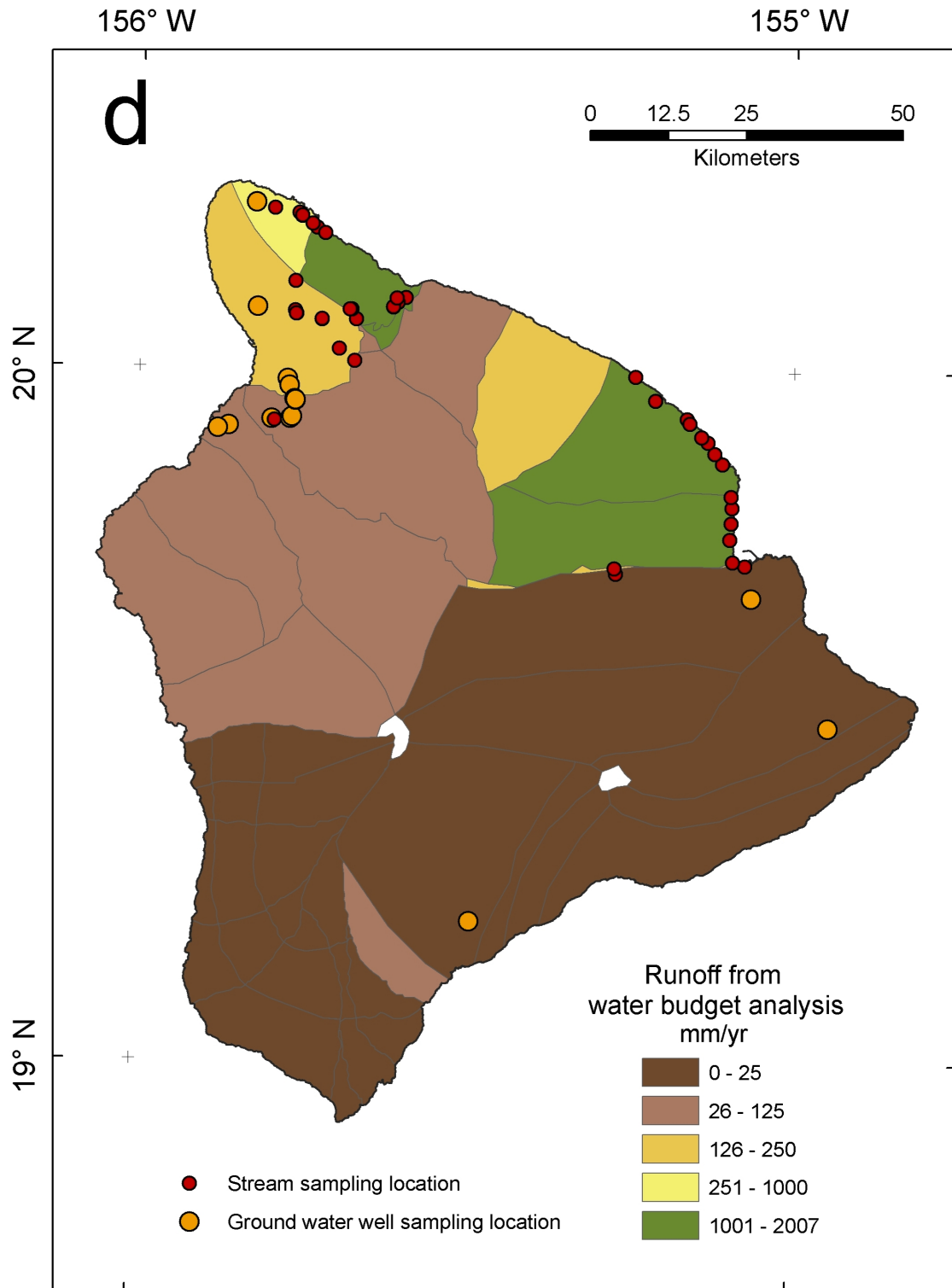
The final map, Figure 3.9f, shows direct runoff as a function of groundwater recharge. In the case of the Big Island, where base flow is a trivial component of the groundwater recharge (see beginning of this section), this number is an indicator of the relative importance of surface runoff (total runoff) versus SGD. SGD exceeds total surface runoff by up to a factor of 10 (in the Hilo and Keauhou aquifers) and in only two aquifers is total surface runoff larger than SGD. These are the Onomea aquifer,

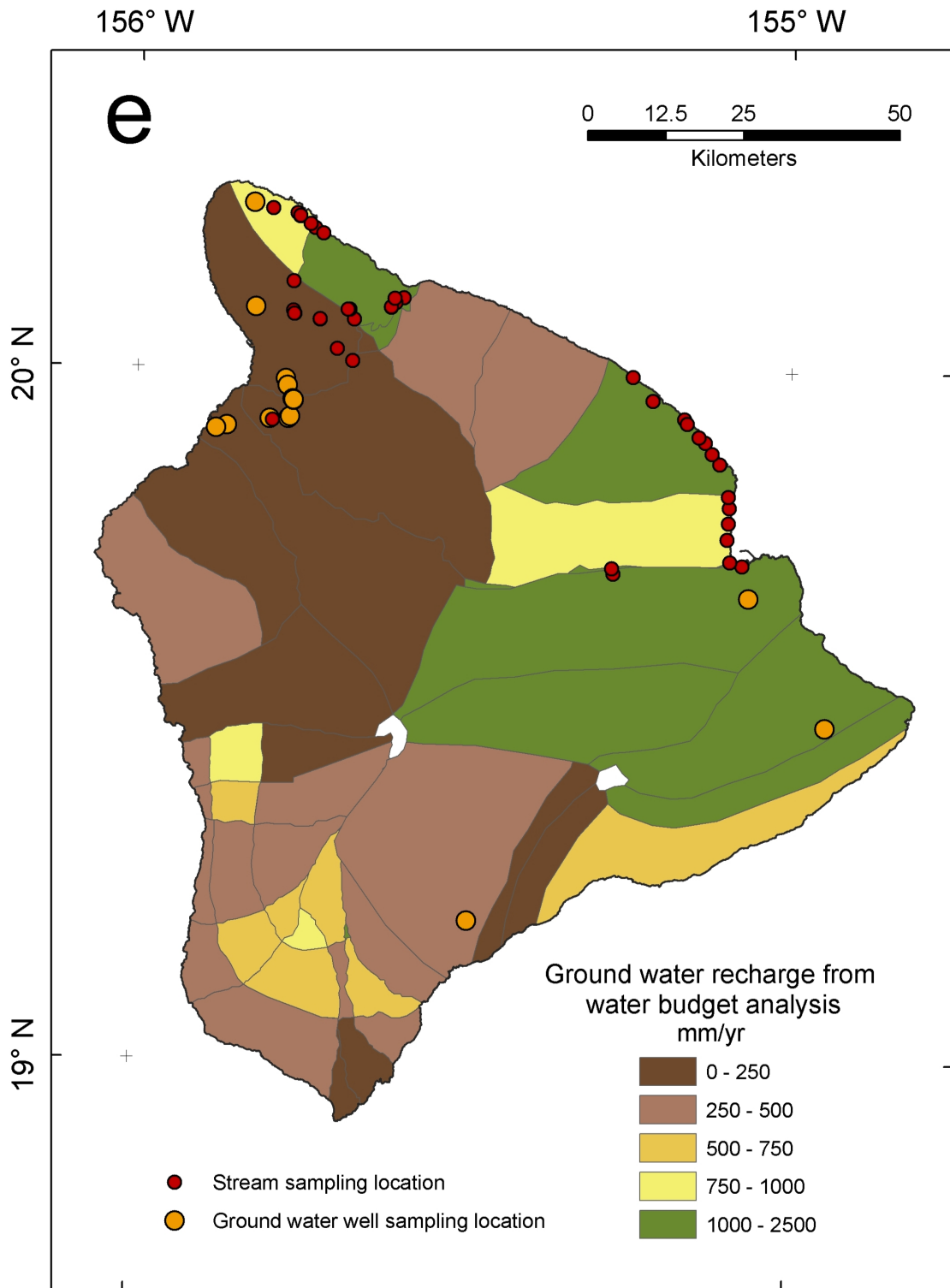
Figure 3.9. Maps of water budget analysis for all aquifers on the Big Island. a) Precipitation from water budget analysis, with rainfall isohyets from Giambelluca et al. (1986), b) Actual evapotranspiration from water budget analysis, c) Actual evapotranspiration from Nullet et al. (1995), annual pan evaporation from Ekern and Chang (1985), d) Runoff from water budget analysis, e) Ground water recharge from water budget analysis, f) Total runoff versus ground water recharge (R/G).

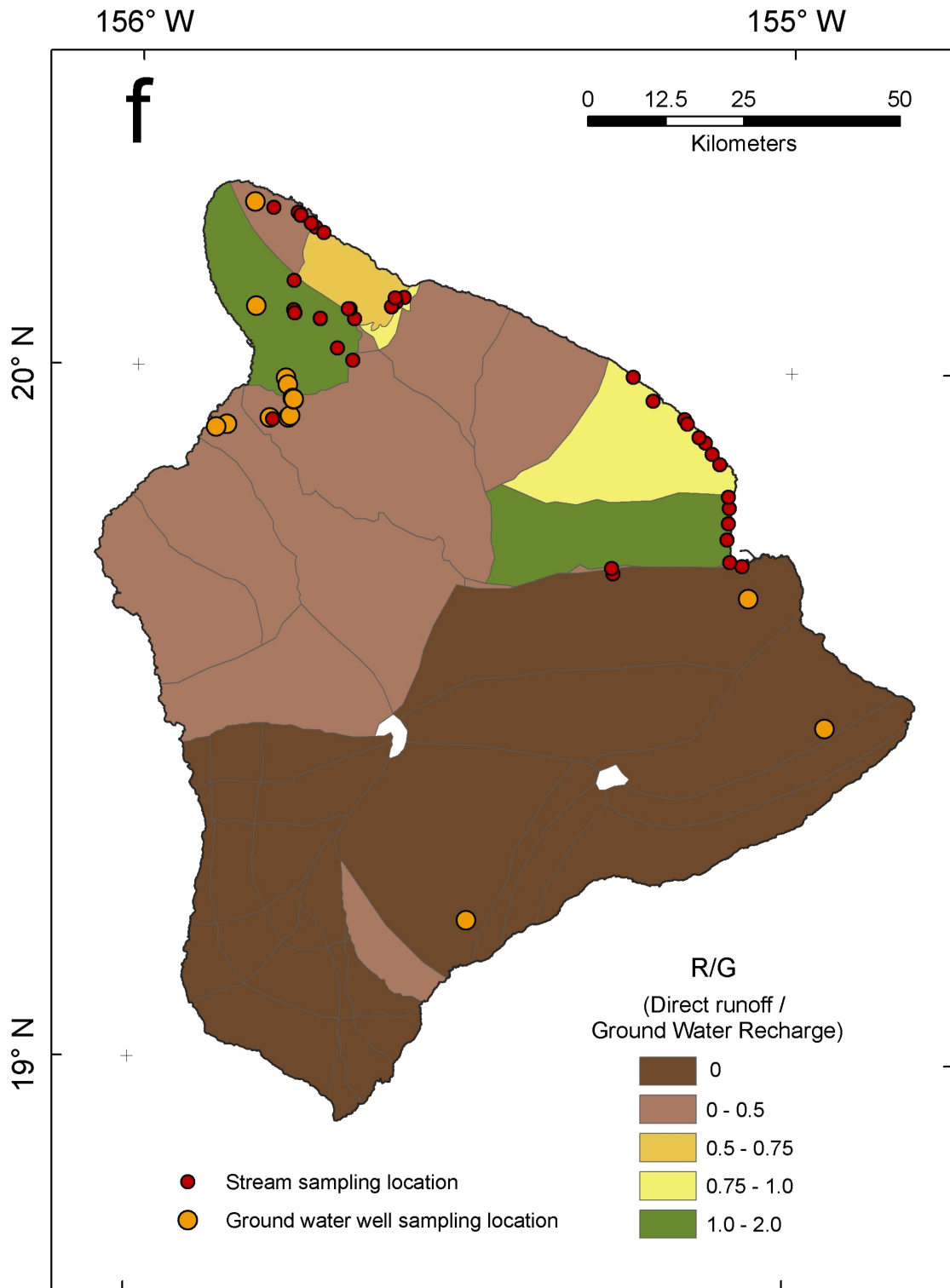












just south of Hilo, and the "C" aquifer on the western half of the Kohala Peninsula. These two aquifers are very different in every other respect; the "C" aquifer for instance is one of the driest regions on the Big Island. The precipitation gradient on Kohala going from east to west is very large and the precipitation maximum occurs just west of the drainage divide that runs along the peninsula from north to south. This rainfall feeds the streams on west Kohala but is usually not enough to keep them flowing all the way to the sea. The bedrock is porous enough that the streams "disappear" into their bed and percolate down to the groundwater level before discharging into the sea. In west Kohala, therefore, one does not have the usual situation where groundwater becomes stream water (i.e., base flow) but the opposite, where stream water (surface runoff) becomes groundwater.

3.4. DISCUSSION AND CONCLUSIONS

This study produced two main data products: 1) A revised estimate of groundwater recharge for Maui and the Big Island of Hawai'i, using and combining data from USGS reports published since 1990 (when the last state-wide water budget was produced) and 2) Surface runoff surfaces for NE/Central Eastern Big Island and Kaua'i.

Groundwater recharge, as defined and calculated by the USGS, exceeds surface runoff in nearly every aquifer investigated. The exceptions are the island of Kaua'i, east Maui and two aquifers on the Big Island of Hawai'i. The uncertainties on groundwater recharge in these reports are substantial, on the order of 35%.

The authors are not aware of other studies that have relied exclusively on monitored discharge in neighboring streams as inputs into kriging models to predict total runoff values in unmonitored watersheds or sub-basins of monitored watersheds, as we do. The good results of our kriging model in Hawai'i justify this approach on volcanic islands.

A major finding of this study is the feasibility of kriging models to predict runoff values, and thereby discharge, in unmonitored basins in Hawai'i. Discharge is a difficult quantity to predict and no comprehensive, fine-scale estimates of it exist for the Hawaiian Islands. Our kriging models for total runoff on Kaua'i and the Big Island, described above, demonstrate the feasibility of kriging as a strategy to predict total runoff in unmonitored watersheds on high-porosity volcanic islands, as long as high-quality, semi-long term discharge data are available for a sufficient number of adjacent streams.

References

- Baddeley A. and Turner R. (2005) spatstat: An R Package for Analyzing Spatial Point Patterns. *Journal of Statistical Software* **12**, 1-42.
- Bear J. (1988) *Dynamics of Fluids in Porous Media*. Dover Publications.
- Berman M. and Turner T.R. (1992) Approximating Point Process Likelihoods with GLIM. *Applied Statistics* **41**, 31-38.
- Ekern P.C. and Chang J. (1985) *Pan Evaporation: State of Hawai'i, 1894-1983*. Report# R74. Honolulu, HI, Department of Land and Natural Resources.
- Engott J.A. and Vana T.T. (2007) *Effects of Agricultural Land-Use Changes and Rainfall on Ground-Water Recharge in Central and West Maui, Hawai'i, 1926-2004*. Report# SIR2007-5103. Reston, VA, U.S. Geological Survey.
- Giambelluca T.W., Nullet M.A. and Schroeder T.A. (1986) *Rainfall Atlas of Hawaii*. Report# R76. Honolulu, HI, Water Resources Research Center, University of Hawaii at Manoa.
- Giambelluca T.W., Loague K., Green R.E. and Nullet M.A. (1996) Uncertainty in recharge estimation: impact on groundwater vulnerability assessments for the Pearl Harbor Basin, O'ahu, Hawai'i, U.S.A. *Journal of Contaminant Hydrology* **23**, 85-112.
- Gribov A. and Krivoruchko K. (2004) Geostatistical Mapping with Continuous Moving Neighborhood. *Mathematical Geology* **36**, 267-281.
- Grigg R.W. and Jones A.T. (1997) Uplift caused by lithospheric flexure in the Hawaiian Archipelago as revealed by elevated coral deposits. *Marine Geology* **141**, 11-25.
- Hengl T. (2006) Finding the right pixel size. *Computers & Geosciences* **32**, 1283-1298.

- Juvik, S.P. and Juvik, J.O. (1998) *Atlas of Hawaii*. 3rd ed. Honolulu, University of Hawai'i Press.
- Knee K., Santoro A., Street J., Boehm A., Berg C. and Paytan A. (2005) Nutrient Subsidies to Hanalei Bay, Kauai, HI From Submarine Groundwater Discharge. In: *Eos Trans. AGU*.
- Knee K., Street J.H., Santoro A., Berg C., Boehm A. and Paytan, A. (2006) Estimating the Importance of Submarine Groundwater Discharge in Hanalei Bay, Kaua'i. In: *Ocean Sci. Meet. Suppl. AGU*, OS15B-20.
- Knee K., Layton B., Street J., Boehm A. and Paytan, A. (2008) Sources of Nutrients and Fecal Indicator Bacteria to Nearshore Waters on the North Shore of Kaua'i (Hawai'i, USA). *Estuaries and Coasts* **31**, 607-622.
- McDougall I. (1964) Potassium-Argon Ages from Lavas of the Hawaiian Islands. *Geological Society of America Bulletin* **75**, 107-128.
- McDougall I. (1979) Age of shield-building volcanism of Kauai and linear migration of volcanism in the Hawaiian island chain. *Earth and Planetary Science Letters* **46**, 31-42.
- McDougall I. and Swanson D.A. (1972) Potassium-Argon Ages of Lavas from the Hawi and Pololu Volcanic Series, Kohala Volcano, Hawaii. *Geological Society of America Bulletin* **83**, 3731-3738.
- Moore J.G. (1987) Subsidence of the Hawaiian Ridge. In: *Volcanism in Hawaii*. USGS Professional Paper. Washington, DC, USGS, pp. 85-100.
- Nielsen D. and Wendroth O. (2003) *Spatial and Temporal Statistics - Sampling Field Soils and Their Vegetation*. Catena-Verlag.
- Nullet D., Juvik J.O. and Wall A. (1995) A Hawaiian mountain climate cross-section. *Climate Research* **05**, 131-137.

- Oki D.S. (2002) *Reassessment of Ground-Water Recharge and Simulated Ground-Water Availability for the Hawi Area of North Kohala, Hawaii*. Report# WRIR 4006. U.S. Geological Survey.
- Oki D.S. (2004) *Trends in Streamflow Characteristics at Long-Term Gaging Stations, Hawaii*. Report# SIR2004-5080. U.S. Geological Survey.
- Oki D.S., Tribble G.W., Souza W.R. and Bolke E.L. (1999) *Ground-Water Resources in Kaloko-Honokohau National Historical Park, Island of Hawaii, and Numerical Simulation of the Effects of Ground-Water Withdrawals*. Report# WRIR99-4070. Honolulu, USGS Pacific Islands Water Science Center.
- Peterson D.W. and Moore R.B. (1987) Geologic History and Evolution of Geologic Concepts, Island of Hawaii. In: *Volcanism in Hawaii*. USGS Professional Paper. USGS, pp.149-189.
- Peterson R.N., Burnett W.C., Glenn C.R. and Johnson A.G. (2009) Quantification of point-source groundwater discharges to the ocean from the shoreline of the Big Island, Hawaii. *Limnology and Oceanography* **54**, 890-904.
- Schmincke H. (2004) *Volcanism*. 1st edition. Springer.
- Shade P.J. (1995a) *Water Budget for the Island of Kaua'i, Hawaii*. Report# WRIR95-4128. Honolulu, HI, U.S. Geological Survey.
- Shade P.J. (1995b) *Water Budget for the Kohala Area, Island of Hawaii*. Report# WRIR95-4114. Honolulu, HI, U.S. Geological Survey.
- Shade P.J. (1997) *Water Budget for the Island of Molokai, Hawaii*. Report# WRIR97-4155. Honolulu, HI, U.S. Geological Survey.
- Shade P.J. (1999) *Water Budget of East Maui, Hawaii*. Report# WRIR98-4159. Honolulu, HI, U.S. Geological Survey.
- Shade P.J. and Nichols W.D. (1996) *Water Budget and the Effects of Land-Use Changes on Ground-Water Recharge, Oahu, Hawaii*. Professional Paper 1412-C. U.S. Geological Survey.

- State of Hawaii (1990) *Water Resources Protection Plan, Volume I and II*. Commission on Water Resource Management, Department of Land and Natural Resources, State of Hawaii.
- Street J.H., Knee K.L., Grossman E.E. and Paytan, A. (2008) Submarine groundwater discharge and nutrient addition to the coastal zone and coral reefs of leeward Hawai'i. *Marine Chemistry* **109**, 355-376.
- Takasaki K.T. (1993) *Ground Water in Kilauea Volcano and Adjacent Areas of Mauna Loa Volcano, Island of Hawaii*. Report# OFR93-82. Honolulu, HI, U.S. Geological Survey.
- Thornthwaite C.W. (1948) An Approach toward a Rational Classification of Climate. *Geographical Review* **38**, 55-94.
- Thornthwaite C.W. and Mather J. (1955) The water balance. *Publications in Climatology* **8**, 1-104.
- USGS (2010) USGS Water Data for the Nation [Internet]. Available from: <<http://waterdata.usgs.gov/nwis/>> [Accessed 15 December 2010].
- Waagepetersen R. (2008) Estimating functions for inhomogeneous spatial point processes with incomplete covariate data. *Biometrika* **95**, 351 -363.
- Waimea Water Services, Inc. (2004) *Water Resources of the South Kona/Ka'u Water Master Plan Area*. Kamuela, HI, Waimea Water Services, Inc.
- Watts A.B. (1978) An Analysis of Isostasy in the World's Oceans 1. Hawaiian-Emperor Seamount Chain. *Journal of Geophysical Research* **83** (B12), 5989-6004.
- Watts A.B. and ten Brink U.S. (1989) Crustal Structure, Flexure, and Subsidence History of the Hawaiian Islands. *Journal of Geophysical Research* **94** (B8), 10,473-10,500.

CHAPTER 4

SURFACE AND SUBSURFACE CHEMICAL WEATHERING FLUXES FROM THE HAWAIIAN ISLANDS

Abstract

Chemical weathering fluxes from the Big Island of Hawai'i and Kaua'i were investigated in early 2005, 2006 and 2008. These two islands were chosen as study sites for representing the extremes in age and landscape development in the Hawaiian archipelago. We sampled streams and groundwater wells on the Big Island and streams only on Kaua'i, and used chemistry data from USGS groundwater wells on Maui, O'ahu and Kaua'i.

Our results indicate that there are no statistically significant differences in area-normalized surface (stream) chemical fluxes from regions on the Big Island compared with regions on Kaua'i. The only exceptions are fluxes of Ca+Mg and weathering carbon sequestration flux, which is significantly elevated in the Hamakua-Hilo region on the Big Island compared to the Kohala peninsula on the Big Island and to East Kaua'i. This result implies that bedrock age is not a primary control on surface chemical weathering fluxes, but could also simply indicate that a more refined error estimate is necessary to detect the impact of bedrock age on these fluxes. In general, we find that carbon export fluxes by surface chemical weathering in Hawai'i are low to average compared to the global average in basaltic settings and identical to slightly higher to the values reported by Dessert et al. (2003). Upon inclusion of chemical weathering fluxes delivered by submarine groundwater discharge (SGD), this picture

changes substantially. Considering the Big Island as a whole, we find that chemical weathering fluxes via SGD are at least an order of magnitude larger than from chemical weathering occurring on the Earth's surface. This ratio decreases as landscapes age: the first traces of landscape incision (Hamakua-Hilo) suffice to bring the ratio of subsurface to surface weathering fluxes down to $\sim 1-1.5$, and in the heavily incised landscapes of Kaua'i the ratio has decreased to ~ 0.5 . These results highlight the importance of groundwater as a pathway for chemical fluxes from volcanic islands to the ocean and demonstrate that groundwater remains a crucial component of the weathering system on volcanic islands during the entire lifespan of these islands.

4.1. INTRODUCTION

4.1.1. Motivation and previous studies

It is well established that the chemical weathering of silicate rocks, especially Ca- and Mg-rich silicates, is an important regulator of atmospheric CO₂-concentrations and thereby global climate (e.g. Berner, 2004). The mechanisms controlling the chemical weathering of silicate rocks, however, are still debated. Initial studies of chemical weathering focused on large rivers ($>100,000 \text{ km}^2$) that collectively drain significant fractions of the world's exorheic area, such as the Amazon (Stallard and Edmond, 1981; 1983; 1987). The drainage basins of large rivers usually comprise different lithologies and a common understanding was that lithology was a relatively insignificant influence on weathering rates, while runoff and relief were regarded as the primary control on chemical weathering rates (Meybeck, 1976 and references therein). Later work (e.g. Meybeck, 1987; Bluth and Kump, 1994) identified lithology

as a major control on weathering fluxes and Gislason et al. (1996) and Louvat and Allegre (1997) highlighted the large weathering fluxes from volcanic islands.

This led to the realization that although volcanic regions comprise only a small fraction of global land area, they have such high chemical weathering fluxes that any compendium of global chemical weathering would need to incorporate island arcs and hot-spot volcanic islands (Gaillardet et al., 1999). Dessert and co-workers (2003) studied the impact of basalt weathering on the global carbon cycle. They found that chemical weathering fluxes from basalt provinces worldwide are highly disproportionate to the area these regions cover: they are responsible for about a third of global silicate weathering fluxes and yet cover less than 10% of the area covered by silicates. Another important contribution to the study of the chemical weathering of volcanic islands (Rad et al., 2007) pointed out the importance of submarine groundwater discharge (SGD) to the chemical budget of weathering. Rainfall infiltrates the highly porous rocks of volcanic islands easily and a large portion of precipitation is routed to groundwater in that manner. Rad et al. (2007) found that subsurface weathering contributed between 60-90% of the total weathering flux from the three volcanic islands they studied. If their results were borne out elsewhere, it would further elevate the importance of volcanic islands as a pathway for dissolved fluxes to the ocean.

The weathering geochemistry of Hawai'i has not been studied in any detail so far. Bluth and Kump (1994) investigated the effects of lithology and climate on stream geochemistry and weathering on the Hawaiian Islands. They reported significant differences in the ratios of cations (expressed as bicarbonate) to silica in streams and conclude that the type of soils in catchments controls the stream geochemistry. Dessert

et al. (2003) reported anomalously low chemical weathering fluxes from Hawai'i (based on publicly available stream chemistry and discharge data from the USGS) compared to other volcanic islands with similar temperatures and runoff.

We investigated the stream geochemistry of Kaua'i and the Big Island of Hawai'i in an effort to further constrain the chemical weathering fluxes from Hawai'i. Given the importance of SGD in Hawaiian hydrology (e.g. Peterson et al., 2009), we also sampled groundwater wells on the Big Island in order to quantify chemical weathering fluxes via groundwater. Chemical data for groundwater wells on Maui, O'ahu and Kaua'i was obtained from the USGS online database (<http://waterdata.usgs.gov/nwis/>).

Spelling of Hawaiian place names follows the one employed in the Atlas of Hawai'i (Juvik and Juvik, 1998). In Hawaiian, the archipelago, the state and the island of Hawai'i are spelled the same, Hawai'i. To avoid confusion, we will use the term "Hawai'i" when referring to the entire archipelago and "the Big Island of Hawai'i", or simply "the Big Island", when we discuss the island of Hawai'i.

4.1.2. Geology and climate

A detailed account of the tectonic setting and climate of the Hawaiian Islands is given in Chapter 3. In this section, the geomorphology and petrology of Kaua'i and the Big Island of Hawai'i will be described and a brief summary of climate and hydrology will be given.

Precipitation on the Hawaiian Islands is in general controlled by the so-called trade winds that come in from the NE, carrying large amounts of moisture that is deposited over the eastern part of the islands from ascending air masses as they encounter land. Due to a rain shadow effect, the western part of all the islands is significantly drier

than the east. The climate is warm (average yearly $T = 25.3^{\circ}\text{C}$) and equitable, with small differences between the coldest and warmest month. Hawaiians recognize two seasons, the wet winter season from October through April and a drier summer from May through September.

The Hawaiian Islands (Figure 4.1) are typical hot-spot islands, formed by the continuous activity of the Hawaiian mantle plume over the last 5-6 Myr (10^6 years). The main rock type is tholeiite basalt, with smaller amounts of alkali lavas erupted at the very beginning and very end of the lifespan of individual volcanoes. The Big Island is still being created by constant volcanism in Kilauea Volcano (at the time of writing, the current eruption has been going on for almost 30 years) and both Mauna Loa and Hualalai Volcanoes are regarded as active (Juvik and Juvik, 1998). Mauna Kea has been inactive for ca. 5000 years and Kohala Volcano, the oldest volcano on the island at ~ 450 kyr (10^3 years) (McDougall and Swanson, 1972), is extinct.

Erosion has not yet changed the constructive volcanic landscape on the Big Island (Figure 4.2) to any great extent, as is evident in the pristine shield surfaces of northern Kohala Peninsula (Figure 4.3, A-A'), Mauna Kea and Mauna Loa (Figure 4.3 D-D', E-E'). The only exception is the east coast of the Kohala Peninsula, where deeply incised valleys (e.g. Honokane Nui, Figure 4.3 B-B', right side) have eroded into the headwall (see Figure 4.3 C-C', far right) of a massive landslide that occurred 385-173 kyr ago (Lamb et al. 2007). In stark contrast with the deep valleys on eastern Kohala, the western side of the peninsula has experienced almost no dissection (Figure 4.3 A-A', B-B', C-C', left side). The reason is the strong focusing of rainfall over eastern Kohala; the western half of the peninsula is largely starved of rainfall throughout the year.

Figure 4.1. Location map of the Hawaiian Islands. Filled triangles represent the approximate location of the atmospheric deposition sites discussed in the text. This study focuses on Kaua'i and the Big Island of Hawai'i.

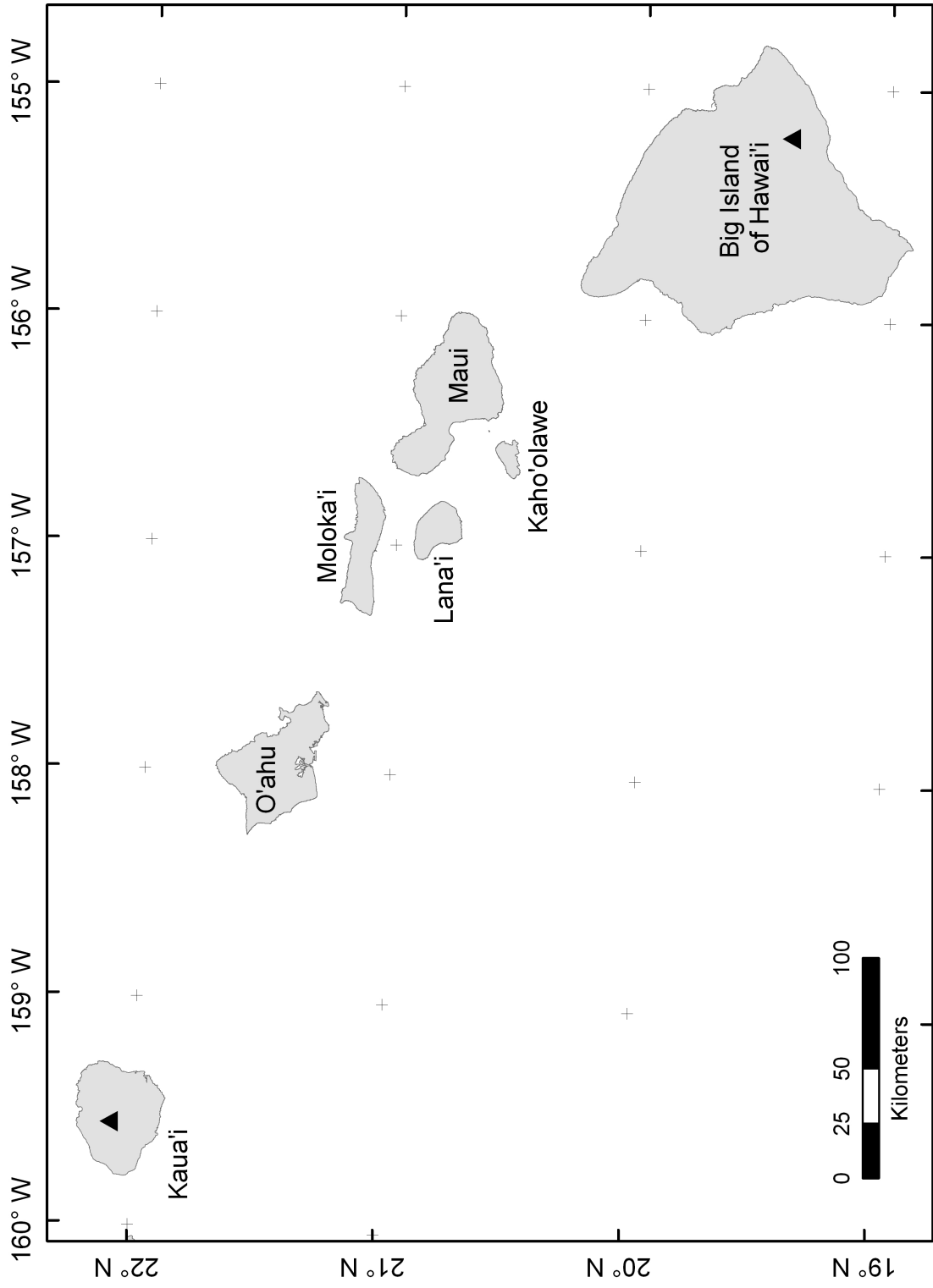


Figure 4.2. Shaded relief map of the Big Island. The five volcanoes that make up the island are labeled. The landscape is smooth and very little erosion has altered the constructive topography of the shield volcanoes, with the exception of deep valleys carved into the headwall of a giant landslide on eastern Kohala. The Hamakua-Hilo region is located along the coastline at the top of the image, on the eastern flanks of Mauna Kea. The Puna/Ka'u region occupies the southeast of the island around Kilauea volcano. Red dots show the location of major towns.

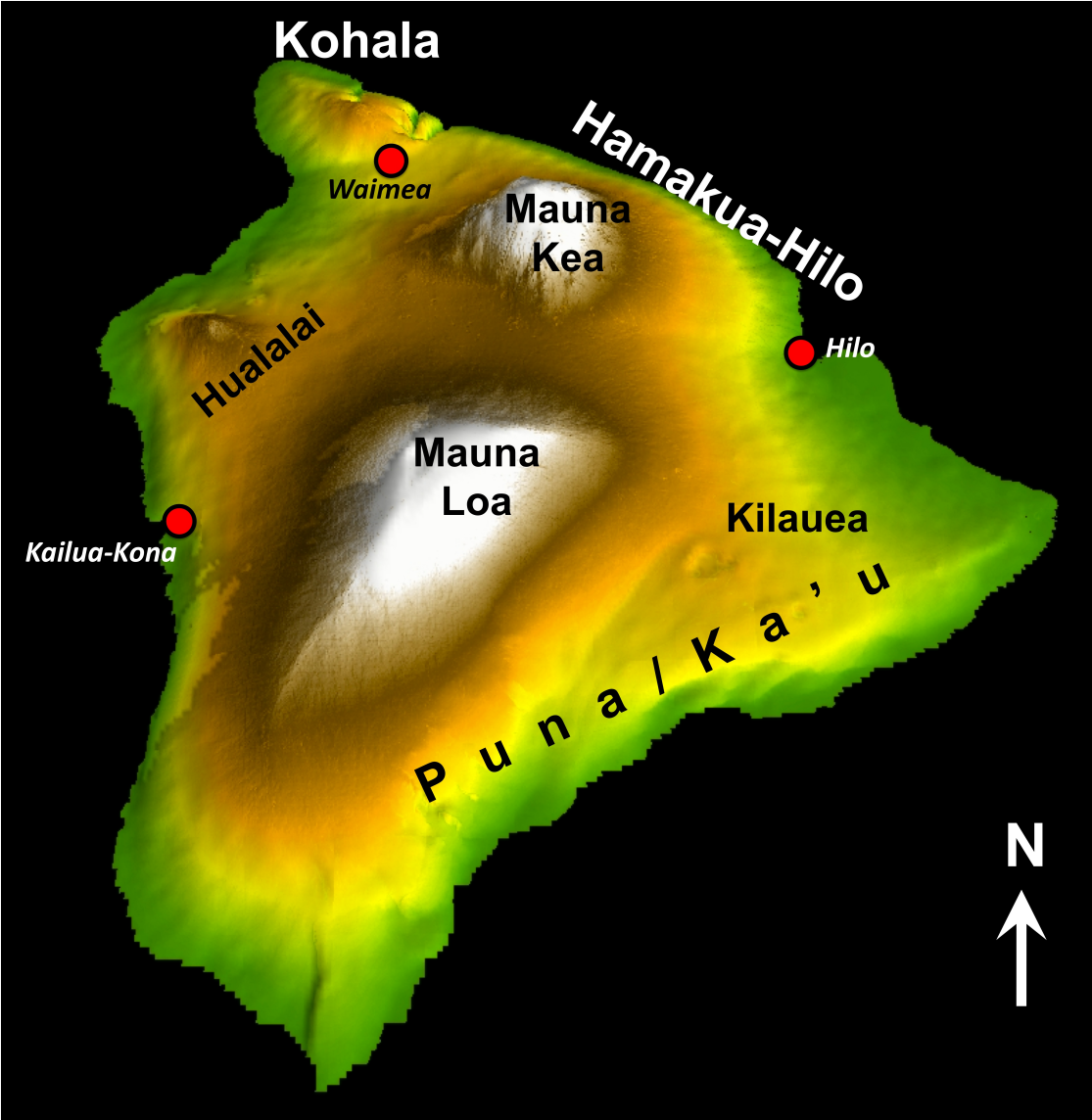
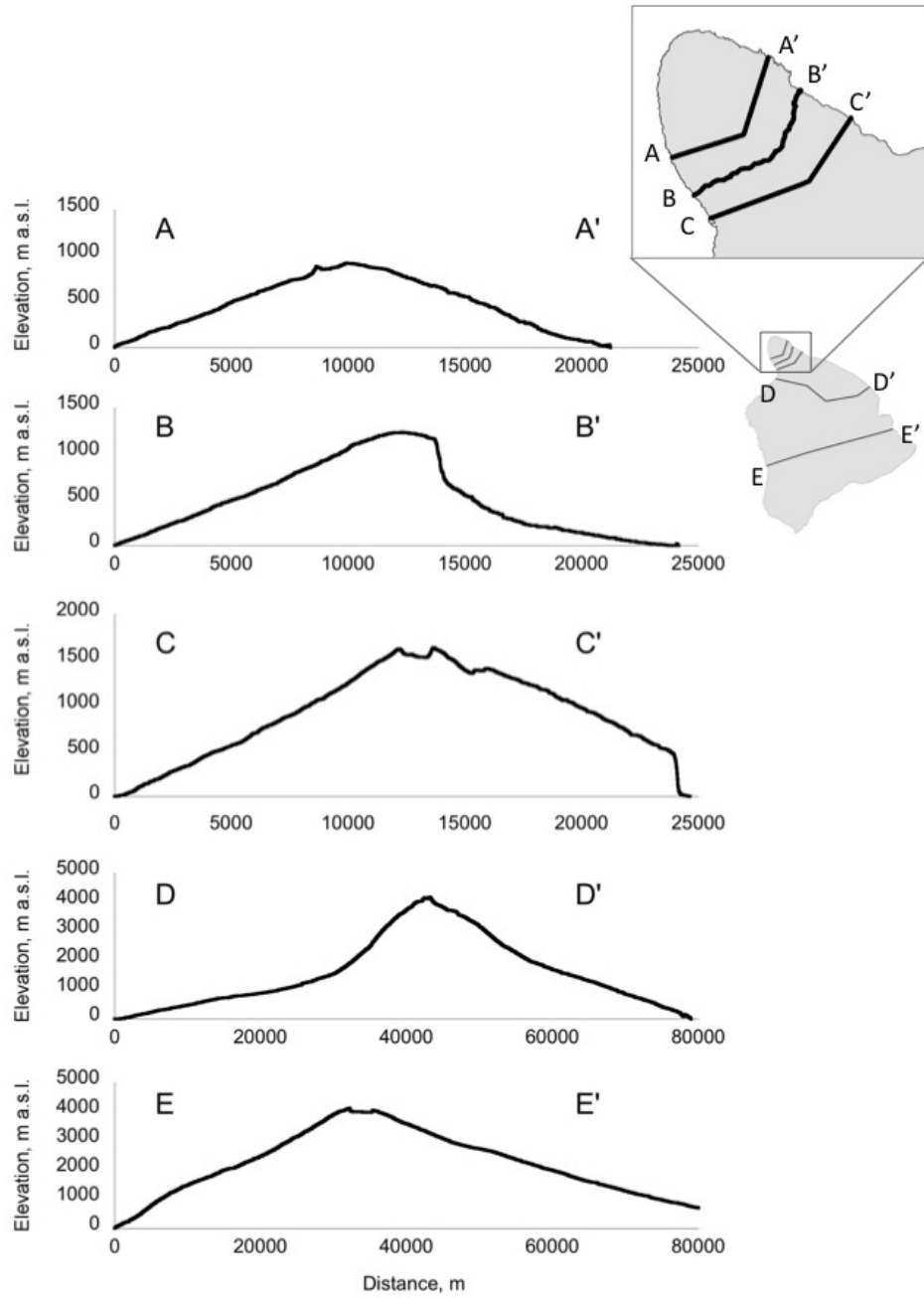


Figure 4.3. Cross-sections through the Big Island illustrate the varying degrees of landscape development on the island. The first three cross-sections (**A** through **C**) slice through the Kohala Peninsula and the latter two go through Mauna Kea (section **D**) and Mauna Loa (section **E**). Section **A-A'** shows the relatively pristine shield surface of northern Kohala, outside the area of influence of the giant landslide of 385-173 kyr ago (Lamb et al., 2007). Late-stage volcanic cones dot the surface of the shield, giving it a slightly uneven appearance. Sections **B-B'** and **C-C'** are complementary in the sense that they describe two possible outcomes from development of the headwall of the giant landslide referred to above. Small streams that have a very limited drainage area do not manage to cut into the headwall effectively and instead plunge off of the cliff in spectacular, up to 500m tall, waterfalls (Section **C-C'**). Streams that manage to capture adjacent drainage basins as they erode the headwall, such as Honokane Nui Stream, end up with a large drainage area and large amounts of runoff to carve deep, V-shaped valleys with steep headwalls and gently curving stream profile (Section **B-B'**). Faults near the summit of Kohala Volcano that channel the abundant rainfall into the deep valleys are responsible for the ability of these streams to capture nearby drainages and thereby for their great erosive power (Lamb et al., 2007). All traverses have 4× vertical exaggeration.



Rainfall rates drop from ~3800 mm/yr at the summit of Kohala Volcano to ~160 mm/yr at the west coast, over a distance of 12 km, creating an exceptionally steep rainfall gradient (Giambelluca et al., 1986).

Kaua'i is the oldest of the large Hawaiian Islands. The oldest shield-building rocks on Kaua'i have been dated at 5.1 Myr (McDougall, 1979). The original constructive shield topography has been profoundly altered by chemical weathering, erosion and sedimentation (Figure 4.4). The Alaka'i Swamp in central western Kaua'i is the only remnant of the original shield surface and covers less than 20% of the island (center section of Figure 4.5 A-A', B-B' and C-C'). A large tectonic basin, the Lihue Basin, occupies much of the eastern part of the island (Figure 4.5 A-A', right side) and deeply incised river valleys characterize the remainder (e.g. Figure 4.5 C-C'). The highest point on Kaua'i is Mt. Wai'ale'ale (1569 m, 5148 ft). The trade winds bring up to 11,000 mm of rain pr. year to Mt. Wai'ale'ale (Giambelluca et al., 1986). The copious rainfall forms very steep terrain (Figures 4.4, 4.5) with lush vegetation on the east side of Kaua'i. The west side is considerably drier, due to a rain shadow effect similar to the one described for the Kohala Peninsula above but not nearly as pronounced.

The two islands studied here represent the extremes of landscape sculpting and weathering progression on the Hawaiian Islands (compare Figures 4.2 and 4.4). Although small enclaves of little to no physical erosion can be found on nearly all the islands (Crews et al., 1995), the dramatic differences in landscapes that unfold along the chain of islands testify to the increasing impact of physical erosion and mass wasting from the younger islands to the older ones. Since rainfall is very easily routed to groundwater through the porous substrate, most streams on the Big Island of Hawai'i are ephemeral, flowing only after intense and/or prolonged rainfall. The

Figure 4.4. Shaded relief map of Kaua'i. Kaua'i is much more eroded than the Big Island, as seen in the knife-edge ridges and deep valleys of the island. The semi-circular structure that occupies much of the western half of the island is the Lihu'e Basin, formed by structural collapse (Reiners et al., 1999). The remains of the original shield surface in the Alaka'i Swamp are visible in the north-central part of the island, upstream from the Waimea River in Waimea Canyon. Mt. Wai'ale'ale is the tallest point on the island and also one of the wettest spots on Earth. Red dots show the location of major towns.

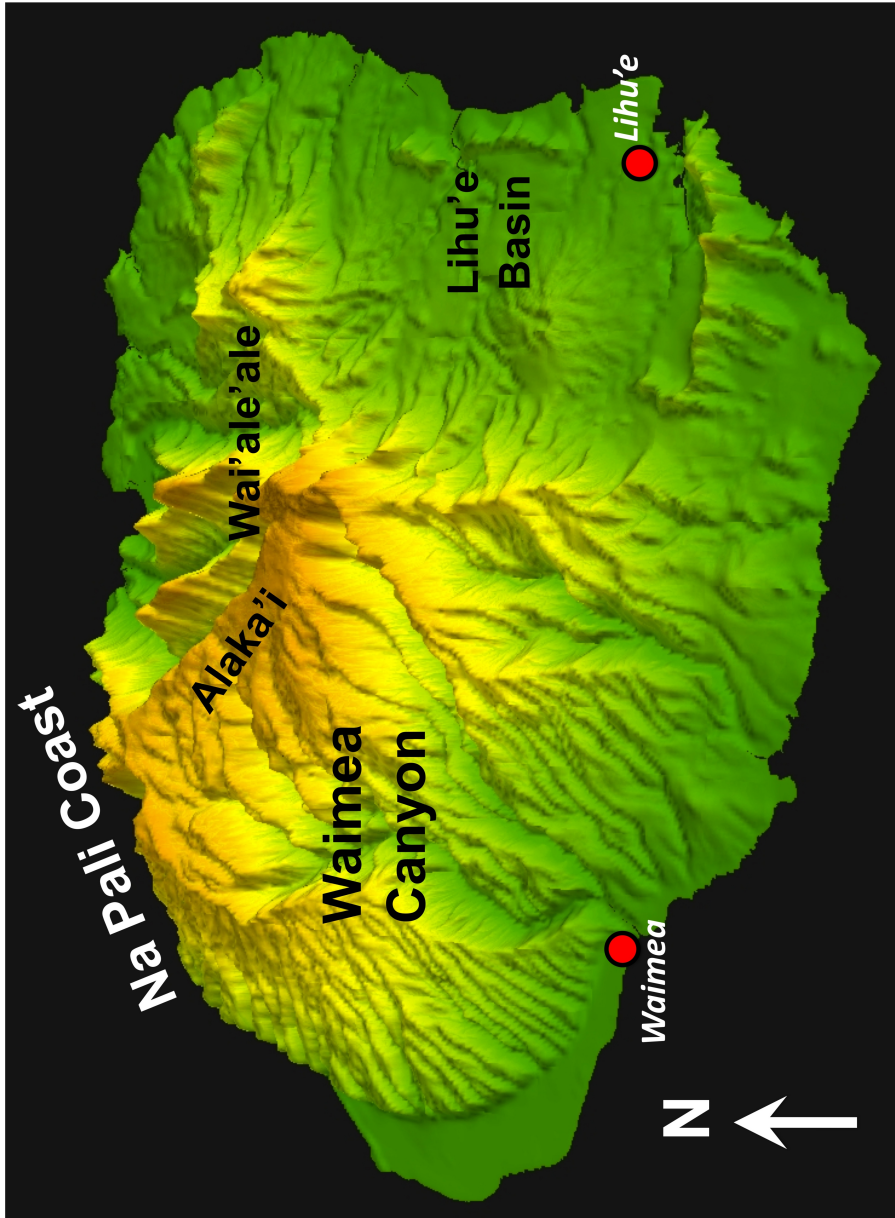
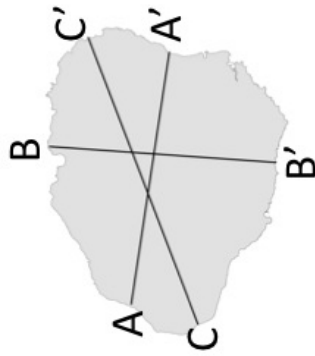
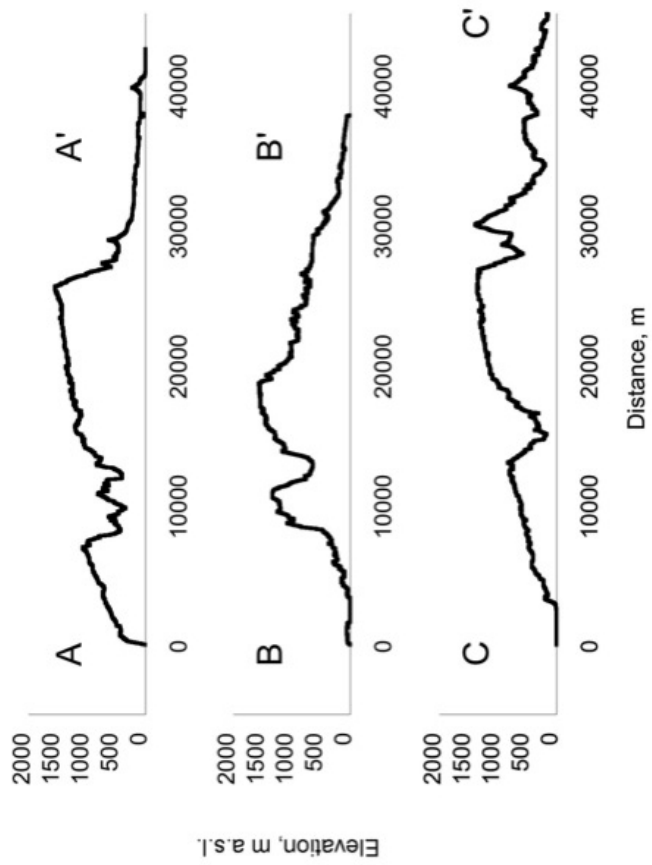


Figure 4.5. Cross-sections through Kaua'i illustrate the different geomorphic regimes on the island. Section **A-A'** cuts from west to east right through the upper reaches of Waimea Canyon and its tributaries (around the 10,000 m mark on the x-axis) and over the Alakai Swamp to the summit of Mt. Wai'ale'ale before plunging steeply into the Lihue Basin. Section **B-B'** traverses the island from north to south, highlighting the high-relief landscape of northern Kaua'i (also seen in the north-east segment of section **C-C'**). In the south, a more gently sloping ridge leads down from Mt. Wai'ale'ale along the eastern wall of Hanapepe Stream valley towards the south coast. A different perspective on the Waimea Canyon is displayed in section **C-C'**, which traverses the Waimea Canyon (at the 15,000m mark on the x-axis) about 3 km downstream from the "Waimea Stream @ dam" sampling site and around 1 km upstream from the "Waimea Stream @ powerhouse" sampling site. The section continues to the east over the Alaka'i Swamp and over the uppermost reaches of the heavily eroded Wainiha Valley before traversing the summit of Mt. Wai'ale'ale and continuing north-east north of the Lihue Basin. All traverses have 4× vertical exaggeration.



largest river on the Big Island, Wailuku River, is located in a zone of rainfall maximum at the boundary between rocks from Mauna Kea and Mauna Loa and is a perennial, largely groundwater-fed, river. A few smaller perennial streams lie immediately north of the Wailuku River but going north along the shore of Mauna Kea, rainfall decreases and streams become ephemeral. On the Kohala Peninsula, abundant rainfall and physical erosion over time combine to form several mostly groundwater-fed streams that can nonetheless dry out after any prolonged absence of rain.

In stark contrast to the Big Island, Kaua'i is home to many perennial streams and rivers, including the only navigable river in Hawai'i, the Wailoa River. Many of these streams have carved spectacular steep-sided river valleys.

4.2. METHODS

4.2.1. Fieldwork

Fieldwork was carried out on Kaua'i and the Big Island of Hawai'i in early 2005 and 2006 and on the Big Island in January 2008. Our primary aim was to characterize the spatial variability in stream geochemistry and the associated chemical weathering rates. Due to the ephemeral nature of many of the streams on the Big Island, we focused our sampling efforts in the wet season when there is a greater chance of finding the streams running.

In 2005, we sampled 16 streams on the Big Island and 12 on Kaua'i. We were granted access to a number of groundwater wells on the Big Island as well, yielding 12 samples of groundwater. In 2006, we sampled 22 streams on the Big Island and 23 on

Kaua'i. During the 2006 Kaua'i sampling campaign, there was an intense prolonged rainstorm on the island. Due to the high rainfall, we observed a dilution effect in those streams sampled also the year before under more average hydrological conditions. It also enabled us to sample small streams on the west side of Waimea Canyon that only flow during storms. The 2008 fieldwork was mainly aimed at sampling inaccessible regions of the Kohala Peninsula on the Big Island. Twenty-two samples were collected. The sampling sites for stream water on the Big Island are shown in Figure 4.6a,b and groundwater well sites in Figure 4.6c. Figure 4.7 shows the stream sampling sites on Kaua'i. Table 4.1a contains a complete list of all streams sampled and Table 4.1b lists all groundwater wells used in this study.

The sampling procedure is described in detail in Chapter 2. We measured pH and temperature in the field. Normally, two samples of 125 mL each were collected from each stream. The water was collected using a 60 mL syringe that was rinsed several times in river water prior to sample collection, and filtered through a 0.2 or 0.45 μ m nitrate cellulose filter directly into an acid washed HDPL sample bottle. The samples were stored in a refrigerator until transport to Cornell University (up to 6 weeks after sample collection). One of the two bottles was acidified to pH \sim 2 with double-distilled HNO₃ or HCl for cation analysis.

4.2.2. Chemistry

Major anions (Cl⁻, SO₄²⁻) were analyzed on a Dionex ICS 2000 ion chromatograph at Cornell University with a precision better than 5%. Major cations (Na⁺, K⁺, Mg²⁺ and Ca²⁺) in samples from 2005 and 2006 were analyzed on a Dionex ICS 2000 ion chromatograph at Cornell University and in samples from 2008 on a Jobin Yvon Ultima ICP-AES at Boston University. The precision in the cation analyses was

Figure 4.6. Sampling sites on the Big Island. a) Streams sampled on the Kohala Peninsula. b) Streams sampled in the Hamakua-Hilo region. c) Heavy black line shows outlines of the full extent of Kohala and Hamakua-Hilo regions as defined here.

Filled boxes show location of groundwater wells used in this study.

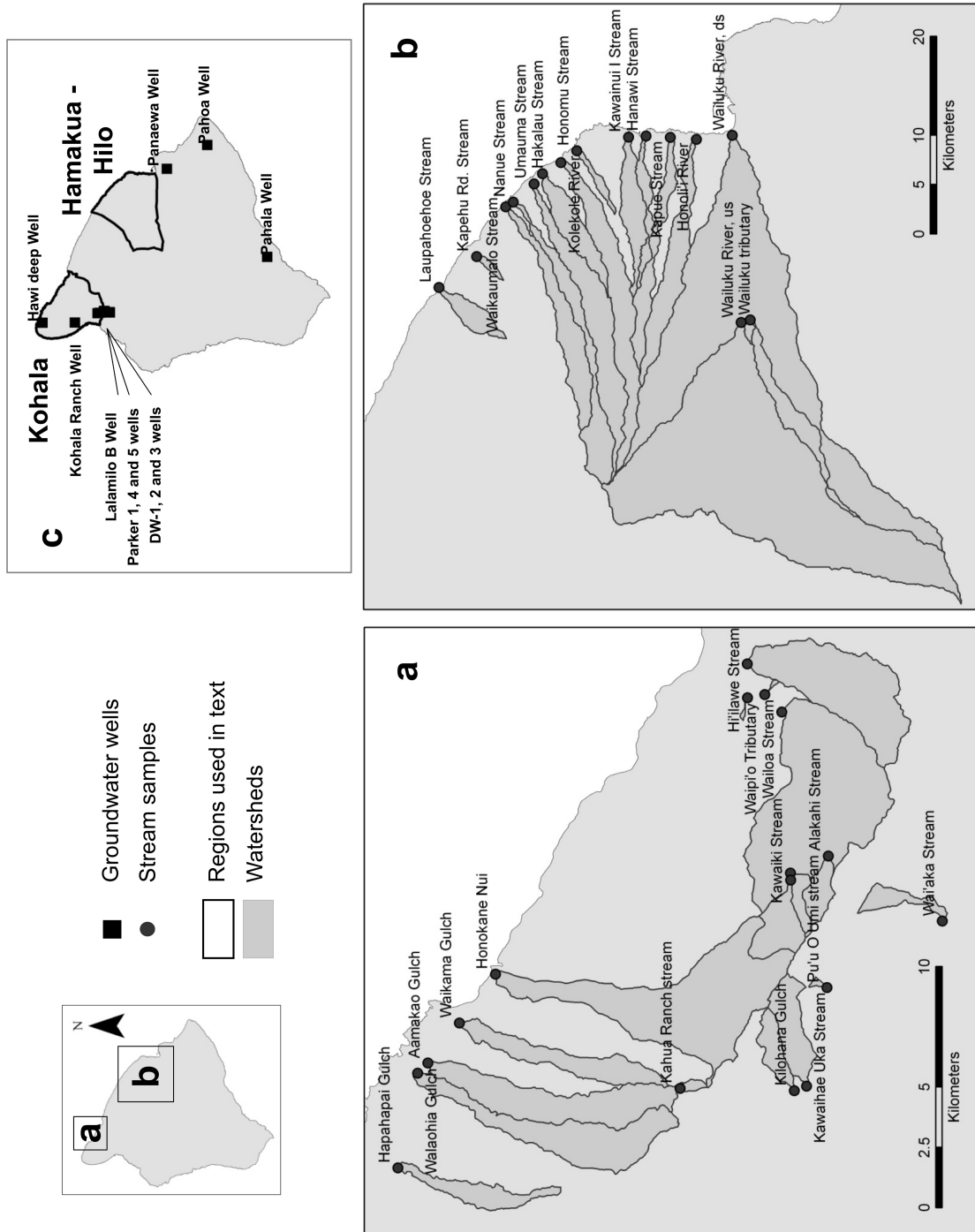


Figure 4.7. Sampling sites on Kaua'i. Heavy black lines delineate the regions used in this study. a) Streams sampled in Waimea. b) Streams sampled on East Kaua'i. Same legend as in Figure 4.6.

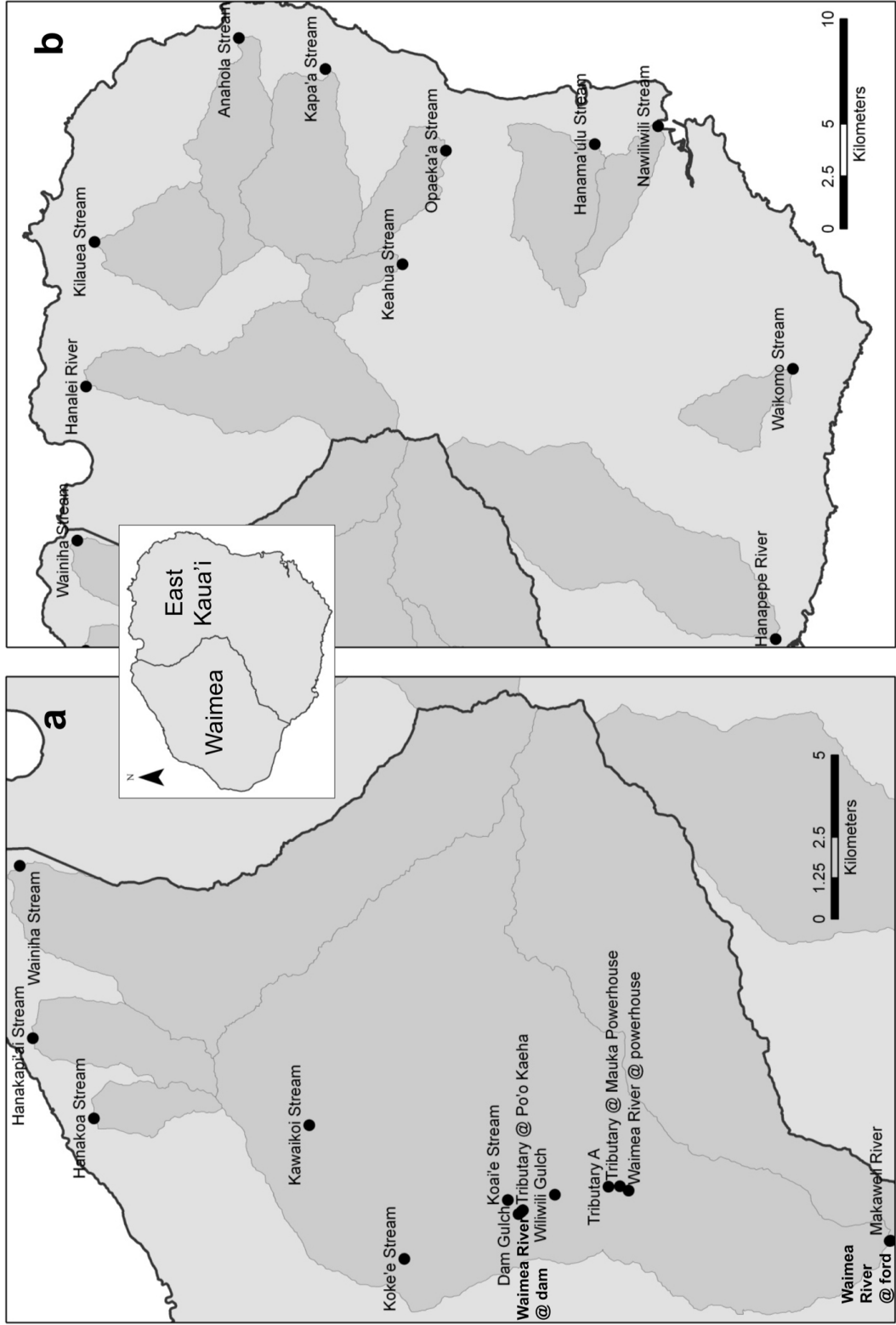


Table 4.1a. Sampling locations in Hawai'i 2005, 2006 and 2008.

Table 4.1a.

River name	Sample ID	Type	Latitude	Longitude	Area, km ²	Runoff, mm/yr	Sampling site, m a.s.l.	Basin, max elevation, m a.s.l.	Basin, average elevation, m a.s.l.	CV
Big Island										
Hamakua-Hilo										
Hakalau Stream	HI-05-41, HI-06-50, HI-08-09	Main	19.899	-155.131	22.4	5236	6	1237	560	50
Hanawi Stream	HI-05-38	Main	19.805	-155.093	10.8	5138	24	1189	583	53
Honoli'i Stream	HI-05-36, HI-06-16, HI-08-02	Main	19.758	-155.096	36.7	3172	5	2022	1049	39
Honomu Stream	HI-05-40, HI-06-07	Main	19.868	-155.109	4.16	5801	85	617	318	41
Kapehu Rd. Stream	HI-06-52, HI-08-06	Main	19.958	-155.212	1.98	2615	207	672	426	24
Kapue Stream	HI-05-37, HI-06-51, HI-08-03	Main	19.782	-155.095	24.3	3331	42	1890	1000	45
Kawainui I Stream	HI-05-39, HI-06-14, HI-08-04	Main	19.820	-155.095	21.9	4953	61	1240	635	42
Kolekole Stream	HI-05-01, HI-05-35, HI-06-13, HI-08-05	Main	19.882	-155.120	53.8	3104	4	3489	1330	56
Laupahoehoe Stream	HI-06-11	Main	19.992	-155.242	12.2	1449	11	1176	643	39
Nanue Stream	HI-05-43, HI-06-12, HI-08-08	Main	19.925	-155.159	37.5	1793	63	3784	2008	48
Umauma Stream	HI-05-42, HI-06-06, HI-08-10	Main	19.906	-155.141	54.2	2458	80	3661	1479	45
Waikaumalo Stream	HI-05-44, HI-06-05, HI-08-07	Main	19.932	-155.163	35.5	2373	62	2708	1391	41
Wailuku River, ds	HI-05-02, HI-05-33, HI-06-15, HI-08-01	Main	19.726	-155.092	638	688	6	4201	1864	42
Wailuku River, us	HI-06-47	Tributary	19.715	-155.272	343	79	1109	4201	2284	27
Wailuku Tributary	HI-06-46	Tributary	19.707	-155.270	24.3	79	1100	2356	1645	15

Table 4.1a. (continued)

River name	Sample ID	Type	Latitude	Longitude	Area, km ²	Runoff, mm/yr	Sampling site, m a.s.l.	Basin, max elevation, m a.s.l.	Basin, average elevation, m a.s.l.	CV
Kohala										
Aamakao Gulch	HI-05-23, HI-06-04, HI-08-23	Main	20.220	-155.755	12.5	1535	47	1222	204	36
Hapahapai Gulch	HI-05-24	Main	20.230	-155.797	3.86	651	142	734	540	14
Hi'ilawe Stream	HI-06-42, HI-08-15	Main	20.103	-155.595	16.2	1661	32	1211	762	19
Honokane Nui Stream	HI-08-21	Main	20.195	-155.720	26.1	2316	8	1676	975	44
Kakeha Stream	HI-08-16	Main	20.096	-155.607	0.07	1826	24	615	496	26
Kawaihae Uka Stream	HI-06-01, HI-08-24	Main	20.078	-155.762	4.57	2853	1066	1668	1377	10
Kilohana Gulch	HI-05-05, HI-06-02	Main	20.082	-155.764	2.30	3128	1084	1541	1292	11
Pu'u O Umi Stream	HI-06-49	Main	20.071	-155.723	0.15	2535	1486	1612	1553	2
Wai'aka Stream	HI-05-04, HI-05-28, HI-06-40, HI-06-41, HI-06-45, HI-08-19, HI-08-20	Main	20.028	-155.696	1.95	4580	747	1358	1047	13
Waikama Gulch	HI-08-22	Main	20.208	-155.739	6.65	1695	122	1139	647	43
Wailoa Stream	HI-06-43, HI-08-17	Main	20.089	-155.614	37.4	1781	42	1627	931	40
Wailoa Tributary	HI-08-18	Main	20.102	-155.609	0.07	2007	10	662	457	41
Walaohia Gulch	HI-06-03	Main	20.223	-155.759	12.4	1094	62	1222	702	38
Kohala - Upper Kohala										
Alakahi Stream	HI-08-11	Tributary	20.071	-155.671	2.17	3292	1187	1598	1315	5
Kahua Ranch Stream	HI-05-03	Tributary	20.125	-155.764	0.37	1969	1146	1428	1211	6
Kawaiki Stream	HI-08-13	Tributary	20.085	-155.678	1.24	2688	1225	1574	1333	5
Kawainui II Stream	HI-08-14	Tributary	20.085	-155.681	3.99	3403	1244	1627	1409	6

Table 4.1a. (continued)

River name	Sample ID	Type	Latitude	Longitude	Area, km ²	Runoff, mm/yr	Sampling site, m a.s.l.	Basin, max elevation, m a.s.l.	Basin, average elevation, m a.s.l.	CV
Kaua'i										
East Kaua'i										
Anahola Stream	HI-06-23	Main	22.142	-159.313	23.9	1438	3	861	273	60
Hanalei River	HI-05-19, HI-06-21	Main	22.207	-159.475	54.3	3455	2	1562	397	47
Hanama'ulu Stream	HI-05-17, HI-06-25	Main	21.989	-159.362	25.6	1348	12	350	147	42
Hanapepe River	HI-06-27	Main	21.911	-159.590	69.2	1575	9	1416	456	68
Kapa'a Stream	HI-06-18	Main	22.105	-159.328	36.2	1634	5	993	305	74
Keahua Stream	HI-06-17	Main	22.072	-159.418	9.25	3046	157	993	418	43
Kilauea Stream	HI-06-22	Main	22.204	-159.408	23.0	2956	85	860	226	60
Opaeka'a Stream	HI-06-26	Main	22.053	-159.365	13.3	1687	85	403	155	41
Waikomo Stream	HI-06-29	Main	21.904	-159.466	11.5	138	61	551	170	48
Waimea										
Dam Gulch	HI-06-33	Tributary	22.073	-159.648	0.10	417	233	807	483	31
Hanakapi'ai Stream	HI-05-21, HI-06-19, TA-2	Main	22.207	-159.597	9.55	1597	17	1296	762	48
Hanakoa Stream	HI-05-20	Main	22.190	-159.620	4.38	1142	158	1297	833	35
Koai'e Stream	HI-05-07	Tributary	22.076	-159.644	29.3	2094	257	1379	1008	26
Makaweli River	HI-05-14, HI-06-30	Main	21.971	-159.656	68.7	2166	3	1599	724	56
Waimea River @ dam	HI-05-06, HI-06-32	Tributary	22.073	-159.648	52.7	906	230	1300	1000	27
Waimea River @ ford	HI-05-12, HI-06-28	Main	21.971	-159.656	151	647	1	1440	842	44
Waimea River @ powerhouse	HI-05-08, HI-06-35	Tributary	22.043	-159.641	113	614	157	1440	975	31
Waimea Tributary @ Po'o Kaeha	HI-06-34	Tributary	22.072	-159.647	0.45	1278	228	1017	652	32

Table 4.1a. (continued)

River name	Sample ID	Type	Latitude	Longitude	Area, km ²	Runoff, mm/yr	Sampling site, m a.s.l.	Basin, max elevation, m a.s.l.	Basin, average elevation, m a.s.l.	CV
Waimea Tributary	HI-06-36	Tributary	22.046	-159.640	1.01	378	160	920	599	28
@ powerhouse										
Waimea Tributary A	HI-05-09, HI-06-37	Tributary	22.049	-159.640	0.23	499	164	613	513	8
Waimiha Stream	HI-06-20	Main	22.211	-159.546	58.3	3641	5	1562	719	58
Wiliwili Gulch	HI-06-31	Tributary	22.063	-159.642	2.66	408	204	991	620	32
Waimea - Alakai										
Kawaikoi Stream	HI-06-39, TA-5	Tributary	22.131	-159.622	10.6	2795	1038	1300	1174	5
Koke'e Stream	HI-05-10, HI-06-38, TA-4	Tributary	22.105	-159.662	4.91	1376	896	1285	1112	5

Table 4.1b. Groundwater wells in Hawai'i used in this study.

Island	Aquifer	Well name	USGS Well #	Sample ID	Latitude	Longitude	Land surface elevation	Mean groundwater level	USGS Well # for nearby well
BI	C	Lalamilo B	8-5946-02	HI-05-25	19.984	-155.774	333	-2.1	334
BI	C	Parker 1*	8-5846-02	HI-05-26	19.974	-155.771	358	1.5	351
BI	B	Hawi deep well 1	n.a.	HI-05-27	20.238	-155.825	161	-	-
BI	C	Kohala Ranch Well 1	n.a.	HI-05-29	20.088	-155.821	441	-	-
BI	Waimea	DW-2	8-5546-01	HI-05-47	19.927	-155.769	363	-	-
BI	Waimea	DW-3	8-5546-02	HI-05-48	19.929	-155.767	379	-	-
BI	Waimea	Parker 4	8-5745-02	HI-05-49	19.953	-155.762	369	-	-
BI	Waimea	DW-1	8-5745-03	HI-05-50	19.955	-155.763	372	3.7	361
BI	Waimea	Parker 5	8-5745-01	HI-05-51	19.954	-155.762	366	-	-
BI	Puna/Ka'u	Panaewa Well 1*	8-4003-01	HI-06-57	19.673	-155.063	62	3.7	59
BI	Puna/Ka'u	Pahoa Well 1*	n.a.	HI-06-58	19.487	-154.944	220	4.6	179
BI	Puna/Ka'u	Pahala Well*	n.a.	HI-06-59	19.204	-155.487	342	340	2
K	Kauai	Kalepa Ridge W-10	2-5921-01	n.a.	21.997	-159.359	92	4.6	88
M	Iao	Waikapu 2	6-5130-02	n.a.	20.862	-156.508	158	3.4	155
M	Iao	Waiehu Deep Monitor Well	6-5430-05	n.a.	20.913	-156.513	116	3	113
O	Pearl Harbor	Waipahu Deep Monitor Well	3-2300-18	n.a.	21.391	-158.002	8	5.2	3
O	Pearl Harbor	Schofield Shaft	3-2901-07	n.a.	21.488	-158.027	259	84	175

*: Groundwater level cited is from a nearby well

1: meters below land surface

generally better than 6%. Si in all samples was measured using the molybdate blue method (Mortlock and Froelich, 1989) at Cornell University with a precision better than 2%. Sr^{2+} in 2005 samples was measured on a Finnigan Element 2 ICP-MS at Cornell University and in all other samples on the Jobin Yvon Ultima ICP-AES at Boston University. The precision on Sr^{2+} -analyses is in general better than 5%. $^{87}\text{Sr}/^{86}\text{Sr}$ in all samples was analyzed on a Fisons Sector 54 thermal ionization mass spectrometer at Cornell University, with an average error of 0.01%. Sr-isotopes on 2006 samples have slightly larger uncertainty because of contamination from the filters used in that year's sampling campaign. Repeated measurements of the NBS987 standard give $^{87}\text{Sr}/^{86}\text{Sr}$ of 0.71025 ± 0.00001 . Bicarbonate concentrations in samples from 2006 were determined by charge balance and have a propagated error of 22%. Alkalinity in all other samples was determined with Gran titration, with a precision better than 2%. Repeat analyses of the M178 standard from the USGS indicate that the accuracy of our methods is better than 6% for anions, 5% for cations and 3% for Si.

4.2.3. Atmospheric correction

Solutes in surface and groundwater derive not only from the chemical weathering of bedrock but also from precipitation and atmospheric dust. The atmospheric contribution to the solute load must be determined in order to isolate the chemical weathering component. We used two methods to determine atmospheric contribution. The first method, the “cyclic salts” method, relies on the assumptions that a) Cl^- behaves conservatively in the weathering environment, b) all Cl^- in water comes from the atmosphere and c) X/Cl -ratios in atmospheric deposition are known. The second method we use relies on Sr-isotopes in stream and groundwater as an indicator of

mixing between two end members, namely Sr from basalt and Sr from atmospheric sources.

4.2.3.1. Cyclic salts - method

The most complete budget of atmospheric deposition in Hawai'i (Carrillo et al., 2002) uses multi-year data from Koke'e State Park on Kaua'i and Hawai'i Volcanoes National Park (HVNP) on the Big Island of Hawai'i (approximate location of sites is labeled with triangles in Figure 4.1). At Koke'e State Park, precipitation amounts and chemistry were measured from 1999 to 2000. The record from HVNP is more complete, incorporating dry, precipitation and fog deposition. We converted the results of Carrillo et al. (2002) into Cl-normalized ratios for Na^+ , K^+ , Ca^{2+} and Mg^{2+} to use in the standard atmospheric correction method. Atmospheric deposition in the vicinity of the volcano is heavily influenced by volcanic gases and the burning of biomass (Carrillo et al., 2002) and the ratios from HVNP might therefore not be applicable to other regions unaffected by volcanism. To investigate this, we compared the Cl-normalized ratios of rainfall, the only data product available for both sites, from the two sites. Mg/Cl and Ca/Cl in rainfall were almost identical at the two sites, suggesting these elements are not significantly impacted by the ongoing volcanism in Kilauea. Na/Cl and K/Cl at HVNP are 2 and 7 times, respectively, higher than the corresponding ratios at Koke'e. Carrillo et al. (2002) attribute the enrichment in K in HVNP to biomass burning by flowing lava and to high concentrations of K in volcanic plumes. The authors do not speculate on the origin of the Na enrichment at HVNP but we conclude that the 2-fold enrichment over the value at Koke'e, and 30% enrichment over sea salt ratios, is significant and most likely influenced by the volcano.

Table 4.2. Cl-normalized atmospheric deposition in Hawai'i.

	Na/Cl	K/Cl	Mg/Cl	Ca/Cl
Rainfall, Koke'e State Park*	0.595	0.011	-	-
All atmospheric deposition, HVNP*	-	-	0.091	0.040
Seawater [#]	0.858	0.019	0.098	0.019

* = Carrillo et al., 2002

= Schlesinger, 1997

Taking all this into consideration, we argue that the most accurate atmospheric correction for Hawai'i is accomplished by using the K/Cl and Na/Cl from precipitation chemistry in Koke'e, and the Mg/Cl and Ca/Cl from total atmospheric deposition at HVNP. These values, listed in Table 4.2, are used for all streams in this study. We assume that all Cl⁻ comes from the atmosphere, and calculate the weathering-derived fraction of element X in sample *j*, [X]_{*j*}^{*}, as (X = Na, K, Ca, Mg):

$$[X]_j^* = [X]_j - [Cl^-]_j \times \left(\frac{X}{Cl} \right)_{atm} \quad (4.1)$$

4.2.3.2. Sr-isotopes – method

We used a simple two-component mixing model to partition the Sr in our samples into relative proportions derived from igneous rock and atmospheric sources:

$$f_i = \frac{R_{spl} - R_{atm}}{R_i - R_{atm}} \times 100 \quad (4.2)$$

where “*f*” refers to fraction in percents, “*R*” refers to $^{87}\text{Sr}/^{86}\text{Sr}$ and the subscripts “*i*”, “*spI*” and “*atm*” refer to igneous rock, sample and atmospheric input, respectively. The average $^{87}\text{Sr}/^{86}\text{Sr}$ of Hawaiian basalt is 0.7035 (Chadwick et al., 2009; and references therein). We use the present-day $^{87}\text{Sr}/^{86}\text{Sr}$ of seawater ($^{87}\text{Sr}/^{86}\text{Sr} = 0.7092$) as our best estimate of the $^{87}\text{Sr}/^{86}\text{Sr}$ of atmospheric deposition in Hawai'i.

4.2.4. Hydrology

A detailed account of hydrological fluxes from the Hawaiian Islands is presented in Chapter 3.

4.2.5. Geomorphology

Watersheds were extracted from a 10m resolution digital elevation model (DEM) downloaded from the USGS seamless server. We used ArcGIS 8 and 9 (ESRI, 2009) to process the DEM for watershed delineation upstream from sampling points. We extracted DEMs for each watershed and calculated the statistics (minimum, mean and maximum elevation, standard deviation of the elevation, and relief) for each.

4.3. RESULTS

The chemical composition of streams and groundwater collected in this study is presented in Table 4.3a (streams) and Table 4.3b (groundwater). Several streams were sampled multiple times. Where discharge data at time of sampling was available, discharge-weighted average concentrations were calculated, otherwise arithmetic average concentrations were used for streams with multiple samples.

Table 4.3a. Chemical composition of stream water on the Big Island of Hawai'i and on
Kaua'i

Table 4.3a.

River name	Sample ID	Date	Q	T	pH	Cl	SO ₄	Na	K	Mg	Ca	Si	Alk	TDS	Sr	⁸⁷ Sr/ ⁸⁶ Sr	± 2σ					
			m ³ /sec	°C	μmol/L													μeq/L	ppm	nmol/L		
Big Island																						
Hamakua-Hilo																						
Hakalau Stream	HI-05-41	5/6/09	n.a.	25.0	7.73	184	24	210	9	158	148	297	593	76	51							
Hakalau Stream	HI-06-50	4/10/10	n.a.	19.5	8.06	146	28	176	8	78	70	129	278	41	307							
Hakalau Stream	HI-08-09	1/17/12	n.a.	18.6	7.49	161	26	153	10	145	121	276	484	65	502							
<i>Hakalau Stream</i>	<i>3 samples</i>			<i>21.0</i>	<i>7.76</i>	<i>164</i>	<i>26</i>	<i>179</i>	<i>9</i>	<i>127</i>	<i>113</i>	<i>234</i>	<i>451</i>	<i>60</i>	<i>287</i>							
Hanawi Stream	HI-05-38	5/6/09	n.a.	23.4	8.07	202	22	214	9	154	139	280	558	73	53							
Honoli'i River	HI-05-36	5/6/09	0.4	23.4	7.78	163	24	275	11	154	153	271	682	80	41							
Honoli'i River	HI-06-16	3/20/10	39.6	n.a.	7.49	71	31	137	7	23	17	56	90	19	109							
Honoli'i River	HI-08-02	1/16/12	0.5	19.3	7.51	133	24	124	8	168	147	304	579	72	418							
<i>Honoli'i River</i>	<i>3 samples</i>			<i>21</i>	<i>7.49</i>	<i>73</i>	<i>31</i>	<i>138</i>	<i>7</i>	<i>26</i>	<i>19</i>	<i>61</i>	<i>101</i>	<i>20</i>	<i>112</i>							
Hononu Stream	HI-05-40	5/6/09	n.a.	22.4	7.91	211	29	347	14	166	181	349	776	96	64							
Hononu Stream	HI-06-07	3/18/10	n.a.	27.0	7.24	187	33	191	10	90	67	272	262	51	574							
<i>Hononu Stream</i>	<i>2 samples</i>			<i>25</i>	<i>7.58</i>	<i>199</i>	<i>31</i>	<i>269</i>	<i>12</i>	<i>128</i>	<i>124</i>	<i>311</i>	<i>519</i>	<i>73</i>	<i>319</i>							
Kapehu Rd. Stream	HI-06-52	4/10/10	n.a.	20.3	7.57	207	27	299	16	244	317	522	1175	135	1165							
Kapehu Rd. Stream	HI-08-06	1/17/12	n.a.	20.3	7.19	159	30	252	15	261	296	556	1160	133	1152	0.70367	0.00010					
<i>Kapehu Rd. Stream</i>	<i>2 samples</i>			<i>20</i>	<i>7.38</i>	<i>183</i>	<i>28</i>	<i>275</i>	<i>15</i>	<i>252</i>	<i>307</i>	<i>539</i>	<i>1168</i>	<i>134</i>	<i>1159</i>	<i>0.70367</i>	<i>0.00010</i>					
Kapue Stream	HI-05-37	5/6/09	n.a.	23.5	8.05	172	25	195	8	156	127	234	543	67	38							
Kapue Stream	HI-06-51	4/10/10	n.a.	20.3	7.57	130	37	139	9	75	65	108	226	36	242							
Kapue Stream	HI-08-03	1/16/12	n.a.	19.2	7.5	151	27	127	7	159	115	251	473	62	377	0.70409	0.00007					
<i>Kapue Stream</i>	<i>3 samples</i>			<i>21</i>	<i>7.71</i>	<i>151</i>	<i>30</i>	<i>153</i>	<i>8</i>	<i>130</i>	<i>102</i>	<i>198</i>	<i>414</i>	<i>55</i>	<i>219</i>	<i>0.70409</i>	<i>0.00007</i>					
Kawainui I Stream	HI-05-39	5/6/09	n.a.	24.8	7.95	174	17	181	8	104	103	233	387	55	40							
Kawainui I Stream	HI-06-14	3/20/10	n.a.	19.2	6.82	68	23	103	6	20	25	44	85	16	112							
Kawainui I Stream	HI-08-04	1/16/12	n.a.	19.1	7.37	156	19	136	10	108	95	237	358	52	437	0.70397	0.00007					
<i>Kawainui I Stream</i>	<i>3 samples</i>			<i>21</i>	<i>7.38</i>	<i>133</i>	<i>20</i>	<i>140</i>	<i>8</i>	<i>77</i>	<i>74</i>	<i>172</i>	<i>277</i>	<i>41</i>	<i>196</i>	<i>0.70397</i>	<i>0.00007</i>					
Kolekole River	HI-05-01	3/31/09	n.a.	20.1	6.6	202	27	58	3	27	25	57	-96	11		0.70373	0.00010					
Kolekole River	HI-05-35	5/5/09	n.a.	24.1	7.43	182	22	189	8	148	150	271	562	71	45							

Table 4.3a. (continued)

River name	Sample ID	Date	Q m ³ /sec	T °C	pH	Cl	SO ₄	Na	K	Mg	Ca	Si	Alk µeq/L	TDS ppm	Sr	⁸⁷ Sr/ ⁸⁶ Sr	± 2σ
Kolekole River	HI-06-13	3/20/10	n.a.	18.9	6.86	45	27	63	6	20	29	55	70	15	93		
Kolekole River	HI-08-05	1/16/12	n.a.	18.4	7.46	138	23	135	9	151	137	280	537	67	429	0.70396	0.00007
<i>Kolekole River</i>	<i>4 samples</i>			<i>20</i>	<i>7.09</i>	<i>142</i>	<i>25</i>	<i>111</i>	<i>7</i>	<i>87</i>	<i>85</i>	<i>166</i>	<i>268</i>	<i>41</i>	<i>189</i>	<i>0.70384</i>	<i>0.00009</i>
Laupahoehoe Stream	HI-06-11	3/20/10	n.a.	19.8	7.25	82	25	258	15	28	22	88	239	32	139		
Nanue Stream	HI-05-43	5/6/09	n.a.	24.1	7.4	186	23	196	9	141	136	270	523	69	45		
Nanue Stream	HI-06-12	3/20/10	n.a.	18.6	6.59	48	23	135	6	15	19	37	117	17	81		
Nanue Stream	HI-08-08	1/17/12	n.a.	17.9	7.47	139	22	138	10	137	118	278	472	62	439	0.70397	0.00007
<i>Nanue Stream</i>	<i>3 samples</i>			<i>20.2</i>	<i>7.15</i>	<i>124</i>	<i>22</i>	<i>156</i>	<i>8</i>	<i>98</i>	<i>91</i>	<i>195</i>	<i>371</i>	<i>49</i>	<i>188</i>	<i>0.70397</i>	<i>0.00007</i>
Umauma Stream	HI-05-42	5/6/09	n.a.	25.5	8.26	177	25	212	10	162	147	280	606	75	45		
Umauma Stream	HI-06-06	3/18/10	n.a.	26.0	7.52	105	25	113	7	59	38	161	159	31	277		
Umauma Stream	HI-08-10	1/17/12	n.a.	19.3	7.78	139	26	134	9	162	126	285	529	67	459		
<i>Umauma Stream</i>	<i>3 samples</i>			<i>23.6</i>	<i>7.85</i>	<i>140</i>	<i>25</i>	<i>153</i>	<i>9</i>	<i>128</i>	<i>104</i>	<i>242</i>	<i>431</i>	<i>58</i>	<i>260</i>		
Waikaumalo Stream	HI-05-44	5/6/09	n.a.	23.6	7.06	223	27	239	12	165	159	339	617	83	51		
Waikaumalo Stream	HI-06-05	3/18/10	n.a.	26.5	7.07	149	26	145	8	64	43	209	168	37	320		
Waikaumalo Stream	HI-08-07	1/17/12	n.a.	18.3	7.51	178	26	162	12	156	136	347	529	73	494	0.70398	0.00007
<i>Waikaumalo Stream</i>	<i>3 samples</i>			<i>22.8</i>	<i>7.21</i>	<i>183</i>	<i>26</i>	<i>182</i>	<i>10</i>	<i>129</i>	<i>113</i>	<i>298</i>	<i>438</i>	<i>64</i>	<i>288</i>	<i>0.70398</i>	<i>0.00007</i>
Wailuku River, ds	HI-05-02	3/31/09	n.a.	19.9	7.2	72	28	198	12	31	32	75	196	28	9		
Wailuku River, ds	HI-05-33	5/5/09	n.a.	22.9	7.99	130	25	165	11	117	119	252	457	60	32		
Wailuku River, ds	HI-06-15	3/20/10	n.a.	n.a.	6.79	47	27	76	6	21	16	64	56	14	105		
Wailuku River, ds	HI-08-01	1/16/12	n.a.	20.2	7.7	139	35	134	13	143	127	301	468	65	354	0.70421	0.00012
<i>Wailuku River, ds</i>	<i>4 samples</i>			<i>21.0</i>	<i>7.42</i>	<i>97</i>	<i>29</i>	<i>143</i>	<i>10</i>	<i>78</i>	<i>73</i>	<i>173</i>	<i>294</i>	<i>42</i>	<i>125</i>	<i>0.70421</i>	<i>0.00012</i>
Wailuku River, us	HI-06-47	4/7/10	n.a.	15.7	7.65	39	22	81	7	42	47	135	182	27	330		
Wailuku Tributary	HI-06-46	4/7/10	n.a.	17.0	7.74	34	28	92	8	40	65	178	219	33	153		
Kohala																	
Aamakao Gulch	HI-05-23	4/29/09	n.a.	22.3	7.89	777	49	646	25	166	132	331	381	99	124		
Aamakao Gulch	HI-06-04	3/17/10	n.a.	28.0	7.75	461	26	540	18	105	58	283	369	75	1267		

Table 4.3a. (continued)

River name	Sample ID	Date	Q m ³ /sec	T °C	pH	Cl	SO ₄	Na	K	Mg	Ca	Si	µeq/L			Sr	⁸⁷ Sr/ ⁸⁶ Sr	± 2σ
													Alk	TDS	ppm			
Aamakao Gulch	HI-08-23	1/22/12	n.a.	19.5	7.31	438	33	435	27	156	108	327	485	85	1168			
<i>Aamakao Gulch</i>	<i>3 samples</i>			<i>23.3</i>	<i>7.65</i>	<i>559</i>	<i>36</i>	<i>541</i>	<i>23</i>	<i>142</i>	<i>99</i>	<i>314</i>	<i>412</i>	<i>86</i>	<i>853</i>			
Hapahapai Gulch	HI-05-24	4/29/09	n.a.	23.1	7.87	553	65	607	24	162	150	402	563	107	139	0.70386	0.00008	
Hi'ilawe Stream	HI-06-42	4/2/10	n.a.	n.a.	7.54	224	54	522	72	233	149	718	975	138	420			
Hi'ilawe Stream	HI-08-15	1/19/12	n.a.	20.6	8.16	193	54	445	68	253	140	771	925	135	399	0.70378	0.00007	
<i>Hi'ilawe Stream</i>	<i>2 samples</i>			<i>20.6</i>	<i>7.85</i>	<i>208</i>	<i>54</i>	<i>483</i>	<i>70</i>	<i>243</i>	<i>144</i>	<i>744</i>	<i>950</i>	<i>137</i>	<i>410</i>	<i>0.70378</i>	<i>0.00007</i>	
Honokane Nui Stream	HI-08-21	1/21/12	n.a.	20.0	7.49	155	22	202	30	159	179	572	705	99	419			
Kakeha Stream	HI-08-16	1/19/12	n.a.	19.3	6.48	249	24	178	13	75	45	142	132	35	120	0.70509	0.00012	
Kawaihae Uka Stream	HI-06-01	3/17/10	n.a.	23.5	6.68	152	6	121	7	19	17	16	35	13	124			
Kawaihae Uka Stream	HI-08-24	1/22/12	n.a.	15.7	5.11	168	8	102	6	24	13	54	-3	13	97			
<i>Kawaihae Uka Stream</i>	<i>2 samples</i>			<i>20</i>	<i>5.90</i>	<i>160</i>	<i>7</i>	<i>111</i>	<i>6</i>	<i>21</i>	<i>15</i>	<i>35</i>	<i>16</i>	<i>13</i>	<i>110</i>			
Kilohana Gulch	HI-05-05	4/12/09	n.a.	n.a.	7	203	14	145	10	29	20	67	17	19	17			
Kilohana Gulch	HI-06-02	3/17/10	n.a.	24.5	6.52	204	11	172	12	27	28	61	69	22	291			
<i>Kilohana Gulch</i>	<i>2 samples</i>			<i>25</i>	<i>6.76</i>	<i>203</i>	<i>12</i>	<i>158</i>	<i>11</i>	<i>28</i>	<i>24</i>	<i>64</i>	<i>43</i>	<i>20</i>	<i>154</i>			
Pu'u O Umi stream	HI-06-49	4/8/10	n.a.	12.5	4.53	178	9	168	9	23	14	24	55	17	51			
Wai'aka Stream	HI-05-04	4/12/09	n.a.	n.a.	7	179	12	131	5	32	15	62	21	17	17			
Wai'aka Stream	HI-05-28	5/3/09	n.a.	23.7	6.45	194	13	250	8	31	22	107	140	30	16	0.70509	0.00010	
Wai'aka Stream	HI-06-40	3/29/10	n.a.	n.a.	6.49	163	13	174	8	37	21	68	110	23	249			
Wai'aka Stream	HI-06-41	3/29/10	n.a.	21.2	6.51	167	14	185	9	37	22	72	116	25	260			
Wai'aka Stream	HI-06-45	4/6/10	n.a.	20.0	6.4	171	13	237	9	36	21	86	163	29	249			
Wai'aka Stream	HI-08-19	1/20/12	n.a.	15.4	6.08	156	11	117	7	36	15	108	48	20	197			
Wai'aka Stream	HI-08-20	1/20/12	n.a.	19.1	5.86	162	11	119	7	35	16	107	44	20	197			
<i>Wai'aka Stream</i>	<i>7 samples</i>			<i>19.9</i>	<i>6.40</i>	<i>170</i>	<i>12</i>	<i>173</i>	<i>8</i>	<i>35</i>	<i>19</i>	<i>87</i>	<i>92</i>	<i>24</i>	<i>169</i>	<i>0.70509</i>	<i>0.00010</i>	
Waikama Gulch	HI-08-22	1/22/12	n.a.	19.0	7.20	408	50	397	27	102	63	318	239	67	692	0.70414	0.00007	
Wailoa Stream	HI-06-43	4/3/10	n.a.	n.a.	7.96	243	43	453	56	199	200	641	970	132	447			
Wailoa Stream	HI-08-17	1/19/12	n.a.	20.5	8.09	173	33	297	39	167	154	575	724	104	362	0.70384	0.00007	
<i>Wailoa Stream</i>	<i>2 samples</i>			<i>20.5</i>	<i>8.03</i>	<i>208</i>	<i>38</i>	<i>375</i>	<i>47</i>	<i>183</i>	<i>177</i>	<i>608</i>	<i>847</i>	<i>118</i>	<i>405</i>	<i>0.70384</i>	<i>0.00007</i>	

Table 4.3a. (continued)

River name	Sample ID	Date	Q m ³ /sec	T °C	pH	Cl	SO ₄	Na	K	Mg	Ca	Si	Alk	TDS	Sr	⁸⁷ Sr/ ⁸⁶ Sr	± 2σ
Waipi'o Tributary	HI-08-18	1/19/12	n.a.	20.3	7.78	180	33	295	36	164	147	508	698	98	467	0.70384	0.00008
Walaohia Gulch	HI-06-03	3/17/10	n.a.	27.0	7.35	426	33	543	23	99	49	281	370	74	790		
Kohala - Upper Kohala																	
Alakahi Stream	HI-08-11	1/18/12	0.01	14.4	6.06	132	9	108	7	49	25	106	115	23	276	0.70387	0.00013
Kahua Ranch stream	HI-05-03	4/9/09	n.a.	n.a.	7.00	225	16	172	14	66	45	145	143	34	55		
Kawaiki Stream	HI-08-13	1/18/12	n.a.	13.2	5.32	137	7	82	5	23	10	48	0	11	66		
Kawainui II Stream	HI-08-14	1/18/12	0.05	13.0	4.79	135	7	78	5	23	11	49	0	11	55		
Kaua'i																	
East Kaua'i																	
Anahola Stream	HI-06-23	3/23/10	n.a.	n.a.	7.11	498	43	454	13	105	36	157	164	55	237		
Hanalei River	HI-05-19	4/23/09	3.3	23.8	7.56	275	14	322	15	248	145	243	816	93	29		
Hanalei River	HI-06-21	3/23/10	11.4	n.a.	7.07	225	13	200	9	110	44	198	264	46	202		
<i>Hanalei River</i>	<i>2 samples</i>			<i>23.8</i>	<i>7.18</i>	<i>236</i>	<i>13</i>	<i>227</i>	<i>11</i>	<i>141</i>	<i>66</i>	<i>208</i>	<i>387</i>	<i>56</i>	<i>163</i>		
Hanama'ulu Stream	HI-05-17	4/23/09	n.a.	23.5	7.56	442	54	491	22	227	129	225	670	96	34		
Hanama'ulu Stream	HI-06-25	3/23/10	n.a.	n.a.	7.23	658	115	630	44	138	88	139	196	77	610		
<i>Hanama'ulu Stream</i>	<i>2 samples</i>			<i>23.5</i>	<i>7.40</i>	<i>550</i>	<i>85</i>	<i>561</i>	<i>33</i>	<i>183</i>	<i>108</i>	<i>182</i>	<i>433</i>	<i>86</i>	<i>322</i>		
Hanapepe River	HI-06-27	3/24/10	n.a.	21.4	7.34	460	32	538	21	157	52	262	448	80	327		
Kapa'a Stream	HI-06-18	3/21/10	n.a.	22.0	7.09	607	52	529	16	162	75	193	293	75	483		
Keahua Stream	HI-06-17	3/21/10	n.a.	21.3	7.35	316	17	251	10	109	39	214	206	48	244		
Kilauea Stream	HI-06-22	3/23/10	n.a.	n.a.	7.21	412	47	371	11	100	43	142	158	50	211		
Opaeka'a Stream	HI-06-26	3/24/10	n.a.	21.9	6.95	579	72	530	20	110	67	121	150	62	400		
Waikomo Stream	HI-06-29	3/24/10	n.a.	23.4	6.91	928	97	758	39	164	83	118	143	84	445		
Waimea																	
Dam Gulch	HI-06-33	3/26/10	n.a.	n.a.	7.66	245	39	360	3	138	65	554	390	82	405		

Table 4.3a. (continued)

River name	Sample ID	Date	Q m ³ /sec	T °C	pH	Cl	SO ₄	Na	K	Mg	Ca	Si	Alk	TDS ppm	Sr	⁸⁷ Sr/ ⁸⁶ Sr	± 2σ
Hanakapi'ai Stream	TA-2	1/2/05	n.a.	19.0	310	17	350	0	185	126	401	629	90	280			
Hanakapi'ai Stream	HI-05-21	4/25/09	n.a.	18.4	7.93	284	15	330	13	191	143	381	696	93	23		
Hanakapi'ai Stream	HI-06-19	3/22/10	n.a.	23.0	7.18	330	18	339	11	115	54	321	322	64	221		
<i>Hanakapi'ai Stream</i>	<i>3 samples</i>			<i>20.1</i>	<i>7.56</i>	<i>308</i>	<i>16</i>	<i>340</i>	<i>8</i>	<i>164</i>	<i>108</i>	<i>368</i>	<i>549</i>	<i>82</i>	<i>174</i>		
Hanakoa River	HI-05-20	4/25/09	n.a.	18.4	7.50	274	14	316	14	169	128	392	620	87	21		
Koai'e Stream	HI-05-07	4/21/09	n.a.	22.3	8.44	214	8	243	15	175	118	381	612	81		0.70425	0.00023
Makaweli River	HI-05-14	4/22/09	n.a.	25.2	7.73	608	29	480	25	456	202	406	1151	146	51		
Makaweli River	HI-06-30	3/25/10	n.a.	n.a.	7.61	520	23	464	17	237	77	356	537	93	495		
<i>Makaweli River</i>	<i>2 samples</i>			<i>25.2</i>	<i>7.67</i>	<i>564</i>	<i>26</i>	<i>472</i>	<i>21</i>	<i>346</i>	<i>140</i>	<i>381</i>	<i>844</i>	<i>120</i>	<i>273</i>		
Waimea River @ dam	HI-05-06	4/21/09	n.a.	22.3	8.81	234	11	265	15	220	139	461	739	97		0.70430	0.00008
Waimea River @ dam	HI-06-32	3/26/10	n.a.	n.a.	7.13	235	13	209	8	109	45	321	257	53	237		
<i>Waimea River @ dam</i>	<i>2 samples</i>			<i>22.3</i>	<i>7.97</i>	<i>234</i>	<i>12</i>	<i>237</i>	<i>11</i>	<i>165</i>	<i>92</i>	<i>391</i>	<i>498</i>	<i>75</i>	<i>237</i>	<i>0.70430</i>	<i>0.00008</i>
Waimea River @ ford	HI-05-12	4/22/09	n.a.	24.6	8.23	561	26	518	20	324	164	307	900	120			
Waimea River @ ford	HI-06-28	3/24/10	n.a.	21.9	7.07	273	17	228	9	113	39	265	215	49	231		
<i>Waimea River @ ford</i>	<i>2 samples</i>			<i>23.3</i>	<i>7.65</i>	<i>417</i>	<i>21</i>	<i>373</i>	<i>15</i>	<i>219</i>	<i>102</i>	<i>286</i>	<i>558</i>	<i>85</i>	<i>231</i>	<i>0.70469</i>	<i>0.00014</i>
Waimea River	HI-05-08	4/21/09	n.a.	24.1	8.76	238	11	259	16	199	117	322	646	82			
@ powerhouse																	
Waimea River	HI-06-35	3/26/10	n.a.	n.a.	7.38	236	14	219	8	114	44	280	268	52	246		
@ powerhouse																	
<i>Waimea River</i>	<i>2 samples</i>			<i>24.1</i>	<i>8.07</i>	<i>237</i>	<i>13</i>	<i>239</i>	<i>12</i>	<i>156</i>	<i>81</i>	<i>301</i>	<i>457</i>	<i>67</i>	<i>246</i>		
@ powerhouse																	
Waimea Tributary	HI-06-34	3/26/10	n.a.	n.a.	7.00	262	25	266	2	126	51	517	296	70	275		
@ Po'o Kaeha																	
Waimea Tributary	HI-06-36	3/26/10	n.a.	n.a.	7.48	227	14	216	8	104	40	276	250	49	216		
@ powerhouse																	
Waimea Tributary A	HI-05-09	4/21/09	n.a.	21.3	7.77	460	32	562	18	800	387	1053	2422	271			
Waimea Tributary A	HI-06-37	3/26/10	n.a.	n.a.	7.87	559	18	561	23	729	153	801	1721	206	789		

Table 4.3.a. (continued)

River name	Sample ID	Date	Q m ³ /sec	T °C	pH	Cl	SO ₄	Na	K	Mg	Ca	Si	Alk µeq/L	TDS ppm	Sr mmol/L	⁸⁷ Sr/ ⁸⁶ Sr	± 2σ
<i>Waimea Tributary A</i>																	
	2 samples			21.3	7.82	509	25	561	20	764	270	927	2071	238	789		
Waimiha Stream	HI-06-20	3/22/10	n.a.	n.a.	7.16	242	11	208	10	121	59	330	313	58	259		
Wiliwili Gulch	HI-06-31	3/26/10	n.a.	n.a.	7.81	460	26	461	7	218	78	593	499	102	417		
Waimea - Alakai																	
Kawaikoi Stream	HI-06-39	3/27/10	3.3	n.a.	6.5	94	8	118	4	21	10	19	74	13	48		
Kawaikoi Stream	TA-5	1/3/05	0.4	15.0	146	7	142	0	20	10	10	35	41	14	86		
<i>2 samples</i>																	
Kawaikoi Stream	TA-4	1/3/05	3.31	15	5.81	100	8	121	4	21	10	21	71	14	52		
Koke'e Stream	HI-05-10	4/22/09	n.a.	16.0	337	18	349	0	144	72	276	409	197	37	245	0.70523	0.00008
Koke'e Stream	HI-06-38	3/27/10	n.a.	n.a.	0	178	12	239	18	66	57	85	301	40	161	0.70523	0.00008
<i>3 samples</i>																	
Koke'e Stream				17	3.55	243	13	264	8	94	56	170	302	48	203	0.70523	0.00008

Table 4.3b. Chemical composition of groundwater on the Hawaiian Islands.

Well name	Sample ID	Date	T °C	pH	Cl	SO ₄	Na	K	Mg	Ca	Si	Alk	TDS	Sr	⁸⁷ Sr/ ⁸⁶ Sr	± 2σ	
																	μmol/L
												μeq/L		ppm		nmol/L	
Hawi deep well 1	HI-05-27	05/2005	28.5	8.04	737	74	1026	57	345	266	796	1421	207		0.70420	0.00007	
Lalamilo well B	HI-05-25	05/2005	26.3	8.07	1166	172	1627	97	573	247	1001	1854	289	699	0.70421	0.00010	
Parker well 1	HI-05-26	05/2005	26.6	8.08	2885	262	3124	119	773	294	993	1970	407	925			
Kohala Ranch Well 1	HI-05-29	05/2005	21.4	7.86	2028	167	1676	119	509	412	916	1275	288	1661	0.70386	0.00008	
Pahoa 1	HI-06-58	04/2006	24.1	7.76	659	107	759	91	131	121	837	480	139	243	0.70387	0.00010	
Panaewa 1	HI-06-57	04/2006	21.0	7.51	1287	25	239	45	112	180	612	639	138	292	0.70407	0.00007	
Pahala Well	HI-06-59	04/2006	20.2	8.13	318	61	275	37	145	190	678	541	107	282	0.70378	0.00017	
DW-2	HI-05-47	05/2005	29	7.90	3365	376	3697	161	886	297	1016	2105	462	1096			
DW-3	HI-05-48	05/2005	28.7	7.99	2263	313	2977	136	787	281	935	2361	407		0.70435	0.00007	
Parker 4	HI-05-49	05/2005	27	7.65	768	168	1485	84	542	213	1028	1974	277	575			
DW-1	HI-05-50	05/2005	27.1	7.50	729	158	1442	94	537	216	1010	1998	275	562	0.70374	0.00007	
Parker 5	HI-05-51	05/2005	27.2	7.50	746	163	1460	84	561	215	1022	2023	279	575	0.70375	0.00010	
Kalepa Ridge W-10	USGS		n.a.	7.68	1062	406	2893	40	497	282	1079	2762	392	n.a.	n.a.	n.a.	
Waikapu 2	USGS		n.a.	8.10	457	94	3219	124	391	299	566	3868	384	n.a.	n.a.	n.a.	
Waiehu Deep	USGS		n.a.	8.20	1386	151	1957	124	232	312	658	1449	254	n.a.	n.a.	n.a.	
Monitor Well*																	
Waipahu Deep	USGS		n.a.	7.20	3686	186	2379	89	708	499	891	1393	377	n.a.	n.a.	n.a.	
Monitor Well**																	
Schofield Shaft	USGS		n.a.	6.90	514	49	587	50	298	321	1049	1049	181	n.a.	n.a.	n.a.	

n.a. = Data not available

* = Average of two samples, least contaminated by sea water (sea water intrudes the aquifer at high tide)

** = One of two available samples, the other one is contaminated by sea water

4.3.1. Topography and regional division:

We split the streams studied into four main groups based on their location, which also correlates with the CV of elevation, which is a measure of the distribution of elevations within a watershed. The groups are: Waimea (heavily eroded, $CV_{\text{elevation}} = 35\% \pm 8\%$, $n=13$) and Eastern Kaua'i (less eroded, $CV_{\text{elevation}} = 54\% \pm 7\%$, $n=10$) on Kaua'i (Figure 4.7), and Kohala (heavily eroded, $CV_{\text{elevation}} = 26\% \pm 7\%$, $n=13$) and Hamakua-Hilo (little eroded, $CV_{\text{elevation}} = 41\% \pm 6\%$, $n=15$) on the Big Island (Figure 4.6). Many of the streams studied, especially in the Waimea and Kohala regions, are tributaries to larger streams that were also sampled further downstream (see Figure 4.6 and 4.7). In the Kohala and Waimea regions, several of these tributaries originate in relatively little eroded, but heavily weathered, plateaux (the topographic manifestation of these plateaux is clearly visible in Figure 4.3 B-B' and Figure 4.5). These tributaries are investigated separately, as the Alaka'i group (headwaters of the Waimea region, $CV_{\text{elevation}} = 5\% \pm 18\%$, $n=2$) and Upper Kohala group (headwaters of the Kohala region, $CV_{\text{elevation}} = 5\% \pm 13\%$, $n=4$).

A low CV means that elevation values in the watershed cluster tightly around the mean, as would be the case in relatively flat watersheds. CV s of 25-35% are observed in watersheds where the elevation distribution is skewed (in this case, usually towards higher values); such watersheds are heavily eroded but retain some of the original landscape characteristics in the uplands (e.g. on the Kohala Peninsula) or have wide amphitheater-like headwaters (e.g. the Hanakoa Stream in the Waimea region of Kaua'i). A high CV of elevation means that no particular elevation interval within the watershed dominates in the watershed, or alternatively, is indicative of a bimodal elevation distribution within the watershed. The highest CV s of elevation in this study

occur in watersheds that are not heavily eroded, such as the ones draining the eastern flanks of Mauna Kea on the Big Island (i.e. in Hamakua-Hilo) and in eastern Kaua'i.

All these streams are investigated with respect to major element chemistry, mineral saturation state and sources of solutes. Tributaries to larger streams are excluded from calculations of total chemical fluxes.

The Puna and Ka'u districts on the Big Island were shown in Chapter 3 to have exceptionally large groundwater recharge. We investigate this region separately from the rest of the Big Island in the following analysis.

4.3.2. Major elements

4.3.2.1. Surface water

In general, Hawaiian streams are dilute to average compared to streams draining other volcanic regions. The lowest mean concentration for every solute is always found in either the Alaka'i Swamp or Upper Kohala. pH-values are highest in the Waimea and Hamakua-Hilo regions (mean = 7.71, up to 8.81) and lowest in Upper Kohala (mean = 5.79, lowest value measured = 4.53). Total dissolved solids (TDS) range from 11 ppm to 271 ppm (in Hamakua-Hilo and Waimea, respectively), compared to 82-916 ppm in volcanic regions in the Philippines (see Chapter 2), 27-460 ppm in the Lesser Antilles (Rad et al., 2006) and 49-211 ppm in Iceland (Gislason et al., 1996). TDS is strongly positively correlated with both alkalinity (Alk) and Si-concentrations and in fact, the highest concentrations of both alkalinity and silica, as well as Mg and Ca (the two major components of alkalinity in Hawaiian streams), are all found in the Waimea region. Si-concentrations in Waimea Canyon are significantly higher than in any other region, including the Alaka'i Swamp that drains into Waimea Canyon. The same

applies in Kohala, where Si-concentrations in streams draining the deep canyons of Honokane Nui, Wailoa and Hi'ilawe Streams are significantly higher than Si-concentrations in streams draining the Upper Kohala plateau into these canyons.

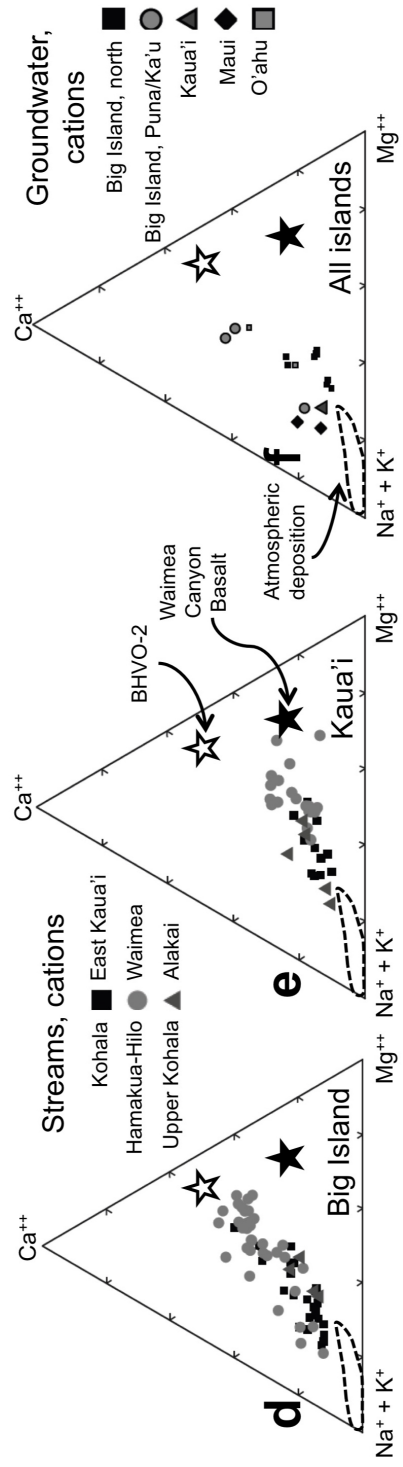
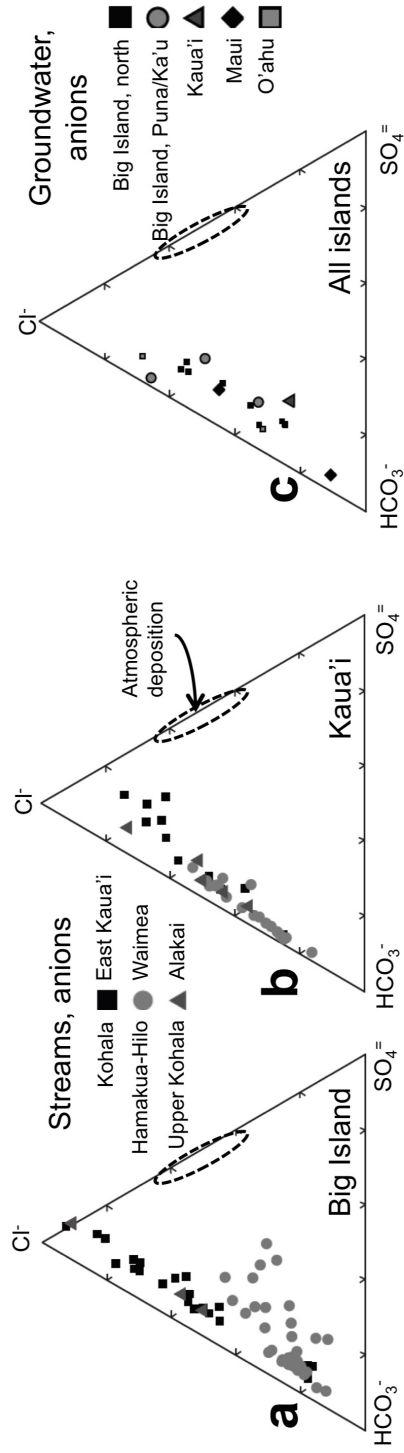
The anion component in streams on both the Big Island and Kaua'i is dominated by Cl^- and HCO_3^- (see Figure 4.8a (Big Island) and Figure 4.8b (Kaua'i)). Sulfate is a small component of water draining Kohala and Upper Kohala but constitutes a significant share of the anion charge in many streams in Hamakua-Hilo. On Kaua'i, sulfate is also a minor component in most cases, except for in a few streams in East Kaua'i. East Kaua'i has the highest $\text{SO}_4^{=}$ -concentrations found in any streams in this study and also has a significantly higher mean $\text{SO}_4^{=}$ than any other region studied. The same applies to Cl^- . Waimea streams, have almost no sulfate and are also relatively poor in Cl^- , while streams draining the Alaka'i swamp in the headwaters of Waimea Canyon have significantly more Cl^- but are still poor in sulfate. Streams in the Hamakua-Hilo region have the largest variability in anion composition and are similar to streams draining Waimea Canyon, with the exception of much larger sulfate contribution to Hamakua-Hilo. Streams draining Kohala range from 20-100% Cl^- by charge, with HCO_3^- and minor sulfate making up the rest.

The cation composition of stream waters, before atmospheric correction, is investigated in Figure 4.8d (Big Island) and Figure 4.8e (Kaua'i). The atmospheric correction generally shifts all data points slightly towards the Ca^{2+} -apex on the plots but not enough to affect our interpretation. On the Big Island, streams draining Kohala and Upper Kohala have in general smaller proportions of the alkaline earth elements than do streams draining Hamakua-Hilo, although the two regions overlap, and the highest K-concentrations in this study are found in Kohala. Streams draining East

Figure 4.8. Ternary diagrams of the anion and cation composition of streams and groundwater in Hawai'i. The upper *row* shows anion content and the lower *row* shows cation composition; the left *column* shows data for streams on the Big Island, the center *column* shows data for Kaua'i and the right *column* shows data for groundwater.

The cation data have not been corrected for atmospheric contributions. Neither streams nor groundwater match the anion composition of rainfall, indicating significant addition of solutes to streams and groundwater from rock-water interaction. Cation contents of streams on the Big Island follow a mixing line between rainfall and congruent dissolution of tholeiite, and the same applies for groundwater on all islands.

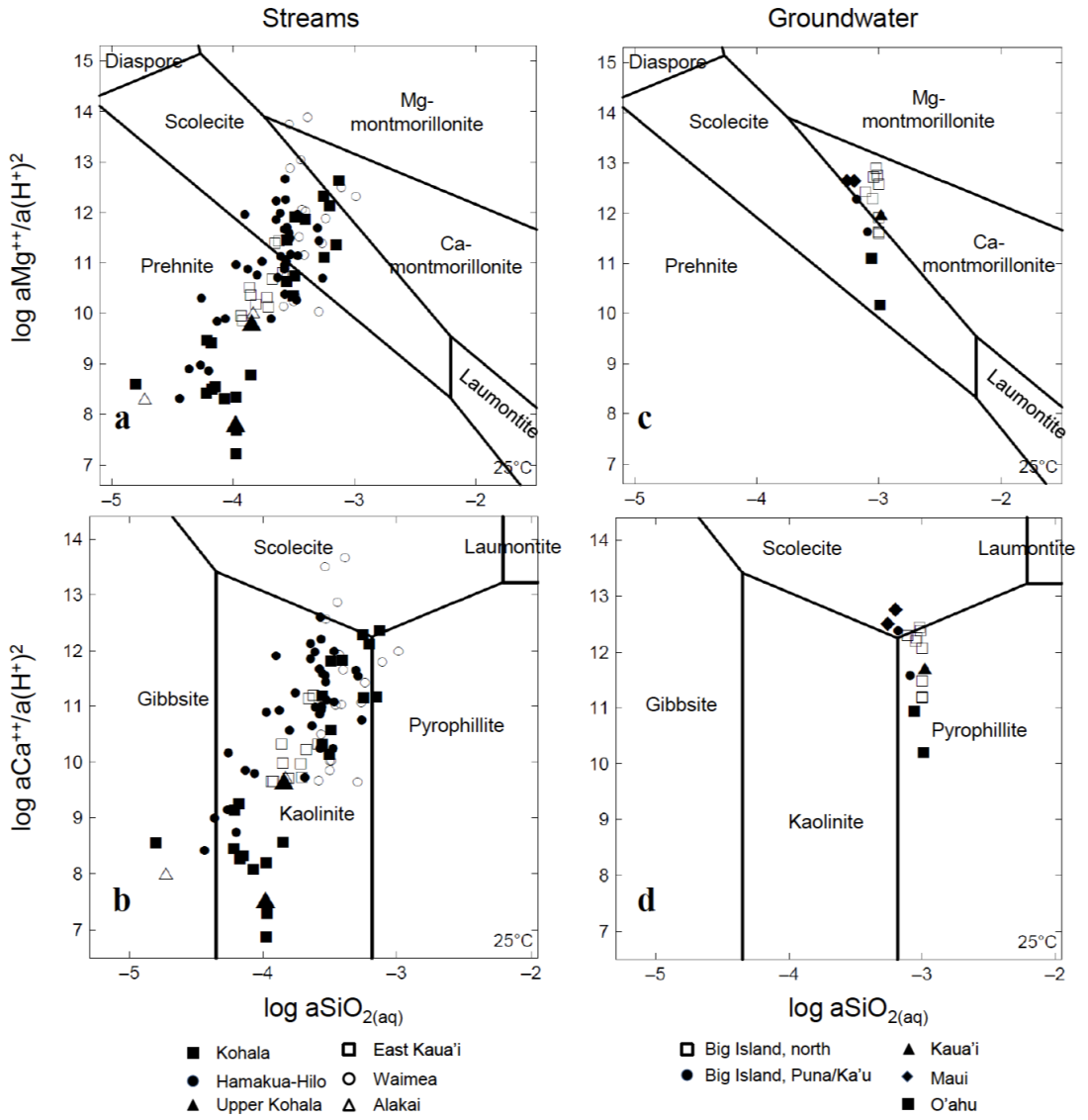
Streams on Kaua'i depart from the mixing trend and veer off to Mg-enrichment, especially streams in Waimea.



Kaua'i and the Alaka'i swamp are, like the majority of Kohala streams, proportionately rich in the alkali metals. The highest mean Na-concentrations are observed in East Kaua'i. The streams draining Hamakua-Hilo have a fairly equal share of Ca^{2+} and Mg^{2+} , which contrasts with streams draining the Waimea Canyon; those also have a small percentage of the alkalis but a high percentage of Mg^{2+} relative to streams in Hamakua-Hilo. For reference, the composition of two representative rock types (the USGS standard BHVO-2 and the average of 6 analyses of Waimea Canyon Basalt, WCB (Feigenson, 1984)) is shown as stars in Figure 4.8.

Geochemical equilibrium modeling was performed in Geochemist's Workbench 7.0 (Bethke, 2007) using the thermo.com.v8.r6+2.dat database. The saturation state of streams with respect to Mg- and Ca-minerals is shown in Figures 4.9a and 4.9b, respectively. All streams are undersaturated with respect to amorphous silica ($\log K = -2.71$) and none reach equilibrium with primary minerals in the basalt. Apart from these overarching observations, the mineral saturation state of the streams is very variable, also within regions, and no differences are observed between islands (open symbols represent Kaua'i, filled symbols represent the Big Island). Streams in the highly weathered but little eroded Alaka'i Swamp and Upper Kohala are generally poor in cations and silica and have high acidity, plotting in the stability fields of kaolinite and gibbsite and even prehnite (although one would not normally expect to find prehnite in soils). Streams draining the highly eroded Waimea Canyon have the highest Si and are sometimes saturated in 2:1 clays, such as montmorillonites, and zeolites, although most of the streams are in equilibrium with kaolinite. East Kaua'i has a relatively restricted range of saturation states, mostly plotting in the stability fields of prehnite and kaolinite. On the Big Island, water draining Kohala and

Figure 4.9. Saturation state of streams and groundwater in Hawai'i with respect to Ca- and Mg-minerals, computed for 25°C. a, b) Streams on Kaua'i (open symbols) and the Big Island (filled symbols); Mg-minerals, a), and Ca-minerals, b). All streams are undersaturated with respect to amorphous Si, which occurs at $\log a\text{SiO}_{2(\text{aq})} = -2.7$ at 25°C. Otherwise, the saturation state of streams on both islands and in all regions is very variable, ranging from predominant saturation with zeolites and 2:1 clays in Waimea and Hamakua-Hilo to predominant saturation with 1:1 clays and gibbsite in Upper Kohala and the Alaka'i Swamp. c, d) Groundwater from the Big Island, Maui, O'ahu and Kaua'i. Groundwater Si-concentrations appear to be buffered by a pyrophyllite-kaolinite buffer and never exceed roughly 1000 μM . In general, groundwater from the north of the Big Island and Maui tends to be more saturated in smectites than groundwater from Puna/Ka'u and O'ahu. Overall, there is a rather small variation in the saturation state of groundwater compared to surface water, suggesting a much more restricted range of weathering environments in the subsurface. Most groundwater plots in the pyrophyllite stability field in d), Only one stream, Tributary A, plots there – all others are Si-poor compared to groundwater.



Hamakua-Hilo has a very large range in saturation states, from saturation in zeolites and 2:1 clays to gibbsite.

4.3.2.2. *Groundwater*

Variability in groundwater composition is considerably smaller than in surface water. The pH of groundwater varies from 6.9 to 8.2. There is no discernible difference in concentrations of Cl^- , SO_4^{2-} and K but Na, Mg, Ca, Si, Alk and TDS concentrations are significantly ($\alpha = 0.05$) lower in Puna/Ka'u (the region modeled by Takasaki, 1993; labeled as aquifer "C" in Chapter 3 and Tables 4.1b, 4.3b) than elsewhere on the islands. Compared to surface water, groundwater is average to high in Si (566-1079 μM) and high in Alk (480-3868 $\mu\text{eq/L}$). TDS is somewhat higher in groundwater than in surface water, ranging in the former from 107 to 462 ppm. This is comparable to TDS levels in surface waters in other volcanic regions, such as the Philippines (Schopka et al., 2011; Chapter 2) and the Lesser Antilles (Rad et al., 2006).

Comparing Figures 4.8a and 4.8b with 4.8c (anions) it is clear that groundwater has a very similar composition to surface water and has a narrower range of compositions. Figures 4.8d, 4.8e and 4.8f (cations) reveal that groundwater cation composition only diverges from that of surface water in the case of Waimea Canyon, which as noted earlier, is enriched in Mg relative to both other surface water and groundwater. The number of groundwater samples is too small to infer about the degree to which differences in groundwater composition from island to island exist or do not exist.

The same conclusion can be drawn from Figures 4.9c and 4.9d, where the saturation state of groundwater is shown. In this projection, it is clear that groundwater has a very constant Si-concentration of around 1000 μM , or around half of amorphous Si

saturation. This high Si-content keeps groundwater oversaturated with the 1:1 clays (kaolinite, gibbsite) and in equilibrium with smectites and/or zeolites.

Assuming that the BHVO-2 standard and/or WCB are representative for the rocks that the groundwater interacts with at depth, we find that groundwater in Puna/Ka'u has X/Si ($X = Ca, Mg$ and Na) statistically indistinguishable from the rocks (Table 4.4). Groundwater elsewhere has significantly higher X/Si ($X = Ca, Mg, Na$ and K) than both BHVO-2 and WCB.

Table 4.4. X/Si values for representative rocks in Hawai'i.

	Na/Si	K/Si	Mg/Si	Ca/Si
WCB ¹	0.081	0.008	0.240	0.228
BHVO-2	0.086	0.013	0.216	0.245

1: Waimea Canyon Basalt (Feigenson, 1984)

4.3.3. Atmospheric inputs

4.3.3.1. Surface water

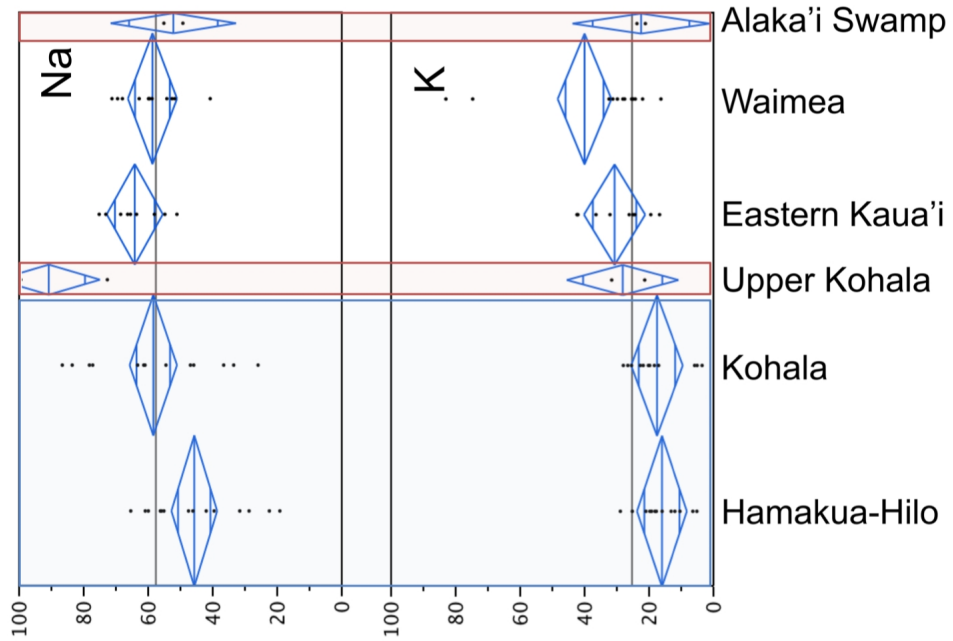
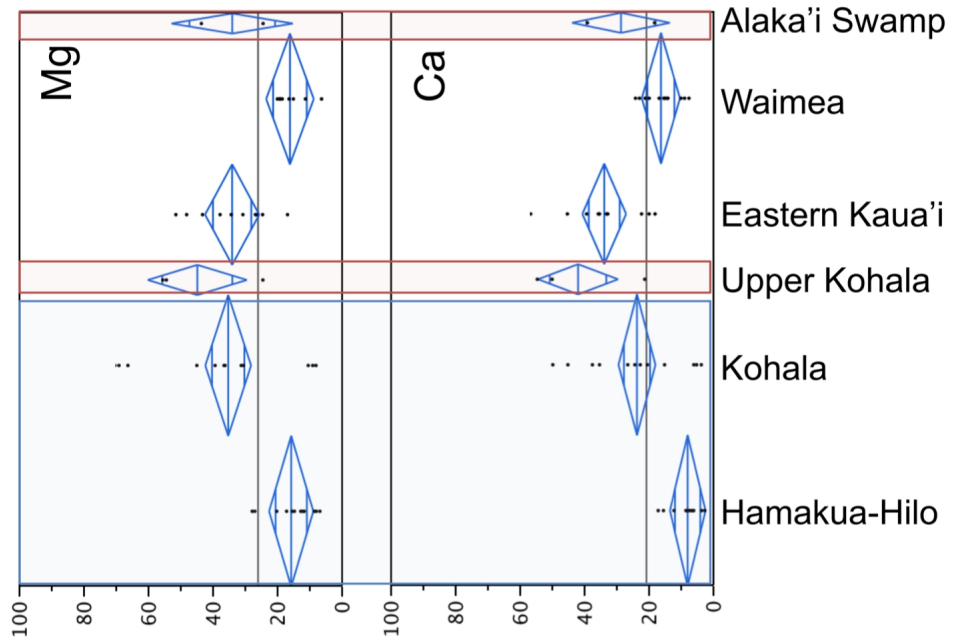
The results from the cyclic salt-correction of stream chemistry are presented in Figure 4.10, grouped by regions. Where more than one sample per stream is available, we calculated an average contribution from cyclic salts per element. The horizontal line that runs through each plot represents the arithmetic average of all values for a particular element, and the diamonds show the mean (horizontal line through center of diamond) and both 90% and 95% confidence interval (upper/lower horizontal lines and upper/lower apex of diamond, respectively) for the mean for each region. In

general, the largest contribution of cyclic salts is observed in Na, with an overall mean of nearly 60%. Only Upper Kohala and Hamakua-Hilo fall off this mean – Upper Kohala gets between 70 and 100% of its Na from the atmosphere while Hamakua-Hilo only receives around 40% from atmospheric sources. Hamakua-Hilo is in fact the only region where the fraction of solutes derived from the atmosphere is always lower than the average fraction over the entire archipelago. K is heavily influenced by vegetation and the results from the atmospheric correction are therefore hard to interpret. The calculated contribution of the atmosphere to K fluxes ranges from ~15% in Kohala and Hamakua-Hilo to ~40% in Waimea.

The alkaline earth metals behave very similarly across different regions, with atmospheric deposition contributing on average 10-45% to solute fluxes. Waimea and Hamakua-Hilo both receive (mostly significantly) lower proportion of their Ca and Mg from the atmosphere than do the other regions. East Kaua'i, Upper Kohala and Kohala all receive large fractions of both Ca and Mg from the atmosphere and streams draining the Alaka'i Swamp land in the middle.

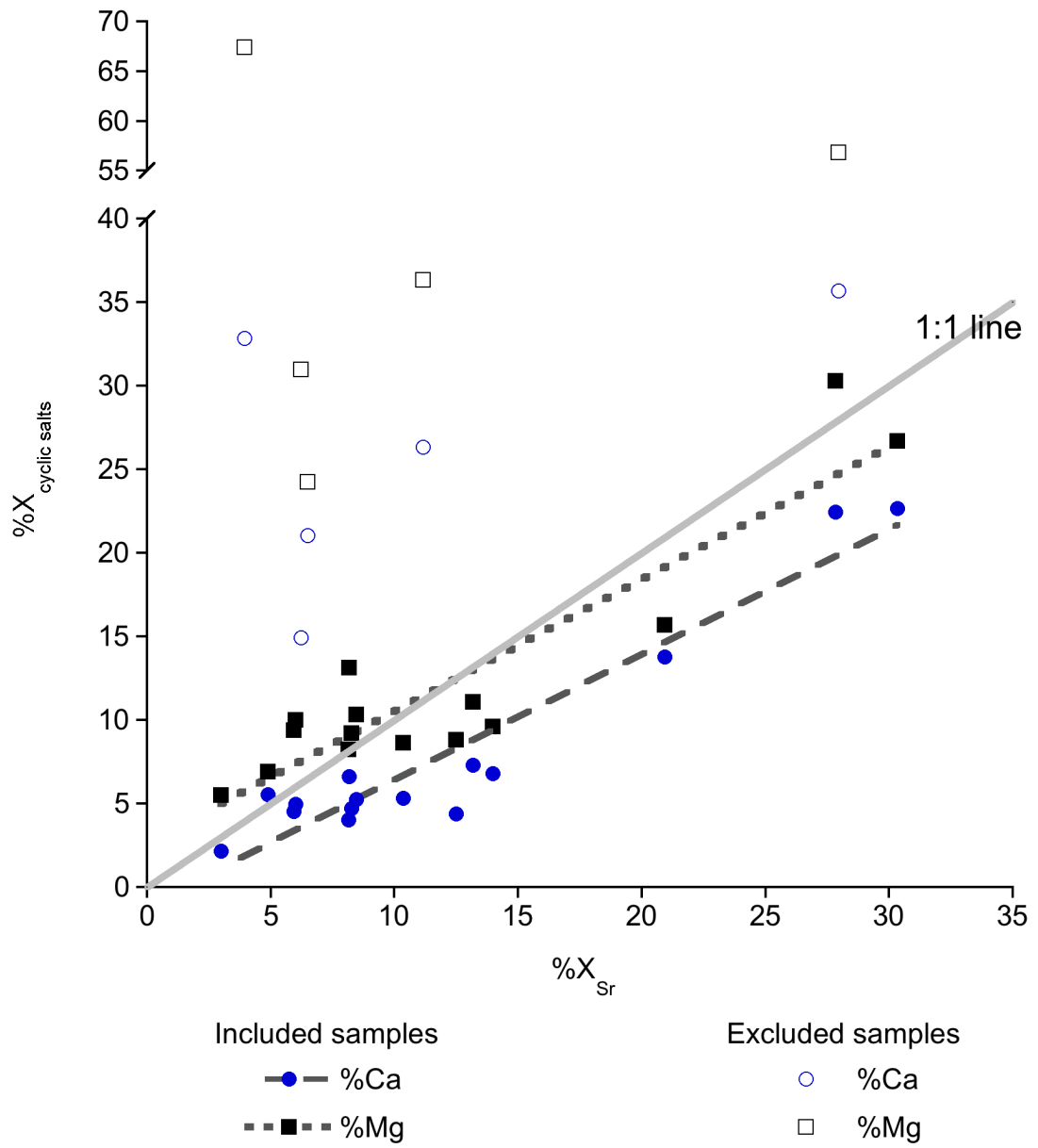
We compared results from cyclic salt correction with results from Sr-isotopes where available (Figure 4.11). In general, there is good agreement between the two techniques, assuming that Sr-isotopes trace the behavior of Ca and Mg. Excluding 5 samples where the cyclic salt correction predicts 2-10 times higher atmospheric contribution than do Sr-isotopes (Kolekole Stream, spl. HI-05-01; Hapahapa'i Gulch, spl. HI-05-24; Wai'aka Stream, spl. HI-05-28; Alakahi Stream, spl. HI-08-11; Waikama Gulch, spl. HI-08-22), we find the relationship $\%Mg_{\text{cyclic salts}} = 0.8 \times \%Mg_{\text{Sr}}$ ($r^2 = 0.84$) and $\%Ca_{\text{cyclic salts}} = 0.75 \times \%Ca_{\text{Sr}}$ ($r^2 = 0.91$), where $\%X_{\text{cyclic salts}}$ refers to atmospheric contribution calculated using the cyclic salts method and $\%X_{\text{Sr}}$

Figure 4.10. One-way ANOVA on proportion of dissolved solids derived from atmospheric deposition, as computed using cyclic salt correction (Chapter 4.2.3.1), grouped by regions. The Hamakua-Hilo region has a consistently lower proportion of atmosphere-derived solutes than the average. Atmospheric deposition contributes on average slightly more of Na and K to the solute load on Kaua'i than on the Big Island. The alkaline earths also follow an internally consistent pattern that differs from that of the alkali metals: the Waimea and Hamakua-Hilo regions have the largest proportion of rock-derived solutes and the Upper Kohala, Eastern Kaua'i and, in the case of Mg, the Kohala regions, are the most affected by atmospheric deposition.



% from cyclic salt deposition

Figure 4.11. Comparison of two different methods to calculate atmospheric contribution to the dissolved load. Fraction of dissolved load derived from the atmosphere, calculated using Sr-isotopes, is shown on the x-axis and the corresponding fraction calculated using the cyclic salts method on the y-axis. If all samples for which Sr-isotope data is available are included, no correlation between the two methods is observed. Excluding five samples (see text), a good correlation is however observed. Sr isotopes predict on average slightly larger atmospheric contribution, as is evidenced by the slope of the regression line being less than unity.



refers to atmospheric contribution calculated using Sr-isotopes. Both relationships are highly significant (p of slope < 0.0001 in both cases). Slope of less than one indicates that in general, Sr-isotopes predict larger atmospheric contribution in Hawai'i than do cyclic salts.

Four of the five streams excluded from the regression above are on the Kohala Peninsula, the fifth one (Kolekole Stream) is in Hamakua-Hilo. The spatial clustering of these outliers is notable but we cannot at present explain these findings in any more detail.

4.3.3.2. Groundwater

Groundwater in Hawai'i is either present as a thin freshwater basal lens, resting on top of seawater that has penetrated the lava layers, or as perched aquifers confined by dikes and/or impermeable tephra layers (see Chapter 3 for further discussion). The basal lens is usually thin, on the order of 1-2 dozen meters, and is found only a few meters above sea level even several kilometers inland. Such aquifers are often impacted by tides far inland and some mixing between sea water and the freshwater lens occurs. We therefore assume that elevated Sr-isotopes in groundwater point to seawater contamination, rather than atmospheric deposition. Sr-isotopes reveal that in groundwater, 4-15% of Sr^{2+} , and by extension Ca^{2+} and Mg^{2+} , come from sources with the $^{87}\text{Sr}/^{86}\text{Sr}$ signature of seawater.

This is supported by the elevated levels of Cl^- in our groundwater samples. There is little doubt that in the recently active volcanoes, some of the Cl^- in groundwater also derives from the host rock and perhaps magmatic gasses but this contribution is assumed to be minor and is not considered further. We use the X/Cl -ratios of seawater (see Table 4.2) to estimate the contribution of seawater to the groundwater, assuming

conservative mixing. We find that on average some 8-10% of Ca^{2+} is contributed by seawater, which matches well with the Sr-isotope correction for Ca^{2+} .

Perched aquifers are less prone to sea water contamination. Only one groundwater sample in our study, HI-06-59, is derived from a perched aquifer. This well, Pahala Well, has the lowest Cl-concentration of all groundwater samples used in this study, and Sr-isotopes indicate an atmospheric contribution of around 5% to the Ca and Mg contents.

4.4. DISCUSSION

4.4.1. Processes controlling chemistry of surface water

The anion composition in streams on both Kaua'i and the Big Island appears to be only slightly controlled by rainfall (Figures 4.6a and 4.6b). Rainfall (Carrillo et al., 2002) is composed of generally less than 5% bicarbonate, with the remainder evenly split between Cl^- and $\text{SO}_4^{=}$. Only six streams come close to this composition, those are all located in East Kaua'i. Five of the six streams most impacted by sulfate line up along the east coast of Kaua'i (from north to south: Kilauea, Anahola, Kapa'a, Opaeka'a and Hanama'ulu Streams). The sixth one, Waikomo Stream, is located in the east of the south coast. Streams in this region have the highest mean concentrations of Cl^- and $\text{SO}_4^{=}$. The location of these streams in the path of the trade winds suggest a large contribution of solutes from sea salts. The high sulfur concentrations are almost certainly caused by deposition of non-sea salt sulfur, formed by the oxidation of biogenic compounds such as dimethyl sulfide and carbonyl sulfide, both relatively insoluble gases that are produced by algae in the ocean (Andrews et al., 1996). We did not correct sulfate for atmospheric deposition due to the high variability in $\text{SO}_4^{=}/\text{Cl}^-$ ratios in atmospheric deposition. The high proportion of sulfate in the anion load of

streams in Hamakua-Hilo is most likely caused by elevated deposition of sulfur from the nearby volcanism at Kilauea (see Figure 4.2 and Figure 4.6). We propose that the high proportion of HCO_3^- in Hawaiian streams in general is due to the fixing of atmospheric carbon by chemical weathering of rocks.

The cation composition of streams on the Big Island falls on a mixing line between atmospheric deposition and BHVO-2 (Figure 4.8d and 4.8e). On Kaua'i, stream cation composition is impacted by the WCB (see Figure 4.8d-f) which is enriched in Mg compared to BHVO-2. The two mixing lines overlap in the Na+K-corner and towards the center of the diagram, diverging only towards the apexes of Ca (BHVO-2) and Mg (WCB). Streams of Hamakua-Hilo and Kohala span almost the entire range between the two end-members. The Kohala streams tend to cluster with the streams in Upper Kohala closer to the rainfall end-member and the Hamakua-Hilo cluster closer to the fresh rock end-member. These results suggest that streams within each region drain a variety of soils, with soils in Kohala being on average more leached than soils in Hamakua-Hilo. This agrees broadly with the observation from activity diagrams (Figure 4.9) that waters from Hamakua-Hilo and Kohala are in equilibrium with a wide range of soil minerals, ranging from 2:1 clays with high ion-exchange capacity to 1:1 kaolinites and finally gibbsite. Figure 4.10 supports this interpretation –the proportion of solutes supplied by atmospheric deposition is most pronounced in Upper Kohala and decreases from there through Kohala to a low in Hamakua-Hilo.

Streams draining the heavily weathered plateaux of Upper Kohala and the Alaka'i Swamp are depleted in the alkaline earth metals relative to fresh rock. This observation matches the observed data on leaching of rock-derived nutrients from Hawaiian soils along the LSAG (Vitousek et al., 1997) relatively well. Rock-derived

nutrients are depleted fast from accumulating soils in the warm and humid climate in Hawai'i, such that nearly all original Si, Ca and Mg has been leached from undisturbed soil formed on 20 kyr old substrate (Vitousek et al., 1997). Ecosystems older than that are mainly sustained by nutrients derived from sea-salt aerosols and dust from the Asian continent (Chadwick et al., 1999). This rhymes with the relatively high proportions of atmospheric-derived solutes in streams draining the un-eroded plateau of Kohala (Figure 4.10). Another confirmation of the leached state of the soils of Upper Kohala and Alaka'i comes from Figure 4.9, where these streams are shown to be in equilibrium with gibbsite and kaolinite. An interesting deviation from this pattern is seen in the Alaka'i Swamp, where atmospheric correction predicts that a smaller fraction of solutes (especially Na) is derived from the atmosphere than in Kohala.

Streams on East Kaua'i have a similar cation composition as streams in Kohala. They are relatively depleted in the alkaline earth metals compared to both BHVO-2 and WCB. Much of East Kaua'i is covered with a veneer of rejuvenation-stage alkali basalts of the Koloa Volcanics underlain by tholeiites of the WCB (e.g. Reiners et al., 1999). Although substantial weathering and leaching of alkali metals from the substrate has been observed in drill cores from the region (Reiners et al., 1999), weathering of this rock may still produce waters that are enriched in Na and K relative to waters draining tholeiite and in fact the highest Na-concentrations in this study are observed in East Kaua'i. There is also a possibility that the depletion in Ca and Mg in East Kaua'i stream waters indicates on average highly weathered soils, this interpretation is supported by the high percentage of solutes from atmospheric deposition in the region (Figure 4.10). The observed chemistry is most likely influenced by both these factors.

Streams draining the Waimea region plot close to the WCB end-member (Figure 4.8e). The streams that exhibit this behavior are the Makaweli River, a large river originating in the highest section of the Alaka'i Swamp (Figure 4.4), and a very small perennial stream at the bottom the Waimea Canyon that we call Tributary A. Tributary A was the only creek we found running along the western wall of the canyon in our 2005 sampling campaign. The creek was flowing at the same rate the following year when we entered the canyon during a prolonged rainfall that brought up every creek on the island, including many on the western wall of the Waimea Canyon. We suspect that Tributary A taps a groundwater spring and that the 2005 sample is representative of groundwater draining into the canyon. The Kaua'i groundwater sample from the USGS that we use is from a well on the east coast of the island and given the difference in stream chemistry in the eastern and western part of the island, it is entirely possible that groundwater in the two regions would differ.

All samples from Tributary A, Makaweli River and Waimea River are undersaturated w/resp. to calcite, with a single exception. An inspection of the activity diagrams of Figure 4.9 reveals that Waimea River is always in equilibrium with scolecite and/or Mg-smectite. Koai'e Stream, which drains into the Waimea Canyon through a deep tributary canyon, is in equilibrium with scolecite like the main channel of the Waimea River. Both our samples from Tributary A are in equilibrium with Ca-smectite and pyrophyllite. Interestingly, Tributary A is the sole stream plotting in the pyrophyllite field in the activity diagrams, where most groundwater samples plot (Figure 4.9d). We cannot say with absolute certainty that Tributary A represents unmixed groundwater, but the available evidence, as well as its similarity to the composition of WCB, suggests that groundwater is at least a significant component of the water in that stream.

4.4.2. Processes controlling chemistry of groundwater

As mentioned above, groundwater on both the Big Island and on Kaua'i plots within the fields defined by streams on these islands on ternary plots (Figure 4.8). This may indicate that common processes control the composition of both surface and groundwater, or it may imply that surface water is largely derived from groundwater.

From Figure 4.9d, it may be inferred that a clay buffer involving pyrophyllite and kaolinite controls the silica content of groundwater. Differential dissolution of minerals may yield a weathering solution that has X/Si different from the whole rock composition of the dissolving rock. The BHVO-2 Si-normalized major element ratios in Puna and Ka'u groundwater indicate that the rocks dissolve congruently in the region. Alternatively, several different weathering regimes may be active in the region and their effects cancel each other out so that on average, the mix of the resulting weathering solutions would look like the original rock. In all other regions, the X/Si ratios of groundwater are significantly higher than those of the parent rock. This may indicate net uptake of Si into secondary minerals and/or a net release of cations into solution, possibly from secondary minerals that are being further weathered into simpler clays. In all cases, further sampling of both groundwater and the rocks that the groundwater interacts with is necessary to further constrain the weathering processes at work in the subsurface.

In summary, the available evidence (major element composition, mineral equilibrium calculations and X/Si ratios in rocks and groundwater) give somewhat conflicting information about weathering processes in the deep subsurface in Hawai'i. From the two former, it may be inferred that processes controlling chemical weathering by

groundwater do not differ significantly from region to region, while the X/Si -ratios may be interpreted to signal spatial differences in rock-water interactions.

4.4.3. Fluxes, calculations and error propagation

Chemical fluxes, F_X , from a region are determined by multiplying the average concentration of the solute of interest, $[X]$, with the total discharge, Q , from the region: $F_X = [X] \times Q$. The average concentration of solutes is listed in Table 4.1a (streams) and Table 4.1b (groundwater). Total discharge from all streams studied is given in Tables 3.2 and 3.6 in this dissertation. Chemical fluxes from land are given in Table 4.5a (total flux per region) and Table 4.5b (area-normalized flux per region) and total groundwater discharge from the regions studied is given in Table 4.5c.

Groundwater recharge is subject to $CV = 35\%$ (see Chapter 3) ($CV =$ coefficient of variation $=$ (standard deviation)/(mean)). Errors on modeled discharge in unmonitored streams, derived from a kriging model of observed CV in streams monitored by the USGS, are listed in Table 3.6 in this dissertation. Wherever USGS discharge data is available for the streams studied here, we use the observed CV from the USGS database (Table 3.2 in this dissertation).

Errors on solute concentrations are listed in Chapter 4.2.2. Where necessary, the errors for individual elements are propagated to give the cumulative error on composite fluxes, such as $Ca+Mg$ or $WCSF$ (see Chapter 4.4.5.).

Uncertainties in the area of watersheds extracted from digital elevation models (DEMs) using ArcGIS are taken from Oksanen and Sarjakoski (2005). When extracted from a DEM with 10m cell size, CV is 24% in watersheds smaller than 2 km^2 , 16% in watersheds between 2 and 22 km^2 and less than 3% in watersheds over 22 km^2 .

Table 4.5a. Regional total fluxes by silicate weathering from the Big Island and Kaua'i

Region	Silicate weathering cation flux ¹		Silicate weathering ²		Silicate Ca*+Mg*		WCEF ³	2 × Si	WCSF ⁴	
	10 ⁶ mol/yr	10 ⁶ eq/yr	t/yr	t/yr	10 ⁶ mol/yr	10 ⁶ eq/yr				
Big Island										
Hamakua-Hilo	13	352	583	10362	26619	230	75	475	541	248
Kohala	11	110	168	3182	9868	58	15	143	223	66
Kaua'i										
Eastern	9	169	250	4478	11042	80	38	179	218	93
Waimea	5	178	302	4937	14686	124	17	258	325	131
Total fluxes										
n	10 ⁶ mol/yr	10 ⁶ eq/yr	t/yr	t/yr	10 ⁶ mol/yr	10 ⁶ eq/yr	10 ⁶ mol/yr	10 ⁶ mol/yr	10 ⁶ mol/yr	10 ⁶ mol/yr
CV%, total fluxes										
Big Island										
Hamakua-Hilo	47	49	47	47	47	46	47	51	46	46
Kohala	54	56	54	54	54	53	53	57	53	53
Kaua'i										
Eastern	58	60	58	58	58	57	57	61	57	57
Waimea	49	51	49	49	49	48	49	52	48	48

1: Silicate cation weathering rate = Na* + K* + Ca* + Mg*

2: Silicate weathering rate = Na* + K* + Ca* + Mg* + SiO₂

3: Weathering carbon export flux = see discussion in section on surface fluxes

4: Weathering carbon sequestration flux = see discussion in section on surface fluxes

Table 4.5b. Regional area-normalized fluxes by silicate weathering from the Big Island and Kaua'i

Region	Silicate weathering cation flux ¹		Silicate weathering ²		SO ₄	WCEF ³	2 × Si	WCSF ⁴		
	mol/km ² /yr	eq/km ² /yr	t/km ² /yr	mol/km ² /yr					Ca*+Mg*	
Area-normalized fluxes ± 1 standard error										
	10 ⁶	10 ⁶	10 ⁶	10 ⁶	10 ⁶	10 ⁶	10 ⁶	10 ⁶		
Big Island	n	mol/km ² /yr	eq/km ² /yr	t/km ² /yr	mol/km ² /yr	eq/km ² /yr	mol/km ² /yr	mol/km ² /yr		
Hamakua-Hilo	13	1.00 ± 0.26	1.67 ± 0.45	29.6 ± 7.72	75.8 ± 19.8	0.67 ± 0.17	0.17 ± 0.04	1.42 ± 0.40	1.54 ± 0.39	0.72 ± 0.18
Kohala	11	0.58 ± 0.26	0.85 ± 0.39	16.4 ± 7.41	49.1 ± 22.2	0.27 ± 0.12	0.10 ± 0.05	0.66 ± 0.31	1.09 ± 0.49	0.31 ± 0.14
Kaua'i										
Eastern	10	0.62 ± 0.25	0.90 ± 0.38	16.4 ± 6.72	37.1 ± 16.7	0.28 ± 0.12	0.24 ± 0.07	0.52 ± 0.25	0.69 ± 0.33	0.33 ± 0.14
Waimea	5	0.68 ± 0.21	1.13 ± 0.36	18.9 ± 5.74	57.9 ± 17.6	0.45 ± 0.14	0.06 ± 0.02	0.98 ± 0.32	1.30 ± 0.38	0.49 ± 0.14
CV%, area-normalized fluxes										
Big Island										
Hamakua-Hilo	94	98	93	94	94	94	93	100	91	93
Kohala	150	153	149	150	150	150	150	154	149	149
Kaua'i										
Eastern	140	142	139	140	140	140	140	144	139	139
Waimea	68	71	67	68	68	68	67	73	66	67

1: Silicate cation weathering rate = Na* + K* + Ca* + Mg*

2: Silicate weathering rate = Na* + K* + Ca* + Mg* + SiO₂

3: Weathering carbon export flux = see discussion in section on surface fluxes

4: Weathering carbon sequestration flux = see discussion in section on surface fluxes

Table 4.5c. Chemical fluxes via groundwater from the Hawaiian Islands.

Region	Q m ³ /yr	Area km ²	Silicate weathering cation flux ¹			Silicate weathering ² t/yr	Silicate Ca*+Mg* 10 ⁶ mol/yr	SO ₄ eq/yr	WCEF ³ mol/yr	2 × Si mol/yr	WCSF ⁴ mol/yr
			10 ⁶ mol/yr	10 ⁶ eq/yr	10 ⁶ t/yr						
Division by groundwater chemistry:											
Puna/Ka'u	4901	3750	1404	2271	47733	252977	867	558	2812	6832	937
All other regions	5985	12243	8851	12735	241757	589228	3884	2443	10908	11566	4618
Sum, Hawaiian Islands	10886	15993	10255	15006	289490	842205	4751	3001	13721	18398	5555
Division by islands and regions:											
Kaua'i	280	1437	414	596	11310	27565	182	114	510	541	216
East Kaua'i		890	256	369	7002	17066	113	71	316	335	134
Waimea		547	158	227	4308	10499	69	44	194	206	82
O'ahu	1095	1542	1619	2330	44231	107803	711	447	1996	2116	845
Molokai	264	675	391	563	10684	26039	172	108	482	511	204
Maui	1517	1888	2243	3227	61267	149324	984	619	2764	2931	1170
Big Island	7729	10456	5587	8289	161980	531428	2702	1713	7967	12298	3119
Hamakua-Hilo		961	1422	2045	38829	94637	624	392	1752	1858	742
Kohala		366	541	779	14791	36049	238	149	667	708	283
Puna/Ka'u	4901	3750	1404	2271	47733	252977	867	558	2812	6832	937
All other regions	1501		2220	3194	60627	147766	974	613	2736	2901	1158
CV%	35	3	37	40	37	37	36	36	41	35	36

1: Silicate cation weathering rate = Na* + K* + Ca* + Mg*

2: Silicate weathering rate = Na* + K* + Ca* + Mg* + SiO₂

3: Weathering carbon export flux = see discussion in section on surface fluxes

4: Weathering carbon sequestration flux = see discussion in section on surface fluxes

The CV for total chemical fluxes in a single watershed i (Ft,i), is calculated as:

$$CV_{Ft,i} = \sqrt{CV_{[X]}^2 + CV_Q^2} \quad (4.3)$$

where Q = discharge. In the case of area-normalized fluxes (Fa) the equation becomes:

$$CV_{Fa,i} = \sqrt{CV_{Ft,i}^2 + CV_{A_i}^2} \quad (4.4)$$

The CV for the total chemical fluxes from a region j (Ft,j) is calculated as:

$$CV_{Ft,j} = \sqrt{\sum_{n=1}^i CV_{Ft,i}^2} \quad (4.5)$$

where n = number of watersheds in the region.

Cumulative errors in average area-normalized fluxes from each region, Fa,j , are calculated as:

$$CV_{Fa,j} = \sqrt{\frac{\sum_{n=1}^i CV_{Fa,i}^2}{\sqrt{n}}} \quad (4.6)$$

4.4.4. Fluxes, metrics

Chemical fluxes from all main watersheds are presented in the appendix (Table A4.1) and summary flux values for each region in Table 4.5a (total fluxes from each region) and Table 4.5b (area-normalized fluxes from each region).

Multiple metrics have been developed to quantify chemical weathering fluxes from watersheds and the appropriateness of each depends on the application and purpose of the study. Silicate-derived cation fluxes are indicative of the total amount of chemical weathering taking place within the watershed and can be expressed as moles, equivalents and/or tons of material. Silicate weathering flux sums cation and silica fluxes and is usually given in tons. We present all these values below in order to facilitate comparison of our data to that of other studies. Fluxes of Ca and Mg are particularly interesting in terms of the influence of silicate weathering on atmospheric CO₂ levels and global climate. This is due to the unique capabilities of Ca and Mg to sequester carbon in the ocean, both directly through precipitation of calcite and/or aragonite shells and indirectly through ion exchange in estuaries and at mid-ocean ridges. Fluxes of sulfate are expected to be high in volcanically active areas where atmospheric deposition of volcanogenic sulfate is high or where geothermal waters, rich in sulfur, impact surface waters.

Many studies of chemical weathering have focused mainly on the carbon sequestration potential of the solute load. A common method for calculating the impact of weathering on atmospheric carbon, the "consumption" as it is frequently called (e.g. Gaillardet 1999) is the total silicate-derived alkalinity - usually calculated as $Alk = \sum z^+ - \sum z^-$, where "z⁺" and "z⁻" refer to positive and negative charge, respectively, from solutes derived from silicate weathering. This is an appropriate measure for the export of silicate alkalinity from a watershed but is a poor predictor of actual sequestration of CO₂ in the ocean, because the alkali metals (Na, K) do not participate in the sequestration reactions to the same extent as the alkaline earth metals (Ca and Mg). In Chapter 5 I propose to use the terms **weathering carbon export flux (WCEF, Φ CO₂)**

for the total silicate alkalinity (a.k.a., "carbon consumption") and **weathering carbon sequestration flux (WCSF, ΔCO_2)** (see also Chapter 1.2.3.):

$$\Delta\text{CO}_2 = \Delta\text{Mg} + \Delta\text{Ca} + 0.15 \times \Delta\text{Na} + 0.1 \times \Delta\text{K} \quad (4.6)$$

(France-Lanord and Derry, 1997) for the proportion of carbon that will be precipitated as carbonate minerals in the marine environment. The proportions of the alkali metals in equation (6) correspond to the current best estimates of their respective participation in carbon sequestration processes in the ocean.

Edmond and Huh (1997) proposed the use of $2 \times F_{\text{Si}}$ as a proxy for carbon consumption (essentially WCEF) and this metric has been used by subsequent workers (e.g. Lyons et al., 2005). We report this metric here as well. Chapter 5 contains a thorough investigation into the various metrics and methods for flux calculations applied in chemical weathering studies and their appropriateness for different bedrock lithologies is assessed. In the following discussion, we will mainly discuss fluxes of silica (Si) and alkalinity (WCEF).

4.4.5. Fluxes, surface water

It is hard to compare absolute, or total, flux values from a given region or watershed to fluxes from other locations. Instead, total fluxes are divided by the area of the region under study to yield an area-normalized flux ($\text{mass} \times \text{area}^{-1} \times \text{time}^{-1}$) that can be compared across regions. The success of the method thus relies heavily on an accurate assessment of the area of the region undergoing weathering. In regions of impermeable bedrock, groundwater infiltration is minimal and watershed boundaries are usually well defined, especially in regions of intermediate and high relief. ArcGIS

(ESRI, 2009) was used to extract watershed from 10-m DEM data from the USGS. Such an automated technique is fast and straightforward to use but it is well known that rivers in highly porous volcanic bedrock do not have easily defined watershed boundaries. To explore this issue, we performed two different one-way ANOVA analyses on the area-normalized surface fluxes from the four major regions studied. First, we performed the ANOVA using the area of each watershed as a weighing factor, essentially dividing the total chemical flux from a region with the total area of that region. We compared these weighted-average fluxes with average fluxes computed in an un-weighted ANOVA (i.e., arithmetic average of area-normalized fluxes).

The mean for any given flux for both regions on Kaua'i is indistinguishable between the two ANOVAs. The results for Kohala and especially Hamakua-Hilo differed between the two ANOVAs. In the Hamakua-Hilo region, the average fluxes *decreased* substantially when fluxes were weighted by the area of each watershed, while in the Kohala region, the average fluxes *increased* somewhat following that same treatment. We have not tested the sameness of the two means statistically but we observe that no pair of the 95% confidence intervals from the two ANOVAs overlaps in the case of the Hamakua-Hilo region (not shown).

We suspect that the large difference between the two ANOVAs in computed regional means for all fluxes from Hamakua-Hilo is caused by an anomaly in the computed watershed area of the Wailuku River. Wailuku is by far the largest river in the Hamakua-Hilo region, measuring 640 km² or nearly 70% of the total area of the region. The automated procedure in ArcGIS traces the boundaries of the Wailuku watershed up to the peaks of both Mauna Loa and Mauna Kea, a region that is

doubtless far too large. Rainfall is sparse at the high altitude in the upper reaches of the watershed and the rocks, largely devoid of soils, are extremely porous. There is no accepted way to define the watershed area of a river such as the Wailuku, making it hard to estimate the "real" area-normalized chemical weathering fluxes. We note, however, that runoff (discharge divided by drainage area) is about 4 times lower in the Wailuku drainage than in other comparable watersheds in Hamakua-Hilo. It might therefore be argued that we are overestimating the area of the Wailuku River by a factor of 4, and indeed, if the observed area-normalized fluxes from the river are multiplied by four, they become comparable to the fluxes elsewhere in the region.

In order to test for the influence of the Wailuku River on the area-weighted ANOVA we excluded it from an iteration of the process (Figure 4.12). The results show that the Wailuku exerts a heavy influence on the area-weighted averages: the area-weighted average area-normalized fluxes from Hamakua-Hilo, excluding the Wailuku, are almost always statistically identical to arithmetic-average fluxes.

Weighing the chemical fluxes by area increases the average chemical fluxes somewhat in the Kohala region. This is directly opposite to what happens in the Hamakua-Hilo region. Rather than some part of the region not contributing to the chemical weathering fluxes (as is the case in Hamakua-Hilo), this must be because some parts of the region contribute more to the chemical fluxes than others. A possible explanation could be that some parts of the region operate as a 3-D system, contributing substantially more to the chemical flux than their 2-D counterparts. By 3-D, we mean a system that has both a surface and subsurface weathering factory contributing to a downstream 2-D (surface weathering only) system. It is likely that the 3-D region is the plateau near the summit of Kohala volcano. Products of surface

weathering in the deep soils of the plateau are transported by headwater streams into the Wailoa River that runs along the bottom of the heavily eroded Waipio Valley. The surface environment weathering products are then augmented by weathering products in groundwater draining the lava pile under the plateau. This groundwater enters the Wailoa stream where the streambed intersects the groundwater table.

The other two regions seem to be insensitive to area-weighting of fluxes (i.e., area-weighted and un-weighted average area-normalized fluxes in the other two regions are statistically identical). To avoid introducing poorly quantified errors into our calculations due to uncertain watershed extent in Hamakua-Hilo, we use the un-weighted area-normalized fluxes in the following analysis. The results from the various ANOVAs reveal the difficulties inherent in defining watershed areas for largely spring-fed streams in highly porous, young volcanic landscapes such as in the Hamakua-Hilo region.

Results from the un-weighted, one-way ANOVA on area-normalized fluxes from all four regions are shown in Figure 4.13 with 1 standard error (s.e.) error bars. The large *CV* of fluxes from Kaua'i and Hamakua-Hilo can mainly be ascribed to the large *CV* in modeled discharge there (see results from kriging modeling on *CV* in Chapter 3). We suspect that the large *CV* on Kaua'i masks some differences between the regions but a refined error model for discharge on the island would have to be constructed to fully investigate the issue.

In general, fluxes from Eastern Kaua'i are smaller than from Waimea, although the effect is never statistically significant at the 1 s.e. level. Fluxes from Kohala and Hamakua-Hilo are markedly different - cation and Ca+Mg export, WCEF and WCSF are all significantly higher from Hamakua-Hilo than from Kohala. Fluxes from

Figure 4.12. Results from three different ANOVAs. As an example, we show the area-normalized weathering carbon sequestration flux (WCSF) from the four different regions under study. a) Area-weighted ANOVA, excluding the Wailuku River in Hamakua-Hilo. b) Area-weighted ANOVA, including the Wailuku River. c) Un-weighted ANOVA on the four regions, including all streams. The inclusion of the Wailuku River in the area-weighted ANOVA has a significant impact on the average fluxes from the Hamakua-Hilo region and other regions are almost entirely insensitive to area-weighting the area-normalized fluxes.

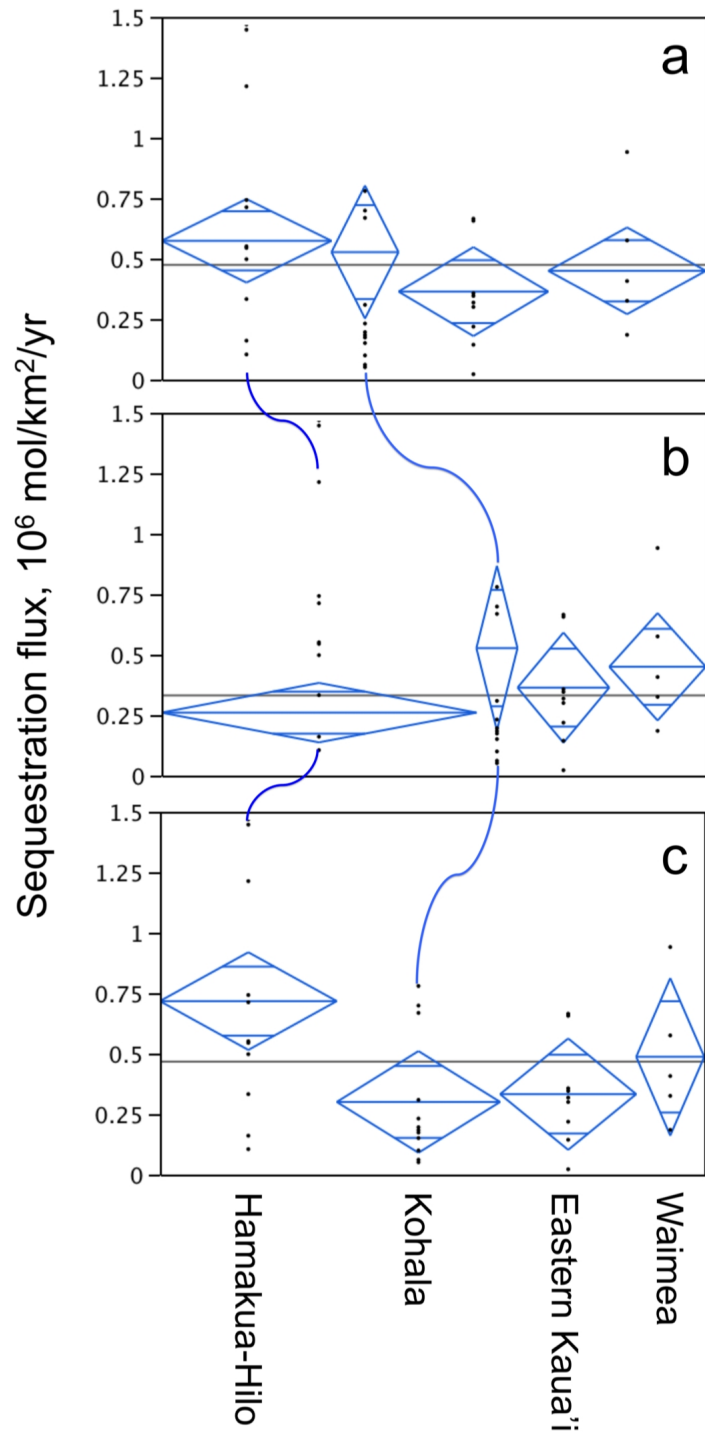
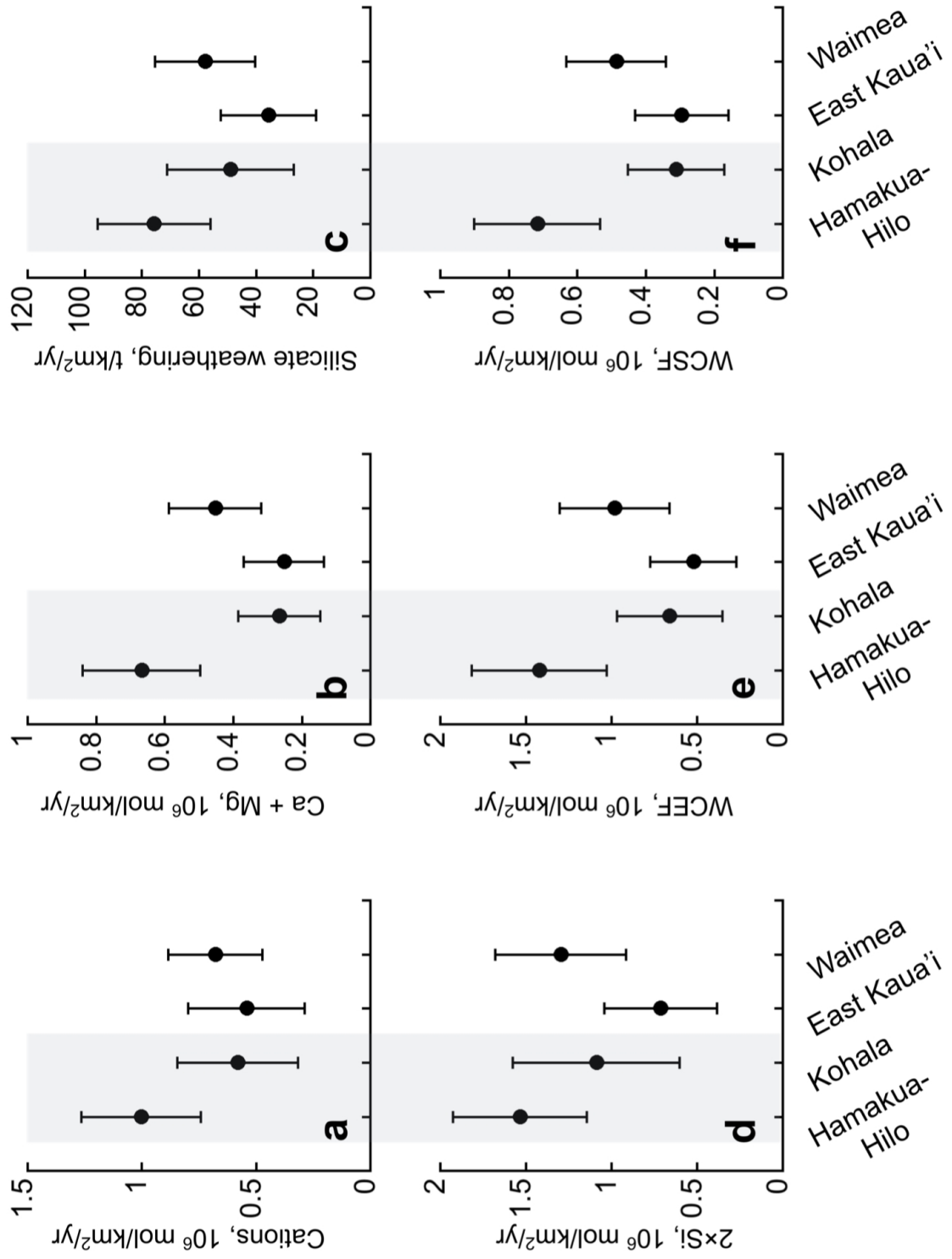


Figure 4.13. One-way un-weighted ANOVA shows the central tendency and 1 s.e. error bars of area-normalized chemical fluxes, by region. Fluxes from the Big Island are shaded. There are no statistical differences between area-normalized weathering fluxes between the two regions on Kaua'i and the Kohala Peninsula on the Big Island. Hamakua-Hilo is the only region that differentiates itself, with significantly higher fluxes of silicate derived $\text{Ca}^{2+} + \text{Mg}^{2+}$ and bicarbonate (WCEF) and WCSF than Kohala and E-Kaua'i. No statistical difference is observed between the Hamakua-Hilo and Waimea regions for any type of flux.



Kohala, on the other hand, are almost always statistically indistinguishable from fluxes from Kaua'i. This indicates that a) un-weighted, area-normalized fluxes on Kaua'i do not differ significantly across the island, b) Kohala, in spite of its proximity both in space and age to Hamakua-Hilo, does not differ appreciably from the older, more highly weathered terrain of Kaua'i in terms of chemical weathering fluxes and c) Hamakua-Hilo has significantly elevated fluxes of the key variables controlling sequestration of atmospheric CO₂ in the oceans.

The surface weathering fluxes reported here (WCEF = 0.52-1.42 × 10⁶ mol/km²/yr) range from the lower end to the center of the range reported in basaltic environments worldwide (Dessert et al., 2003) and are substantially lower than the fluxes reported from other tropical volcanic islands such as the Philippines (Chapter 2, WCEF = 2.04-6.16 × 10⁶ mol/km²/yr), and Reunion and Mt. Cameroon (WCEF = 2.26 and 3.44 × 10⁶ mol/km²/yr, respectively) (cited in Dessert et al., 2003). They are, on average, slightly higher than the value given for Hawaiian streams (WCEF = 0.66 × 10⁶ mol/km²/yr) reported by Dessert et al. (2003). They did not investigate streams in the Waimea region on Kaua'i or any streams in Hamakua-Hilo - the two regions where chemical fluxes are the highest. This probably goes a long way to explaining the highly anomalous values for chemical weathering in Hawai'i reported by Dessert and her coworkers (2003).

The lack of statistical difference between regions in this study should not necessarily be taken as evidence that the chemical fluxes from these regions are identical. Rather, this highlights a need for a more rigorous control on error, mainly in the water budget. Put another way, we propose that the poorly constrained, but relatively well quantified, errors in our results mask significant differences that only further testing and modeling

will reveal. These results also highlight the need for rigorous and explicit error propagation in studies of this kind. The kind of large uncertainties on chemical fluxes that we find in Hawai'i are likely to be found elsewhere but authors rarely carry out an error analysis of the kind done here.

4.4.6. Fluxes, groundwater (subsurface)

Groundwater recharge was compiled from USGS reports as described in Chapter 3. Groundwater chemistry for all wells used in this study is shown in Table 4.3b.

Variability in groundwater chemistry is not as large as in surface water chemistry (average *CV* for groundwater chemical concentrations is 43%, compared to 83% for surface water). Since groundwater in the Puna/Ka'u districts is a) significantly more dilute in the solutes that are the most important components of the weathering fluxes that we are calculating (see Chapter 4.3.2.2.) and b) groundwater recharge rates in the Puna/Ka'u region are very high (see Chapter 3), we treat the Puna/Ka'u region separately with respect to groundwater chemical fluxes and calculate separate recharge-weighted average concentrations for the region. There is little to no statistical difference between chemical concentrations in groundwater elsewhere on the Big Island and on the other islands. No further regional groundwater chemistry distinction is therefore made and instead we calculate a single recharge-weighted average concentration for groundwater elsewhere in Hawai'i. The two regions will be referred to as the "Puna/Ka'u" region and the "rest of Hawai'i" region.

We use the recharge-weighted average concentration of the "rest of Hawai'i" groundwater to calculate chemical fluxes from all aquifers excluding the Puna/Ka'u, for which we use the recharge-weighted average concentration of the Pahala, Pahoa and Panaewa wells (Table 4.3b, Figure 4.6). The groundwater chemical fluxes for the

four regions defined for this study (Waimea, East Kaua'i, Kohala and Hamakua-Hilo) are listed in Table 4.5c and chemical fluxes for all other aquifers are listed in Table A4.2.

The Puna/Ka'u aquifers (Takasaki, 1993) cover a little less than a quarter of the total area of the Hawaiian Islands and receive around 40% of the total groundwater recharge. Total annual fluxes of solutes from the Puna/Ka'u aquifer are 13-34% of total groundwater solute fluxes from all of Hawai'i. 34% of the flux of dissolved flux of Si via groundwater occurs from the Puna/Ka'u aquifer, and only 13% of sulfate. As shown in Fig 4.9a, b, groundwater mineral equilibria do not vary between the Puna/Ka'u region and other regions. This would suggest that weathering processes do not differ between the Puna/Ka'u groundwater system and other aquifers, although the X/Si ratios do suggest that such differences exist (see Chapters 4.3.2.2. and 4.4.2.). Since evidence for differences in secondary mineral assemblages between the Puna/Ka'u region and other regions is not unequivocal, we conclude that the large export fluxes of Si from the Puna/Ka'u are essentially a consequence of the large volumes of water moving through the system.

4.4.7. Magnitude of surface and subsurface fluxes

It is not straightforward to area-normalize groundwater chemical fluxes, mainly because of uncertainty about the extent of the weathering zone in the subsurface. Groundwater takes flow paths that do not necessarily match surface topography, aided by dikes and variable permeability in different rock layers, and this causes considerable uncertainty about the areal extent of the region through which the groundwater has passed. Furthermore, there may be several lenses or layers of groundwater at different levels in the lava pile (Thomas et al., 1996), with each of

these groundwater lenses interacting with the rocks it passes through. The groundwater system is therefore a highly 3-D system (as mentioned briefly above). Because of this, we compare the total magnitude of subsurface (groundwater) and surface fluxes ($R_{\text{sub/sur}}$) (Figure 4.14, Table 4.6), instead of comparing area-normalized fluxes of subsurface and surface fluxes.

First, we look at $R_{\text{sub/sur}}$ on the Big Island. We find that $R_{\text{sub/sur}}$ of WCSF is ~ 10 and ~ 13 for WCEF. $R_{\text{sub/sur}}$ of silicate weathering flux and Si-flux is ~ 15 -16, and for sulfate it is almost 18. These numbers show that on young hot-spot volcanic islands such as the Big Island, groundwater is at least an order of magnitude more important for transporting chemicals from weathering than is surface water. This finding has implications for the overall fluxes of chemicals from basaltic oceanic islands and their impact on ocean chemistry.

Looking at individual regions reveals that groundwater is a larger vector for chemical fluxes in Hamakua-Hilo and Kohala than in either region on Kaua'i. The ratio of subsurface to surface fluxes ($R_{\text{sub/sur}}$) in Hamakua-Hilo is 1.0-1.8 with a mean of 1.5, and in Kohala it ranges from 0.9 to 2.1, with an average of 1.4. Thus, on average around 60% of total chemical fluxes from the two regions on the Big Island come from subsurface weathering. On Kaua'i, $R_{\text{sub/sur}}$ is on average 0.5 in both regions, Waimea and East Kaua'i. In other words, around a third of total chemical weathering fluxes from Kaua'i originate in subsurface weathering. The range of $R_{\text{sub/sur}}$ observed in East Kaua'i is very small (0.5-0.7) but fairly large in Waimea (0.3-1.3). Sulfate is a special case in Waimea ($R_{\text{sub/sur}} = 1.3$) - this is due to the low concentrations of sulfate in surface water in the region. Excluding sulfate fluxes, the average $R_{\text{sub/sur}}$ in Waimea is 0.4.

Figure 4.14. Ratios of subsurface to surface chemical fluxes ($R_{\text{sub/sur}}$), by region. The y-scale is broken for clarity. For reference, $R_{\text{sub/sur}} = 1$ is displayed with a heavy gray line. In Hamakua-Hilo, groundwater contributes more to the overall flux of all metrics inspected than does surface water. The same is true for Kohala. In Waimea and East Kaua'i, stream flow is more important for solute fluxes than groundwater is, usually supplying around 60% of solutes ($R_{\text{sub/sur}} \sim 0.5$). Analysis of stream and groundwater chemistry shows that on Kaua'i, streams are heavily influenced by groundwater inputs, which tends to decrease the actual $R_{\text{sub/sur}}$.

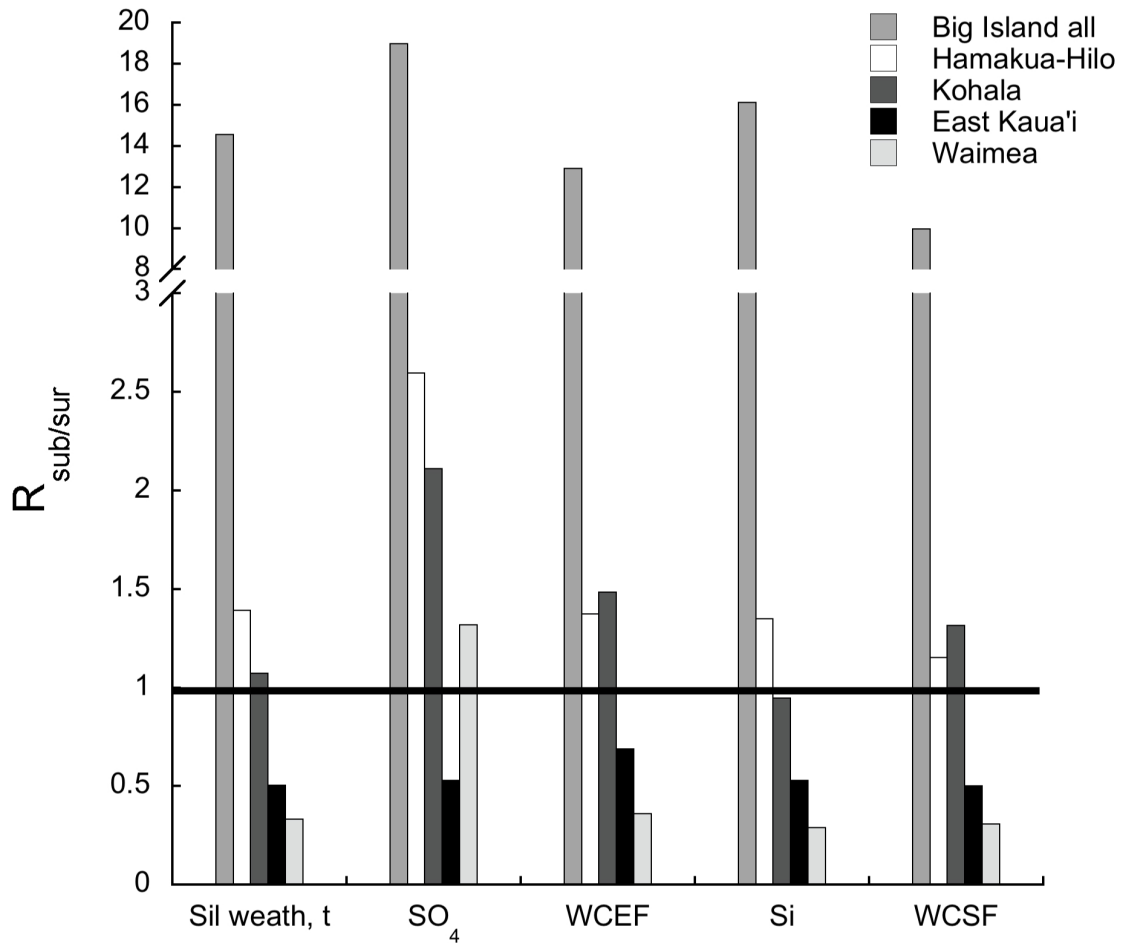


Table 4.6. Ratio of subsurface chemical fluxes to surface chemical fluxes on the Big Island of Hawai'i and on Kaua'i.

	Silicate weathering cation flux ¹		Silicate weathering ²		Silicate Ca*+Mg*		SO ₄	WCEF ³	2 × Si	WCSF ⁴
	mol/yr	eq/yr	t/yr	t/yr	mol/yr	mol/yr				
					eq/yr	mol/yr				
Big Island										
Whole island	12	11	12	15	19	9.4	13	16	10	
Hamakua-Hilo	1.8[#]	1.5	1.6	1.5	2.6	1.0	1.4	1.3	1.2	
Kohala	1.6	1.5	1.5	1.1	2.1	1.2	1.5	0.9	1.3	
Kaua'i										
East Kaua'i	0.5	0.5	0.5	0.5	0.5	0.5	0.7	0.5	0.5	
Waimea	0.5	0.4	0.5	0.3	1.3	0.3	0.4	0.3	0.3	

1: Silicate cation weathering rate = Na* + K* + Ca* + Mg*

2: Silicate weathering rate = Na* + K* + Ca* + Mg* + SiO₂

3: Weathering carbon export flux = see discussion in section on surface fluxes

4: Weathering carbon sequestration flux = see discussion in section on surface fluxes

#: Numbers in bold show cases where subsurface chemical fluxes are larger than surface chemical fluxes.

The immediate conclusion to draw from these calculations is that groundwater chemical fluxes are an important component of chemical weathering budgets on the Hawaiian Islands, transporting 30-95% of the total flux of chemical weathering products from the islands. A similar conclusion was reached by Rad et al. (2007), whose study called attention to the concept of groundwater chemical fluxes from volcanic islands but did not look in sufficient detail at the phenomenon. Rad et al. (2007) use both low-temperature and high-temperature (i.e., boiling and sub-boiling water from geothermal systems) groundwater in their study and conclude that groundwater fluxes supply 60-95% of total chemical fluxes from the volcanic islands they studied (Martinique, Guadeloupe and Reunion). Our study does not include any high-temperature weathering solutions and our results are therefore not directly comparable to the results of Rad et al. (2007).

The decrease in $R_{\text{sub/sur}}$ with age of the substrate (Big Island < 0.35 Myr, Kaua'i ~ 4 Myr) is coupled with the general decrease of groundwater recharge as soils mantle the landscape and porosity in the lava pile is filled in with secondary minerals. It may also reflect the decreased availability of easily weathered material as dissolution of fresh primary minerals in the lava pile and immobilization of elements in secondary minerals proceed. Weathering fluxes from a new volcanic edifice are initially the highest in the subsurface, as is the case in Kilauea. As soils form and retain precipitation in the surface environment, surface weathering increases although groundwater is still the main producer and transport vector for chemical weathering fluxes (Hamakua-Hilo and Kohala, with some exceptions that will be discussed below). On Kaua'i, where very thick soils mantle large parts of the land, groundwater is a much diminished, but still significant, contributor to chemical weathering fluxes. We do not have enough data from Maui, Moloka'i and O'ahu to constrain at what stage

in the lifespan of the islands the effects of surface fluxes become dominant, but they do appear to have overshadowed groundwater fluxes by the time the last vestiges of the original shield geomorphology disappear. At that point, the volume of thick piles of lava has perhaps been diminished sufficiently to not support a vigorous groundwater system any longer.

The addition of groundwater fluxes raises total fluxes from Hawai'i by 40-150%. This allows us to re-calculate the area-normalized flux to include sub-surface weathering, so that $WCEF_{total} = 0.88-3.40 \times 10^6 \text{ mol/km}^2/\text{yr}$. This raises the fluxes from Hawai'i to the levels observed in for instance Reunion and Philippines. Other tropical, basaltic regions should also have significant groundwater recharge (e.g. Join et al., 2005; Prada et al., 2005; Lee and Kim, 2007) and chemical fluxes via that pathway will only further increase the overall fluxes (Rad et al., 2007). Although groundwater chemical fluxes are a significant addition to surface chemical weathering fluxes from Hawai'i, it seems unlikely that the addition of groundwater to area-normalized fluxes from Hawai'i closes the “gap” in magnitude of fluxes between Hawai'i and other tropical, basaltic regions. This raises important questions about the nature of chemical weathering in Hawai'i and the reason for the rather low surface weathering fluxes reported here which we cannot answer at present.

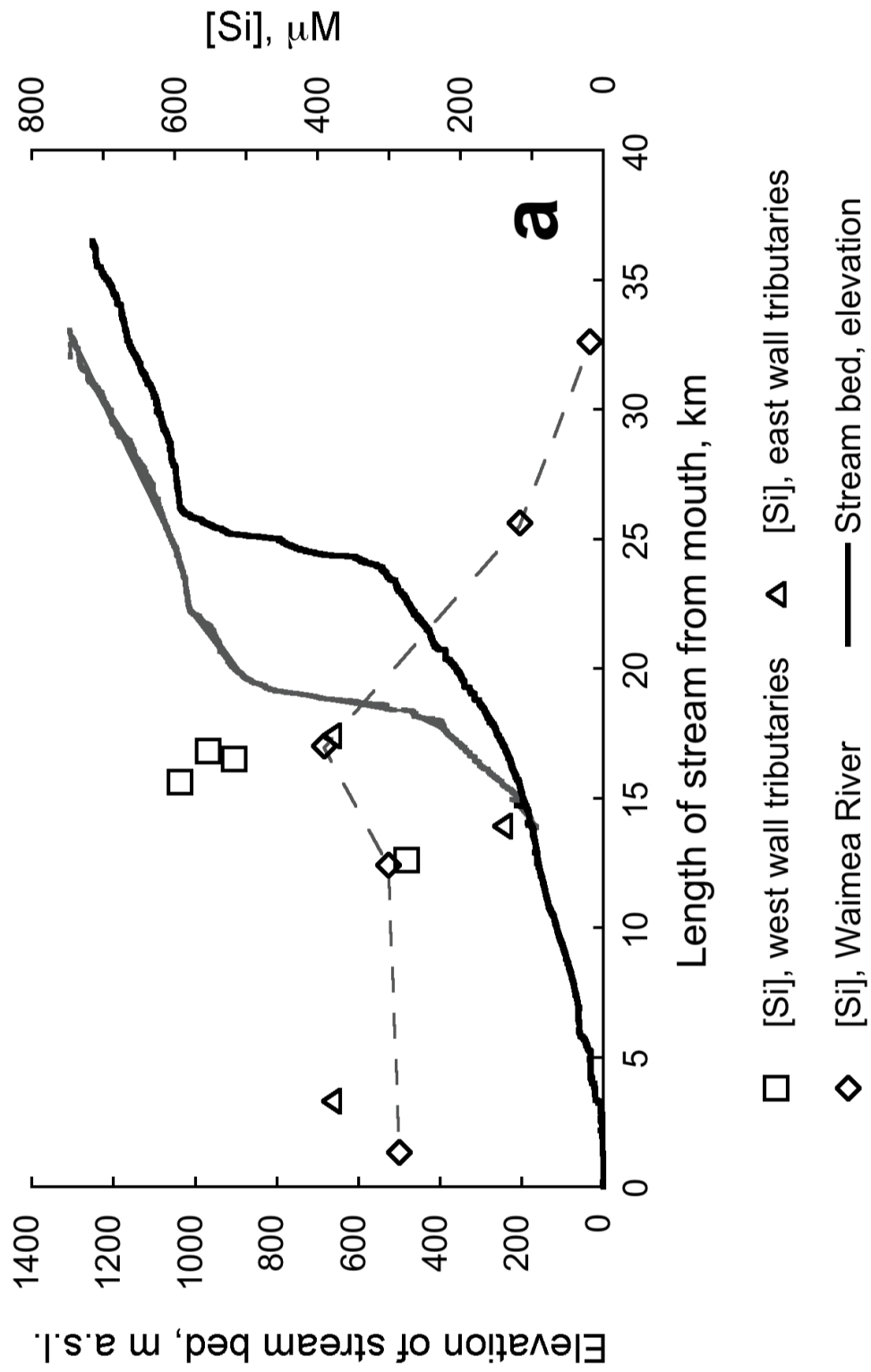
4.4.8. Groundwater and geomorphology

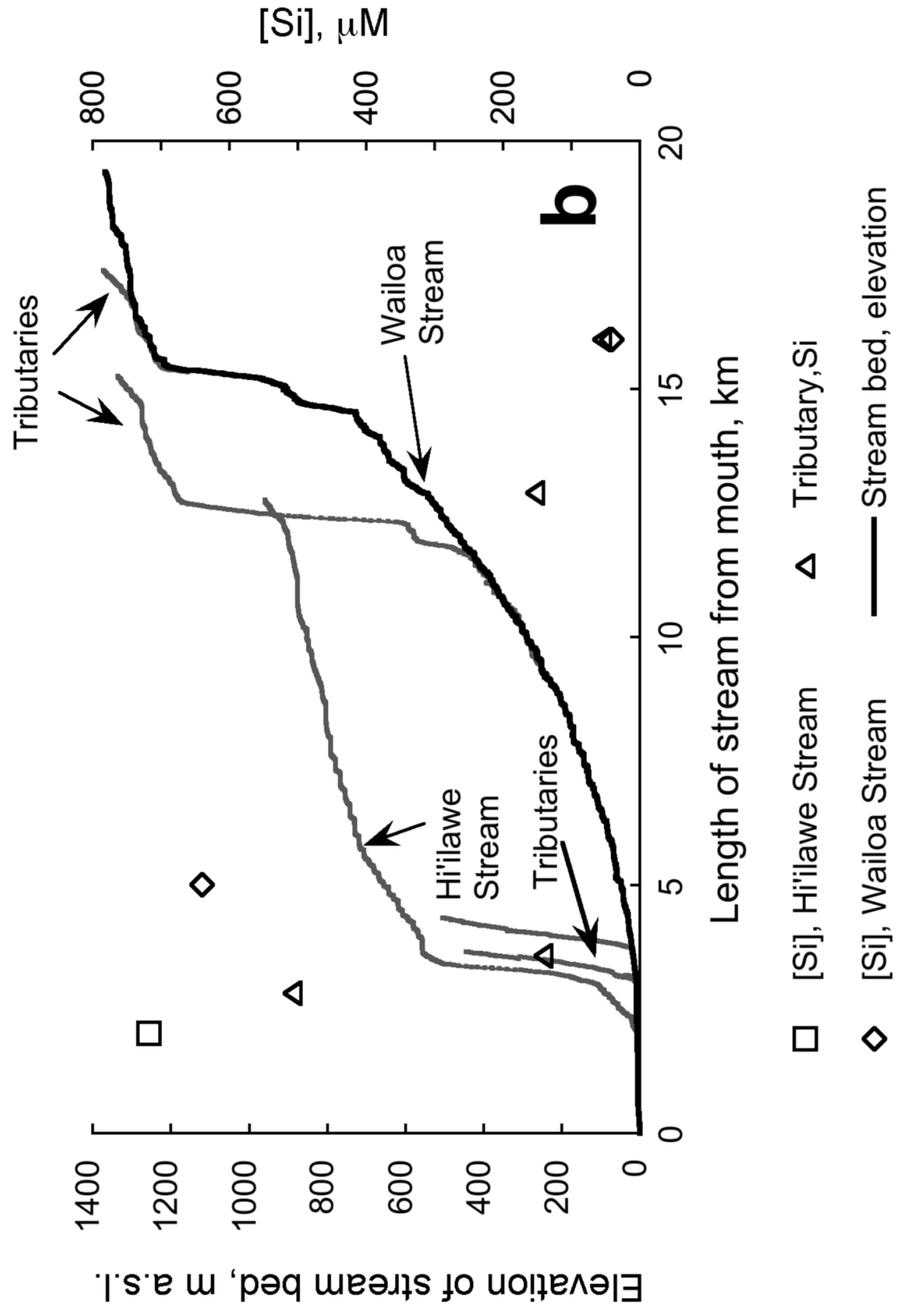
Although weathering and hydrological regimes have so far in this chapter been divided into the rather simplistic terms “surface” and “groundwater”/“subsurface”, this division is not clear-cut. According to data from the USGS, base flow (i.e., the groundwater component of stream flow) supplies around 17% of discharge to streams on the Big Island (this number is very approximate, based on 2 data points) and

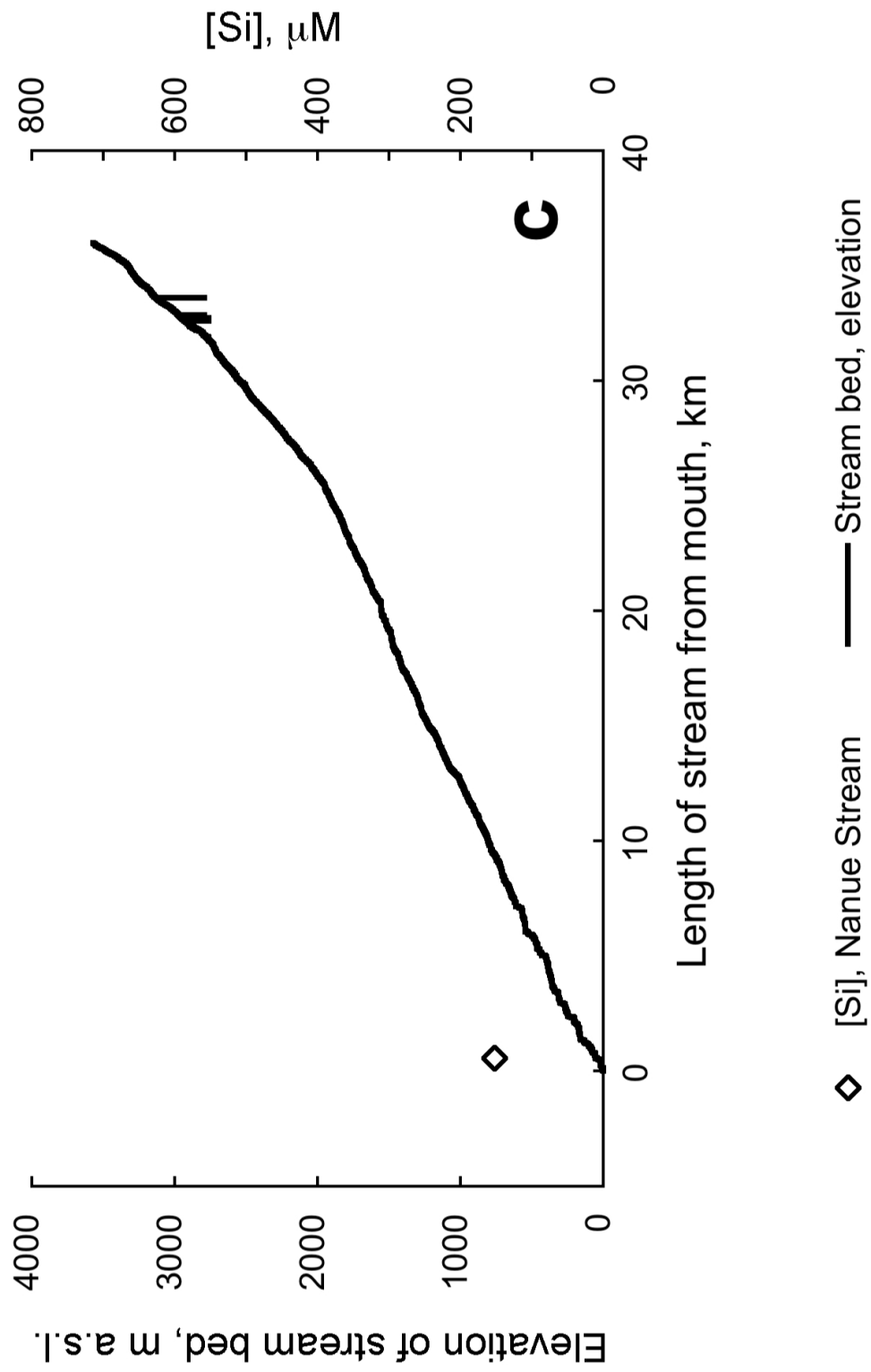
around 50% to streams on Kaua'i (n=4). An alternative explanation for the apparently diminished importance of groundwater contributions to solute flux on highly weathered Kaua'i therefore exists: Since a large fraction of the groundwater recharge on the island discharges on land rather than directly into the sea, a large share of the groundwater contribution is already counted in the surface fluxes, artificially bringing down the $R_{\text{sub/sur}}$ in highly eroded regions. The concentrations of solutes in groundwater, particularly Si, are usually much higher than in streams and even a small influx of groundwater will affect the chemical composition of stream water considerably. For instance, assuming groundwater has $[\text{Si}] = 1000 \mu\text{M}$ and stream water has $[\text{Si}] = 100 \mu\text{M}$, it takes only 11% groundwater by volume to double the $[\text{Si}]$ of the stream.

Figure 4.15a shows average concentrations of Si in Waimea River in Waimea Canyon on Kaua'i and from several tributaries sampled on both sides of the river, overlain on a river profile which shows the dramatic contrasts in landscape within the drainage basin of the river, from the flat highlands via a drop of 500 meters into the narrow Waimea Canyon. Tributaries draining the west wall of the canyon descend steeply down from a knife-edge ridge, have very small drainage areas and only flow during heavy rainfall. Most east bank tributaries drain the Alaka'i Swamp, then descend steeply into tributary canyons where they flow for a few kilometers before joining the main trunk of the river. A clear downstream increase in the concentration of Si is seen in the main trunk of Waimea River as the dilute water coming into the canyon from the Alaka'i Swamp mixes with more concentrated water inside the canyon. Based on the composition of Tributary A (discussed in Chapter 4.4.1.), groundwater draining into the canyon from springs and seeps has an average $[\text{Si}] = 927 \mu\text{M}$. To elevate the composition of the west wall ephemeral tributaries from an assumed $\sim 10 \mu\text{M}$ $[\text{Si}]$ in

Figure 4.15. Comparison of stream profiles and [Si] of stream samples. Heavy lines: Stream bottom, from the stream mouth (left) to its headwaters (right). The x-axis shows the distance upstream from the stream mouth, in km. Note the double y-axis, with elevation in m a.s.l. on the left axis and [Si] in $\mu\text{mol/L}$ on the right axis. **a)** The Waimea River originates in the Alaka'i Swamp and plunges into the Waimea Canyon. Numerous tributaries enter the main trunk of Waimea River from the Alaka'i Swamp to the east of the canyon. There are no perennial tributaries along the west wall of the canyon but many ephemeral ones. The open symbols show [Si] in the main trunk of Waimea River, closed symbols show [Si] in tributaries. [Si] in tributaries along the west canyon wall (circles) are considerably higher than in the main trunk of the stream, even during a very heavy rain, but fairly similar to the main trunk in the eastern tributaries. **b)** A scenario similar to the Waimea Canyon is encountered in the Waipi'o Valley on Kohala Peninsula. Deep erosion has formed a steep-sided valley with very steep headwalls leading up to a high plateau supporting a deeply weathered but little eroded swamp. The open diamonds show the [Si] of the main trunk of Wailoa Stream, the main stream draining Waipi'o Valley. [Si] in tributaries along the main trunk are shown with open triangles and open boxes. Again, the [Si] of the main trunk increases dramatically downstream. **c)** Stream erosion along the Hamakua-Hilo coastline has not modified the original shield surface to any significant extent. All streams were sampled close to the mouth and all have fairly low [Si], indicating a negligible contribution of groundwater to stream flow.







rainfall to the $\sim 500 \mu\text{M}$ commonly observed in the tributaries, a volume contribution of $\sim 50\%$ groundwater is needed. This value is much too high, given that Tributary A had a very low flow rate compared with the tributaries encountered in the canyon during the 2006 field campaign, and that the flow rate of Tributary A was nearly identical during the two sampling trips. The elevated Si in the tributaries may instead be produced by mobilization of dissolved Si (opal) from the soils in the canyon (Derry et al., 2005); an investigation of the Ge/Si in the water would help to clarify the issue.

It is possible to calculate the likely contribution of groundwater to the Si-budget of the Waimea River, based on the average [Si] of the groundwater end-member (Tributary A, [Si] = $930 \mu\text{M}$), surface weathering solution end-member (Kawaikoi Stream, [Si] = $20 \mu\text{M}$) and the average composition of the Waimea River at the sampling station furthest downstream (Waimea at ford, [Si] = $300 \mu\text{M}$). This formulation assumes that Si behaves like a conservative element (which it is not), and that the tributaries draining the west wall of Waimea Canyon are ephemeral and that their chemical composition will not normally influence the composition of the Waimea River. It furthermore assumes that groundwater seeps and springs have the same composition as Tributary A throughout the canyon and that the east-wall tributaries have acquired the same composition as the Waimea River by the time they reach the main trunk. We calculate a total groundwater flux into the Waimea River of $\sim 30\%$ by volume, considerably less than the average for the island based on the USGS hydrograph-separation techniques. The discrepancy is likely due to the non-conservative behavior of Si, i.e. net uptake of Si into vegetation or precipitation into secondary minerals.

A similar pattern is observed in the Waipi'o Valley on Kohala Peninsula and displayed in Figure 4.15b (compare the streambed of the Wailoa Stream in Figure 4.15b to the

Honokane Nui Stream in Figure 4.3 B-B'). The Wailoa Stream (diamonds) is very dilute ($[\text{Si}] \sim 50 \mu\text{M}$) just before it plunges into the valley from the summit plateau, just like the tributaries (triangles) sampled up on the plateau. The drop from the plateau into the steep-walled Waipi'o Valley is 500-600 m and rivals that of the Waimea Canyon. Ten kilometers further downstream, the $[\text{Si}]$ in Wailoa Stream has increased by an order of magnitude, through mixing with up to 60% by volume groundwater. Hi'ilawe Stream, a large tributary immediately south of the main trunk of Wailoa Stream, has an average and practically invariant $[\text{Si}]$ of $744 \mu\text{M}$, suggesting $\sim 80\%$ volume contribution by groundwater. A small tributary on the north wall of the valley has $[\text{Si}] = 500 \mu\text{M}$ and a second one, named Kakeha Stream here and sampled on the same day as the north wall tributary, has $[\text{Si}] = 142 \mu\text{M}$. These values suggest a groundwater contribution of $\sim 15\text{-}50\%$ to tributaries draining the walls of Waipi'o Valley. This volume fraction is too small to account for the groundwater contribution to the main trunk ($\sim 60\%$ based on mixing calculations) and we conclude that groundwater enters the stream via springs and/or seeps close to the bottom of the valley, rather than admixing with the tributaries draining the steep valley walls.

Along the Hamakua-Hilo coast, this pronounced effect of groundwater on the chemical composition of water is not seen (Figure 4.15c). The figure shows stream profiles or all streams sampled for this study, in order of occurrence along the coastline from Laupahoehoe in the north to Wailuku in the south. The distance between the stream profiles on the graph is proportional to the actual distance between the streams. Si-concentrations are mostly $< 200 \mu\text{M}$ and only two samples have Si in excess of $300 \mu\text{M}$. One of those is Kapehu stream, which has average and almost invariant $[\text{Si}] = 539 \mu\text{M}$. This stream, which is very small, undoubtedly receives a

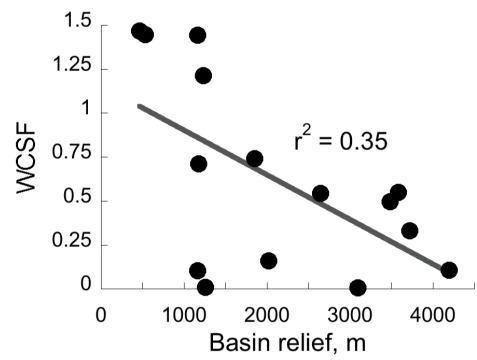
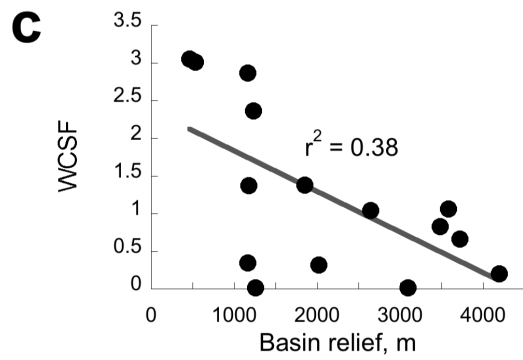
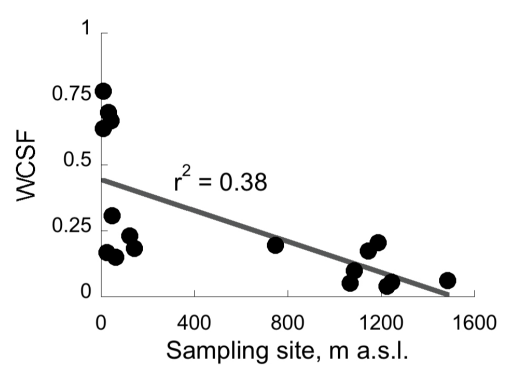
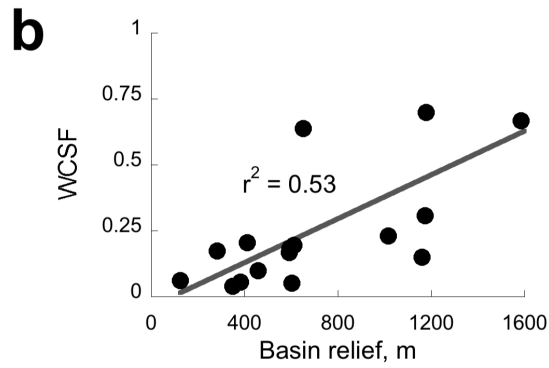
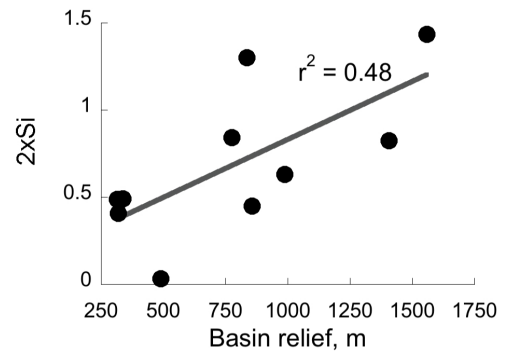
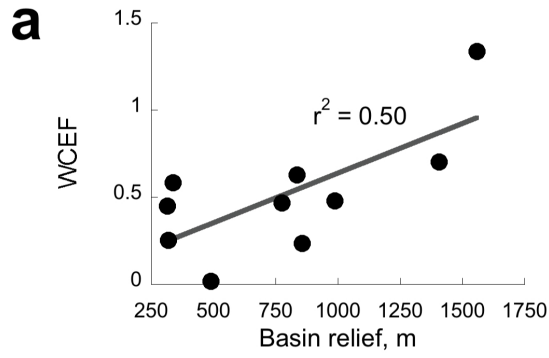
significant volume fraction of groundwater. The green line towards the top of the graph represents the average [Si] of groundwater in Hawai'i.

The stream profile of Figure 4.15c are markedly different from the ones in Figures 4.15a-b. Physical erosion in Hamakua-Hilo has not changed the constructive volcanic landscape to any great extent and the streambeds still have the overall shape of the volcanic edifice (compare Figure 4.15c to Figure 4.3 D-D'). Minor canyon inception is observed in Laupahoehoe Stream, the northernmost of the sampled streams and the northernmost stream we found running in the Hamakua-Hilo region. Although the stream profiles for some of the streams are defined by ArcGIS all the way to near the summit of Mauna Kea (~4000 m a.s.l.), there is hardly any precipitation at elevations above 1500-3000 m a.s.l. and these high regions do not contribute any meaningful amount of water to the watershed. The evidence from [Si] in streams for relatively small volume contribution of groundwater to surface runoff, coupled with the low degree of erosion in the Hamakua-Hilo watersheds, supports the interpretation above that groundwater enters streams mostly close to the bottom of canyons formed by extensive physical erosion.

4.4.9. Surface water and geomorphology

We further investigated the connection between the topography of drainage basins and the area-normalized fluxes through them via a regression of fluxes against various landscape variables, namely elevation of sample site, basin relief, basin maximum elevation, basin mean elevation and the *CV* of elevation within the basin (Figure 4.16). Significant relationships ($p_{\text{slope}} < 0.05$) were only found in East Kaua'i, Kohala and Hamakua-Hilo. Maximum elevation and relief of basin have the strongest correlation with area-normalized fluxes in Eastern Kaua'i (Figure 4.16a), where both are

Figure 4.16. Topographic characteristics of streams studied are in some cases significantly correlated with chemical fluxes. a) In East Kaua'i, basin relief is positively correlated with WCEF and Si-flux. On Kaua'i, high relief is only found in regions of deep erosion. The positive correlation between chemical fluxes and relief in East Kaua'i therefore suggests that groundwater seeping into the bottom of deep stream valleys in the region makes an important contribution to chemical weathering fluxes, just as in Kohala and the Waimea Canyon. b) These figures echo Figure 4.15b and Figure 4.16a. High-relief streams on Kohala are located in deeply eroded valleys and receive a significant input of groundwater, which increases chemical weathering fluxes from the watershed. Since sampling these streams at low elevations guarantees the inclusion of the groundwater component in the sample, high chemical weathering fluxes are seen in the streams that are sampled at the lowest elevation. Streams at high elevation, such as in the Upper Kohala swamp, drain highly weathered rocks that contribute a small part of the overall chemical fluxes from the region. c) In Hamakua-Hilo, all area-normalized fluxes are negatively correlated with maximum elevation and relief as well as with mean elevation. This may be caused by lack of groundwater feeding into the little eroded streams, or because of the size (area) of these watersheds being systematically overestimated.



positively correlated with 2×Si-fluxes and WCEF. Mean basin elevation is also significantly positively correlated with 2×Si but not with WCEF. Relief and maximum elevation are highly auto-correlated in East Kaua'i ($r^2 = 0.99$, $p_{\text{slope}} < 0.0001$). It is therefore sufficient to inspect one only. Streams with high relief are expected to have high area-normalized fluxes since they likely occur in deep valleys with significant groundwater input and this is indeed observed in East Kaua'i. This implies that a similar process as the one described above is at work in the deep valleys of East Kaua'i. A significant negative correlation was observed between all area-normalized fluxes and elevation of sampling site in Kohala (Figure 4.16b), testifying to the impact of groundwater addition in lower reaches of deeply eroded valleys to the chemical fluxes. In Kohala, relief is also significantly positively correlated with area-normalized fluxes, for the same reason as in East Kaua'i above. *CV* of elevation and relief are significantly auto-correlated in Kohala and Waimea ($r^2 = 0.59$, $p_{\text{slope}} < 0.0022$ and $r^2 = 0.70$, $p_{\text{slope}} < 0.0004$, respectively) but no significant correlation between any landscape metric and area-normalized fluxes is found in Waimea.

In Hamakua-Hilo (Figure 4.16c), all area-normalized fluxes are negatively correlated with maximum elevation and relief (again, these two metrics are highly auto-correlated, $r^2 = 0.92$ and $p_{\text{slope}} < 0.0001$), as well as with mean elevation. The negative correlation in Hamakua-Hilo has two possible explanations: 1) Groundwater is not entering the streams to the same extent as in the highly eroded valleys of East Kaua'i and Kohala, and 2) the maximum elevation of drainage basins in Hamakua-Hilo, and thereby the relief (and mean elevation), is systematically overestimated by the inclusion of large areas that do not contribute to weathering in the basin.

4.5. CONCLUSIONS

Surface water and groundwater in Hawai'i have distinct chemical compositions, mainly with respect to saturation state of minerals and concentrations of major elements. Surface area-normalized chemical fluxes are highest in the Hamakua-Hilo region, that drains the flanks of Mauna Kea, and in Waimea, that drains the oldest and most highly eroded shield volcano in the Hawaiian Islands. The sources of the high surface weathering fluxes in the two regions are distinct – in Hamakua-Hilo, sheer volume of water going through the system coupled with an abundance of fresh, easily weathered material combine to produce the high fluxes, whereas in Waimea, a large fraction of the surface fluxes is groundwater that drains into the highly eroded, deep canyons and valleys of the region.

A comparison of total chemical fluxes via groundwater and surface water, as observed in streams and rivers, reveals that on the Big Island, groundwater contributes on average 60% of total chemical weathering fluxes to the ocean. Looking at the Big Island as a whole, the predominance of groundwater chemical fluxes is even more dramatic – up to 95% of solutes released from rocks during weathering is transported to the ocean via groundwater. This percentage falls to 30%, on Kaua'i, the oldest island. As is discussed above, a large fraction of surface fluxes on Kaua'i is actually derived from groundwater and this raises the fraction of chemical fluxes attributable to groundwater (subsurface) weathering in Kaua'i to well above 30%. Groundwater is therefore an important pathway for delivery of solutes from land to ocean across the entire archipelago, regardless of subsurface age.

Groundwater is always present in the landscape, it seems – it is the only large-scale weathering agent in very young volcanic edifices that have not yet developed soils

and/or a moss cover to intercept precipitation and retain it on the surface. It becomes a major component of stream flow as soon as fluvial erosion reaches the groundwater table and remains an important component of the water budget for the lifetime of the fluvial system as investigated here.

In global context, the area-normalized surface fluxes calculated here (WCEF = 0.52-1.42 x 10⁶ mol/km²/yr) place in the lower end to center of the range for volcanic regions worldwide (see Table 2.6, Chapter 2) and lower than in the Philippines (Table 2.5, Chapter 2). The addition of groundwater fluxes raises these fluxes to WCEF = 0.88-3.40 x 10⁶ mol/km²/yr, or by 40-150%. This raises the fluxes from Hawai'i to the levels observed in for instance Reunion and Philippines. However, groundwater fluxes were not included in the weathering calculations for these locations and their inclusion would increase the total fluxes. It therefore appears that even after the inclusion of groundwater fluxes in the total weathering budget of Hawai'i, chemical weathering fluxes on the islands are still relatively low compared to other similar regions. The reasons for this discrepancy are not well understood and we cannot adequately explain them at this point.

References

- Andrews J.E., Brimblecombe P., Jickells T.D. And Liss P.S. (1996) *An Introduction to Environmental Chemistry*. 1st ed. Blackwell Science.
- Berner R.A. (2004) *The Phanerozoic Carbon Cycle*. 1st ed. Oxford University Press.
- Bethke C. (2007) *The Geochemist's Workbench*. Hydrogeology Program, University of Illinois.
- Bluth G.J.S. and Kump L.R. (1994) Lithologic and climatologic controls of river chemistry. *Geochimica et Cosmochimica Acta* 58, 2341-2359.
- Carrillo J.H., Hastings M.G., Sigman D.M and Huebert B.J. (2002) Atmospheric deposition of inorganic and organic nitrogen and base cations in Hawaii. *Global Biogeochemical Cycles* 16, 1076.
- Chadwick O.A., Derry L.A., Vitousek P.M., Huebert B.J. and Hedin L.O. (1999) Changing sources of nutrients during four million years of ecosystem development. *Nature* 397, 491-497.
- Chadwick O.A., Derry L.A., Bern C.R. and Vitousek, P.M. (2009) Changing sources of strontium to soils and ecosystems across the Hawaiian Islands. *Chemical Geology* 267, 64-76.
- Crews T.E., Kitayama K., Fownes J.H., Riley R.H., Herbert D.A., Mueller-Dombois D. and Vitousek P.M. (1995) Changes in Soil Phosphorus Fractions and Ecosystem Dynamics across a Long Chronosequence in Hawaii. *Ecology* 76, 1407.
- Derry L.A., Kurtz A.C., Ziegler K. and Chadwick O.A. (2005) Biological control of terrestrial silica cycling and export fluxes to watersheds. *Nature* 433, 728-731.

- Dessert C., Dupre B., Gaillardet J., Francois L.M. and Allegre C.J. (2003) Basalt weathering laws and the impact of basalt weathering on the global carbon cycle. *Chemical Geology* **202**, 257-273.
- Edmond J.M. and Huh Y. (1997) Chemical Weathering Yields from Basement and Orogenic Terrains in Hot and Cold Climates. In: *Tectonic uplift and climate change*. New York, Plenum Press, pp.330-351.
- ESRI (2009) *ArcGIS – The Complete Geographic Information System [online]*. Redlands: ESRI.
- Feigenson M. (1984) Geochemistry of Kauai volcanics and a mixing model for the origin of Hawaiian alkali basalts. *Contributions to Mineralogy and Petrology* **87**, 109-119.
- France-Lanord C. and Derry L.A. (1997) Organic carbon burial forcing of the carbon cycle from Himalayan erosion. *Nature* **390**, 65-67.
- Gaillardet J., Dupre B., Louvat P. and Allegre C.J. (1999) Global silicate weathering and CO₂ consumption rates deduced from the chemistry of large rivers. *Chemical Geology* **159**, 3-30.
- Giambelluca T.W., Nullet M.A. and Schroeder T.A. (1986) *Rainfall Atlas of Hawaii*. Honolulu, HI, Water Resources Research Center, University of Hawaii at Manoa.
- Gislason S.R., Arnorsson S. and Armannsson H. (1996) Chemical weathering of basalt in Southwest Iceland; effects of runoff, age of rocks and vegetative/glacial cover. *American Journal of Science* **296**, 837-907.
- Join J.L., Folio J.L. and Robineau B. (2005) Aquifers and groundwater within active shield volcanoes. Evolution of conceptual models in the Piton de la Fournaise volcano. *Journal of Volcanology and Geothermal Research* **147**, 187-201.
- Juvik S.P. and Juvik J.O. (1998) *Atlas of Hawai'i*. 3rd ed. Honolulu, University of Hawai'i Press.

- Lamb M.P., Howard A.D., Dietrich W.E. and Perron J.T. (2007) Formation of amphitheater-headed valleys by waterfall erosion after large-scale slumping on Hawai'i. *Geological Society of America Bulletin* **119**, 805-822.
- Lee J. and Kim G. (2007) Estimating submarine discharge of fresh groundwater from a volcanic island using a freshwater budget of the coastal water column. *Geophysical Research Letters* **34**, L11611.
- Louvat P. and Allègre C.J. (1997) Present denudation rates on the island of Réunion determined by river geochemistry: Basalt weathering and mass budget between chemical and mechanical erosions. *Geochimica et Cosmochimica Acta* **61**, 3645-3669.
- Lyons W.B., Carey A.E., Hicks D.M. and Nezat C.A. (2005) Chemical weathering in high-sediment-yielding watersheds, New Zealand. *Journal of Geophysical Research-Earth Surface* **110**, F01008.
- McDougall I. (1979) Age of shield-building volcanism of Kauai and linear migration of volcanism in the Hawaiian island chain. *Earth and Planetary Science Letters* **46**, 31-42.
- McDougall I. and Swanson D.A. (1972) Potassium-Argon Ages of Lavas from the Hawi and Pololu Volcanic Series, Kohala Volcano, Hawaii. *Geological Society of America Bulletin* **83**, 3731-3738.
- Meybeck M. (1976) Total Mineral Dissolved Transport By World Major Rivers / Transport en sels dissous des plus grands fleuves mondiaux. *Bulletin of the International Association of Scientific Hydrology* **21**, 265-284.
- Meybeck M. (1987) Global chemical weathering of surficial rocks estimated from river dissolved loads. *American Journal of Science* **287**, 401-428.
- Mortlock R.A. and Froelich P.N. (1989) A simple method for the rapid determination of biogenic opal in pelagic marine sediments. *Deep Sea Research Part A. Oceanographic Research Papers* **36**, 1415-1426.

- Oksanen J. and Sarjakoski T. (2005) Error propagation analysis of DEM-based drainage basin delineation. *International Journal of Remote Sensing* **26**, 3085-3102.
- Peterson R.N., Burnett W.C., Glenn C.R. and Johnson A.G. (2009) Quantification of point-source groundwater discharges to the ocean from the shoreline of the Big Island, Hawaii. *Limnology and Oceanography* **54**, 890-904.
- Prada S., da Silva M. and Cruz J. (2005) Groundwater behaviour in Madeira, volcanic island (Portugal). *Hydrogeology Journal* **13**, 800-812.
- Rad S., Louvat P., Gaillardet J. and Allegre C.J. (2006) Time scale of erosion in volcanic islands: relationship with chemical and physical erosion. In: *Eos Trans. AGU*.
- Rad S.D., Allegre C.J. and Louvat P. (2007) Hidden erosion on volcanic islands. *Earth and Planetary Science Letters* **262**, 109-124.
- Reiners P.W., Nelson B.K. and Izuka S.K. (1999) Structural and petrologic evolution of the Lihue basin and eastern Kauai, Hawaii. *Geological Society of America Bulletin* **111**, 674-685.
- Schopka H., Derry L. and Arcilla C. (2011) Chemical weathering, river geochemistry and atmospheric carbon fluxes from volcanic and ultramafic regions on Luzon Island, the Philippines. *Geochimica et Cosmochimica Acta*, , **75**, 978-1002.
- Stallard R.F. and Edmond J.M. (1981) Geochemistry of the Amazon .1. Precipitation Chemistry and the Marine Contribution to the Dissolved-Load at the Time of Peak Discharge. *Journal of Geophysical Research-Oceans and Atmospheres* **86**, 9844-9858.
- Stallard R.F. and Edmond J.M. (1983) Geochemistry of the Amazon .2. The Influence of Geology and Weathering Environment on the Dissolved-Load. *Journal of Geophysical Research-Oceans and Atmospheres* **88**, 9671-9688.

Stallard R.F. and Edmond, J.M. (1987) Geochemistry of the Amazon .3. Weathering Chemistry and Limits to Dissolved Inputs. *Journal of Geophysical Research-Oceans* **92**, 8293-8302.

Takasaki K.T. (1993) *Ground Water in Kilauea Volcano and Adjacent Areas of Mauna Loa Volcano, Island of Hawaii*. Honolulu, HI, U.S. Geological Survey.

Thomas D.M., Paillet F.L. and Conrad M.E. (1996) Hydrogeology of the Hawaii Scientific Drilling Project borehole KP-1 2. Groundwater geochemistry and regional flow patterns. *Journal of Geophysical Research* **101**, 11,683-11,694.

Vitousek P.M., Chadwick O.A., Crews T.E., Fownes J.H., Hendricks D.M. and Herbert D. (1997) Soil and ecosystem development across the Hawaiian Islands. *GSA Today* **7**, 1-10.

CHAPTER 5

CRITICAL ASSESSMENT OF METRICS TO QUANTIFY THE IMPACT OF CHEMICAL WEATHERING ON RATES OF ATMOSPHERIC CARBON DRAWDOWN

Abstract

Studies of the impact of chemical weathering of silicate rocks on the carbon budget of the atmosphere are hampered by a lack of consensus among workers about what metrics should be used to quantify this impact. A number of metrics have been proposed in the scientific literature. Some of these metrics quantify the total drawdown of carbon from the atmosphere via silicate weathering, regardless of whether that carbon removal is permanent on geological timescales or not, while others strive to account for only the portion of atmospheric carbon that may be permanently removed from the atmosphere. Authors are often not explicit about this important distinction. Furthermore, not all methods are directly comparable with each other, making comparison between studies cumbersome at best and unreliable at worst.

In this chapter, I critically assess the three main types of metrics commonly used in the scientific literature to quantify drawdown of atmospheric CO₂ due to the weathering of silicate rocks. These types of metrics rely on either the total bicarbonate flux, the total silica flux or the flux of the alkaline earth metals. Important variations exist within the

general concept within the first and the last types of methods. The term **weathering carbon export flux (WCEF, ΦCO_2)** is proposed for the first general type of method, and the corresponding term **weathering carbon sequestration flux (WCSF, ΔCO_2)** is proposed for the last general type of methods. I argue that the total silica-method is unreliable for estimating carbon drawdown in all lithologies except for ophiolites, where it is moderately successful at predicting WCSF.

5.1. INTRODUCTION

One of the main purposes of weathering studies in silicate areas is to estimate the consumption of atmospheric CO_2 (e.g. Gaillardet et al., 1999 and Dessert et al., 2003). To date there is, however, no consensus among workers in the field as to how to calculate that essential quantity, or even what exactly is meant by the term “consumption” in this context. The term is found in the literature describing:

1. Total silicate-derived alkalinity flux (e.g. Dessert et al., 2003; Hren et al., 2007; Dessert et al., 2009; Hartmann, 2009; Wolff-Boenisch et al., 2009). Sometimes alkalinity is measured directly and sometimes it is found by charge balance
2. $2 \times$ Silica flux (e.g. Edmond and Huh, 1997; Lyons et al., 2005)
3. Ca- and Mg-silicate derived alkalinity flux (e.g. Wolff-Boenisch et al., 2009)

All of these different definitions have their merit but they are not equivalent. This makes comparison between studies awkward at best and often unreliable (Wolff-Boenisch et al., 2009). We critically assess the three methods most commonly used in the literature and compare them to our weathering data from the Philippines, New

Zealand, Iceland, Russia and Hawai'i, in order to investigate the performance of each method in different lithologies.

5.2. BACKGROUND

It is well understood that the weathering of carbonate rocks has only a temporary (10^4 – 10^5 yrs) effect on the CO_2 budget of the atmosphere and introduction of “new” Ca and Mg into the weathering system from breakdown of silicate minerals is needed for long-term ($\geq 10^6$ yr) stabilization of carbonate minerals in the marine environment (Berner, 2004). Weathering of silicates with CO_2 -derived acids results in a bicarbonate flux, approximately equal to alkalinity flux, to the oceans.

A simplified silicate weathering reaction and the associated carbon consumption can be represented by:

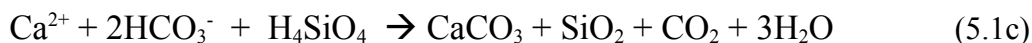


for Ca-silicates, and for Na-silicates:



It is common to estimate the total bicarbonate flux from silicate weathering (equations 5.1a and 5.1b) as the atmospheric CO_2 consumption (e.g. Edmond and Huh, 1997; Louvat and Allègre, 1997; 1998; Dessert et al., 2003; 2009). Since the weathering of all silicic minerals in carbonic acid produces bicarbonate, the bicarbonate in a given river may be charge balanced by any of the major cations (Na, K, Ca, Mg). The alkali metals do not participate in the formation of stable carbonate minerals in the oceans,

thus the weathering of alkali silicates does not have the same long-term impact on CO₂ as does the weathering of alkaline earth silicates. Therefore the total bicarbonate flux more correctly refers to the “export” flux from the landscape to the oceans. The “export” flux does not account for the permanent removal by carbonate precipitation, where one mole CO₂ is released back to the atmosphere:



The net reaction for reactions 5.1a and 5.1c is well known and the stoichiometry is simple for Ca and Mg:



Since Na⁺ (or K⁺) is not removed from the oceans by carbonate formation, the only pathway for the alkali cations to remove CO₂ is by exchange reactions with Ca²⁺ and/or Mg⁺⁺. These processes may occur in estuarine mixing, during sediment diagenesis, and during alteration of the oceanic crust. Available data indicate that the overall efficiency of exchange of alkali metals for alkaline earths in the marine environment is modest on a global scale, but the uncertainties remain large (France-Lanord and Derry, 1997).

It is evident from equation 5.1c that ΣHCO₃⁻ is always at least twice as large as the amount of carbon that can be sequestered in the ocean. In the limiting case where all bicarbonate is balanced by Ca and Mg, a maximum of 0.5 × ΣHCO₃⁻ can be sequestered, and the proportion decreases with increased alkaline earth metal content of the water.

5.3. DESCRIPTION OF METHODS TESTED

A first step in any calculation of silicate weathering fluxes is to separate contributions from the weathering of carbonate, silicate and evaporates in mixed-lithology catchments, as well as contributions from the atmosphere (mainly sea salts, atmospheric pollutants and dust). The statistical inversion of end member elemental ratios in river solute loads was introduced by Negr el et al. (1993) as a means to accomplish this. Others have used various forms of end member mixing models to attribute solutes to the various sources (Gislason et al., 1996; Galy and France-Lanord, 1999; Schopka et al., 2011)

Once the silicate derived cation flux is extracted from the data by any of these methods, the carbon "consumption", ΦCO_2 , is found. There are several ways of determining this quantity:

- a) The most direct method is a Gran titration to directly determine the alkalinity, assuming that an overwhelming majority of the alkalinity in the solution is comprised of carbonate species.
- b) Another way of determining the alkalinity is to perform a charge balance on the solution, again assuming that the main component of alkalinity is carbonate species:

$$\Phi CO_2 = Alk = F_{HCO_3^-} = \sum (Z^+) - \sum (Z^-) \quad (5.2a)$$

where Z^+ refers to the sum of positive ions and Z^- refers to the sum of negative ions.

- c) In basins of uniformly silicate lithology (igneous and metamorphic rocks), the carbon consumption ΦCO_2 may be approximated as

$$\Phi CO_2 = F_{\Sigma(+*)} \approx F_{HCO_3^-} \quad (5.2b)$$

i.e. the bicarbonate flux is balanced by and thus equal to the cation charge derived from silicate weathering, $\Sigma(+*)$ (Edmond and Huh, 1997). This method of calculating carbon consumption has not been extensively used in the literature as far as we are aware.

d) The next method was also first proposed by Edmond and Huh (1997), for use in lithologically complex basins (containing limestones and dolomites). Citing the work of Garrels (1967) they "conservatively" (Edmond and Huh, 1997, p. 333) choose a scaling factor of 2 to go from silica fluxes to carbon consumption:

$$F_{HCO_3^-} \equiv 2 \times F_{Si} \quad (5.3)$$

Combining equations (5.2) and (5.3), we get:

$$\Phi CO_2 \approx F_{\Sigma(+*)} \equiv 2 \times F_{Si} \quad (5.4)$$

Equation (5.3) is a quick and easy way to make a rough first estimate of CO_2 consumption. It can, however, by no means be assumed that the cat:Si ratio of dissolving minerals in all silicate basins is 2 (see equation 5.4 and Tables 5.1 and 5.2). If equation (5.3) is to be employed, the scaling factor should be adjusted to reflect the lithology in question. From Tables 5.1 and 5.2, it is evident that only dissolution of pyroxenes, amphiboles and micas produces a solution with a Si: HCO_3^- close to 0.5, as is needed for the $2 \times$ Si-method to yield correct results for carbon consumption. The dissolution of feldspars, the most abundant minerals on Earth's surface (Kauffman and van Dyk, 1994), yields a solution with Si: HCO_3^- of 1-3. The lowest values are produced when Ca-plagioclase dissolves to form gibbsite. Values of 2 and 3 occur

when Na- and K-feldspars dissolve to form kaolinite and gibbsite, respectively.

Clearly, the $2 \times \text{Si}$ method will overestimate carbon consumption by a factor of 2 to 6 in regions with feldspar-rich rocks.

To sum up, we do not recommend using equation (5.3) for assessment of silicate weathering carbon fluxes. The exact weighted Alk:Si ratio produced by dissolving minerals in any basin is never fully known and any estimates would be subject to large uncertainties. A precedent for using Si to estimate fluxes of silicate weathering-derived carbon is found in Walker et al. (1981); they used dissolved Si as a proxy for the flux of silicate weathering-derived carbon to the oceans. Equation (5.3) has been employed by e.g. Lyons et al. (2005) and Goldsmith et al. (2008).

Table 5.1. Stoichiometry of congruent dissolution of olivine and pyroxene minerals, calculated in the React-module of Geochemist's Workbench 7 (Bethke, 2007). Olivine and pyroxenes dissolve to yield dissolved silica, cations and bicarbonate.

	Olivine	Pyroxene			
	Mg-olivine	Ca,Mg-px	Fe-px	Mg-px	Ca-px
	Forsterite	Diopside	Ferrosilite	Enstatite	Wollastonite
Si/Mg	0.5	2		1	
Si/Ca		2			1
Si/Na					
Si/K					
Si/HCO ₃ ⁻	0.25	0.5	0.5	0.5	0.5

The four above-mentioned methods deal with the total flux from a basin of inorganic carbon dissolved from the atmosphere and fixed in water by silicate weathering processes. For calculating atmospheric carbon consumption, it does not matter if that

Table 5.2. Stoichiometry of incongruent dissolution of feldspar, amphibole and mica minerals, calculated in the React-module of Geochemist's Workbench 7 (Bethke, 2007). These minerals dissolve to form secondary clays ('residue' in table) in addition to dissolved silica, cations and bicarbonate. We model the secondary clays as kaolinite and gibbsite. In the former case, silica is left in the clay structure, whereas in gibbsite, all silica has disappeared (i.e., weathering has proceeded farther).

Table 5.2.

	Feldspar				Amphibole				Mica			
	Ca-plag	K-fsp	Na-fsp		Ca,Mg amphibole	Ca,Mg,Na amphibole			K-mica	K,Mg-mica		
Residue	Anorthite	K-feldspar	Albite		Tremolite	Pargasite			Muscovite	Phlogopite		
	kaolinite	kaolinite	kaolinite	gibbsite	kaolinite	kaolinite	gibbsite	kaolinite	kaolinite	kaolinite	gibbsite	gibbsite
Si/Mg					1.6	0.75	1.6	0.75		0.67		1
Si/Ca	2				4	1.5	4	1.5				
Si/Na			2	3		3		3			3	3
Si/K		2	2	3					3		3	3
Si/HCO ₃ ⁻	1	2	2	3	0.57	0.23	0.57	0.23	3	0.29	3	0.43

carbon was dissolved directly into the water from the atmosphere or if it was cycled through vegetation on its way from atmosphere to weathering solution - the end result (carbon removal from the atmosphere) is the same.

Other methods take into account the fact that when calcite is precipitated, one mole of CO₂ is degassed to the atmosphere for every mole of CO₂ that is incorporated into a calcite molecule (see eq. 5.1c). The maximum amount of carbon that can be sequestered in this process is half of the bicarbonate flux and then only if all silicate-derived alkalinity is balanced by Ca²⁺ and Mg²⁺.

Two distinct but closely related methods are used to calculate the amount of carbon that may be converted to carbonate minerals in the ocean:

$$e) \quad F_{Mg^{2+}} + F_{Ca^{2+}} = F_{HCO_3} \quad (5.5)$$

This method of calculating the sequestration of atmospheric CO₂ by silicate weathering is based on the observation that Ca and Mg form carbonates in the ocean that permanently remove CO₂ from the atmosphere-ocean system (see Berner et al., 1983 and references therein). It has been used by e.g. Wolff-Boenisch et al. (2009).

4) France-Lanord and Derry (1997) calculated the long term sequestration flux from the silicate derived cation fluxes as

$$\Delta CO_2 = \Delta Mg + \Delta Ca + 0.15 \times \Delta Na + 0.1 \times \Delta K \quad (5.6)$$

This equation measures the amount of carbon that can be sequestered into carbonate sediments on the seafloor. It assumes a 100% efficiency of the Mg > Ca ion exchange process in the oceanic crust. The coefficients for Na and K were introduced to account

for the indirect effect of alkali fluxes to the oceans on carbonate formation, where about 30% of Na and 20% of K in stream water are exchanged for Ca in ion exchange processes in estuaries (and in shallow buried sediments). It also assumes that 100% of Ca in the ocean is eventually removed from the ocean via carbonate sedimentation and it takes into account the amount of CO₂ degassed upon precipitation of calcite. This method has been used by workers including Evans et al. (2004; 2008) and Schopka et al. (2011).

In the limiting case that the alkalinity flux contains only Ca²⁺ and Mg²⁺ equation 5.6 reduces to equation 5.5, which describes an upper limit on long-term atmospheric CO₂ consumption by silicate weathering in a given system, if reactions involving the sulfur cycle are not considered. The upper limit is caused by the fact that for every mole of Ca or Mg precipitated as carbonate, one mole of C is precipitated and another mole of C is degassed as CO₂.

It is therefore theoretically impossible to remove into long-term sequestration more than half of the carbon "consumed" during silicate weathering. Not all the literature on the subject of silicate weathering carbon uptake is clear on this point. We propose that the term **weathering carbon export flux (WCEF, ΦCO_2)** be used to describe river output (i.e., the total silicate-derived alkalinity flux, found by Gran titration or equation (5.2a)) and that the term **weathering carbon sequestration flux (WCSF, ΔCO_2)** be reserved for estimates of the long-term removal of CO₂, including the carbonate sedimentation step (i.e., equation 5.6). This small but important change in the use of terminology would help clarify the issue and make comparison between different studies more reliable.

5.4. CASE STUDIES

We assembled data from a number of published studies of river geochemistry in silicate watersheds and re-calculated values for carbon consumption and sequestration based on the methods presented in the preceding section. Alkalinity (calculated as $F_{2 \times Si}$) and carbon sequestration (i.e., WCSF) fluxes are presented as a function of WCEF, or the carbon export flux.

Quite a few studies of weathering in volcanic basins measure and report all the parameters (average annual discharge, basin area, HCO_3^- , Ca^{2+} , Mg^{2+} , Na^+ , K^+ , Si) needed for a thorough comparison of these methods. Finding studies of silicic but non-volcanic regions where all these parameters were available was not as easy, with the exception of the study of Lyons et al. (2005). Importantly, most weathering studies of non-volcanic bedrock include basins heavily influenced by carbonate and/or evaporite dissolution and it is beyond the scope of this study to do all the corrections necessary to separate the solutes from non-silicate weathering from the dissolved load. We use data from volcanic regions and ophiolites in the Philippines (Schopka et al., 2011), basaltic watersheds in Hawai'i (this dissertation, Chapter 4) and Iceland (Gislason et al., 1996) and rhyolite/tephra regions from Lyons et al. (2005). In the absence of appropriate data from monolithologic silicic but non-volcanic watersheds, we use data from Karelia and the Kola Peninsula (granites and gneisses, syenites, sandstones and conglomerates, minor volcanics) (Zakharova et al., 2007) and from greywacke/argillite watersheds reported by Lyons et al. (2005) to demonstrate the impact of lithology on the different methods of calculating carbon fluxes.

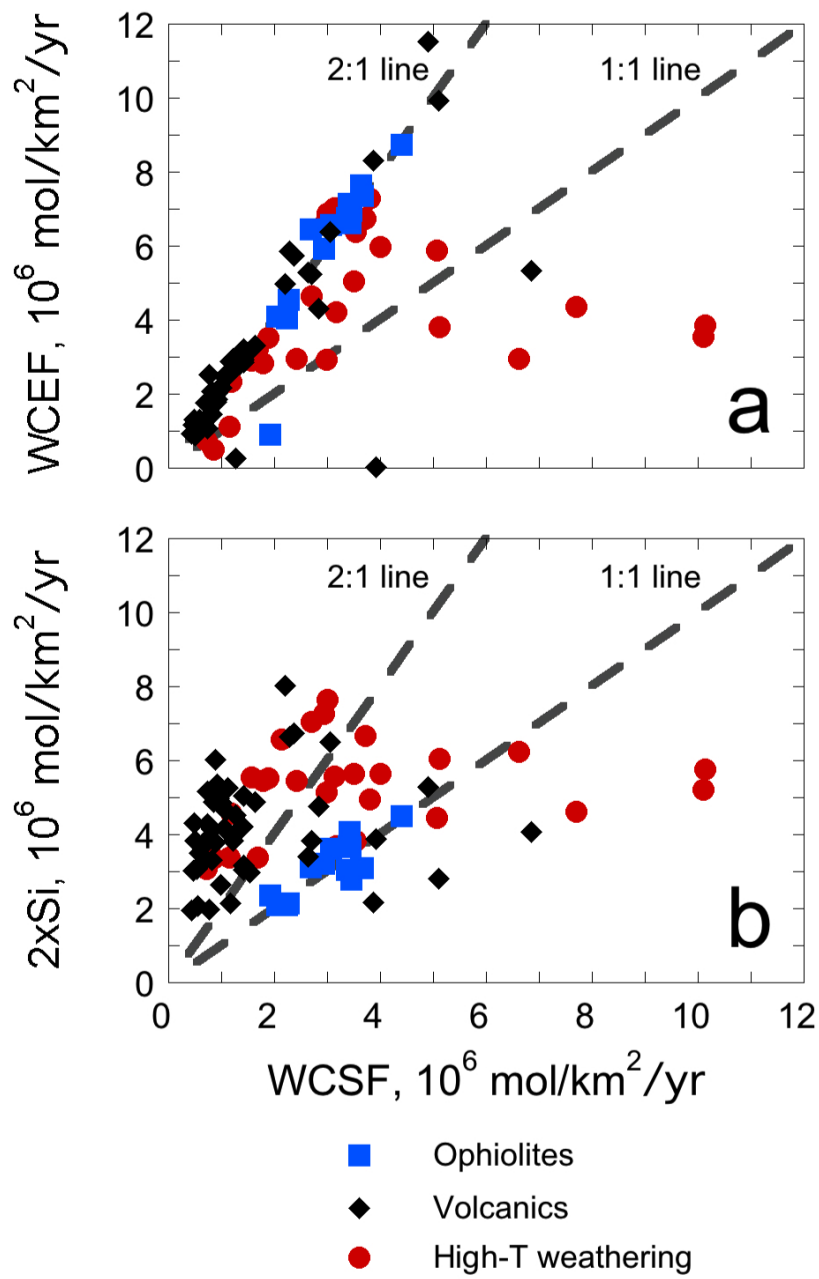
5.4.1. Arc volcanics and ophiolites - Philippines

WCEF and WCSF exhibit a very good correlation in both volcanic and ultramafic regions in the Philippines (Figure 5.1a). The slope of the regression is close to 2, as is expected based on the high Ca- and Mg- content of the rocks. The ophiolitic rocks we studied in the Philippines are largely composed of peridotites comprising ~75% Fo_{90} and ~24% pyroxene (Evans and Hawkins Jr., 1989). The Si:Mg-ratio of olivine, the main constituent of ultramafic rocks, ranges from 0.5 (Fo_{100}) through ~1 ($\text{Fo}_{50}\text{Fa}_{50}$) to infinity in Fa_{100} ; Si:Mg and Si:Ca in pyroxene ranges from 1-3. This yields a weighted average Si:(Ca, Mg) in ophiolitic rocks of 0.7-1.2 and accordingly, the 2xSi-method works fairly well for predicting WCSF in ophiolitic rocks (see Figure 5.1b). It systematically overestimates WCSF in volcanic regions, well in excess of a factor of 2 (see Figure 5.1b). Again, this result was expected, due to the higher abundance of Na- and K-containing minerals in volcanic rocks compared to ophiolitic rocks.

Streams impacted by hydrothermal activity behave very differently from other streams. First, they tend to have much lower WCEF and 2xSi than would be expected in non-hydrothermal streams with a similar WCSF (Figure 5.1a and 5.1b). The low WCEF, or alkalinity, is caused by charge balance in the water being achieved with other anions, mainly strong acids such as Cl^- and SO_4^{2-} . The strong acids come from the hydrothermal systems and dissolve minerals without creating alkalinity. The lack of Si in the water is probably due to precipitation of amorphous silica - although there is less Si in the water than expected based on WCSF, the Si-content is still very high and precipitation may occur (Schopka et al., 2011).

In summary, the 2xSi-method gives a reasonable first estimate of WCSF for rivers draining ophiolitic rocks. It tends to either over- or underestimate WCSF significantly

Figure 5.1. Ophiolites and volcanics in the Philippines, (data from Schopka et al., 2011). All data are corrected for atmospheric inputs. The 1:1 and 2:1 lines serve as visual aids in interpretation of data. a) WCEF vs. WCSF. b) $2 \times \text{Si}$ vs. WCSF.



for volcanic streams. WCEF appears to be relatively insensitive to rock type in our study sites in the Philippines, overestimating the WCSF consistently by a factor of 2 or more for both ophiolites and volcanic rocks. Both $2xSi$ and WCEF are very poor predictors of WCSF in streams that receive additions of hydrothermal fluids, for reasons explained above.

5.4.2. OIB and MORB - Hawai'i and Iceland

In general, a good correlation is observed between WCEF and WCSF in both Hawai'i and Iceland (Figure 5.2a). Like in the Philippines, the slope of the regression is close to 2:1 and again, this is due to the high Ca- and Mg- content of the rocks. In Iceland, the WCEF tends to overestimate the WCSF by a factor of slightly more than 2, indicating that Icelandic streams are proportionally richer in alkali metals than are Hawaiian streams. The $2\times Si$ -method (Figure 5.2b) overestimates WCSF in all cases in both regions. The magnitude of the overestimate is variable with an average of around 3 times.

5.4.3. Felsic volcanics, greywacke, argillite and other mixed silicic rocks - New Zealand and Russia

Moving away from high-Ca and high-Mg rocks, we now investigate felsic volcanics and mixed silicic rocks that may contain some carbonates (Figure 5.3) (Lyons et al., 2005). In the case of greywacke/argillite (GA), we find a reasonably good correlation between WCEF and WCSF, with a slope of ~ 1.7 (Figure 5.3a). In basins where atmospheric CO_2 is the only acid dissolving silicate rocks, the WCEF/WCSF will never be less than 2. We interpret the WCEF/WCSF of 1.7 to indicate the presence of other acids, such as sulfuric acid derived from oxidation of pyrite, supplying protons

Figure 5.2. Hawai'i and Iceland, volcanic rocks only (data from Chapter 4, this dissertation and Gislason et al., 1996). All data are corrected for atmospheric inputs.

a) WCEF vs. WCSF. b) $2 \times \text{Si}$ vs. WCSF.

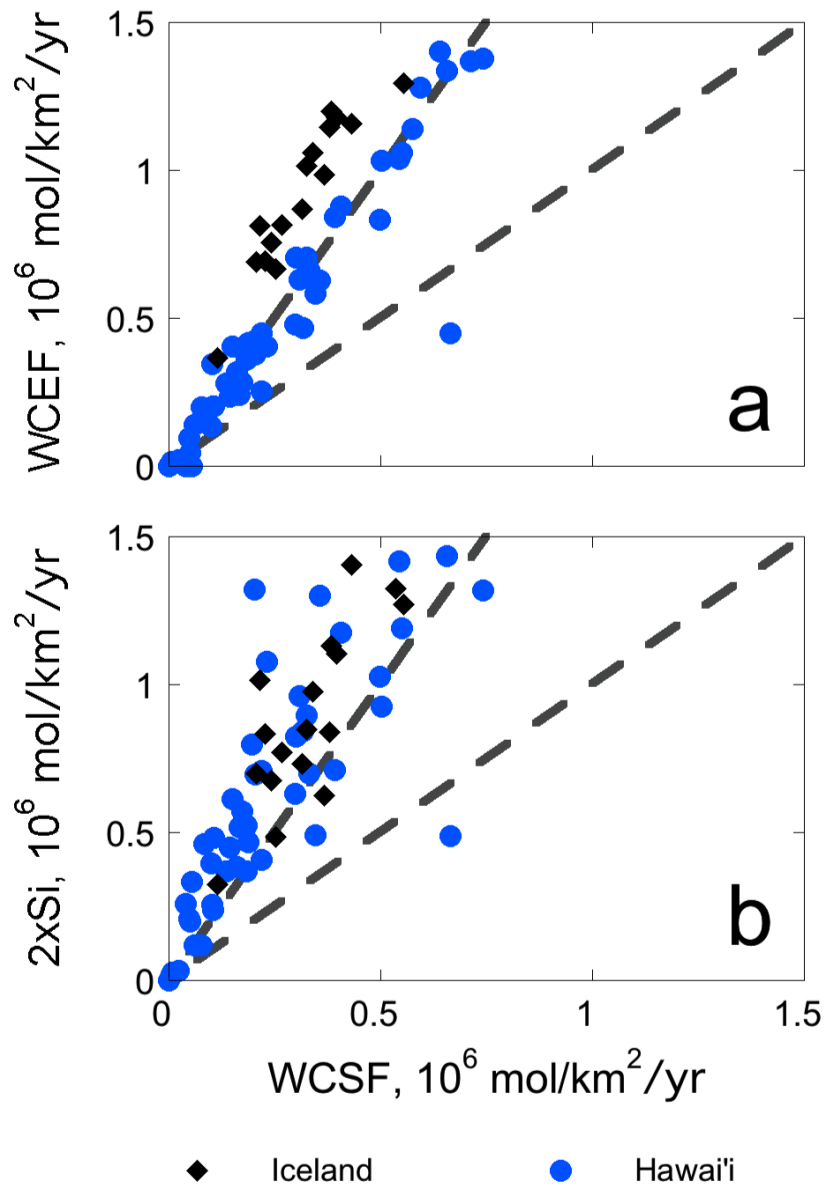
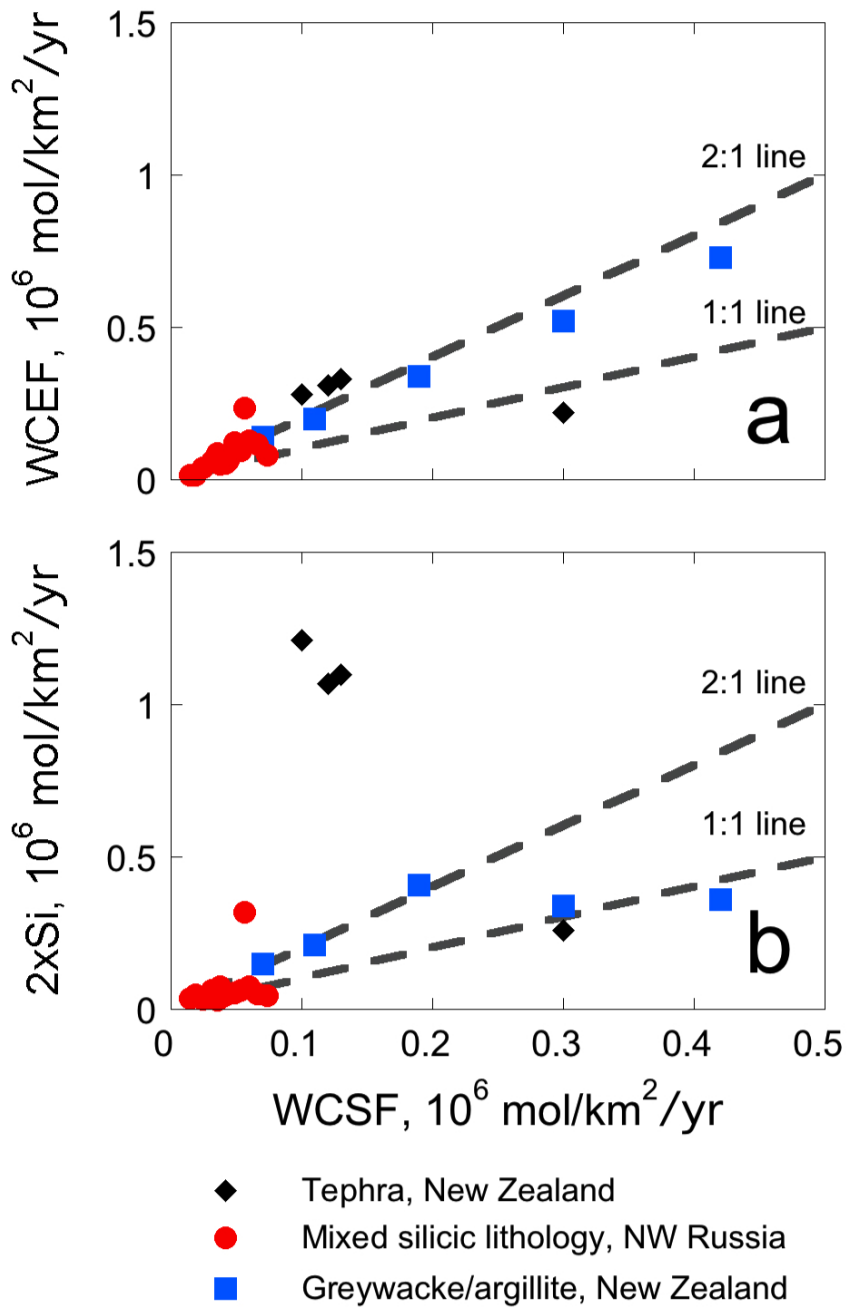


Figure 5.3. Data from New Zealand are from (Lyons et al., 2005) and include watersheds underlain by greywacke /argillite (GA) and tephra/rhyolite (T). These data are not corrected for atmospheric, carbonate or evaporite additions. Data for "mixed silicic" watersheds (see text for composition) are from Zakharova et al. (2007) and were corrected for cyclic salts by the present authors.



for the breakdown of silicate minerals. The $2 \times \text{Si}$ -method is unreliable as a proxy for WCSF, remaining essentially constant across the whole range of WCSF-values in GA rocks (Figure 5.3b). This may tell of high Ca- and Mg-contents in the GA, or of the presence of carbonates whose dissolution dominates the cation composition of the rivers.

The "mixed silicic" watersheds of Figure 5.3 (Zakharova et al., 2007) are composed of granites and gneisses of Archaean age, basalts and volcanic rocks (2.5–2.0 Ga), alkaline rocks of Khibiny massif (nepheline or K-feldspar syenites (371–365 Ma)) and sedimentary rocks (Neoproterozoic sandstones and conglomerates (900–1050 Ma)). Chemical fluxes from watersheds underlain by mixed silicic rocks (Zakharova et al., 2007) are very low in general. Since calculation of WCSF requires data for Na and K- fluxes in units of moles and the alkali metals are given as aggregate ([Na]+[K] in ppm) in (Zakharova et al., 2007), [Na]+[K] were converted to molar units using the average molecular weight of the two elements. WCSF was calculated using that quantity $\times 0.10$ instead of the usual alkali metal treatment in WCSF. The WCSF of these mixed silicate lithology basins should therefore be interpreted with caution. Ca and Mg (but not the alkali metals) were corrected for atmospheric deposition using X/Cl -ratios for sea salt (using data on sea-salt composition from Schlesinger, 1997) assuming all Cl^- comes from precipitation.

Excluding data from the Malaya Belaya, which is a clear outlier, a fair correlation (slope 1.7, $r^2 = 0.67$) between WCEF and WCSF emerges (but, see caution regarding calculation of WCSF above) (Figure 5.3a). As above, we interpret this low WCEF/WCSF to indicate the presence of acids other than carbonic acid in the water.

There is no correlation at all between $2\times\text{Si}$ and WCSF (Figure 5.3b). Interestingly, this is the same trend as we observed in the GA basins above. We therefore assume that carbonates contribute a significant amount of cations to the dissolved load in the mixed silicic basins, most likely from veins of carbonate in the sedimentary rocks.

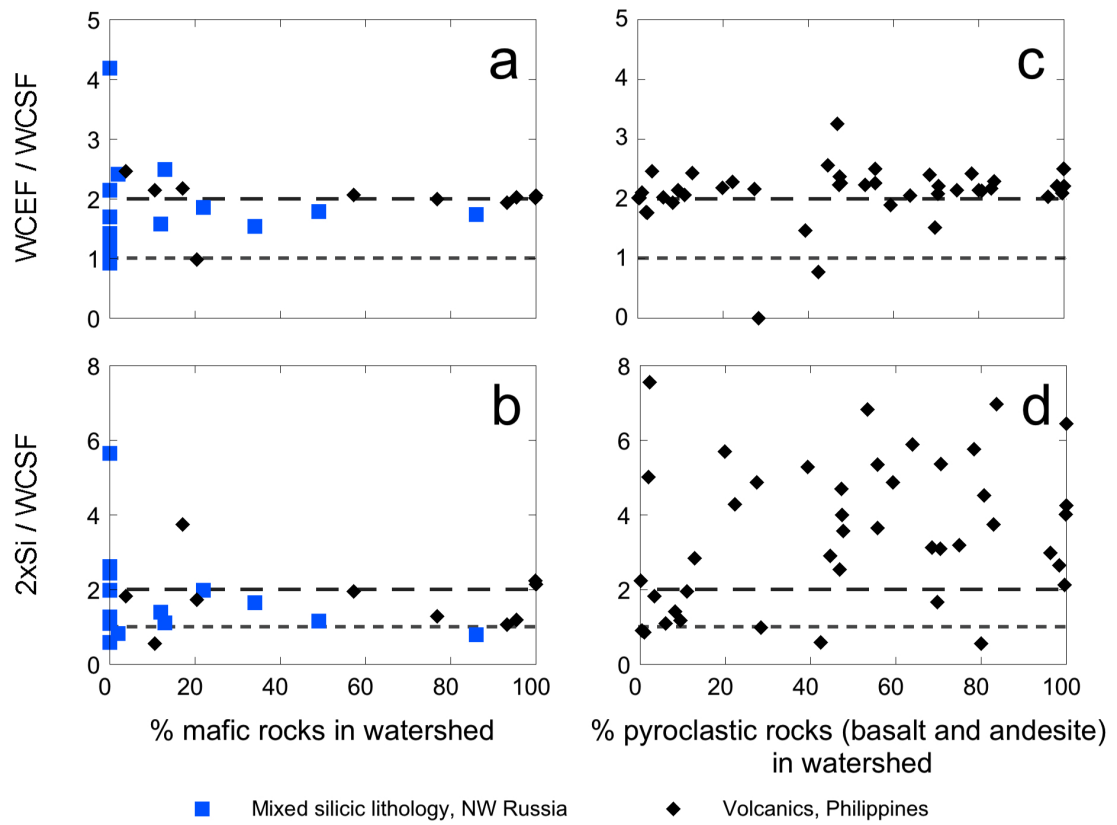
In felsic (alkali metal rich) volcanic rocks (T in Figure 5.3) (Lyons et al., 2005), $2\times\text{Si}$ clearly hugely overestimates both WCSF and WCEF (Figure 5.3a and b). WCEF is roughly 2.5 times higher than WCSF, testifying to a significant contribution of alkali metals to the cation charge in water draining felsic rocks. In these lithologies, using the WCEF as a measure of long-term carbon sequestration potential overestimates that potential by 2-3 times and using $2\times\text{Si}$ as a proxy overshoots it by approximately an order of magnitude.

5.4.4. The impact of lithology

A useful way of looking at the different flux metrics is to normalize them to WCSF, i.e. the sequestration flux of France-Lanord and Derry (1997) (Figure 5.4). As explained earlier, we assert that this metric is currently the best one available for quantifying the expected long-term sequestration of CO_2 via chemical weathering of silicate rocks. Normalizing other flux metrics to that one reveals to what extent these other metrics over- or underestimate long-term carbon sequestration.

In their study of weathering fluxes from silicic basins in western Russia, Zakharova et al. (2007) report the fraction of basic rocks in each watershed. A plot of WCSF-normalized fluxes vs. %(basic rocks) in a watershed reveals that as the proportion of basic rocks in the watershed increases, the ability of both WCEF (Figure 5.4a) and

Figure 5.4. WCEF and $2\times\text{Si}$ normalized to WCSF, plotted as a function of the percentage of different lithologies in watershed. a) WCEF/WCSF vs. % mafic rocks. b) $2\times\text{Si}/\text{WCSF}$ vs. % mafic rocks. c) WCEF/WCSF vs. % pyroclastics in watershed. d) $2\times\text{Si}/\text{WCSF}$ vs. % pyroclastics in watershed. Streams in the Karelia and Kola regions of Russia (blue squares) drain mixed silicic lithologies (see text for composition) (Zakharova et al., 2007). Streams draining mafic rocks in the Philippines (black diamonds) (Schopka et al., 2011 and Chapter 2, this dissertation).



$2\times\text{Si}$ (Figure 5.4b) to predict WCSF becomes better constrained. At low proportions of basaltic rocks in a silicate basin, WCEF and $2\times\text{Si}$ may or may not perform well as predictors of WCSF; at high proportions of basic rocks in a silicate basin, WCEF and $2\times\text{Si}$ are likely to perform relatively well and predictably as predictors of WCSF.

A similar story emerges from data from the Philippines. As the percentage of basic material in the basin (the remaining bedrock in each basin is mostly silicic, although not necessarily volcanic) increases, the ability of both WCEF and $2\times\text{Si}$ to predict WCSF improves (Figure 5.4a and b).

A plot of WCSF-normalized fluxes vs. proportion of basic and andesitic pyroclastic rocks shows no trend at all for either WCEF/WCSF (Figure 5.4c) or $2\times\text{Si}$ /WCSF (Figure 5.4d), clearly showing why silica is a very poor proxy for carbon sequestration in silicic and/or pyroclastic terranes. WCEF/WCSF remains nearly constant with varying proportions of basic and andesitic pyroclastic rocks in a watershed, indicating that WCEF's ability to predict WCSF is invariant in basaltic and andesitic regions in the Philippines.

5.5. RESULTS AND DISCUSSION

5.5.1. The $2\times\text{Si}$ -method of Edmond and Huh (1997)

We have shown that the $2\times\text{Si}$ -method (Edmond and Huh, 1997) is an unreliable proxy for both weathering export fluxes (WCEF) and weathering sequestration fluxes (WCSF) of carbon from most volcanic watersheds (Figures 5.1 and 5.2) where it tends to either over- or underestimate WCSF significantly. The largest deviation from WCSF is observed in felsic volcanic rocks in New Zealand (Lyons et al., 2005), where

$2\times\text{Si}$ overestimates WCSF by an order of magnitude ("T" in Figure 5.3). Silica fluxes do, however, provide a reasonable first estimate of WCSF for rivers draining ophiolitic rocks.

In non-volcanic rocks there is no correlation between $2\times\text{Si}$ -fluxes and WCSF (Figure 5.3, GA and "mixed silicic"). This is interpreted as an effect of the presence of carbonates that add Ca and Mg to the water without any accompanying addition of Si.

5.5.2. Weathering carbon export flux (WCEF)

As explained above, when silicate weathering proceeds through the action of only carbonic acid, WCEF is always at least two times larger than WCSF. In the case where only Ca- and Mg-silicates are being weathered, $\text{WCEF}/\text{WCSF} = 2$, and it increases from there with increased content of alkali silicates. Since the fluxes of alkali metals are scaled down by a factor of 0.1 (K) and 0.15 (Na) in calculations of WCSF, a relatively large addition of alkali metals is required for the ratio of WCEF/WCSF to go much above 2. This is evident in the mafic to intermediate volcanic terranes of the Philippines (Figure 5.1) and Hawai'i (Figure 5.2) where streams plot on or very close to the 2:1 line on plots of WCEF vs. WCSF.

A different story emerges in the felsic volcanic rocks shown in Figure 5.3 (Lyons et al., 2005). The large contribution of alkali metals to the weathering flux elevates the WCEF significantly, resulting in a WCEF/WCSF of ~ 2.5 . Using WCEF as a measure of the long-term CO_2 -drawdown potential due to weathering in these lithologies would thus result in an overestimate of WCSF of up to 2.5 times.

Comparisons of WCEF and WCSF in the mixed silicic lithologies of Figure 5.3 (Zakharova et al., 2007) is complicated by our inability to correctly compute WCSF (see Chapter 5.4.3.). Nonetheless, the correlation observed between WCEF and WCSF in the mixed silicic lithologies is good and has a slope of 1.7. The same ratio of WCEF/WCSF is observed in the GA lithology of Lyons et al. (2005) (Figure 5.3). The low WCEF/WCSF ratio indicates that some acid in addition to carbonic acid is dissolving silicate rocks, probably sulfuric acid from the oxidation of pyrite.

5.6. CONCLUSIONS

In this chapter, we have highlighted the need for a greater awareness among workers in the field of silicate weathering of the metrics used to quantify the impact of silicate weathering on atmospheric CO₂-levels. We argue that a more explicit treatment of carbon fluxes via silicate weathering is needed in order to facilitate comparison between studies. Currently, workers often do not distinguish sufficiently between the export flux (short-term uptake) and the sequestration flux (long-term uptake) potential of the silicate weathering environment, resulting in published estimates of carbon uptake that greatly exceed the actual potential sequestration.

We critically assessed three metrics commonly used in the silicate weathering community for quantifying the carbon uptake. A major result of this assessment is that silica fluxes are a very poor predictor of carbon uptake via silicate weathering in all environments except for possibly in ophiolites. WCEF, i.e. export flux of carbon via silicate weathering, is relatively insensitive to the exact composition of volcanic rocks and ranges from 2-3x higher than WCSF. In mixed silicic rocks it is often lower than 2, indicating the input of strong acids into the weathering environment.

We recommend that the silicate weathering community of scholars adopt the metrics proposed in this chapter, namely **weathering carbon export flux (WCEF, ΦCO_2)** (equation 5.2a) and **weathering carbon sequestration flux (WCSF, ΔCO_2)** (equation 5.6). This small but important change in how carbon fluxes via weathering are calculated and reported would greatly enhance the usefulness of such studies and make comparison between different studies significantly easier and more reliable.

References

- Berner R.A. (2004) *The Phanerozoic Carbon Cycle*. 1st ed. Oxford University Press.
- Berner R.A., Lasaga A.C. and Garrels R.M. (1983) The carbonate-silicate geochemical cycle and its effect on atmospheric carbon dioxide over the past 100 million years. *Am J Sci* **283**, 641-683.
- Bethke C. (2007) *The Geochemist's Workbench*. Hydrogeology Program, University of Illinois.
- Dessert C., Dupre B., Gaillardet J., Francois L.M. and Allegre C.J. (2003) Basalt weathering laws and the impact of basalt weathering on the global carbon cycle. *Chemical Geology* **202**, 257-273.
- Dessert C., Gaillardet J., Dupre B., Schott J. and Pokrovsky O.S. (2009) Fluxes of high- versus low-temperature water-rock interactions in aerial volcanic areas: Example from the Kamchatka Peninsula, Russia. *Geochimica et Cosmochimica Acta* **73**, 148-169.
- Edmond J.M. and Huh Y. (1997) Chemical Weathering Yields from Basement and Orogenic Terrains in Hot and Cold Climates. In: *Tectonic uplift and climate change*. New York, Plenum Press, 330-351.
- Evans C. and Hawkins Jr. J.W. (1989) Compositional heterogeneities in upper mantle peridotites from the Zambales Range Ophiolite, Luzon, Philippines. *Tectonophysics* **168**, 23-41.
- Evans M.J., Derry L.A. and France-Lanord C. (2004) Geothermal fluxes of alkalinity in the Narayani river system of central Nepal. *Geochemistry Geophysics Geosystems* **5**, Q08011.
- Evans M.J., Derry L.A. and France-Lanord C. (2008) Degassing of metamorphic carbon dioxide from the Nepal Himalaya. *Geochemistry Geophysics Geosystems* **9**, Q04021.

- France-Lanord C. and Derry L.A. (1997) Organic carbon burial forcing of the carbon cycle from Himalayan erosion. *Nature* **390**, 65-67.
- Gaillardet J., Dupre B., Louvat P. and Allegre C.J. (1999) Global silicate weathering and CO₂ consumption rates deduced from the chemistry of large rivers. *Chemical Geology* **159**, 3-30.
- Galy A. and France-Lanord C. (1999) Weathering processes in the Ganges-Brahmaputra basin and the riverine alkalinity budget. *Chemical Geology* **159**, 31-60.
- Garrels R.M. (1967) Genesis of some groundwaters from igneous rocks. In: *Researches in geochemistry*. New York, John Wiley & Sons Inc, 405-420.
- Gislason S.R., Arnorsson S. and Armannsson H. (1996) Chemical weathering of basalt in Southwest Iceland; effects of runoff, age of rocks and vegetative/glacial cover. *American Journal of Science* **296**, 837-907.
- Goldsmith S.T., Carey A.E., Lyons W.B. and Hicks D.M. (2008) Geochemical fluxes and weathering of volcanic terrains on high standing islands: Taranaki and Manawatu-Wanganui regions of New Zealand. *Geochimica et Cosmochimica Acta* **72**, 2248-2267.
- Hartmann J. (2009) Bicarbonate-fluxes and CO₂-consumption by chemical weathering on the Japanese Archipelago -- Application of a multi-lithological model framework. *Chemical Geology* **265**, 237-271.
- Hren M.T., Chamberlain C.P., Hilley G.E., Blisniuk P.M. and Bookhagen B. (2007) Major ion chemistry of the Yarlung Tsangpo-Brahmaputra river: Chemical weathering, erosion, and CO₂ consumption in the southern Tibetan plateau and eastern syntaxis of the Himalaya. *Geochimica et Cosmochimica Acta* **71**, 2907-2935.
- Kauffman R. and van Dyk D. (1994) Feldspars. In: D. Carr ed. *Industrial minerals and rocks*. Littleton Colo., Society for Mining Metallurgy and Exploration.

- Louvat P. and Allègre C.J. (1997) Present denudation rates on the island of Réunion determined by river geochemistry: Basalt weathering and mass budget between chemical and mechanical erosions. *Geochimica et Cosmochimica Acta* **61**, 3645-3669.
- Louvat P. and Allègre C.J. (1998) Riverine erosion rates on Sao Miguel volcanic island, Azores archipelago. *Chemical Geology* **148**, 177-200.
- Lyons W.B., Carey A.E., Hicks D.M. and Nezat C.A. (2005) Chemical weathering in high-sediment-yielding watersheds, New Zealand. *Journal of Geophysical Research-Earth Surface* **110**, F01008.
- Négrel P., Allègre C.J., Dupré B. and Lewin E. (1993) Erosion sources determined by inversion of major and trace element ratios and strontium isotopic ratios in river water: The Congo Basin case. *Earth and Planetary Science Letters* **120**, 59-76.
- Schlesinger W. (1997) *Biogeochemistry: An Analysis of Global Change, 2nd edition*. San Diego, Calif., Academic Press.
- Schopka H.H., Derry L.A. and Arcilla C. (2011) Chemical weathering, river geochemistry and atmospheric carbon fluxes from volcanic and ultramafic regions on Luzon Island, the Philippines. *Geochimica et Cosmochimica Acta* **75**, 978-1002.
- Walker J.C.G., Hays P.B. and Kasting J.F. (1981) A negative feedback mechanism for the long-term stabilization of Earth's surface temperature. *Journal of Geophysical Research* **86** (C10), 9776-9782.
- Wolff-Boenisch D., Gabet E.J., Burbank D.W., Langner H. and Putkonen J. (2009) Spatial variations in chemical weathering and CO₂ consumption in Nepalese High Himalayan catchments during the monsoon season. *Geochimica et Cosmochimica Acta* **73** (11), 3148-3170.
- Zakharova E., Pokrovsky O.S., Dupre B., Gaillardet J. and Efimova L. (2007) Chemical weathering of silicate rocks in Karelia region and Kola peninsula, NW Russia: Assessing the effect of rock composition, wetlands and vegetation. *Chemical Geology* **242** (1-2), 255-277.

APPENDICES

Appendix 2.1. Sensitivity analysis for solute source allocations

To estimate the impact of variability in chemical ratios used to calculate sources of solutes (see Chapter 2.4.3, “Sources of solutes”), a sensitivity analysis was performed. The range of plausible values for element ratios in the relevant end-members (rainfall, hydrothermal fluids representative of high-temperature weathering) and the range of possible values for [Cl⁻] in rainfall were identified from literature data. Twenty-seven scenarios were constructed from all possible combinations of smallest, average and highest values for the three variables (element ratios in rainfall, element ratios in hydrothermal fluids and Cl-content of rainfall). For each scenario, the percentage contribution of each source (precipitation, high-temperature weathering and low-temperature weathering) was calculated for each stream. These values were then aggregated into an average (volcanic vs. ophiolite streams) percent contribution from each source for each solute within each scenario. Finally, the average percent contributions of each source to each solute from each of the 27 scenarios were compiled and the CV calculated for all solutes and sources. The results are discussed in terms of CV, to emphasize not the absolute average percentage of a given solute deriving from a given source but to emphasize the variability of the possible results as a function of differences in input parameters.

Depending on what Cl-concentration is assumed for rainfall, the number of streams that have modeled contribution of high-T weathering products increases from 24 through 29 to 40, out of 65 streams in volcanic regions.

The percent contribution of precipitation to the solute load, especially to K-contents, is

more sensitive to changes in the input parameters than either high-T weathering or low-T weathering. The average contribution of rainfall to the solute load in volcanic regions is 27% of Na, 10% of K, 6% of Mg and 1% of Ca. The CV of %Ca and %K in volcanic regions is high, around 70%, but since the contribution of rainfall to both K and especially Ca is small, the large CV does not impact weathering flux calculations significantly. In ophiolites, a significant fraction of both Na and K are derived from precipitation (average of 33% for Na and 41% for K) whereas Ca and Mg are overwhelmingly sourced from low-T weathering. The variability in %Na from rainfall in ophiolites is small, around 10%, whereas the variability in %K from rainfall is around 50%. K constitutes a very small part of the cation flux in ophiolites and the high CV leads to trivial differences in the allocation of solutes to low-T weathering in ophiolites. %Ca from rainfall in ophiolites is even higher, 70%, but in general, Ca is only to a small degree sourced from rainfall and just like with K, the high CV results in a trivial impact on low-T weathering fluxes from ophiolites.

In volcanic regions, the CV of contribution of low-temperature weathering products to the total cation load is modest for Na and K (6 and 10%, respectively) and very low for Ca and Mg (2%). This indicates that our results for low-T weathering fluxes are very robust and insensitive to the choice of input parameters when solutes are allocated to sources. A similar result is obtained for ophiolites, where the CV of low-T weathering products to the total cation load is >1% for Ca and Mg, 5% for Na and 35% for K. Since K is hardly present in ophiolite waters and the high CV for %K from low-T weathering is therefore of trivial importance.

High-temperature is assumed to only occur in volcanic regions. CV of the average contribution of high-T fluids to the total cation chemical flux is on the order of 20%

(16% for K and Na, 20% for Ca and 22% for Mg). The contribution of high-T fluids to the total cation load of volcanic streams ranges from an average of 8% for Na to an average of 16% for K, and a CV of 20% thus has only a minor impact on the overall calculated high-T contribution to weathering in the Philippines.

Overall, these results suggest that our conclusions about low-temperature weathering fluxes from our study region are reasonably insensitive to variability in the magnitude of key parameters used to allocate solutes to their sources. The main exception is K, which is mainly sensitive to variations in K/Cl in rainfall. K is a minor component of river waters in ophiolite regions and constitutes on average less than 10% of the cation load of rivers in volcanic regions; the high sensitivity of this solute to model parameters is therefore of little consequence for our results of low-T weathering fluxes. The same may be said for high-temperature weathering, which is included in the final silicate weathering flux in this paper.

Table A2.1: Chemical composition of representative volcanic rocks on Luzon

Location	Sample	SiO ₂	TiO ₂	Al ₂ O ₃	FeO*	MnO	MgO	CaO	Na ₂ O	K ₂ O	P ₂ O ₅	Total	Rock type	Source
Bicol Volcanic Arc														
Mt. Malinao	CW02	58.33	0.64	17.76	2.73	0.12	3.17	5.95	3.45	2.27	0.23	98.99	Andesite	a
Mt. Malinao	CW22	51.83	0.97	19.42	4.17	0.15	5.02	9.28	2.94	1.43	0.25	100.04	Basalt	a
Mayon	1885-1887	51.95	0.61	19.05	8.69	0.16	4.6	9.52	3.42	1.01		99.01	Basalt	b
Mayon	1814	54.45	0.82	18.03	8.83	0.19	4.1	8.38	3.44	1.02	0.29	99.54	Basaltic andesite	b
Luzon Volcanic Arc														
Mt. Arayat	168	47.80	0.98	13.71	10.92	0.18	11.27	11.15	2.27	1.01	0.35	99.60	Basalt	c
Taal	T1	50.88	0.72	17.3	9.54 [#]	0.17	5.81	10.7	2.6	0.9	0.14	89.22	Basalt	d
Pinatubo	P17	55.11	1.17	17.46	8.76 [#]	0.15	7.15	10.23	3.48	0.92	0.21	95.88	Basaltic andesite	d
Taal	T2	55.57	0.89	17.45	9.46 [#]	0.18	4.61	9.01	3.44	1.41	0.22	92.78	Basaltic andesite	d
Pinatubo	7-1-91-1a	59.2	0.64	16.1	6.13 [#]	0.12	4.86	7.17	3.91	1.56	0.28	100	Andesite scoria	e
Pinatubo	PIN1-3	64.2	0.48	15.6	4.43 [#]	0.11	2.49	5.2	4.64	1.56	0.16	100	Dacite pumice	e
Pinatubo	P18	64.31	0.66	16.9	5.71 [#]	0.13	4.04	6.08	4.51	1.48	0.18	98.29	Dacite	d
Taal	T3	65.09	0.63	15.87	6.06 [#]	0.12	1.62	4.34	4.18	2.91	0.21	94.97	Dacite	d
Pinatubo	P20b	73.75	0.53	19.43	4.39 [#]	0.1	2.38	5.45	4.93	1.57	0.18	108.32	Rhyolite	d
Zambales Ophiolite														
Subic-Olongapo	Zo2	50.85	0.62	11.55	10.44 [#]	0.17	8.85	11.98	2.04	2.34	0.36	99.2	Basalt	f
Subic-Olongapo	SBFZ62	47.14	0.4	13.87	13.06 [#]	0.29	9.85	12.62	1.39	0.03	0.04	98.69	Diabase	f

#: Total iron as Fe₂O₃

Sources: a- Knittel-Weber and Knittel, 1990; b - Castillo and Newhall, 2004; c - Defant et al., 1989; d - DuFrane et al., 2006; e - Pallister et al., 1992;

f - Yumul et al., 2000.

Table A2.2: Sr-isotope composition of volcanic rocks on Luzon.

Location	Sample	$^{87}\text{Sr}/^{86}\text{Sr} \pm 2\sigma$	Source
Bicol Volcanic Arc			
Mayon	1814	0.703771 ± 9	Castillo and Newhall 2004
Mayon	1881–1882	0.703797 ± 8	Castillo and Newhall 2004
Mayon	1938	0.703783 ± 14	Castillo and Newhall 2004
Mayon	1993	0.703779 ± 17	Castillo and Newhall 2004
Mayon	Q8	0.703829 ± 9	Castillo and Newhall 2004
Mayon	SD38	0.703826 ± 9	Castillo and Newhall 2004
Mayon	SV35	0.703696 ± 15	Castillo and Newhall 2004
Mayon	Mi39	0.703807 ± 21	Castillo and Newhall 2004
Mayon	An4	0.70372 ± 14	Castillo and Newhall 2004
Mayon	SD39	0.703713 ± 14	Castillo and Newhall 2004
Mayon	Lignon1	0.703799 ± 9	Castillo and Newhall 2004
Mayon	Pac8	0.703779 ± 12	Castillo and Newhall 2004
Sharp Peak	B-107B	0.70375	McDermott et al., 2005
Irosin Ignimbrite	B-1B	0.7039	McDermott et al., 2005
Bintacan	B-148	0.70385	McDermott et al., 2005
Gate	B-220	0.70399	McDermott et al., 2005
Gate	90-10	0.70387	McDermott et al., 2005
Bulusan	B9	0.703934 ± 15	DuFrane et al., 2006
Bulusan	B10	0.703913 ± 15	DuFrane et al., 2006
Bulusan	B11	0.703976 ± 11	DuFrane et al., 2006
Iriga	I12	0.703680 ± 14	DuFrane et al., 2006
Iriga	I13	0.703753 ± 13	DuFrane et al., 2006
Iriga	I14	0.703753 ± 13	DuFrane et al., 2006
Iriga	I15	0.703751 ± 18	DuFrane et al., 2006
Luzon Volcanic Arc			
Taal	T1	0.704572 ± 11	DuFrane et al., 2006
Taal	T2	0.704553 ± 13	DuFrane et al., 2006
Taal	T3	0.704601 ± 15	DuFrane et al., 2006
Taal	T4	0.70449 ± 10	DuFrane et al., 2006
Taal	T5	0.704521 ± 11	DuFrane et al., 2006
Taal	BAL1f	0.704590 ± 40	DuFrane et al., 2006
Taal	BM8	0.704580 ± 40	DuFrane et al., 2006
Taal	B4	0.704570 ± 20	DuFrane et al., 2006
Taal	CAL1	0.704520 ± 40	DuFrane et al., 2006
Taal	CY3	0.704580 ± 20	DuFrane et al., 2006
Taal	MB5	0.704540 ± 20	DuFrane et al., 2006
Pinatubo	P16	0.704176 ± 15	DuFrane et al., 2006
Pinatubo	P17	0.704207 ± 14	DuFrane et al., 2006
Pinatubo	P18	0.704251 ± 10	DuFrane et al., 2006
Pinatubo	P19	0.704251 ± 10	DuFrane et al., 2006
Pinatubo	P20	0.704213 ± 11	DuFrane et al., 2006
Pinatubo	P20b	0.704139 ± 14	DuFrane et al., 2006
Pinatubo	P21	0.704232 ± 12	DuFrane et al., 2006
Pinatubo	P22	0.704237 ± 11	DuFrane et al., 2006

Table A2.3. Fluxes of silicate weathering-derived major cations and Ca+Mg from individual watersheds, Luzon, Philippines

Location name	Type	Area km ²	Silicate weathering cation flux ¹						Silicate weathering Ca*+Mg* flux		
			10 ⁶ mol/km ² /yr		10 ⁶ eq/km ² /yr		t/km ² /yr		10 ⁶ mol/km ² /yr		
			low-T	high-T	Total	low-T	high-T	Total	low-T	high-T	Total
Angat Ophiolite, region ZA³											
Hanginan River	Main	10	4.09	4.09	7.41	7.41	129	129	3.31	3.31	3.31
Lacotan River	Main	7	3.98	3.98	7.31	7.31	124	124	3.32	3.32	3.32
Zambales Ophiolite, region ZA³											
Alasa River	Main	80	1.92	1.92	3.84	3.84	54	54	1.92	1.92	1.92
Bulsa River, us ²	Tributary	295	3.64	3.64	6.62	6.62	107	107	2.98	2.98	2.98
Bulsa River, ds ²	Main	442	3.65	3.65	6.47	6.47	108	108	2.81	2.81	2.81
Mababo River	Tributary	27	4.06	4.06	7.67	7.67	122	122	3.61	3.61	3.61
Cabarabuan River	Main	38	3.83	3.83	7.21	7.21	115	115	3.38	3.38	3.38
Camiling River, us	Tributary	256	3.77	3.77	7.07	7.07	110	110	3.29	3.29	3.29
Camiling River, ds	Main	298	3.96	3.96	7.54	7.54	115	115	3.58	3.58	3.58
Dumloc River	Main	38	4.95	4.95	9.25	9.25	147	147	4.30	4.30	4.30
Lawis River, us	Tributary	115	2.13	2.13	4.17	4.17	56	56	2.04	2.04	2.04
Lawis Tributary I	Tributary	21	2.31	2.31	4.56	4.56	58	58	2.26	2.26	2.26
Lawis River, ds	Main	138	2.30	2.30	4.52	4.52	59	59	2.22	2.22	2.22
Lawis Tributary II	Main	8	3.47	3.47	6.87	6.87	86	86	3.40	3.40	3.40
Masinloc River	Main	40	2.87	2.87	5.53	5.53	72	72	2.66	2.66	2.66
Bicol Volcanic Arc, region Bicol											
Bulawan River	Main	17	1.82	1.82	2.79	2.79	56	56	0.96	0.96	0.96
Dobgon River	Main	38	1.75	1.75	2.77	2.77	54	54	1.02	1.02	1.02
Guinobatan River	Main	65	4.29	0.58	7.61	0.88	18	159	3.32	0.30	3.62
Joroel River	Main	10	0.96	0.96	1.60	1.60	31	31	0.64	0.64	0.64
Kinastilohan River	Main	4	1.79	1.79	2.72	2.72	56	56	0.93	0.93	0.93
Naga River	Main	14	1.05	1.05	1.73	1.73	34	34	0.69	0.69	0.69
Naga River Tributary	Main	8	1.11	0.04	1.91	0.06	1	39	0.80	0.02	0.82
Paulog River	Main	29	2.86	0.08	4.55	0.12	2	91	1.68	0.04	1.72

Table A2.3 (continued)

Location name	Type	Area km ²	Silicate weathering cation flux ¹						Silicate weathering Ca*+Mg* flux					
			10 ⁶ mol/km ² /yr		10 ⁶ eq/km ² /yr		t/km ² /yr		10 ⁶ mol/km ² /yr					
			low-T	high-T	Total	low-T	high-T	Total	low-T	high-T	Total	low-T	high-T	Total
Pio Duran River	Main	66	5.72	5.72	10.7	10.7	180	180	180	5.00	5.00	5.00		
Quinale River	Main	86	1.38	1.38	2.22	2.22	43	43	43	0.84	0.84	0.84		
Santo Domingo River	Main	8	2.43	2.43	3.68	3.68	74	74	74	1.25	1.25	1.25		
Yawa River	Main	57	6.80	1.13	7.93	10.8	1.72	190	34	224	4.00	0.58	4.58	
Bicol Volcanic Arc, region Camarines														
Daet River	Main	69	0.77	0.77	1.27	1.27	24	24	24	0.50	0.50	0.50		
Inarihan River	Main	1	0.97	0.97	1.38	1.38	30	30	30	0.41	0.41	0.41		
Matogdon Tributary	Tributary	2	0.86	0.86	1.26	1.26	26	26	26	0.41	0.41	0.41		
Matogdon River	Main	28	1.06	1.06	1.70	1.70	33	33	33	0.65	0.65	0.65		
Pinaglabanan River	Main	12	1.90	1.90	3.07	3.07	59	59	59	1.17	1.17	1.17		
Ragay River	Main	120	1.61	1.61	2.78	2.78	54	54	54	1.17	1.17	1.17		
Rangas River	Main	18	4.52	4.52	8.34	8.34	164	164	164	3.82	3.82	3.82		
San Vicente River	Main	1	0.85	0.85	1.38	1.38	28	28	28	0.54	0.54	0.54		
Pulantuna River	Tributary	189	0.59	0.59	1.00	1.00	19	19	19	0.41	0.41	0.41		
Sipocot River	Main	487	1.12	1.12	1.84	1.84	34	34	34	0.72	0.72	0.72		
Bicol Volcanic Arc, region Sorsogon														
Bacolod River	Main	10	2.62	0.43	3.04	4.38	0.65	5.03	83	13	96	1.77	0.22	1.99
Bacon River	Main	12	1.83	1.83	3.16	3.16	59	59	59	1.34	1.34	1.34		
Bangon River	Main	24	0.27	2.37	2.64	0.27	3.27	6	64	70	0.00	0.90	0.90	
Barcelona River	Main	27	1.20	1.20	1.87	1.87	37	37	37	0.67	0.67	0.67		
Karangan Stream	Tributary	1	1.25	1.25	2.01	2.01	40	40	40	0.76	0.76	0.76		
Cadacan River, us	Tributary	34	2.32	1.06	3.38	4.04	1.60	5.64	70	32	102	1.72	0.54	2.26
Cadacan River, ds	Main	125	4.13	1.16	5.29	6.75	1.75	8.50	121	35	156	2.62	0.59	3.21
Pawa River	Main	26	0.89	0.12	1.01	1.49	0.18	1.67	28	4	32	0.60	0.06	0.66
San Bartolome River	Main	17	1.22	1.22	2.06	2.06	39	39	39	0.84	0.84	0.84		
San Francisco River	Main	23	1.37	1.37	2.18	2.18	43	43	43	0.81	0.81	0.81		

Table A2.3 (continued)

Location name	Type	Area km ²	Silicate weathering cation flux ¹						Silicate weathering Ca*+Mg* flux					
			low-T		high-T		Total	low-T		high-T		Total		
			10 ⁶ mol/km ² /yr	10 ⁶ eq/km ² /yr	10 ⁶ mol/km ² /yr	10 ⁶ eq/km ² /yr	t/km ² /yr	10 ⁶ mol/km ² /yr						
San Juan Stream	Main	5	1.35	2.23	2.23	44	44	0.88	0.88	0.88	0.88			
San Juan II Stream	Main	1	1.21	2.00	2.00	39	39	0.79	0.79	0.79	0.79			
Solinao River	Tributary	17	1.26	1.92	1.92	38	38	0.66	0.66	0.66	0.66			
San Ramon (Magsaysay) River	Main	53	1.49	2.30	2.30	46	46	0.82	0.82	0.82	0.82			
Unnamed waterfall	Main	0	0.82	1.28	1.28	27	27	0.46	0.46	0.46	0.46			
Luzon Volcanic Arc, region BLM³														
Balanac River	Main	160	1.29	0.36	1.65	2.22	0.55	2.76	40	11	51	0.93	0.19	1.11
Buso-Buso River	Main	18	3.37	5.88	3.37	5.88	106	106	2.51	2.51	106	2.51	2.51	2.51
Catmon River	Tributary	18	1.75	2.92	1.75	2.92	54	54	1.17	1.17	54	1.17	1.17	1.17
Diwa River	Main	94	2.05	3.28	2.05	3.28	63	63	1.23	1.23	63	1.23	1.23	1.23
Pagsanjan River	Main	207	1.43	2.35	1.43	2.35	45	45	0.92	0.92	45	0.92	0.92	0.92
Pangil River	Main	53	1.19	1.96	1.19	1.96	37	37	0.77	0.77	37	0.77	0.77	0.77
San Antonio River	Main	13	1.94	0.38	2.31	3.32	0.57	3.89	61	11	72	1.39	0.19	1.58
Santa Cruz River, us	Tributary	22	1.68	2.57	1.68	2.57	51	51	0.89	0.89	51	0.89	0.89	0.89
Santa Cruz River, ds	Main	107	1.63	0.61	2.24	2.79	0.92	3.71	49	19	68	1.16	0.31	1.47
Tanay River	Main	44	4.23	8.05	4.23	8.05	155	155	3.82	3.82	155	3.82	3.82	3.82
Luzon Volcanic Arc, region Pinatubo³														
Bamban River	Main	88	3.91	1.96	5.87	6.59	2.97	9.55	124	59	184	2.67	1.01	3.68
Bucao River	Main	557	9.41	0.70	10.1	15.4	1.00	16.4	289	20	309	5.99	0.30	6.28
Gumain River, us	Tributary	127	1.79	3.73	5.52	2.52	5.76	8.28	52	111	163	0.73	2.03	2.76
Caulaman River	Tributary	49	2.41	2.41	2.41	3.91	3.91	3.91	75	75	75	1.50	1.50	1.50
Gumain River, ds	Main	255	2.70	3.58	6.28	3.88	5.46	9.34	70	108	178	1.18	1.88	3.06
Maloma River	Main	153	3.23	3.23	3.23	5.85	5.85	5.85	90	90	90	2.62	2.62	2.62
Bangot River	Tributary	96	3.87	3.87	3.87	6.53	6.53	6.53	124	124	124	2.66	2.66	2.66
O'Donnell River	Main	279	0.03	10.8	10.8	0.07	17.9	18.0	1	347	349	0.03	7.15	7.18

Table A2.3 (continued)

Location name	Type	Area km ²	Silicate weathering cation flux ¹						Silicate weathering Ca*+Mg* flux					
			low-T		high-T		Total	low-T		high-T		Total		
			10 ⁶ mol/km ² /yr	10 ⁶ mol/km ² /yr	10 ⁶ eq/km ² /yr	10 ⁶ eq/km ² /yr	10 ⁶ eq/km ² /yr	t/km ² /yr	10 ⁶ mol/km ² /yr					
Tabang River	Main	167	4.88	0.05	4.93	8.22	0.07	8.30	147	1	148	3.34	0.02	3.37
Luzon Volcanic Arc, region Quezon														
Agus River	Main	931	1.42		1.42	2.55		2.55	47		47	1.13		1.13
Balabag River	Main	3	1.67	0.02	1.69	3.03	0.03	3.06	57	1	58	1.36	0.01	1.37
Kiloloram River	Main	0	1.66		1.66	3.04		3.04	54		54	1.38		1.38
Liabak River	Main	6	0.81		0.81	1.33		1.33	25		25	0.51		0.51
Tignoan River	Main	87	1.84		1.84	3.31		3.31	59		59	1.48		1.48
Luzon Volcanic Arc, region Taal														
Obispo Stream	Tributary	19	3.43		3.43	5.44		5.44	105		105	2.01		2.01
Balayan River	Main	82	4.53	0.04	4.58	7.27	0.06	7.33	142	1	144	2.74	0.02	2.76
Dacanlao River	Main	56	4.40	0.28	4.68	6.91	0.43	7.34	133	9	142	2.51	0.14	2.65
Langgangan River	Main	1	5.39	0.22	5.61	8.69	0.33	9.03	169	7	176	3.31	0.11	3.42
Laurel River	Main	32	5.04		5.04	7.77		7.77	154		154	2.73		2.73
Mabacao River	Main	244	3.70		3.70	5.85		5.85	114		114	2.15		2.15
Mangapol River	Main	39	3.25	1.77	5.02	4.66	2.68	7.34	93	54	147	1.41	0.91	2.32
Naic River	Main	77	5.10	0.46	5.56	7.60	0.70	8.29	152	14	166	2.50	0.24	2.73
Palico River	Main	161	3.54		3.54	5.62		5.62	109		109	2.08		2.08
Palsara River	Main	15	8.27		8.27	12.6		12.6	253		253	4.35		4.35
Pele River	Main	2	1.44		1.44	2.26		2.26	45		45	0.82		0.82

1: Silicate weathering cation flux = Na* + K* + Ca* + Mg*

2: ds = downstream, us = upstream

3: ZA = Zambales and Angat Ophiolites

BLM = Bataan, Laguna and Macolod

Pinatubo = comprises both streams draining exclusively Pinatubo and the adjacent Zambales ophiolite

Table A2.4. Silicate weathering rate, sulfur flux, carbon export flux and carbon sequestration flux from individual watersheds, Luzon, Philippines

Location name	Type	Area km ²	Silicate weathering				SO ₄ flux				Silicate weathering carbon export flux ²				Silicate weathering carbon sequestration flux ³	
			low-T		high-T		atm		high-T		atm		high-T		Total	
			rate ¹ t/km ² /yr	Total	rate ¹ t/km ² /yr	Total	atm	high-T	atm	high-T	atm	high-T	atm	high-T	Total	Total
10 ⁶ mol/km ² /yr																
Angat Ophiolite, region ZA⁵																
Hanginan River	Main	10	240	240	0.05	0.05	0.05	6.63	6.63	0.05	0.05	6.63	6.63	6.63	3.56	
Lacotan River	Main	7	247	247	0.01	0.01	0.01	6.92	6.92	0.01	0.01	6.92	6.92	6.92	3.44	
Zambales Ophiolite, region ZA⁵																
Alasa River	Main	80	125	125	0.61	0.61	0.61	0.90	0.90	0.61	0.61	0.90	0.90	0.90	2.96	
Bulsa River, us ⁴	Tributary	295	216	216	0.02	0.02	0.02	6.59	6.59	0.02	0.02	6.59	6.59	6.59	3.12	
Bulsa River, ds ⁴	Main	442	204	204	0.01	0.01	0.01	5.94	5.94	0.01	0.01	5.94	5.94	5.94	2.96	
Mababo River	Tributary	27	215	215	0.01	0.01	0.01	7.36	7.36	0.01	0.01	7.36	7.36	7.36	3.69	
Cabarabuan River	Main	38	199	199	0.01	0.01	0.01	6.95	6.95	0.01	0.01	6.95	6.95	6.95	3.47	
Camiling River, us	Tributary	256	202	202	0.01	0.01	0.01	6.78	6.78	0.01	0.01	6.78	6.78	6.78	3.39	
Camiling River, ds	Main	298	209	209	0.02	0.02	0.02	7.64	7.64	0.02	0.02	7.64	7.64	7.64	3.70	
Dumloc River	Main	38	283	283	0.01	0.01	0.01	8.75	8.75	0.01	0.01	8.75	8.75	8.75	4.43	
Lawis River, us	Tributary	115	119	119	0.01	0.01	0.01	4.09	4.09	0.01	0.01	4.09	4.09	4.09	2.08	
Lawis Tributary I	Tributary	21	122	122	0.01	0.01	0.01	4.54	4.54	0.01	0.01	4.54	4.54	4.54	2.29	
Lawis River, ds	Main	138	122	122	0.01	0.01	0.01	4.05	4.05	0.01	0.01	4.05	4.05	4.05	2.26	
Lawis Tributary II	Main	8	198	198	0.01	0.01	0.01	7.14	7.14	0.01	0.01	7.14	7.14	7.14	3.44	
Masinloc River	Main	40	165	165	0.01	0.01	0.01	6.45	6.45	0.01	0.01	6.45	6.45	6.45	3.28	
Bicol Volcanic Arc, region Bicol																
Bulawan River	Main	17	196	196	0.02	0.02	0.02	2.48	2.48	0.02	0.02	2.48	2.48	2.48	1.14	
Dobgon River	Main	38	213	213	0.03	0.03	0.03	2.51	2.51	0.03	0.03	2.51	2.51	2.51	1.18	
Guinobatan River	Main	65	289	18	0.04	0.74	0.78	6.90	0.39	0.04	0.74	6.90	7.29	7.29	3.90	
Joroel River	Main	10	131	131	0.02	0.02	0.02	1.29	1.29	0.02	0.02	1.29	1.29	1.29	0.73	
Kinastillohan River	Main	4	182	182	0.02	0.02	0.02	2.48	2.48	0.02	0.02	2.48	2.48	2.48	1.10	
Naga River	Main	14	151	151	0.04	0.04	0.04	1.08	1.08	0.04	0.04	1.08	1.08	1.08	0.84	
Naga River Tributary	Main	8	139	1	0.04	0.05	0.09	0.49	0.03	0.04	0.05	0.49	0.52	0.52	0.96	

Table A2.4. (continued)

Location name	Type	Area km ²	Silicate weathering				SO ₄ flux				Silicate weathering				Silicate weathering					
			rate ¹		Total		atm		high-T		Total		atm		high-T		Total		Total	
			low-T	high-T	t/km ² /yr	t/km ² /yr	10 ⁶ eq/km ² /yr	10 ⁶ eq/km ² /yr	10 ⁶ mol/km ² /yr											
Paulog River	Main	29	255	2	257	0.04	0.10	0.14	3.48	0.05	3.53	2.00								
Pio Duran River	Main	66	264		264	0.03		0.03	9.94		9.94	5.18								
Quinale River	Main	86	190		190	0.02		0.02	2.02		2.02	0.96								
Santo Domingo River	Main	8	226		226	0.02		0.02	3.20		3.20	1.48								
Yawa River	Main	57	323	34	358	0.04	1.44	1.48	5.13	0.76	5.89	5.17								
Bicol Volcanic Arc, region Camarines																				
Daet River	Main	69	117		117	0.03		0.03	1.18		1.18	0.61								
Inarihan River	Main	1	160		160	0.01		0.01	1.32		1.32	0.52								
Matogdon Tributary	Tributary	2	116		116	0.02		0.02	1.17		1.17	0.52								
Matogdon River	Main	28	146		146	0.03		0.03	1.76		1.76	0.77								
Pinaglabanan River	Main	12	195		195	0.04		0.04	0.26		0.26	1.38								
Ragay River	Main	120	169		169	0.04		0.04	2.95		2.95	1.33								
Rangas River	Main	18	280		280	0.03		0.03	0.03		0.03	3.98								
San Vicente River	Main	1	133		133	0.04		0.04	1.31		1.31	0.67								
Pulantuna River	Tributary	189	78		78	0.03		0.03	0.92		0.92	0.50								
Sipocot River	Main	487	93		93	0.03		0.03	2.52		2.52	1.26								
Bicol Volcanic Arc, region Sorsogon																				
Bacolod River	Main	10	280	13	293	0.04	0.54	0.59	3.82	0.29	4.11	2.24								
Bacon River	Main	12	186		186	0.04		0.04	2.88		2.88	1.50								
Bangon River	Main	24	108	64	172	0.04	0.29	0.33	0.00	1.13	1.13	1.26								
Barcelona River	Main	27	193		193	0.03		0.03	1.71		1.71	0.82								
Karangan Stream	Tributary	1	165		165	0.03		0.03	1.46		1.46	0.90								
Cadacan River, us	Tributary	34	235	32	267	0.04	1.34	1.39	2.24	0.71	2.95	2.52								
Cadacan River, ds	Main	125	291	35	326	0.04	1.47	1.51	4.29	0.77	5.06	3.61								
Pawa River	Main	26	121	4	124	0.04	0.15	0.20	0.67	0.08	0.75	0.82								

Table A2.4. (continued)

Location name	Type	Area km ²	Silicate weathering				SO ₄ flux				Silicate weathering				Silicate weathering	
			low-T		high-T		atm		high-T		atm		high-T		carbon export flux ²	carbon sequestration flux ³
			t/km ² /yr	rate ¹	Total	rate ¹	Total	atm	high-T	Total	atm	high-T	Total	atm	high-T	Total
San Bartolome River	Main	17	153	153	0.04	0.04	0.04	0.04	1.98	1.98	1.98	1.98	1.98	0.98	0.98	
San Francisco River	Main	23	224	224	0.04	0.04	0.04	1.98	1.98	1.98	1.98	1.98	0.98	0.98		
San Juan Stream	Main	5	193	193	0.03	0.03	0.03	2.11	2.11	2.11	2.11	2.11	1.02	1.02		
San Juan II Stream	Main	1	186	186	0.03	0.03	0.03	1.91	1.91	1.91	1.91	1.91	0.92	0.92		
Solinao River	Tributary	17	166	166	0.03	0.03	0.03	1.80	1.80	1.80	1.80	1.80	0.82	0.82		
San Ramon (Magsaysay) River	Main	53	207	207	0.04	0.04	0.04	1.86	1.86	1.86	1.86	1.86	1.00	1.00		
Unnamed waterfall	Main	0	142	142	0.04	0.04	0.04	0.90	0.90	0.90	0.90	0.90	0.60	0.60		
Luzon Volcanic Arc, region BLM⁵																
Balanac River	Main	160	177	188	0.04	0.13	0.18	2.09	0.24	2.33	2.09	0.24	2.33	1.29	1.29	
Buso-Buso River	Main	18	209	209	0.01	0.01	0.01	5.28	5.28	5.28	5.28	5.28	2.67	2.67		
Catmon River	Tributary	18	175	175	0.02	0.02	0.02	2.69	2.69	2.69	2.69	2.69	1.29	1.29		
Diwa River	Main	94	188	188	0.03	0.03	0.03	2.81	2.81	2.81	2.81	2.81	1.41	1.41		
Pagsanjan River	Main	207	125	125	0.03	0.03	0.03	2.20	2.20	2.20	2.20	2.20	1.05	1.05		
Pangil River	Main	53	137	137	0.03	0.03	0.03	2.07	2.07	2.07	2.07	2.07	0.89	0.89		
San Antonio River	Main	13	162	174	0.04	0.28	0.32	2.97	0.25	3.22	2.97	0.25	3.22	1.79	1.79	
Santa Cruz River, us	Tributary	22	197	197	0.02	0.02	0.02	2.16	2.16	2.16	2.16	2.16	1.04	1.04		
Santa Cruz River, ds	Main	107	216	235	0.04	0.23	0.27	2.50	0.41	2.91	2.50	0.41	2.91	1.68	1.68	
Tanay River	Main	44	220	220	0.02	0.02	0.02	8.33	8.33	8.33	8.33	8.33	3.92	3.92		
Luzon Volcanic Arc, region Pinatubo⁵																
Bamban River	Main	88	294	353	0.04	2.50	2.54	4.66	1.32	5.98	4.66	1.32	5.98	4.10	4.10	
Bucao River	Main	557	411	432	0.04	0.73	0.78	4.72	0.61	5.33	4.72	0.61	5.33	6.95	6.95	
Gumain River, us	Tributary	127	163	274	0.04	2.54	2.58	1.57	2.65	4.22	1.57	2.65	4.22	3.27	3.27	
Caulaman River	Tributary	49	222	222	0.01	0.01	0.01	3.32	3.32	3.32	3.32	3.32	1.66	1.66		
Gumain River, ds	Main	255	186	294	0.04	4.63	4.67	3.92	2.46	6.38	3.92	2.46	6.38	3.63	3.63	

Table A2.4. (continued)

Location name	Type	Area km ²	Silicate weathering				SO ₄ flux				Silicate weathering				Silicate weathering				
			rate ¹		t/km ² /yr		atm		high-T		atm		high-T		carbon export flux ²		carbon sequestration flux ³		
			low-T	high-T	Total	low-T	high-T	Total	atm	high-T	Total	atm	high-T	Total	atm	high-T	Total	atm	high-T
Maloma River	Main	153	205	205	205	0.01	0.01	0.01	5.23	5.23	5.23	0.01	0.01	0.01	5.23	5.23	2.74	2.74	
Bangot River	Tributary	96	266	266	266	0.03	0.03	0.03	4.31	4.31	4.31	0.03	0.03	0.03	4.31	4.31	2.89	2.89	
O'Donnell River	Main	279	140	347	488	0.04	13.80	13.84	0.00	4.37	4.37	0.00	4.37	4.37	0.00	4.37	7.81	7.81	
Pasig River	Main	56	482	175	657	0.04	7.32	7.37	0.00	3.56	3.56	0.00	3.56	3.56	0.00	3.56	10.20	10.20	
Porac River us	Tributary	42	427	62	489	0.04	2.58	2.62	1.59	1.36	2.95	0.04	2.58	2.62	1.59	1.36	6.72	6.72	
Porac River ds	Main	120	376	41	416	0.04	1.70	1.74	2.92	0.90	3.81	0.04	1.70	1.74	2.92	0.90	5.21	5.21	
Sacobia River	Main	33	589	61	650	0.04	2.54	2.59	2.52	1.34	3.86	0.04	2.54	2.59	2.52	1.34	10.24	10.24	
Santol River	Main	18	251	5	256	0.04	0.20	0.24	2.74	0.10	2.84	0.04	0.20	0.24	2.74	0.10	1.88	1.88	
Tabang River	Main	167	333	1	334	0.05	0.06	0.11	3.50	0.03	3.53	0.05	0.06	0.11	3.50	0.03	3.72	3.72	
Luzon Volcanic Arc, region Quezon																			
Agus River	Main	931	111	111	111	0.02	0.02	0.02	2.88	2.88	2.88	0.02	0.02	0.02	2.88	2.88	1.49	1.49	
Balabag River	Main	3	152	1	153	0.04	0.02	0.06	2.83	0.02	2.85	0.04	0.02	0.06	2.83	0.02	1.52	1.52	
Kiloloram River	Main	0	146	146	146	0.03	0.03	0.03	2.93	2.93	2.93	0.03	0.03	0.03	2.93	2.93	1.50	1.50	
Llabak River	Main	6	88	88	88	0.02	0.02	0.02	1.20	1.20	1.20	0.02	0.02	0.02	1.20	1.20	0.61	0.61	
Tignoan River	Main	87	149	149	149	0.03	0.03	0.03	3.17	3.17	3.17	0.03	0.03	0.03	3.17	3.17	1.60	1.60	
Luzon Volcanic Arc, region Taal																			
Obispo Stream	Tributary	19	347	347	347	0.03	0.03	0.03	4.99	4.99	4.99	0.03	0.03	0.03	4.99	4.99	2.49	2.49	
Balayan River	Main	82	373	1	374	0.04	0.05	0.10	6.85	0.03	6.88	0.04	0.05	0.10	6.85	0.03	3.11	3.11	
Dacanalao River	Main	56	352	9	360	0.04	0.36	0.40	6.39	0.19	6.58	0.04	0.36	0.40	6.39	0.19	3.23	3.23	
Langgangan River	Main	1	370	7	376	0.04	0.28	0.32	6.60	0.15	6.74	0.04	0.28	0.32	6.60	0.15	3.82	3.82	
Laurel River	Main	32	349	349	349	0.04	0.04	0.04	6.39	6.39	6.39	0.04	0.04	0.04	6.39	6.39	3.14	3.14	
Mabacao River	Main	244	316	316	316	0.03	0.03	0.03	5.76	5.76	5.76	0.03	0.03	0.03	5.76	5.76	2.45	2.45	
Mangapol River	Main	39	305	54	358	0.04	1.07	1.11	3.47	1.18	4.65	0.04	1.07	1.11	3.47	1.18	2.81	2.81	
Naic River	Main	77	320	14	334	0.04	0.58	0.63	6.72	0.31	7.03	0.04	0.58	0.63	6.72	0.31	3.23	3.23	
Palico River	Main	161	309	309	309	0.03	0.03	0.03	5.85	5.85	5.85	0.03	0.03	0.03	5.85	5.85	2.56	2.56	

Table A2.4. (continued)

Location name	Type	Area km ²	Silicate weathering rate ¹			SO ₄ flux			Silicate weathering carbon export flux ²			Silicate weathering carbon sequestration flux ³		
			low-T	high-T	Total	atm	high-T	Total	atm	high-T	Total	atm	high-T	Total
			t/km ² /yr	10 ⁶ eq/km ² /yr	10 ⁶ mol/km ² /yr				10 ⁶ mol/km ² /yr					
Palsara River	Main	15	412	412	0.04	0.04	0.04	11.53	11.53	11.53	4.99	4.99	4.99	
Pele River	Main	2	196	196	0.03	0.03	0.03	1.79	1.79	1.79	0.98	0.98	0.98	

1: Silicate weathering rate = Silicate cation weathering rate + SiO₂ = Na* + K* + Ca* + Mg* + SiO₂

2: Total bicarbonate flux, also called "carbon consumption" in published studies

3: See France-Lanord and Derry (1997), p. 66.

4: ds = downstream, us = upstream

5: ZA = Zambales and Angat Ophiolites

BLM = Bataan, Laguna and Macolod

Pinatubo = comprises both streams draining exclusively Pinatubo and the adjacent Zambales ophiolite

Table A4.1. Chemical fluxes from all watersheds studied on the Big Island of Hawai'i and Kaua'i

River name	Area km ²	Silicate weathering cation flux ¹			Silicate weathering ²			Silicate Ca*+Mg*			SO ₄	WCEF ³	2 × Si	WCSF ⁴
		10 ⁶			10 ⁶			10 ⁶						
		mol/km ² /yr	eq/km ² /yr	t/km ² /yr	mol/km ² /yr	t/km ² /yr	mol/km ² /yr	eq/km ² /yr	mol/km ² /yr	eq/km ² /yr				
Big Island of Hawai'i														
Aamakao Gulch	12.5	0.60	0.86	16.5	45.4	0.26	0.11	0.63	0.96	0.31				
Alakahi Stream	2.17	0.30	0.49	8.55	29.5	0.19	0.06	0.38	0.70	0.20				
Hakalau Stream	22.4	1.61	2.76	47.9	122	1.15	0.27	2.36	2.45	1.21				
Hanawi Stream	10.8	1.89	3.25	56.3	143	1.37	0.22	2.87	2.88	1.44				
Hapahapai Gulch	3.86	0.35	0.50	9.71	25.4	0.16	0.08	0.37	0.52	0.18				
Hi'ilawe Stream	16.2	1.31	1.90	36.2	110	0.60	0.18	1.58	2.47	0.70				
Honokane Nui	26.1	1.06	1.79	32.6	112	0.73	0.10	1.63	2.65	0.78				
Honoli'i River	36.7	0.43	0.55	11.2	22.8	0.11	0.20	0.32	0.38	0.16				
Hononu Stream	4.16	2.24	3.55	64.7	173	1.31	0.36	3.01	3.60	1.45				
Kahua Ranch stream	0.37	0.26	0.42	7.57	24.7	0.16	0.06	0.28	0.57	0.17				
Kakeha Stream	0.07	0.23	0.39	6.79	22.4	0.16	0.09	0.24	0.52	0.17				
Kapehu Rd. Stream	1.98	1.87	3.27	57.8	142	1.40	0.15	3.05	2.82	1.47				
Kapue Stream	24.3	0.94	1.65	28.0	67.6	0.71	0.20	1.38	1.32	0.74				
Kawaihae Uka Stream	4.57	0.10	0.15	3.01	8.96	0.04	0.04	0.05	0.20	0.05				
Kawaiki Stream	1.24	0.05	0.09	1.54	9.34	0.04	0.04	0.00	0.26	0.04				
Kawainui I Stream	21.9	1.00	1.66	29.8	80.8	0.66	0.20	1.37	1.70	0.71				
Kawainui II Stream	3.99	0.06	0.12	2.04	12.1	0.05	0.05	0.00	0.33	0.06				
Kilohana Gulch	2.30	0.22	0.30	6.52	18.5	0.08	0.08	0.13	0.40	0.10				
Kolekole River	53.8	0.62	1.10	19.1	50.0	0.48	0.15	0.83	1.03	0.50				
Laupahoehoe Stream	12.2	0.38	0.44	9.52	17.2	0.06	0.07	0.35	0.26	0.10				
Nanue Stream	37.5	0.47	0.78	13.8	34.8	0.31	0.08	0.66	0.70	0.33				
Pu'u O Umi stream	0.15	0.21	0.25	5.44	9.05	0.04	0.05	0.14	0.12	0.06				
Umauma Stream	54.2	0.71	1.24	21.1	56.9	0.52	0.12	1.06	1.19	0.55				
Wai'aka Stream	1.95	0.50	0.64	13.0	36.9	0.14	0.11	0.42	0.80	0.20				
Waikama Gulch	6.65	0.49	0.68	13.3	45.7	0.19	0.17	0.41	1.08	0.23				

Table A4.1. (continued)

River name	Area km ²	Silicate weathering cation flux ¹				Silicate weathering ²		Silicate Ca*+Mg*		SO ₄ 10 ⁶ eq/km ² /yr	WCEF ³ 2 × Si	WCSF ⁴
		10 ⁶		10 ⁶		10 ⁶		10 ⁶				
		mol/km ² /yr	eq/km ² /yr	t/km ² /yr	t/km ² /yr	mol/km ² /yr	mol/km ² /yr	eq/km ² /yr	eq/km ² /yr			
Waikamalo Stream	35.5	0.71	1.23	21.3	63.8	0.52	0.12	1.04	1.42	0.54		
Wailoa Stream	37.4	1.12	1.71	32.6	97.7	0.59	0.14	1.51	2.17	0.67		
Wailuku River, ds	638	0.16	0.26	4.68	11.8	0.10	0.04	0.20	0.24	0.11		
Wailuku River, us	343	0.01	0.02	0.34	0.99	0.01	0.00	0.01	0.02	0.01		
Wailuku Tributary	24.3	0.01	0.02	0.43	1.27	0.01	0.00	0.02	0.03	0.01		
Waipi'o Tributary	0.07	1.02	1.60	29.7	91.0	0.58	0.13	1.40	2.04	0.64		
Walaohia Gulch	12.4	0.44	0.54	11.1	29.5	0.10	0.07	0.40	0.61	0.15		
Kaua'i												
Anahola Stream	23.9	0.35	0.46	8.64	22.2	0.11	0.12	0.24	0.45	0.14		
Dam Gulch	0.10	0.16	0.23	4.15	18.0	0.07	0.03	0.16	0.46	0.08		
Hanakapi'ai Stream	9.55	0.63	1.00	17.5	52.8	0.37	0.05	0.88	1.17	0.41		
Hanakoa River	4.38	0.49	0.78	13.8	40.7	0.30	0.03	0.71	0.90	0.33		
Hanaiei River	54.3	0.94	1.54	25.9	69.0	0.61	0.09	1.34	1.44	0.66		
Hanama'ulu Stream	25.6	0.65	0.94	17.7	32.4	0.29	0.23	0.58	0.49	0.35		
Hanapepe River	69.2	0.68	0.91	17.1	41.9	0.23	0.10	0.70	0.82	0.30		
Kapa'a Stream	36.2	0.55	0.80	14.4	33.4	0.26	0.17	0.48	0.63	0.30		
Kawaikoi Stream	10.6	0.23	0.28	5.79	9.33	0.05	0.05	0.20	0.12	0.08		
Keahua Stream	9.25	0.54	0.86	14.3	53.4	0.33	0.10	0.63	1.30	0.36		
Kilauea Stream	23.0	0.65	0.91	16.8	42.1	0.26	0.28	0.47	0.84	0.32		
Koai'e Stream	29.3	0.82	1.38	23.7	71.6	0.56	0.04	1.28	1.60	0.59		
Koke'e Stream	4.91	0.34	0.50	9.08	23.1	0.16	0.04	0.42	0.47	0.19		
Makaweli River	68.7	1.22	2.11	33.8	83.4	0.89	0.11	1.83	1.65	0.94		
Opaeka'a Stream	13.3	0.50	0.67	13.3	25.6	0.17	0.24	0.25	0.41	0.22		
Tributary @ Mauka Powerhouse	1.01	0.08	0.12	2.02	8.29	0.04	0.01	0.09	0.21	0.05		

Table A4.1. (continued)

River name	Area km ²	Silicate weathering cation flux ¹		Silicate weathering ²		SO ₄ 10 ⁶ eq/km ² /yr	WCEF ³ 2 × Si 10 ⁶ mol/km ² /yr	WCSF ⁴	
		10 ⁶ mol/km ² /yr	10 ⁶ eq/km ² /yr	t/km ² /yr	mol/km ² /yr				
Tributary @ Po'o Kaaha	0.45	0.32	0.51	8.49	48.2	0.06	0.38	1.32	0.20
Tributary A	0.23	0.62	1.10	17.0	44.8	0.02	1.03	0.93	0.50
Waikomo Stream	11.5	0.05	0.07	1.33	2.31	0.03	0.02	0.03	0.02
Waimea River @ dam	52.7	0.30	0.51	8.50	29.8	0.02	0.45	0.71	0.22
Waimea River @ ford	151	0.26	0.43	7.17	18.3	0.03	0.36	0.37	0.18
Waimea River @ powerhouse	113	0.19	0.32	5.38	16.5	0.02	0.28	0.37	0.14
Wainiha Stream	58.3	0.80	1.34	22.3	94.4	0.08	1.14	2.40	0.58
Wiliwili Gulch	2.66	0.17	0.27	4.50	19.0	0.02	0.20	0.48	0.11

1: Silicate cation weathering rate = Na* + K* + Ca* + Mg*

2: Silicate weathering rate = Na* + K* + Ca* + Mg* + SiO₂

3: Weathering carbon export flux = see discussion in section on surface fluxes

4: Weathering carbon sequestration flux = see discussion in section on surface fluxes

Table A4.2. Uncertainties in chemical fluxes from all watersheds studied on the Big Island of Hawaii'i and Kauai'i

River name	Area km ²	Silicate weathering cation flux ¹ km ²	Silicate weathering ²		SO ₄	WCEF ³	2 × Si	WCSF ⁴
			Ca*+Mg*	Ca*+Mg*				
CV, %								
Big Island of Hawaii'i								
Aamakao Gulch	12.5	79	80	79	79	81	78	79
Alakahi Stream	2.17	37	40	37	36	42	36	36
Hakalau Stream	22.4	34	37	34	33	38	32	33
Hanawi Stream	10.8	36	39	36	35	40	34	35
Hapahapai Gulch	3.86	197	198	197	197	198	197	197
Hi'ilawe Stream	16.2	58	59	58	57	60	56	57
Honokane Nui	26.1	40	42	40	39	44	38	39
Honoli'i River	36.7	35	38	35	34	39	33	34
Honomu Stream	4.16	33	36	33	32	38	31	32
Kahua Ranch stream	0.37	58	59	58	57	60	56	57
Takeha Stream	0.07	46	48	46	45	50	45	45
Kapehu Rd. Stream	1.98	47	49	47	46	50	45	46
Kapue Stream	24.3	42	45	42	41	46	41	41
Kawaihae Uka Stream	4.57	45	47	45	44	49	44	44
Kawaiki Stream	1.24	45	47	45	44	48	43	44
Kawainui I Stream	21.9	36	39	36	35	41	34	35
Kawainui II Stream	3.99	34	37	34	33	39	32	33
Kilohana Gulch	2.30	43	45	43	42	47	41	42
Kolekole River	53.8	47	49	47	46	50	45	46
Laupahoehoe Stream	12.2	71	72	71	70	73	70	70
Nanue Stream	37.5	74	76	75	74	77	74	74
Pu'u O Umi stream	0.15	50	52	50	49	53	49	49
Umauma Stream	54.2	58	60	58	58	61	57	58
Wai'aka Stream	1.95	35	38	35	34	39	33	34
Waikama Gulch	6.65	67	69	67	66	69	66	66

Table A4.2. (continued)

River name	Area km ²	Silicate weathering cation flux ¹	Silicate weathering ²		SO ₄	WCEF ³ 2 × Si	WCSF ⁴	
			Ca*+Mg*	CV, %				
Waikaumalo Stream	35.5	58	60	58	58	61	57	58
Wailoa Stream	37.4	18	23	18	16	26	14	16
Wailuku River, ds	638	47	50	47	47	51	46	47
Wailuku River, us	343	49	51	49	48	52	48	48
Wailuku Tributary	24.3	49	51	49	48	52	48	48
Waipi'o Tributary	0.07	48	51	48	48	52	47	48
Walaohia Gulch	12.4	111	112	111	110	112	110	110
Kaua'i								
Anahola Stream	23.9	69	71	69	69	72	68	69
Dam Gulch	0.10	261	261	261	261	262	261	261
Hanakapi'ai Stream	9.55	32	35	32	31	37	30	31
Hanakoa River	4.38	36	39	36	35	40	34	35
Hanalei River	54.3	22	26	22	20	29	19	20
Hanama'ulu Stream	25.6	101	102	101	101	103	100	101
Hanapepe River	69.2	76	77	76	76	78	75	76
Kapa'a Stream	36.2	65	67	65	64	68	64	64
Kawaikoi Stream	10.6	35	38	35	34	39	33	34
Keahua Stream	9.25	45	47	45	44	48	43	44
Kilauea Stream	23.0	44	46	44	43	48	43	43
Koai'e Stream	29.3	56	58	56	55	59	55	55
Koke'e Stream	4.91	85	86	85	84	87	84	84
Makaweli River	68.7	61	63	61	61	64	60	61
Opaeka'a Stream	13.3	73	74	73	72	75	72	72
Tributary @ Mauka Powerhouse	1.01	373	373	373	373	373	373	373

Table A4.2. Uncertainties in chemical fluxes from all watersheds studied on the Big Island of Hawai'i and Kaua'i

River name	Area km ²	Silicate weathering ² cation flux ¹		Silicate weathering ² cation flux ¹		SO ₄	WCEF ³ 2 × Si	WCSF ⁴	
		283	284	283	284				
Tributary @ Po'o Kaeoha	0.45	283	284	283	283	283	284	283	283
Tributary A	0.23	232	232	232	232	232	232	231	232
Waikomo Stream	11.5	156	156	156	156	155	157	155	155
Waimea River @ dam	52.7	34	37	34	34	33	38	32	33
Waimea River @ ford	151	53	55	53	53	52	56	51	52
Waimea River @ powerhouse	113	65	66	65	65	64	67	64	64
Wainiha Stream	58.3	38	41	38	38	37	42	36	37
Wiliwili Gulch	2.66	277	277	277	277	277	277	277	277

1: Silicate cation weathering rate = Na* + K* + Ca* + Mg*

2: Silicate weathering rate = Na* + K* + Ca* + Mg* + SiO₂

3: Weathering carbon export flux = see discussion in section on surface fluxes

4: Weathering carbon sequestration flux = see discussion in section on surface fluxes